REVIEWS OF MODERN PHYSICS VOLUME 44, NUMBER 2 APRIL 1972

Optical Pumping*

WILLIAM HAPPER
Columbia Radiation Laboratory, Department of Physics, Columbia University, New York, New York 10027

Optical pumping of ground-state and metastable atoms and ions is reviewed. We present a critical survey of the literature on pumping mechanisms, light propagation, relaxation mechanisms, spin exchange, and experimental details on the various atomic species which have been successfully pumped.

CONTENTS

* This work was supported by the Joint Services Electronics Program (U.S. Army, U.S. Navy, and U.S. Air Force) under Contract DAAB07-69-C083, and in part by the U.S. Air Force Office of Scientific Research under Contract AFOSR-68-1454B.

I. INTRODUCTION

Ever since the pioneering work of Hanle (Han24) on the magnetic depolarization of resonance light, it has been known that the excited atomic states that are produced by the absorption of anisotropic resonance light are strongly polarized. This atomic polarization results from the directionality or polarization of the light beam. Perhaps the most important aspect of polarized excited atoms is that the degree of atomic polarization can be determined with great sensitivity by observing the intensity and polarization of the fluorescent light. Unfortunately, very little work was devoted to the interrelationships between polarized atoms and resonance light in the two decades following Hanle's original work. In 1949, Kastler (Kas50) again drew attention to the remarkable properties of the interaction of resonance light with atoms. Kastler pointed out that the absorption and scattering of resonance light could lead to large population imbalances in atomic ground states as well as in excited states. Ground-state polarization by optical pumping was soon observed experimentally by Brossel, Kastler, and Winter (Bro52b) and by Hawkins and Dicke (Haw53).

A simple optical pumping experiment is illustrated in Fig. 1. An atom with a $^2S_{1/2}$ ground state and a $^2P_{1/2}$ excited state is illuminated by circularly polarized resonance radiation which propagates along the direction of a small magnetic field H. Ground-state atoms in the $+\frac{1}{2}$ sublevel cannot absorb light since they cannot accommodate the additional angular momentum of the photon in the $^2P_{1/2}$ excited state. However, ground-state atoms in the $-\frac{1}{2}$ sublevel can absorb a photon and jump to the $+\frac{1}{2}$ sublevel of the excited state. Atoms in the $+\frac{1}{2}$ excited-state sublevel decay very quickly and fall back to either the $-\frac{1}{2}$ ground-state sublevel or the $+\frac{1}{2}$ ground-state sublevel. The atom is twice as likely to fall to the $-\frac{1}{2}$ sublevel as to the $+\frac{1}{2}$ sublevel, but nevertheless, in the absence of any relaxation mechanisms, all atoms will eventually be "pumped" into the $+\frac{1}{2}$ sublevel.

This pumping can be detected in two ways. We notice that when all atoms have been pumped into the $+\frac{1}{2}$ sublevel, the vapor will become transparent. Consequently, the pumping light will no longer be attenuated, and photodetector A will receive the full intensity of the pumping light. Thus, observing the intensity of the transmitted pumping light, or *transmission monitoring*, is one important way to detect optical pumping. It is also clear that when complete pumping has taken place there will no longer be any resonantly scattered light, and the intensity of fluorescent light at photodetector B will vanish. Consequently, pumping can also be detected by observing the fluorescent light or by *fluorescence monitoring*. There are many variants of each method. For instance, transmission monitoring can be done with nonresonant light, since a polarized atomic vapor may change the polarization of the light even though the total intensity of the light is not affected.

It is also possible to detect optical pumping in an atomic beam experiment by using inhomogeneous magnetic fields to state select the pumped atoms. Such experiments were first used by Buck, Rabi, and Senitsky (Buc56) to measure the quadrupole interactions of

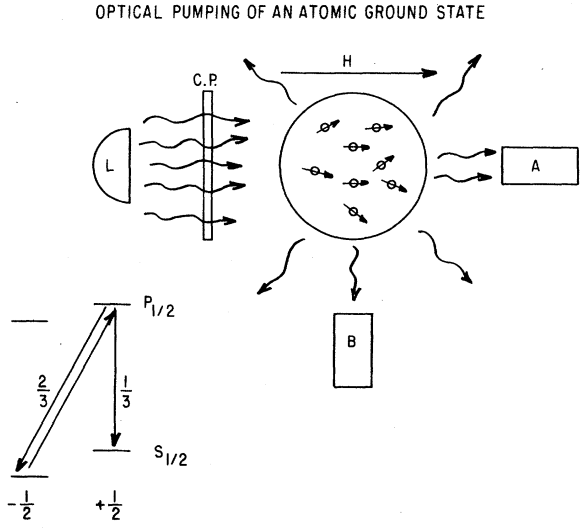

FIG. 1. A simple optical pumping experiment. Atoms are polarized by the scattering of circularly polarized resonant light. Either the transmitted light at A or the fluorescently scattered light at B can be used to monitor the atomic polarization.

excited alkali atoms. However, such experiments are not as sensitive, except in the case of radioactive atoms, as experiments based on optical monitoring. Recently Bucka (Buc66) has reconsidered these atomic beam techniques.

The ultimate degree of polarization that can be attained in an optical pumping experiment depends critically on the relaxation rates in the ground state. Pumping rates with conventional lamps rarely exceed a few thousand photon absorptions per second; and, consequently, relaxation times from collisions and other dissipative mechanisms can be no shorter than a few milliseconds if large degrees of polarization are to be attained. Long relaxation times can be obtained in a number of ways. The simplest is to place the atoms in a very large evacuated container or atomic beam so that the time between interatomic collisions or wall collisions is long. The first successful optical pumping experiments by Brossel *et al.* (Bro52b, 53) and by Hawkins and Dicke (Haw53) were done with atomic beams of sodium, and Barrat (Bar54) reported successful pumping of sodium vapor in a large (12-cm diameter) quartz cell shortly thereafter. It was apparent that nearly every collision of a sodium atom with the wall destroyed the polarization of the atom.

The problem of wall relaxation of optically pumped alkali atoms was overcome in two ways. Brossel *et al.* (Bro55b), Dicke's group in Princeton, and a number of other workers (Coh57), (Deh57a), (Ska57), (Har58) discovered that the molecules of certain simple gases such as hydrogen, nitrogen, or the inert gases could make millions of collisions against polarized alkali atoms without destroying the atomic polarization. These weakly relaxing gases can therefore be used as buffer gases which, at pressures of a few Torr, greatly increase the times for diffusion of the polarized atoms to the walls. Spin-relaxation times on the order of seconds can be obtained in buffered cells.

A second technique that has proved useful in optical pumping work with alkali atoms is coating the container walls with a nonrelaxing material. Dehmelt, Ensberg, and Robinson (Rob58) discovered that various paraffins and organosilanes are effective wall coatings against which an atom can make thousands of collisions without loss of polarization. Wall relaxation is not as serious a problem for diamagnetic species such as mercury, cadmium, helium-3, and lead, and these atoms are usually pumped in unbuffered, uncoated cells.

In this brief introduction we have already touched on three of the most important aspects of optical pumping: pumping, relaxation, and optical monitoring. In the remainder of this paper we shall examine these three topics in more detail.

In undertaking this review we had originally hoped to cover the entire subject of the interaction of resonance radiation with atomic vapors as well as peripheral fields of interest that have geen generated by optical pumping. These include the interaction of atoms with strong rf fields and the elegant experimental techniques of optical double-resonance and level-crossing spectroscopy of excited states. However, a closer acquaintance with the extensive and growing literature soon convinced us of the futility of these plans, and we have therefore limited this discussion to optical pumping of ground-state atoms and long-lived metastable states. Pumping of the excited state is discussed only insofar as it is necessary for an understanding of the ground-state pumping.

In the first six sections of this paper we review three basic phenomena, optical pumping, light propagation, and relaxation, which are common to most experiments. We have tried to present a reasonably complete outline of the basic theory of these phenomena, and wherever possible we have reproduced experiments from the literature which illustrate particularly important aspects of the physics. Sections VII–X contain a more detailed discussion of the various atomic and ionic species which have been pumped to date. These latter sections can be read without reference to the first six sections for a rapid review of the experimental situation. An extensive bibliography and cross reference list has been prepared, and we have tried to include all papers published through 1970. Because of the extensiveness of the literature some excellent papers have undoubtedly been overlooked and we apologize in advance to their authors.

Earlier reviews of optical pumping have been written by Kastler (Kas57), Skalinski (Ska60), deZafra (deZ60), Skrotskii and Izyumova (Skr61), Carver (Car63), Cohen–Tannoudji and Kastler (Coh66c), and Major (Maj68). A monograph and collection of reprints on Optical Pumping has been published by Bernheim (Ber65b).

II. MATHEMATICAL FRAMEWORK

A. The Atomic Hamiltonian

We shall assume that the evolution of an individual atom of the vapor is described by the Schroedinger equation

$$i\hbar(\partial/\partial t)\,|\,\psi\rangle=\mathcal{H}\,|\,\psi\rangle. \tag{II.1}$$

We assume that the Hamiltonian operator $\mathcal{H}$ is the sum of a large static part $\mathcal{H}_0$, which is the same for all atoms in the vapor, and a small perturbation V, which may represent a randomly fluctuating collisional interaction, an external radio-frequency field, or other processes. The unperturbed Hamiltonian $\mathcal{H}_0$ will define a number of eigenstates $|\,i\rangle$:

$$\mathcal{H}_0\,|\,i\rangle=E_i\,|\,i\rangle. \tag{II.2}$$

In optical pumping experiments we will usually be interested in a set of ground-state basis functions, which we shall designate by Greek letters μ, ν, etc., and a set of excited-state wave functions, which we shall designate with Latin letters m, n, etc. We shall find it useful to

define a ground-state Hamiltonian as

$$\mathcal{H}_g = \sum_{\mu\nu} |\mu\rangle\langle\mu|(\mathcal{H}-E_g)|\nu\rangle\langle\nu|, \quad \text{(II.3)}$$

where E_g is the mean energy of the ground-state sublevels. We may define the excited-state Hamiltonian $\mathcal{H}_e$ in an analogous way. Both the ground-state and excited-state Hamiltonians are traceless, e.g.,

$$\mathrm{Tr}[\mathcal{H}_g] = \sum_{\mu} \langle\mu|\mathcal{H}_g|\mu\rangle = 0. \quad \text{(II.4)}$$

For an atom of nuclear spin I and electronic spin J, the truncated Hamiltonians $\mathcal{H}_e$ and $\mathcal{H}_g$ can be represented to sufficient accuracy by an effective Hamiltonian of the form

$$hA\mathbf{I}\cdot\mathbf{J}+hB[3(\mathbf{I}\cdot\mathbf{J})^2+(3/2)(\mathbf{I}\cdot\mathbf{J}) - I(I+1)J(J+1)]/2I(2I-1)J(2J-1) + g_J\mu_0\mathbf{J}\cdot\mathbf{H}-(\mu_I/I)\mathbf{I}\cdot\mathbf{H}. \quad \text{(II.5)}$$

The magnetic dipole- and electric quadrupole-interaction constants are A and B, respectively, the gyromagnetic ratio of the electronic spin J is g_J, and the nuclear moment is μ_I. The atoms are subject to an external magnetic field $\mathbf{H}$.

B. The Density Matrix

One is seldom interested in the wave function of an individual atom. The signals observed in any optical pumping experiment always turn out to be proportional to the mean value $\langle M\rangle$ of some atomic observable M. For instance, M might be some component of the atomic angular momentum. Suppose that each atom of the vapor can be described by a wave function $|\psi_i\rangle$. Then the average value of M for a vapor of N atoms is

$$\langle M\rangle = (1/N)\sum_{i=1}^{N}\langle\psi_i|M|\psi_i\rangle. \quad \text{(II.6)}$$

Note that Eq. (II.6) can also be written as

$$\langle M\rangle = \mathrm{Tr}[\rho M] = \sum_n \langle n|\rho M|n\rangle, \quad \text{(II.7)}$$

where the density matrix ρ is defined by

$$\rho = (1/N)\sum_{i=1}^{N}|\psi_i\rangle\langle\psi_i|. \quad \text{(II.8)}$$

The probability of finding a given atom of the vapor in the sublevel $|n\rangle$ is $\langle n|\rho|n\rangle$. Thus, in order to calculate the average value of atomic observables it is only necessary to know the density matrix of the atoms. One need not know the wave functions of the individual atoms; and, in fact, because of interactions between the atoms themselves and between the atoms and the light, a wave function for each individual atom may not exist. Nevertheless, one can always define a density matrix ρ such that Eq. (II.7) is valid.

A more profound discussion of the limitation of the wave function and the advantages of the density matrix as a description of physical systems is contained in a review article by Fano (Fan57).

The description of optical pumping experiments usually requires two types of observables: ground-state observables and excited-state observables. Consequently, it is convenient to write the density matrix as the sum of a ground-state component ρ_g and an excited-state component ρ_e:

$$\rho = \rho_g + \rho_e + \cdots. \quad \text{(II.9)}$$

Here ρ_g and ρ_e are the projections of ρ within the ground state and excited state, respectively, of the atom.

C. The Liouville Equation

The rate of change of the density matrix is often described by a first order differential equation called the Liouville equation:

$$(\partial/\partial t)\rho = (1/i\hbar)[\mathcal{H}_0, \rho] + L(\rho). \quad \text{(II.10)}$$

The commutator $[\mathcal{H}_0, \rho]$ follows directly from the Schroedinger equation (II.1). The term $L(\rho)$ represents relaxation and pumping mechanisms and all other processes which cannot be included in $\mathcal{H}_0$. We shall find that the Liouville operator for an optically pumped ground-state atom is composed to three main parts:

$$L(\rho) = (d^{(1)}/dt)\rho + (d^{(2)}/dt)\rho + (d^{(3)}/dt)\rho\cdots. \quad \text{(II.11)}$$

Here the first term represents depopulation pumping, which is discussed in detail in Sec. III.A. The basic formula for depopulation pumping is Eq. (III.7). The second term in Eq. (II.11) represents repopulation pumping, which is discussed in Sec. III.C. The basic formula for repopulation pumping is Eq. (III.87). The last term in Eq. (II.11) represents relaxation, which is discussed in Sec. V. Relaxation is an extremely diverse and complicated phenomenon and cannot be summarized by one formula.

D. The Interaction Representation

We shall frequently make use of the interaction representation to analyze optical pumping experiments. The interaction-picture density matrix σ is defined by

$$\sigma = \tilde{\rho} = \exp(i\mathcal{H}_0 t/\hbar)\rho\exp(-i\mathcal{H}_0 t/\hbar). \quad \text{(II.12)}$$

More generally, a tilde over any operator always indicates that it has been subjected to the transformation of Eq. (II.12). The goal of this transformation to the interaction picture is to simplify the Liouville equation, which now becomes

$$(d/dt)\sigma = \tilde{L}(\rho). \quad \text{(II.13)}$$

That is, the interaction-picture density matrix would be constant if there were no pumping or relaxation mechanisms. Analogous transformations can be made if $\mathcal{H}_0$ is time dependent; for instance, if the atom is subject to an oscillating or rotating magnetic field (Rab54), (Ale64).

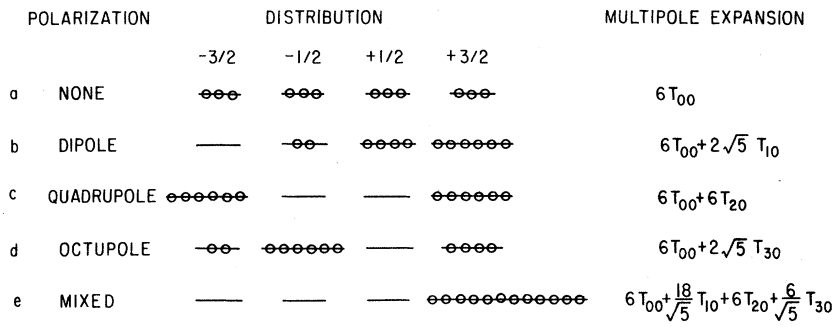

FIG. 2. Multipole polarizations for a spin-$\frac{3}{2}$ atom. The pure multipole population distributions have characteristic effects on the absorption or emission of light, and they often relax by simple exponential decay.

In terms of σ, the expectation value of any operator M is

$$\langle M\rangle = \mathrm{Tr}\,[\sigma\tilde{M}]. \qquad \text{(II.14)}$$

E. The Secular Approximation

One frequently finds that the rate of change of the density matrix in the interaction picture is given by an equation of the form

$$(d/dt)\sigma_{ij}=A_{ij}+\sum_k B_{ij}(\omega_k)\,\exp\,(i\omega_k t). \qquad \text{(II.15)}$$

That is, the rate of change of the density matrix is the sum of slowly varying parts A_{ij} and rapidly oscillating parts $B_{ij}(\omega_k)\,\exp\,(i\omega_k t)$. We assume that the oscillation frequencies ω_k are very large compared to the components of A and B, i.e.,

$$\omega_k \gg A_{ij},$$
$$\omega_k \gg B_{ij}(\omega_r). \qquad \text{(II.16)}$$

We also assume that the elements of A and B are of comparable orders of magnitude. Under these conditions one finds that an adequate description of the atomic evolution can be obtained by simply ignoring the rapidly oscillating terms and solving the simplified equation

$$(d/dt)\sigma_{ij}=A_{ij}. \qquad \text{(II.17)}$$

This procedure, called the secular approximation, is quite useful in discussing the relaxation of an atomic ensemble. Barrat and Cohen-Tannoudji (Bar61d,e) discuss the limits of the secular approximation in more detail.

F. Atomic Polarization

Let us suppose there are G sublevels of the atomic ground state. If the atoms of a vapor were distributed at random among the ground-state sublevels, the probability of finding the atom in any given sublevel would be $1/G$, and the density matrix would be

$$\rho_g=(1/G)\sum_\mu |\,\mu\rangle\langle\mu\,| = 1/G. \qquad \text{(II.18)}$$

For brevity we shall always suppress projection operators such as $\sum_\mu |\,\mu\rangle\langle\mu\,|$ when no confusion can arise. The density matrix of Eq. (II.18) describes a completely unpolarized ensemble. It is natural to define the polarization P of an atomic vapor as the difference between the actual density matrix and the density matrix of an unpolarized ensemble. Thus, the polarization of the ground-state density matrix ρ_g is

$$P_g=\rho_g-(1/G)\,\mathrm{Tr}\,\rho_g. \qquad \text{(II.19)}$$

The excited-state polarization is defined in like manner. The polarization operators are always traceless, i.e.,

$$\mathrm{Tr}\,P=0. \qquad \text{(II.20)}$$

We shall call the diagonal matrix elements of the polarization "population excesses." Thus, $\langle\mu\,|\,P_g\,|\,\mu\rangle$ is the excess population of the ground-state sublevel μ with respect to a random population distribution. Off-diagonal components of the polarization or of the density matrix are called coherences. Thus, $\langle\mu\,|\,\rho_g\,|\,\nu\rangle$ or $\langle\mu\,|\,P_g\,|\,\nu\rangle$ is the coherence between the levels μ and ν.

In the absence of optical pumping or other polarizing mechanisms the polarization of the ground state is

$$P=-\mathcal{K}_g/GkT. \qquad \text{(II.21)}$$

Here T is the absolute temperature, and k is Boltzmann's constant. We assume that the energy splittings of the ground state are much smaller than kT, so that the thermal polarization is always very small. By optically pumping the ground state, one can produce much larger polarizations than the thermal polarization of Eq. (II.21).

G. Spherical Tensor Representations of ρ

For many problems which arise in optical pumping, it is convenient to represent the density matrix in terms of spherical basis operators. This is entirely analogous to the description of the surface of a solid with spherical harmonics. The systematic use of spherical basis operators seems to have been first suggested by Fano (Fan57), and the spherical tensor formalism has been popularized in optical pumping work by Dyakonov and Perel (Dya65), Omont (Omo65b), and Happer and Mathur (Hap67c).

To see why these "multipole polarizations" are useful, consider a ground-state atom with nuclear spin $I=\frac{3}{2}$ (e.g., ^{201}Hg). In Fig. 2, five different types of

population distribution are shown for an ensemble of such atoms. In case (a), there is a random distribution with no polarization. In case (b), there is a pure dipole polarization; that is, the average value of the magnetic dipole moment is nonzero, but all other multipole moments are zero. In case (c), there is a pure quadrupole polarization, and in case (d), there is a pure octupole polarization. The polarization of case (e) is mixed; that is, it is a linear superposition of a dipole, a quadrupole, and an octupole polarization. In a certain sense, the polarizations (a)–(d) correspond to the first four Legendre (more precisely, Gram) polynomials, while the polarization (e) corresponds to a Dirac delta function.

A few examples will indicate the significance of these different types of multipole distributions. First, it is easy to show that static or oscillating magnetic fields cannot change the multipolarity of a distribution, since magnetic fields simply rotate the atomic ensemble. A rotated dipole distribution is still a dipole distribution. Also, under the isotropic conditions which often prevail when a polarized ensemble relaxes toward a random ensemble, each multipole polarization is decoupled from all other multipole polarizations, and each multipole relaxes with a characteristic decay time that may be different for different multipoles. Furthermore, one can show that the absorption (or spontaneous emission) of light is affected only by dipole or quadrupole polarizations, but not by octupole or higher-order polarizations. That is, the distribution d of atoms would absorb or emit light in precisely the same way as a random distribution of the same number of atoms. Thus, regardless of the atomic spin, one need only consider the dipole and quadrupole components of polarization when analyzing most optical pumping experiments. This can result in a considerable simplification for high-spin atoms. It is convenient to describe the multipole polarizations with spherical basis operators. Consider two atomic multiplets which can be described by angular momentum basis states $|Fm\rangle$ and $|F'm'\rangle$. Here F and m label, respectively, the total angular momentum and the axial angular momentum of the state. Spherical basis operators for the atom are then defined by

$$T_{LM}(FF')=\sum_m |Fm\rangle\langle F'm-M|(-1)^{m-M-F'} \times C(FF'L;m,M-m). \quad \text{(II.22)}$$

These operators form an orthonormal basis system in the sense that they satisfy the condition

$$\mathrm{Tr}\,[T_{LM}^{\dagger}(FF')T_{lm}(ff')]=\delta_{Ll}\delta_{Mm}\delta_{Ff}\delta_{F'f'}. \quad \text{(II.23)}$$

Consequently, one can expand the density matrix of the atom in terms of the basis operators

$$\rho=\sum (-1)^{F-F'+M}\rho_{LM}(FF')T_{L-M}(F'F), \quad \text{(II.24)}$$

where the summation extends over the complete range of the indices L, M, F, and F'. We note that the Hermitian conjugate of a basis operator is

$$T_{LM}^{\dagger}(FF')=(-1)^{F-F'+M}T_{L-M}(F'F). \quad \text{(II.25)}$$

Equations (II.23), (II.24), and (II.25) imply the condition

$$\rho_{LM}(FF')=\mathrm{Tr}\,[\rho T_{LM}(FF')]. \quad \text{(II.26)}$$

For an atomic state of electronic angular momentum J and nuclear spin I, it is often convenient to express the density matrix in terms of the basis operators $T_{KM}(II)$ and $T_{LN}(JJ)$. Thus, we can write

$$\rho=\sum (-1)^{M+N}\rho(KM;LN)T_{K,-M}(II)T_{L,-N}(JJ), \quad \text{(II.27)}$$

where the summation extends over the range of the labels K, M, L, and N, and

$$\rho(KM;LN)=\mathrm{Tr}\,[\rho T_{KM}(II)T_{LN}(JJ)]. \quad \text{(II.28)}$$

We shall refer to Eqs. (II.24) and (II.27) as coupled and uncoupled expansions of ρ. The formulas for transforming between the coupled and the uncoupled expansions are listed at the end of this section.

As an example, let us consider the ground state of an alkali atom. We can always write the density matrix in the form

$$\rho=\alpha+\mathbf{A}\cdot\mathbf{S}, \quad \text{(II.29)}$$

where $\mathbf{S}$ is the electron spin, and α, A_x, A_y, and A_z are purely nuclear operators. We note that since the electronic spin is $\frac{1}{2}$, we have

$$\sqrt{2}S_\mu=T_{1\mu}(JJ), \quad \text{(II.30)}$$

so that Eq. (II.29) is a version of the uncoupled expansion of Eq. (II.27); and, in fact, we have

$$\alpha=(1/\sqrt{2})\sum_{LM}(-1)^M\rho(L-M;00)T_{LM}(II), \quad \text{(II.31)}$$

where $\rho(L-M;00)$ is one of the expansion coefficients in Eq. (II.27).

We can also express α in terms of the coupled basis operators, and we can use the transformation formulas summarized at the end of this section to write Eq. (II.31) as [here $[F]=(2F+1)$ etc.]

$$\alpha=\sum[(-1)^M/2]([F][F'][f][f'])^{1/2} \times W(JIF'L;FI)W(f'JLI;If)\rho_{L-M}(FF')T_{LM}(ff'). \quad \text{(II.32)}$$

Similar expressions can be found for $\mathbf{A}\cdot\mathbf{S}$. We note that the expectation value of the electron spin is

$$\langle\mathbf{S}\rangle=\mathrm{Tr}_I\,[\mathbf{A}]/2, \quad \text{(II.33)}$$

and the nuclear multipole moments are

$$\langle T_{LM}(II)\rangle=2\,\mathrm{Tr}_I\,[\alpha T_{LM}(II)]. \quad \text{(II.34)}$$

Here Tr_I means that the trace is to be performed only over the nuclear sublevels.

We shall sometimes find it convenient to work with the Zeeman projections of the electronic and nuclear multipole operators. We shall denote such a projection by a bar over the operator, e.g.,

$$\bar{T}_{LM}(JJ)=\sum_{Fm,m'}|Fm\rangle\langle Fm|T_{LM}(JJ)|Fm'\rangle\langle Fm'|. \tag{II.35}$$

Such operators are not orthogonal to each other or to the original multipole operators, but they play an important role in the description of many optical pumping experiments because they appear naturally when one makes the secular approximation.

In conclusion we list some important transformation equations for the multipole operators. Since the multipole operators $T_{LM}(FF')$ are in essence four angular momenta (I, J, I, and J) coupled to a total angular momentum L and z projection M, the coupled and uncoupled multipole operators are related to each other with a $9j$ symbol. Consequently, we have the equation

$$T_{LM}(FF')=\sum_{jj'}[(2F+1)(2F'+1)(2j+1)(2j'+1)]^{1/2}\times\begin{bmatrix}I & I & j\\ J & J & j'\\ F & F' & L\end{bmatrix}[T_j(II)T_{j'}(JJ)]_{LM}. \tag{II.36}$$

The symbol $[\cdots j\cdots j']_{LM}$ indicates that the angular momenta j and j' have been coupled to a total angular momentum L and z projection M. The inverse of Eq. (II.36) follows from the orthogonality properties of the $9j$ symbols:

$$[T_j(II)T_{j'}(JJ)]_{LM}=\sum_{FF'}[(2F+1)(2F'+1)(2j+1)(2j'+1)]^{1/2}\times\begin{bmatrix}I & I & j\\ J & J & j'\\ F & F' & L\end{bmatrix}T_{LM}(FF'). \tag{II.37}$$

Important special cases of Eq. (II.37) are

$$T_{LM}(II)=\sum_{FF'}[(2F+1)(2F'+1)]^{1/2}\times W(F'JLI;IF)T_{LM}(FF') \tag{II.38}$$

and

$$T_{LM}(JJ)=\sum_{FF'}[(2F+1)(2F'+1)]^{1/2}\times W(IFJL;JF')T_{LM}(FF'), \tag{II.39}$$

where the symbol W denotes a Racah coefficient.

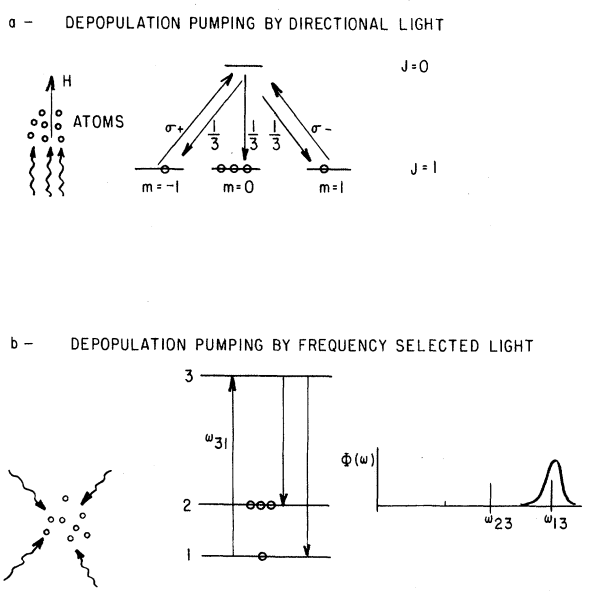

FIG. 3. Some simple examples of depopulation pumping. Population excesses are created in weakly absorbing sublevels, and population deficiencies are created in strongly absorbing sublevels.

III. PUMPING

A. Depopulation Pumping

The transfer of order from a light beam to an atomic vapor takes place as a result of two different mechanisms, depopulation pumping and repopulation pumping. Depopulation pumping occurs when certain ground-state sublevels absorb light more strongly than others. Since atoms are removed more rapidly from the strongly absorbing sublevels, an excess population will tend to build up in the weakly absorbing sublevels.

Depopulation pumping can occur if the pumping light is anisotropic or polarized, or if the frequency spectrum of the light departs from that of a blackbody for frequencies in the neighborhood of the atomic absorption lines.

Depopulation pumping by anisotropic light is illustrated in Fig. 3(a). This type of pumping is sometimes used with metastable helium atoms. Unpolarized light is incident, along the z axis, on an atom with a spin-1 ground state and a spin-0 excited state. Since the atom must absorb ±1 units of angular momentum from the light beam, no transitions can occur out of the $m=0$ sublevel of the ground state. However, an atom which has been excited from the $m=\pm1$ sublevel has a probability of 1/3 of falling back to the ground-state sublevel $m=0$. Consequently, in the absence of any relaxation mechanisms, all atoms will eventually be pumped into the $m=0$ sublevel of the ground state.

Depopulation pumping by isotropic light with a nonequilibrium-frequency profile is illustrated in Fig. 3(b). Pumping of this type is used in the alkali atoms to

produce population imbalances between the hyperfine multiplets. Consider an atom with two well-resolved ground-state levels (or multiplets) and one excited-state level (or multiplet). Light of frequency ω_{13} is incident on the atoms in such a way that atoms in level 1 are excited but atoms in level 2 are not, since the pumping light is off-resonance for the transition 2→3. The atoms can decay spontaneously to either of the two ground-state levels. Consequently, in the absence of relaxation, all atoms will eventually be pumped into level 2.

1. Elementary Theory of Depopulation Pumping

The transition rate $R_{\mu m}$ from a sublevel μ of the ground-state to a sublevel m of the excited state can be calculated from elementary perturbation theory. Let us represent the electric field of a monochromatic light wave by

$$\mathbf{E}=\boldsymbol{\mathcal{E}}\exp i(\mathbf{k}\cdot\mathbf{r}-\omega t)+\text{c.c.}, \tag{III.1}$$

where c.c. denotes the complex conjugate. Then the atom will experience an oscillating perturbation

$$V=-\mathbf{E}\cdot\mathbf{D}, \tag{III.2}$$

where $\mathbf{D}$ is the electric dipole-moment operator of the atom.

From simple perturbation theory, we find that the light wave will induce transitions from the ground-state sublevel μ to the excited-state sublevel m at a rate

$$R_{\mu m}=\{(1/\hbar^2)|\,\boldsymbol{\mathcal{E}}\cdot\mathbf{D}_{m\mu}\,|^2/[(\Gamma/2)+i(\omega_{m\mu}+\mathbf{k}\cdot\mathbf{v}-\omega)]\}+\text{c.c.}, \tag{III.3}$$

where Γ is the spontaneous decay rate of the excited state, $\mathbf{v}$ is the velocity of the atom, and

$$\omega_{m\mu}=(1/\hbar)(E_m-E_\mu) \tag{III.4}$$

is the resonant frequency of the transition. Let us denote the total rate of depletion of the ground state caused by transitions into all excited-state sublevels by

$$\delta\Gamma_{\mu\mu}=\sum_m R_{\mu m}. \tag{III.5}$$

Then the depletion of population in the ground-state sublevel μ resulting from depopulation pumping is described by the equation

$$(d^{(1)}/dt)\rho_{\mu\mu}=-\delta\Gamma_{\mu\mu}\rho_{\mu\mu}. \tag{III.6}$$

2. The Effective Hamiltonian

Equation (III.6) is useful only if no coherence exists in the ground state. Barrat and Cohen-Tannoudji (Bar61d,e) have shown that the correct generalization of Eq. (III.6) is

$$i\hbar(d^{(1)}/dt)\rho=\delta\mathcal{H}\rho-\rho\delta\mathcal{H}^\dagger, \tag{III.7}$$

where the effective Hamiltonian $\delta\mathcal{H}$ is a ground-state operator whose matrix elements are

$$\langle\mu'\,|\,\delta\mathcal{H}\,|\,\mu\rangle=(1/\hbar)\times\sum_m \boldsymbol{\mathcal{E}}^*\cdot\mathbf{D}_{\mu' m}\mathbf{D}_{m\mu}\cdot\boldsymbol{\mathcal{E}}/[(\omega-\omega_{m\mu}-\mathbf{k}\cdot\mathbf{v})+i\Gamma/2]. \tag{III.8}$$

The effective Hamiltonian is not Hermitian, but it can be written in terms of a Hermitian light-shift operator $\delta\mathcal{E}$ and a Hermitian light-absorption operator $\delta\Gamma$:

$$\delta\mathcal{H}=\delta\mathcal{E}-i\hbar\delta\Gamma/2. \tag{III.9}$$

In the original work of Barrat and Cohen–Tannoudji (Bar61d,e), the effective Hamiltonian was designated by

$$\delta\mathcal{H}_{\mu\mu'}=A_{\mu\mu'}(\Delta E'-i/2T_p)\hbar, \tag{III.10}$$

where the parameters $\Delta E'$ and $1/T_p$ were rates proportional to the light intensity, and $A_{\mu\mu'}$ was a dimensionless matrix proportional to the numerator of Eq. (III.8). The form of Eq. (III.10) is not as general as that of Eq. (III.8) because it implies that the light-shift operator and the light-absorption operator are both multiples of the same matrix $A_{\mu\mu'}$. This is true only in certain simple cases, and it is not true, for instance, for heavy alkali atoms such as rubidium and cesium.

3. The Effective Hamiltonian and The Polarizability

From Eq. (III.8) we see that the effective Hamiltonian can be written in the form

$$\delta\mathcal{H}=-\boldsymbol{\mathcal{E}}^*\cdot\boldsymbol{\alpha}\cdot\boldsymbol{\mathcal{E}}=\delta\mathcal{E}-i\hbar\delta\Gamma/2, \tag{III.11}$$

where the dyadic operator $\boldsymbol{\alpha}$ is defined by its matrix elements

$$\langle\mu\,|\,\boldsymbol{\alpha}\,|\,\mu\rangle=(-1/\hbar)\times\sum_m \mathbf{D}_{\mu' m}\mathbf{D}_{m\mu}/[(\omega-\omega_{m\mu}-\mathbf{k}\cdot\mathbf{v})+i\Gamma/2]. \tag{III.12}$$

Happer and Mathur (Hap67c) have shown that the expectation value of $\boldsymbol{\alpha}$ is the polarizability of the atom, i.e., that the dipole moment $\langle\mathbf{D}\rangle$ induced in the atom by the electric field E of Eq. (III.1) is

$$\langle\mathbf{D}\rangle=\langle\boldsymbol{\alpha}\rangle\cdot\boldsymbol{\mathcal{E}}\exp i(\mathbf{k}\cdot\mathbf{r}-\omega t)+\text{c.c.}. \tag{III.13}$$

4. The Mean Pumping Rate

Let us denote the statistical weight of the ground state by G. Then the mean pumping rate of the light beam is defined as

$$R=(1/G)\ \text{Tr}\,[\delta\Gamma]. \tag{III.14}$$

We shall see that the mean pumping rate plays a role in the ground state analogous to the role of the spontaneous decay rate of the excited state.

5. Velocity Averages

Suppose that the probability of finding the atomic velocity $\mathbf{v}$ in the volume element d^3v is $N(\mathbf{v})d^3v$. Then

for a Maxwell–Boltzmann distribution of velocities at a temperature T we have

$$N(\mathbf{v})\,d^3v=(M/2\pi RT)^{3/2}\exp(-Mv^2/2RT)\,d^3v, \tag{III.15}$$

and the polarizability of an atomic vapor should be replaced by the velocity-averaged polarizability

$$\boldsymbol{\alpha}=\int\boldsymbol{\alpha}(\mathbf{v})N(\mathbf{v})\,d^3v. \tag{III.16}$$

The velocity average can be conveniently expressed in terms of the plasma-dispersion function (Fri61)

$$Z(\zeta)=(1/\pi^{1/2})\int_{\infty}^{\infty}du[\exp(-u^2)](u-\zeta)^{-1}, \tag{III.17}$$

and the polarizability becomes

$$\langle\mu'\mid\boldsymbol{\alpha}\mid\mu\rangle=(1/\hbar k)(M/2RT)^{1/2}\sum_m\langle\mu'\mid\mathbf{D}\mid m\rangle\times\langle m\mid\mathbf{D}\mid\mu\rangle Z[x(m\mu)+iy], \tag{III.18}$$

where we have

$$x(m\mu)=(1/k)(M/2RT)^{1/2}(\omega-\omega_{m\mu}) \tag{III.19}$$

and

$$y=(1/k)(M/2RT)^{1/2}\Gamma/2. \tag{III.20}$$

6. *Pressure Broadening and Shifting of the Optical Absorption Lines*

One usually assumes that the effects of small collisional broadening and shifting of the optical absorption line can be accounted for by making the replacements

$$\omega_{m\mu}\rightarrow\omega_{m\mu}+\Delta\omega, \tag{III.21}$$

$$\Gamma/2\rightarrow\Gamma/2+\gamma_c, \tag{III.22}$$

in Eqs. (III.19) and (III.20). Here $\Delta\omega/2\pi$ is the collisionally induced shift of the absorption frequency, and γ_c is the collisionally induced dephasing rate for optical coherence. These approximations seem to work reasonably well, but no definitive studies of the influence of optical collision broadening and pressure shifts on optical pumping experiments have been made. More careful consideration of these phenomena will eventually be necessary. For instance, the pressure-broadened lines are known to deviate from a simple Lorentzian shape, so that a plasma-dispersion function is not the correct line shape function. A review of the pressure broadening and shifting of optical lines has been written by Chen and Takeo (Che57).

7. *Oscillator Strengths and Lifetimes*

The magnitudes of the dipole-matrix elements which enter into the effective Hamiltonian [Eq. (III.8)] or the polarizability [Eq. (III.12)] are conveniently expressed in terms of the oscillator strength of the optical transition. A number of different definitions of oscillator strengths are in use, and to avoid confusion, we shall briefly review the more widespread conventions.

Suppose that an atomic multiplet of angular momentum J_e can decay to an atomic multiplet of electronic angular momentum J_g by an electric dipole transition. The energies of the upper and lower states are E_e and E_g, respectively. Then the "absorption-oscillator strength" is

$$f_{ge}=f(J_e,J_g)=2m\omega^2[3e^2(2J_g+1)(E_e-E_g)]^{-1}\times\sum_{m,\mu}\langle J_em\mid\mathbf{D}\mid J_g\mu\rangle\cdot\langle J_g\mu\mid\mathbf{D}\mid J_em\rangle. \tag{III.23}$$

Here the notation f_{ge} is that used by Foster (Fos64), while the notation $f(J_e,J_g)$ is that used by Condon and Shortley (Con53). Extensive, critically evaluated Tables of absorption oscillator strengths have been prepared by Wiese, Smith, and Glennon (Wie66). We note that

$$(2J_g+1)f(J_e,J_g)=-(2J_e+1)f(J_g,J_e). \tag{III.24}$$

Condon and Shortley's "emission-oscillator strength" $f(J_gJ_e)$ is a negative number. The product of the absolute value of the emission-oscillator strength and the statistical weight of the upper state

$$gf=\mid f(J_g,J_e)\mid(2J_e+1) \tag{III.25}$$

is also widely used, and extensive tables of gf values can be found in the work of Corliss and Bozman (Cor62). However, while the relative values of emission-oscillator strengths for a single element are usually fairly accurate, the absolute values can be in error by as much as an order of magnitude.

The oscillator strength can also be written in terms of the momentum operator $\mathbf{p}$ of the atom, since we have

$$\langle J_em\mid\mathbf{p}\mid J_g\mu\rangle=(im/e\hbar)(E_e-E_g)\langle J_em\mid\mathbf{D}\mid J_g\mu\rangle. \tag{III.26}$$

For spontaneous electric dipole transitions from the state e to the state g, the decay rate is

$$\Gamma(J_e\rightarrow J_g)=2e^2\omega^2(mc^3)^{-1}(2J_g+1)f_{ge}/(2J_e+1). \tag{III.27}$$

Very reliable estimates of oscillator strengths can be inferred from atomic lifetime measurements with the aid of Eq. (III.27).

In this paper, we shall always make use of the absorption-oscillator strengths f_{ge} defined in Eq. (III.23), and the oscillator strength will always refer to an electronic transition. We shall not use oscillator strengths for transitions between ground-state and excited-state hyperfine multiplets (e.g., F_g and F_e), since, for allowed transitions, these are related by simple angular factors to the more fundamental electronic oscillator strength.

8. *The Spectral Profile of the Pumping Light*

Most optical pumping experiments are done with incoherent light from a conventional lamp. We can

think of such light as a superposition of many monochromatic waves of the form (III.1) with different frequencies and random relative phases. Let $\Phi(\nu)d\nu$ represent the energy flux carried by waves whose frequencies lie between ν and $\nu+d\nu$. Let us assume that the light has a well-defined polarization $\hat{e}$ (i.e., the electric field amplitude of a monochromatic wave such as that of Eq. (III.1) is $\mathcal{E}=|\mathcal{E}|\hat{e}$). Then we have

$$\Phi(\nu)d\nu=(c/2\pi)\mathcal{E}^2, \tag{III.28}$$

and the effective Hamiltonian [Eq. (III.11)] becomes

$$\delta\mathcal{H}=-(2\pi/c)\int\hat{e}^*\cdot\boldsymbol{\alpha}\cdot\hat{e}\,\Phi(\nu)d\nu. \tag{III.29}$$

If the light is only partially polarized, it is convenient to define a flux dyadic (Coh67),

$$\boldsymbol{\Phi}(\nu)=c(2\pi\Delta\nu)^{-1}\sum_i\boldsymbol{\mathcal{E}}_i\boldsymbol{\mathcal{E}}_i^*, \tag{III.30}$$

where the summation extends over all waves i whose frequencies lie within the interval ν to $\nu+\Delta\nu$. Then Eq. (III.29) becomes

$$\delta\mathcal{H}=-(2\pi/c)\int_0^\infty\boldsymbol{\alpha}:\boldsymbol{\Phi}d\nu. \tag{III.31}$$

The flux dyadic $\boldsymbol{\Phi}$ and the electric field $\boldsymbol{\mathcal{E}}$ are analogous, respectively, to a density matrix and a wave function description of the light.

If the pumping light beam is modulated, correlations between the different frequencies of the light beam must be considered.

9. *Light with a Flat Spectral Profile*

Let us assume that the light intensity is independent of frequency in the neighborhood of the absorption lines. Then the flux is

$$\Phi(\nu)=cu, \tag{III.32}$$

where u is the energy density per unit frequency interval of the light beam. The integral of Eq. (III.29) may be calculated without difficulty, and one finds the results

$$\delta\mathcal{E}=0 \tag{III.33}$$

and

$$\delta\Gamma=(2\pi/\hbar^2)u\sum_m\hat{e}^*\cdot\mathbf{D}\,|\,m\rangle\langle m\,|\,\mathbf{D}\cdot\hat{e}. \tag{III.34}$$

One can show that the mean pumping rate (III.14) for light of a flat spectral profile is

$$R(J_gJ_e)=\lambda r_0cf_{ge}u(2\hbar)^{-1}, \tag{III.35}$$

where λ is the mean wavelength of the transition $(J_g\rightarrow J_e)$, r_0 is the classical electron radius, and f_{ge} is the absorption-oscillator strength of the transition $J_g\rightarrow J_e$.

For an atom with hyperfine structure, the spectral profile may be flat only for transitions from one ground-state multiplet F_g to one excited-state multiplet F_e. Then the light-absorption operator of Eq. (III.34) may be thought of as operating only within the multiplet F_g, and the sum on m extends only over sublevels of the multiplet F_e. Under these circumstances, we designate the mean pumping rate by $R(F_gF_e)$, and we find

$$R(F_gF_e)=\lambda r_0cf_{ge}u(2\hbar)^{-1}\times W^2(J_eF_eJ_gF_g;I1)(2J_g+1)(2F_e+1), \tag{III.36}$$

where u is the energy density at the frequency of the transition $F_g\rightarrow F_e$.

10. *Multipole Representation of* $\boldsymbol{\alpha}$

We shall often find it convenient to write the polarizability $\boldsymbol{\alpha}$ in terms of its irreducible components. For instance, for an atom devoid of hyperfine structure both in the ground state and in the excited state, the polarizability is (Hap67c)

$$\boldsymbol{\alpha}=\sum_L(-1)^L\frac{3r_0\lambda^2f_{ge}}{8\pi^2}\left(\frac{Mc^2}{2RT}\right)^{1/2}\times Z(J_eJ_g)(2J_g+1)W(1LJ_eJ_g;1J_g)\mathfrak{Q}_L\cdot T_L(J_gJ_g). \tag{III.37}$$

The irreducible basis dyadics are defined in analogy to Eq. (II.22) as

$$\mathfrak{Q}_{LM}=\sum\hat{\imath}_\mu(\hat{\imath}_{\mu-M})^*(-1)^{\mu-M-1}C(11L;\mu,M-\mu). \tag{III.38}$$

In the future, we shall call the $L=0$ component of $\boldsymbol{\alpha}$ the isotropic part, the $L=1$ component of $\boldsymbol{\alpha}$ the gyrotropic part, and the $L=2$ component of $\boldsymbol{\alpha}$ the birefringent part. In view of Eq. (III.11), we see that both the light-shift operator $\delta\mathcal{E}$ and the light-absorption operator $\delta\Gamma$ will have a multipole expansion analogous to Eq. (III.37). For instance, the light-absorption operator corresponding to Eq. (III.37) is

$$\delta\Gamma=3R\sum_{L=0}^{2}(2J_g+1)W(1LJ_eJ_g;1J_g)E_L\cdot T_L(J_gJ_g). \tag{III.39}$$

Here R is the mean pumping rate defined in Eq. (III.14), and the polarization tensor E_{LM} is defined by

$$E_{LM}=\hat{e}\cdot\mathfrak{Q}_{LM}\cdot\hat{e}^*, \tag{III.40}$$

for light with a polarization vector $\hat{e}$.

For an atom with well-defined hyperfine multiplets, the light-absorption operator which corresponds to the transition $F_g\rightarrow F_e$ is

$$\delta\Gamma=3R(F_gF_e)\sum(2F_g+1)W(1LF_eF_g;1F_g)\times E_L\cdot T_L(F_gF_g). \tag{III.41}$$

It is also useful to write the polarizability [Eq. (III.37)] in the form

$$\boldsymbol{\alpha}=\alpha_0+i\alpha_{gt}\mathbf{J}\times x+\alpha_{br}\mathfrak{Q}, \tag{III.42}$$

where α_0, α_{gt}, and α_{br} are scalar functions of frequency,

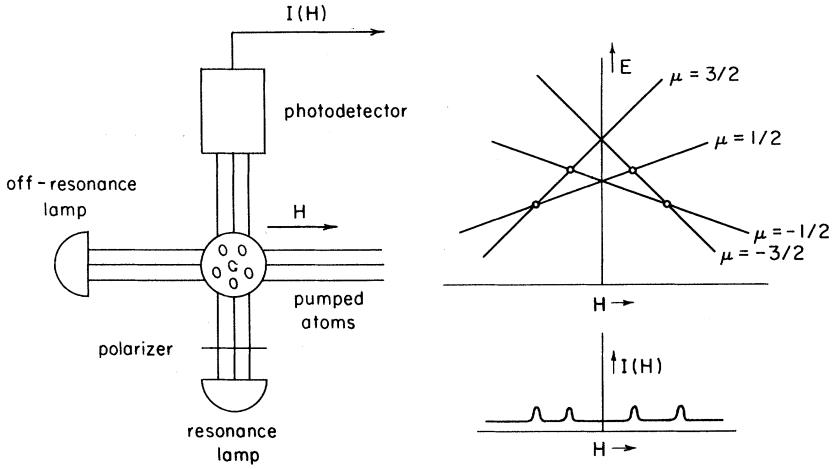

FIG. 4. Production of static coherence by optical pumping. Coherence can be produced by unmodulated light only when two levels intersect. In this experiment, a magmetic field and a tensor light shift caused by a coaxial beam of off-resonant light are used to produce level crossings. The coherence is produced and detected by the resonant light beam [from (Dup68b)].

J is the angular momentum operator of the atom (J is supposed to form a vector cross product with any vector to the right of it), and the quadrupole operator $\mathfrak{Q}$ is

$$\mathfrak{Q}(J_g J_g) = \mathfrak{Q}_2 \cdot T_2(J_g J_g). \quad \text{(III.43)}$$

11. The Polarization Produced by Weak Pumping Light

Some insight into the mechanism of optical pumping can be gained by considering the polarization produced by weak pumping light. This procedure was suggested by Ensberg (Ens67a). For simplicity, let us assume that the ground-state polarization decays with a single relaxation rate γ. More realistic relaxation processes will be considered later. Then the evolution of the ground-state density matrix is given by

$$(d/dt)\rho = (-1/2)(\delta\Gamma\rho + \rho\delta\Gamma) - \gamma P + (d^{(2)}/dt)\rho + (1/i\hbar)[\mathfrak{H}', \rho]. \quad \text{(III.44)}$$

The Hamiltonian

$$\mathfrak{H}' = \mathfrak{H}_g + \delta\mathcal{E} \quad \text{(III.45)}$$

is the sum of the static, unperturbed Hamiltonian and the light-shift operator $\delta\mathcal{E}$. Suppose that the pumping light is weak, causing the mean pumping rate R to be much smaller than the decay rate γ of the polarization. Under these conditions, it is reasonable to seek a steady-state solution for the density matrix as a power series in the parameter

$$\lambda = R/\gamma \ll 1. \quad \text{(III.46)}$$

That is, we assume

$$\rho_g = \rho^{(0)} + \rho^{(1)} + \rho^{(2)} + \cdots, \quad \text{(III.47)}$$

where the nth order contribution to ρ_g is

$$\rho^{(n)} = \lambda^n P^{(n)}, \quad \text{(III.48)}$$

and $P^{(n)}$ is an operator which is independent of λ. Substituting Eqs. (III.47) and (III.48) into Eq. (III.44), one finds that the zeroth order contribution to ρ_g is

$$\rho^{(0)} = 1/G. \quad \text{(III.49)}$$

The first-order contribution is composed of two terms

$$\rho^{(1)} = P_d^{(1)} + P_r^{(1)}, \quad \text{(III.50)}$$

which we can identify as the polarization produced by depopulation and repopulation pumping, respectively. The polarization due to depopulation pumping is

$$\langle \mu \mid P_d^{(1)} \mid \mu' \rangle = -\langle \mu \mid \delta\Gamma \mid \mu' \rangle / G(\gamma + i\omega_{\mu\mu'}). \quad \text{(III.51)}$$

From Eq. (III.51), we see that population imbalances can be produced by depopulation pumping only if the diagonal matrix elements of the light-absorption operator differ from each other, i.e., only if the pumping rates out of the different sublevels are not all the same. The first-order polarization produced by repopulation pumping is

$$\langle \mu \mid P_r^{(1)} \mid \mu' \rangle = [1/(\gamma + i\omega_{\mu\mu'})] \langle \mu \mid (d^{(2)}/dt)(1/G) \mid \mu' \rangle. \quad \text{(III.52)}$$

We shall discuss the polarization due to repopulation pumping in more detail in Sec. III.C.

12. Ground-State Hanle Effect and Level-Crossing Effect

Note that the coherences ($\mu \neq \mu'$) in Eqs. (III.51) and (III.52) depend explicitly on the energy difference $\hbar\omega_{\mu\mu'}$ between the sublevels μ and μ'. Sizeable coherence can be produced only if

$$\omega_{\mu\mu'} \lesssim \gamma, \quad \text{(III.53)}$$

i.e., only if the energy splitting is comparable to or less than the collisional relaxation rate γ. Thus, static coherence can be produced in optical pumping experiments only when the energies of the corresponding sublevels are nearly equal; this condition can easily occur at zero magnetic field. The first experimental studies of

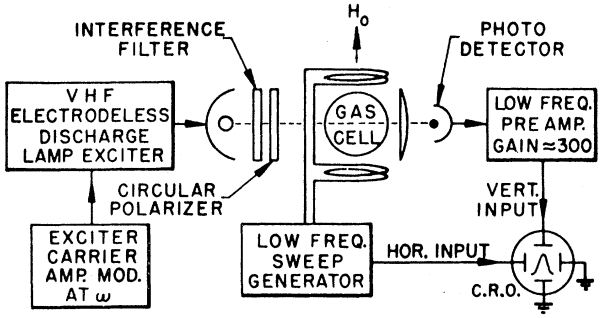

FIG. 5. Production of oscillatory coherence by optical pumping (optically driven spin precession). When the pumping light is modulated at a ground-state transition frequency, coherence may be generated between the corresponding sublevels. The coherence causes a change in the mean intensity of the transmitted pumping light [from (Bel61b)].

the production of static coherence were made at zero field with optically pumped ^{111}Cd by Lehmann and Cohen–Tannoudji (Leh64b,67). The phenomenon is closely related to the excited-state phenomena of level crossing and the Hanle effect. A particularly interesting example of the resonant increase of coherence when ground-state sublevels intersect has been investigated by Dupont-Roc and Cohen–Tannoudji (Dup68b), whose results are illustrated in Fig. 4. The ground-state Hanle effect has been observed in rubidium and cesium by Schmieder *et al.* (Sch70c).

For an atom with a single Zeeman multiplet in the ground state, the polarization is most conveniently described in the multipole representation. Let a magnetic field define the z axis of the coordinate system, and let ω be the Larmor frequency of the atoms in the field. Then the polarization due to depopulation pumping is

$$P_d^{(1)}(LM) = -\delta\Gamma_{LM}[G(\gamma - iM\omega)]^{-1}, \quad \text{(III.54)}$$

and the polarization due to repopulation pumping is

$$P_r^{(1)}(LM) = [1/(\gamma - iM\omega)][(d^{(2)}/dt)(1/G)]_{LM}. \quad \text{(III.55)}$$

We note that if the ground-state relaxation is not uniform, but if the multipole moments T_{LM} have a characteristic relaxation time γ_{LM}, one can simply replace γ by γ_{LM} in Eqs. (III.54) and (III.55).

13. *Pumping by Modulated Light*

Suppose the pumping light is intensity modulated so that one component of the light-absorption operator has the form

$$\delta\Gamma = \delta\Gamma(\omega)\exp(-i\omega t), \quad \text{(III.56)}$$

where $\delta\Gamma(\omega)$ is a time-independent operator. For weak pumping light, one can easily generalize the procedure of the preceding sections to show

$$\langle\mu \mid P_d^{(1)} \mid \mu'\rangle = -\exp(-i\omega t)\langle\mu \mid \delta\Gamma(\omega) \mid \mu'\rangle \times[\gamma + i(\omega_{\mu\mu'} - \omega)] \quad \text{(III.57)}$$

and

$$\langle\mu \mid P_r^{(1)} \mid \mu'\rangle = \exp(-i\omega t) \times\langle\mu \mid (d^{(2)}/dt)(1/G)_\omega \mid \mu'\rangle/[\gamma + i(\omega_{\mu\mu'} - \omega)], \quad \text{(III.58)}$$

where the repopulation rate is assumed to be of the form

$$(d^{(2)}/dt)(1/G) = \exp(-i\omega t)(d^{(2)}/dt)(1/G)_\omega. \quad \text{(III.59)}$$

Hence, if the excitation rate is modulated at a frequency ω, it is possible to produce sizeable, oscillating coherence between the levels μ and μ' when the condition

$$|\omega - \omega_{\mu\mu'}| \lesssim \gamma \quad \text{(III.60)}$$

holds. Pumping with modulated light in order to produce coherence was first suggested by Dehmelt (Bel61b), and the first experiments of this type were performed by Bell and Bloom (Bel61b), who called the effect optically driven spin precession (see Fig. 5). Such experiments can be thought of as ground-state Hanle-effect or level-crossing experiments in a rotating coordinate system.

Analogous experiments have been described by Pokazan'ev (Pok68a), where the stationary states of the atom are defined by a precessing magnetic field. Resonances are observed when the modulation frequency of the light in the precessing coordinate system appears to be equal to the precession frequency of the atom about the effective static field.

14. *Absence of Depopulation Pumping by Light of a Very Broad Spectral Profile*

Depopulation pumping is often found to be effective only for light of a limited spectral width. For instance, the diamagnetic $^1S_0$ ground states of Hg, Cd, and Zn and the $^3P_0$ ground state of lead cannot undergo depopulation pumping if all hyperfine components of the pumping light have equal intensities. The light-absorption operator is found to be isotropic, regardless of the polarization of the pumping light. A similar situation arises for the alkali atoms if the two D lines have equal intensities. Also, no depopulation pumping of the metastable $^3S_1$ state of helium can occur if the D_1, D_2, and D_3 lines all have equal intensities. In all of these cases the ground-state polarization is not affected by the absorption of light, but is transferred unchanged into the excited state. The polarization imparted to the atom by the photon is carried by a second, independent angular momentum, which is nonzero only in the excited state; e.g., if the ground state is $^3S_1$, the ground-state polarization is carried by the electronic spin **S**, and the photon polarization is imparted to the orbital angular momentum **L** of the ^3P_J excited states. The absorption probability is completely independent of the initial ground-state polarization, and, since this implies that $\delta\Gamma$ is isotropic, no depopulation pumping can occur. One can prove formally that $\delta\Gamma$ is isotropic under the conditions stated above by summing the expressions of

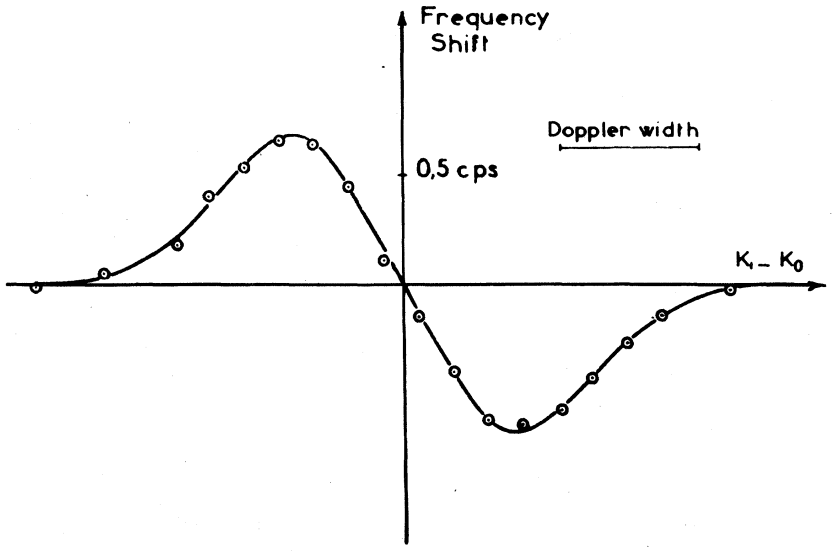

FIG. 6. Frequency dependence of the light shift due to virtual transitions. The shift is proportional to the index of refraction of the vapor [from (Coh62a, b)].

Eqs. (III.39) or (III.41) over the appropriate excited states.

15. Depopulation Pumping at Very High Magnetic Fields

Light-absorption operators of the form of Eq. (III.39) are obtained only if the Zeeman splitting of the atomic absorption lines is assumed to be much less than the Doppler widths of the lines. When the Zeeman splitting is comparable to or greater than the Doppler width, a number of interesting qualitative changes should occur in the character of depopulation pumping (Hap69). For example, anisotropic population imbalances could be produced by depopulation pumping using isotropic light if the frequency of the light were such that it could cause preferential absorption from one Zeeman sublevel of the ground state.

There are a number of technical problems associated with optical pumping at high magnetic fields. Frequently, it is difficult to obtain a pumping lamp whose emission profile overlaps the Zeeman-shifted absorption profile of the pumped atoms. Franz (Fra71) has shown that one can use white light from an incandescent lamp to pump cesium atoms in fields of 100 kG, and Gibbs and Slusher (Gib70c) have used a mercury laser to pump rubidium atoms at 74.5 kG.

16. Light Shifts due to Virtual Absorption of Light

An interesting aspect of depopulation pumping is the phenomenon of "light shifts due to virtual transitions." Barrat and Cohen-Tannoudji (Bar61c), (Coh62a,b) have pointed out that the Hermitian part of the effective Hamiltonian [Eq. (III.9)] will cause a frequency shift

$$\Delta\omega_{\mu\nu}=(1/\hbar)\,(\delta\mathcal{E}_{\mu\mu}-\delta\mathcal{E}_{\nu\nu}) \qquad \text{(III.61)}$$

of the resonance frequency $\omega_{\mu\nu}$. These light shifts may be thought of as the mean Stark shifts produced by the oscillating electric field of the light wave. Light shifts due to virtual transitions were first observed by Arditi and Carver (Ard61) in the 0–0 transition frequency of optically pumped alkali vapors. Light shifts of the Zeeman-transition frequencies of rubidium have been observed by White *et al.* (Whi68). Light shifts in helium have been observed by Schearer (Sch62,68e), and shifts in mercury were first observed by Cohen-Tannoudji (Coh61a). Shifts due to virtual absorption of light are by no means small, and shifts of 20 times the resonance linewidth have been reported by Dupont-Roc (Dup67b). Related shifts have been induced using intense laser light by Aleksandrov *et al.* (Ale66) and Bonch-Bruevich *et al.* (Bon66).

Since the light-shift operator $\delta\mathcal{E}$ is closely related to the real part of the polarizability operator of the atoms [see Eq. (III.11)], the frequency dependence of the light shift will be similar to the frequency dependence of the index of refraction of the vapor. The results of a frequency-scanning experiment for the light shift are shown in Fig. 6. This is data obtained by Cohen-Tannoudji (Coh61a,62a,b) in experiments on ^{199}Hg.

The tensor properties of the light-shift operator have been investigated by Mathur and Happer (Hap67c). They showed that for a simple Zeeman multiplet the light-shift operator can always be written in the form

$$\delta\mathcal{E}=\delta\mathcal{E}_0-\delta\mathbf{H}\cdot\boldsymbol{\mu}-(1/6)\,\delta\boldsymbol{\nabla}\mathbf{E}:\mathfrak{Q}, \qquad \text{(III.62)}$$

where $\delta\mathcal{E}_0$ is a common upward or downward shift of all

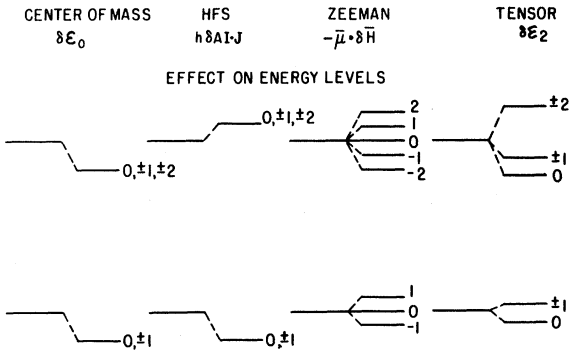

FIG. 7. Multipole components of the light shift. The light shift due to virtual transitions can be represented by fictitious magnetic and electric fields and by modifications of the hyperfine coupling constants [from (Mat68b)].

the Zeeman sublevels, $\delta\mathbf{H}$ is an effective magnetic field which is proportional to the photon spin, and $\delta\nabla\mathcal{E}$ is an effective electric field gradient which interacts with the electric quadrupole moment Ω of the multiplet. We may call these three components the scalar, vector, and tensor parts of the light-shift operator. The characteristic splittings caused by each component are illustrated in Fig. 7.

The effective fields which enter into Eq. (III.62) are completely equivalent to real electromagnetic fields insofar as the evolution of the atomic ground state is concerned. For instance, Happer and Mathur (Hap67b) have shown that an oscillating effective magnetic field can cause transitions between the sublevels of a Zeeman multiplet, and Cohen-Tannoudji and Dupont-Roc (Dup67a) have shown that an atom will precess freely around the effective field if all real fields are canceled. Dupont-Roc and Cohen-Tannoudji (Dup68c) have shown that an oscillating effective electric field gradient will cause $\Delta m=2$ transitions, and they have performed ground-state level-crossing experiments (Dup68b) with a coaxial effective electric field gradient and a real magnetic field (see Fig. 4). Cohen-Tannoudji and Dupont-Roc have also demonstrated that the tensor light shift couples multipole moments of different angular momentum (Coh69).

A detailed theory of the light shifts in alkali atoms has been developed by Mathur, Tang, and Happer (Mat68b) and applied to the case of ^{87}Rb. Experimental confirmation of some aspects of the theory was obtained. Analogous work for ^{85}Rb was carried out by Stern (Ste71). Reviews of light shifts due to virtual transitions have been published by Kastler (Kas63) and Happer (Hap71).

B. The Excited State

One excited atom is produced for every photon absorbed from the pumping light. It is necessary to consider the behavior of these excited atoms in order to understand two important aspects of optical pumping: the production of fluorescent light and the repopulation of the ground state. The evolution of the excited atoms is of considerable interest in its own right, since it can furnish precise information about the lifetime of the excited state, about the hyperfine interactions in the excited state, about the interactions of the excited atom with external electric and magnetic fields, and about collisional relaxation of the excited atoms. We shall only discuss those aspects of the excited-state evolution which are essential for an understanding of ground-state pumping.

1. Generation of the Excited State

We can use the transition rates $R_{\mu m}$ of Eq. (III.3) to write the rate of generation of atoms in the excited-state sublevel m as

$$(d^{(2)}/dt)\rho_{mm}=\sum_{\mu}R_{\mu m}\rho_{\mu\mu}. \qquad \text{(III.63)}$$

Equation (III.63) is valid only when there is no coherence. Happer (Hap67c) has shown that the generalization of Eq. (III.63) to include coherence yields an equation of the form

$$(d^{(2)}/dt)\rho_{mm'}=(1/\hbar^2)\sum_{\mu\mu'}\langle m\mid\boldsymbol{\mathcal{E}}\cdot\mathbf{D}\mid\mu\rangle\rho_{\mu\mu'}$$
$$\times\langle\mu'\mid\boldsymbol{\mathcal{E}}^*\cdot\mathbf{D}\mid m'\rangle/[(\Gamma/2)+i(\omega_{m\mu}+\mathbf{k}\cdot\mathbf{v}-\omega)]+\text{c.c.} \qquad \text{(III.64)}$$

Barrat and Cohen-Tannoudji (Bar61d,e) have shown that in the limit of a broad spectral profile, Eq. (III.64) becomes

$$(d^{(2)}/dt)\rho_e=(2\pi/\hbar^2)u\hat{e}\cdot\mathbf{D}\rho_g\hat{e}^*\cdot\mathbf{D}, \qquad \text{(III.65)}$$

where u is the energy density, and $\hat{e}$ is the polarization of the pumping light.

The polarization which is generated in the excited state originates both from the polarization of the light and from the polarization of the ground state. As an example, let us write Eq. (III.65) in the uncoupled multipole representation:

$$(d^{(2)}/dt)\rho_e=3R(2J_g+1)$$
$$\times\sum_{\Lambda\lambda,LL',M\mu}[(2\Lambda+1)(2L'+1)]^{1/2}X(1J_eJ_g;\,1J_eJ_g;\,L'\Lambda L)$$
$$\times[E_{L'}T_\Lambda(J_eJ_e)]_{LM}T_{\lambda\mu}(II)\rho_g(L,-M;\,\lambda,-\mu)(-1)^{M+\mu}. \qquad \text{(III.66)}$$

The mean pumping rate R was defined in Eq. (III.35). Equation (III.66) shows that the excited-state polarization can be expressed as a rather complicated coupling of the polarization tensor E_{LM}, the light, and the polarization $\rho_g(LM;\lambda\mu)$ [see Eq. (II.27)] of the ground state.

For future reference we consider several important special cases of Eq. (III.66). Suppose that the ground state is unpolarized. Then we have

$$\rho_g(LM;\lambda\mu)=\delta_{L0}\delta_{M0}\delta_{\lambda0}\delta_{\mu0},$$
$$\times[(2J_g+1)(2I+1)]^{-1}, \qquad \text{(III.67)}$$

and Eq. (III.66) becomes

$$(d^{(2)}/dt)\rho_e=[3R/(2I+1)]$$
$$\times\sum_{L=0}^{2}W(J_gJ_e1L;1J_e)(-1)^L E_L\cdot T_L(J_eJ_e). \quad \text{(III.68)}$$

Thus, only electronic orientation ($L=1$) and alignment ($L=2$) are produced by broad-line excitation. No nuclear polarization is generated in the excitation process. However, because of the hyperfine coupling of the nucleus to the electrons, some of the electronic polarization can be converted into nuclear polarization if the excited atom lives for a sufficiently long time. Also, we should emphasize that only for broad-line excitation is no nuclear polarization generated at the instant of excitation. For narrow-line excitation it is quite possible to produce nuclear polarization "instantaneously" in the excited state by the absorption of polarized light.

As another interesting special case, let us consider excitation by unpolarized light. Then we have the conditions

$$E_{LM}=\delta_{L0}\delta_{M0}(\sqrt{3})^{-1} \quad \text{(III.69)}$$

and

$$(d^{(2)}/dt)\rho_e(LM;\lambda\mu)$$
$$=R(2J_g+1)W(1J_gJ_eL;J_eJ_g)\rho_g(LM;\lambda\mu). \quad \text{(III.70)}$$

Thus, each multipole moment of the excited state is generated from the corresponding multipole moment of the ground state. We shall see that Eq. (III.70) is completely analogous to the rate of transfer of polarization from an excited atom to a ground-state atom by the mechanism of spontaneous decay [see Eq. (III.83)].

2. *Evolution of the Excited State*

The initial polarization of the optically excited atoms may be greatly modified before the atoms decay. There are three main causes for this change in polarization: the hyperfine interaction between the electrons and the nucleus, the coupling of the excited atom to external magnetic or electric fields, and the relaxation mechanisms. Thus, the rate of change of the excited state can be described by the differential equation

$$(d/dt)\rho_e=(d^{(2)}/dt)\rho_e+(1/i\hbar)[\mathcal{H}_e,\rho_e]+(d^{(3)}/dt)\rho_e-\Gamma\rho_e. \quad \text{(III.71)}$$

Here the excited-state Hamiltonian $\mathcal{H}_e$ describes the hyperfine interactions and interactions with external fields. The optical excitation rate $(d^{(2)}/dt)\rho_e$ was discussed in the previous section. The spontaneous decay rate of the excited atom is Γ. The relaxation of the excited state is represented by the term $(d^{(3)}/dt)\rho_e$.

3. *Steady Excitation*

Let us consider the solutions to Eq. (III.71) for a few important special cases. We shall be concerned with steady-state conditions, i.e., with the long-term behavior of the atoms after the transients, which occur when the excitation begins, have died away. For the time being, we shall neglect relaxation of the excited state. Suppose that the excitation rate is time independent. Then the steady-state density matrix ρ_e will also be time independent, and the solution to Eq. (III.71) is

$$\langle m\mid\rho_e\mid n\rangle=[1/(\Gamma+i\omega_{mn})]\langle m\mid(d^{(2)}/dt)\rho_e\mid n\rangle. \quad \text{(III.72)}$$

We see that for time independent excitation, sizeable coherence is generated between the sublevels m and n only when the frequency ω_{mn} is comparable to or less than the natural decay rate Γ of the excited state. Experiments based on this phenomenon, such as Hanle-effect experiments (Lur64), or level-crossing experiments (Fra61), have been used to make precise determinations of the lifetimes hyperfine structures, polarizabilities, and g values of the excited states of atoms. We shall not discuss these experiments further here, but the reader can find reviews of this type of experiment in articles by Budick (Bud67) and Happer (Hap68).

Since the polarization of the excited state can be measured directly by observing the fluorescently scattered light (see Sec. IV-B), the excitation process represented by Eq. (III.72) has been studied in great detail. For unpolarized ground-state atoms, optical double-resonance (Bro52) and level-crossing (Sch70c) experiments have shown that Eq. (III.72) describes experimental observations to the limits of experimental accuracy, even for very complicated excited-state hyperfine structure.

Baylis (Bay68) and Krainska-Miszczak (Kra67,69) have studied the influence of ground-state polarization on the polarization of the excited state. They find good qualitative agreement between experiment and theory, but quantitative comparisons are difficult to obtain because the ground-state polarization cannot usually be measured precisely.

4. *Modulated Excitation*

Let us consider the case where the excitation rate is modulated. This can occur if the atom is excited by modulated light or if the ground-state density matrix has modulated components. For simplicity, let us assume that the excitation rate is

$$(d^{(2)}/dt)\rho_e=S\exp(-i\omega t), \quad \text{(III.73)}$$

where S is a constant source operator. Then the solution to Eq. (III.71) leads to oscillating components of ρ_e of the form

$$\langle m\mid\rho_e(t)\mid n\rangle=\{\exp(-i\omega t)[\Gamma+i(\omega_{mn}-\omega)]^{-1}\}$$
$$\times\langle m\mid S\mid n\rangle. \quad \text{(III.74)}$$

We see that sizeable excited-state coherence can be

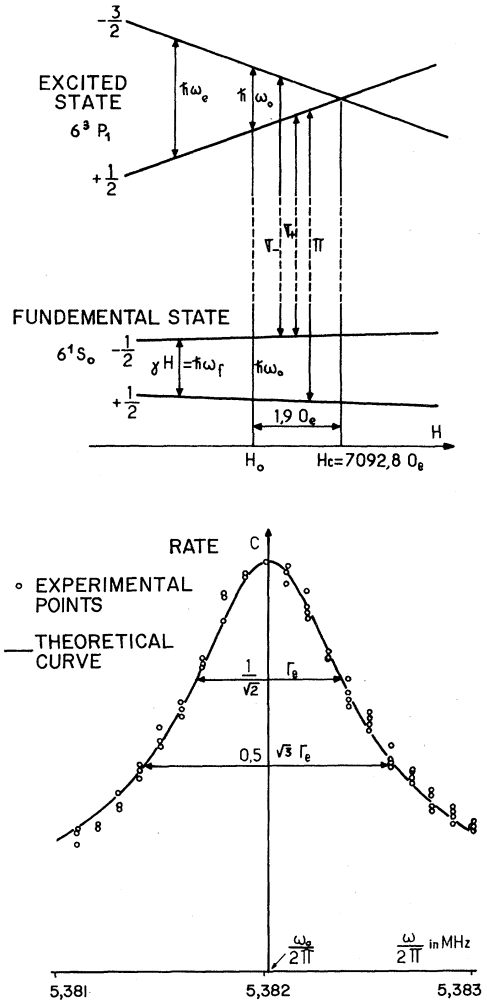

FIG. 8. Resonant transfer of coherence to the excited state of ^{199}Hg. (a) The energy splitting between a pair of ground-state sublevels becomes equal to the energy splitting between a pair of excited-state sublevels at a magnetic field of 7091 Gauss. (b) The modulation index of the fluorescent light is plotted as a function of the ground-state magnetic resonance frequency. The light is most strongly modulated when the ground-state and excited-state energy splittings are equal [from (Qua66)].

produced by an oscillatory excitation rate when the driving frequency ω of the excitation process does not differ from the coherence frequency ω_{mn} by more than the natural width of the excited state, i.e., when we have the condition

$$|\omega-\omega_{mn}| \lesssim \Gamma. \tag{III.75}$$

Kastler (Kas61) has pointed out that one way to produce a modulated excitation rate such as that of Eq. (III.73) is to illuminate atoms with modulated light. Experimental studies of the excitation of atoms with modulated light were initiated by Aleksandrov (Ale63a), and a review of recent work is contained in the article by Novikov *et al.* (Nov70). Such experiments can provide information complimentary to that obtained from level-crossing experiments.

A very important type of modulated excitation occurs when oscillatory coherence exists in the ground state. Suppose that the component $\langle\mu|\rho_g|\nu\rangle$ of the ground-state density matrix oscillates at a frequency ω, which we shall assume to be close to the resonant frequency $\omega_{\mu\nu}$; i.e.,

$$\langle\mu|\rho_g|\nu\rangle = \exp(-i\omega t)\langle\mu|\sigma_g|\nu\rangle, \tag{III.76}$$

where $\langle\mu|\sigma_g|\nu\rangle$ is a constant and

$$\omega\simeq\omega_{\mu\nu}. \tag{III.77}$$

Then from Eqs. (III.74) and (III.65), one finds that unmodulated pumping light will generate oscillating components of ρ_e of the form

$$\langle m|\rho_e|n\rangle=(2\pi/\hbar^2)u\exp(-i\omega t)\times\langle m|\hat{e}\cdot\mathbf{D}|\mu\rangle\langle\mu|\sigma_g|\nu\rangle\langle\nu|\hat{e}^*\cdot\mathbf{D}|n\rangle\times[\Gamma+i(\omega_{mn}-\omega_{\mu\nu})]^{-1}. \tag{III.78}$$

Thus, Eq. (III.78) implies that the excited-state coherence $\langle m|\rho_e|n\rangle$ can be coupled to the ground-state coherence $\langle\mu|\rho_g|\nu\rangle$ by an unmodulated light beam only if the coherence frequencies do not differ by much more than the natural width of the excited state, i.e., only if

$$|\omega_{mn}-\omega_{\mu\nu}| \lesssim \Gamma. \tag{III.79}$$

This resonant increase of the coupling of ground-state to excited-state coherence has been investigated experimentally by Quarré and Omont (Qua66) in ^{199}Hg. They observed a strong resonant increase in the modulated component of the fluorescent light when the condition of Eq. (III.79) was satisfied (see Fig. 8). Similar studies in sodium have been carried out by Rosinski (Ros67). In all cases, the agreement between experiment and theory was excellent.

In Sec. III.C.7, we shall show that the resonance condition (III.79) has an important bearing on light shifts due to real transitions.

Rosinski (Ros65,66), Skalinski and Rosinski (Ska65), and Franzen *et al.* (Fra68) have studied the transfer of ground-state coherence into the excited state for both $\Delta m=1$ transitions and $\Delta m=2$ double quantum transitions in sodium. Rosinski points out that for N quantum transitions, coherence is generated at the Nth harmonic of the driving frequency ω, so that the fluorescent light may be modulated at harmonics of the driving frequency.

Series (Ser66) has studied the transfer of coherence at very low fields between the ground state and excited state, and he concludes that for sufficiently strong coupling of the ground state and excited state by the pumping light, modulation of the fluorescent light at 4ω and higher multiples of the driving frequency can be observed.

5. *Optical Double Resonance*

For completeness, let us mention one more very common type of experiment which is described by the excitation Eq. (III.71). These are experiments in which a strong oscillating field is used to induce transitions between the sublevels of the excited state before the atom decays. Such optical double-resonance experiments were first performed by Brossel and Bitter (Bro52) and since then, similar experiments have yielded an enormous amount of information about the excited states of atoms. Since the techniques and results of optical double-resonance experiments have been reviewed in articles by Series (Ser59) and zu Putlitz (zu P65), we shall not discuss optical double resonance in detail here. The oscillating magnetic fields used in most ground-state optical pumping experiments are far too small to have any influence on the evolution of the excited-state polarization.

C. Repopulation Pumping

In addition to depopulation pumping, a second pumping mechanism, which we shall call repopulation pumping, occurs in many optical pumping experiments. Repopulation pumping can occur when the atomic ground state is repopulated as a result of spontaneous decay of a polarized excited state. Some simple examples of repopulation pumping are illustrated in Fig. 9. In Fig. 9(a) a completely polarized $^2P_{1/2}$ excited-state atom decays spontaneously to a $^2S_{1/2}$ ground state. Since the atoms which are initially in the $+\frac{1}{2}$ sublevel of the excited state are twice as apt to fall to the $-\frac{1}{2}$ ground-state sublevel as to the $+\frac{1}{2}$ ground-state sublevel, the ground state will be partially polarized in the opposite sense from the excited state after all excited atoms have decayed. Figure 9(b) illustrates how hyperfine polarization of an excited $^2P_{1/2}$ state can be transferred to a $^2S_{1/2}$ state.

1. *Theory of Repopulation Pumping*

According to simple perturbation theory, the rate of spontaneous decay from the excited-state sublevel m to the ground-state sublevel μ is

$$A_{m\mu}=(4e^2\omega/3m^2c^3\hbar)\,|\langle m\,|\,\mathbf{p}\,|\,\mu\rangle|^2, \qquad \text{(III.80)}$$

where $\mathbf{p}$ is the momentum operator of the atom. The rate of population of the ground-state sublevel μ is therefore

$$(d^{(2)}/dt)\,\rho_{\mu\mu}=\sum_m A_{m\mu}\rho_{mm}$$
$$=(4e^2\omega/3m^2c^3\hbar)\,\boldsymbol{\Sigma}\,\langle\mu\,|\,\mathbf{p}\,|\,m\rangle\cdot\rho_{mm}\langle m\,|\,\mathbf{p}\,|\,\mu\rangle. \qquad \text{(III.81)}$$

Equation (III.81) is valid only when there is no atomic coherence. Barrat and Cohen-Tannoudji (Bar61d,e) have shown that Eq. (III.81) can be generalized to

$$(d^{(2)}/dt)\,\rho_g=(4e^2\omega/3m^2c^3\hbar)\,\mathbf{p}\cdot\rho_e\mathbf{p}. \qquad \text{(III.82)}$$

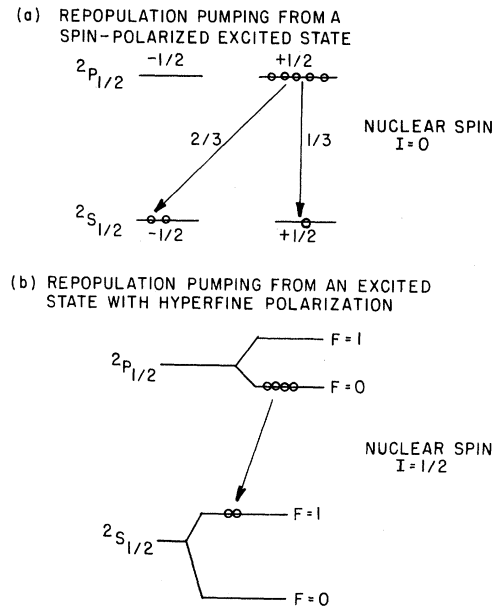

FIG. 9. Some simple examples of repopulation pumping. Excited-state polarization can be partially transferred to the ground-state by spontaneous emission.

Equation (III.82) describes the repopulation pumping of the ground state. We note that Eq. (III.82) can be written in the uncoupled multipole representation as

$$(d^{(2)}/dt)\,\rho_g(LM;\Lambda\mu)=\Gamma(2J_e+1)$$
$$\times W(1J_eJ_gL;J_gJ_e)\,\rho_e(LM;\Lambda\mu). \qquad \text{(III.83)}$$

That is, the various multipole components of the ground state are generated at a rate which is proportional to the corresponding multipole component of the excited state. Equation (III.83) should be compared to Eq. (III.70). We see that spontaneous decay and pumping with isotropic light are completely analogous. The spontaneous decay rate Γ can be regarded as the isotropic pumping rate which is caused by zero-point fluctuations of the electromagnetic field. Systematic studies of the transfer of coherence by spontaneous decay have been made by Duclay and Dumont (Duc68), and by Dumont and Decomps (Dum68). They observed the fluorescent light emitted by neon atoms in cascade transitions and found excellent agreement with the predictions of Eqs. (III.82) and (III.83).

Note that for isotropic pumping light, equilibrium between the ground-state and excited-state populations, N_g and N_e, respectively, occurs when

$$N_gR=N_e(\Gamma+G_gR/G_e). \qquad \text{(III.84)}$$

Here G_g and G_e are the statistical weights of the ground state and the excited state, respectively. One can introduce an effective temperature T of the light by requiring that the condition

$$N_e/N_g=(G_e/G_g)\,\exp\left[-(E_e-E_g)/kT\right] \qquad \text{(III.85)}$$

be satisfied. The effective temperature is therefore

$$T=[(E_g-E_e)/k]\ln G_gR/(G_e\Gamma+G_gR). \quad \text{(III.86)}$$

The effective temperature T is typically several thousands of degrees Kelvin; i.e., the effective temperature is on the order of the excitation temperature of the light source.

2. Transfer of Polarization through the Excited State

An important aspect of the optical pumping process is that the polarization of a ground-state atom may be partially retained after the atom has absorbed and re-emitted a photon. Combining Eqs. (III.82), (III.72), and (III.65), we find that this polarization transfer can be described by the equation

$$(d^{(2)}/dt)\langle\mu\mid\rho_g\mid\nu\rangle=\sum_{\mu'\nu'}B(\mu\nu;\mu'\nu')\langle\mu'\mid\rho_g\mid\nu'\rangle, \quad \text{(III.87)}$$

where the coupling coefficient is

$$B(\mu\nu;\mu'\nu')=(8\pi/3)[e^4u/m^4c^3\hbar^3\omega]\times\sum\langle\mu\mid\mathbf{p}\mid m\rangle\cdot\langle n\mid\mathbf{p}\mid\nu\rangle\times\langle m\mid\hat{e}\cdot\mathbf{p}\mid\mu'\rangle\langle\nu'\mid\hat{e}^*\cdot\mathbf{p}\mid n\rangle/[\Gamma+i(\omega_{mn}-\omega_{\mu'\nu'})]^{-1}. \quad \text{(III.88)}$$

Equations (III.87) and (III.88) were first derived by Barrat and Cohen-Tannoudji (Bar61d,e).

For computational convenience, it is useful to introduce the dimensionless matrix elements

$$(\mu\mid\mathbf{p}\mid m)=\langle\mu\mid\mathbf{p}\mid m\rangle/\langle J_g\|p\|J_e\rangle. \quad \text{(III.89)}$$

Then Eq. (III.88) can be written as

$$B(\mu\nu;\mu'\nu')=3R\Gamma\sum_{mn}[(\mu\mid\mathbf{p}\mid m)\cdot(n\mid\mathbf{p}\mid\nu)\times(m\mid\hat{e}\cdot\mathbf{p}\mid\mu')(\nu'\mid\hat{e}^*\cdot\mathbf{p}\mid n)]\times[(\Gamma+i(\omega_{mn}-\omega_{\mu'\nu'})^{-1}]. \quad \text{(III.90)}$$

The self-coupling coefficient is

$$B(\mu\nu;\mu\nu)=3R\Gamma(2J_g+1)[(2J_e+1)]^{-1}\times\sum_{m,n,\sigma}[|e_{-\sigma}|^2(m\mid p_\sigma\mid\mu)^2(n\mid p_\sigma\mid\nu)^2]\times\{[\Gamma+i(\omega_{mn}-\omega_{\mu\nu})]^{-1}\}. \quad \text{(III.91)}$$

3. Repopulation Pumping by Weak Light

From Eq. (III.52) we find that the first-order polarization produced by weak repopulation pumping is

$$\langle\mu\mid P_r^{(1)}\mid\nu\rangle=[1/G(\gamma+i\omega_{\mu\nu})]\sum_{\mu'}B(\mu\nu;\mu'\mu')=3R\Gamma[G(\gamma+i\omega_{\mu\nu})]^{-1}\times\sum_{mn,\mu'}(\mu\mid\mathbf{p}\mid m)\cdot(n\mid\mathbf{p}\mid\nu)\times(m\mid\hat{e}\cdot\mathbf{p}\mid\mu')(\mu'\mid\hat{e}^*\cdot\mathbf{p}\mid n)/(\Gamma+i\omega_{mn}). \quad \text{(III.92)}$$

For an atom with no nuclear spin ($I=0$), Eq. (III.92) reduces to

$$P_r^{(1)}(LM)=[3R/(\gamma-iM\omega_g)][\Gamma(2J_e+1)/(\Gamma-i\omega_eM)]\times W(1J_eJ_gL;J_gJ_e)W(J_gJ_e1L;1J_e)(-1)^LE_{LM}. \quad \text{(III.93)}$$

4. Degradation of Repopulation Pumping due to Collisional Depolarization of the Excited State

Since repopulation pumping rates are proportional to the excited-state polarization, any depolarization of the excited state by collisions will decrease the efficiency of repopulation pumping. At high buffer-gas pressures the excited state may be almost completely depolarized by collisions so that almost no repopulation pumping can occur, even though the ground state may still be strongly polarized by depopulation pumping. Such situations can arise because of the tremendous differences which sometimes exist between excited-state and ground-state depolarization cross sections. For an alkali atom in a helium buffer gas, for instance, the ground-state depolarization cross sections are about 10^{10} times smaller than the excited-state depolarization cross sections. Hence, it is quite possible to choose a buffer-gas pressure which causes negligible ground-state depolarization but almost complete excited-state depolarization.

As a simple example, let us consider a hypothetical alkali atom with no nuclear spin. Let us denote the spontaneous decay rate of the excited state by Γ and the collisionally induced relaxation rate for the excited-state orientation by $N\bar{v}\sigma$, where N is the number density of the buffer-gas molecules, $\bar{v}$ is the mean relative velocity between a buffer-gas molecule and a polarized atom, and σ is the mean depolarization cross section. Then the total relaxation rate for orientation is

$$\Gamma_1=\Gamma+N\bar{v}\sigma. \quad \text{(III.94)}$$

For weak pumping light we can use Eqs. (III.93), (III.54), and (III.39) to show that the polarization produced by D_1 light is

$$P^{(1)}(10)=-(R_1E_{10}/\gamma)[1-\tfrac{1}{3}(\Gamma/\Gamma_1)], \quad \text{(III.95)}$$

while for D_2 pumping light we find

$$P^{(1)}(10)=(R_2E_{10}/\gamma)[(1/2)-5\Gamma/6\Gamma_1]. \quad \text{(III.96)}$$

As the excited-state relaxation rate Γ_1 varies from Γ to ∞, that is, from no collisional depolarization to complete collisional depolarization, the ground-state polarization (in units of R_1E_{10}/γ) produced by weak D_1 pumping light varies from $-\frac{2}{3}$ to -1, while the ground-state polarization (in units of R_2E_{10}/γ) produced by weak D_2 pumping light varies from $-\frac{1}{3}$ to $+\frac{1}{2}$. From Eq. (III.96) it follows that the polarization produced by weak D_2 pumping light is zero when we have

$$\Gamma_1=5\Gamma/3. \quad \text{(III.97)}$$

Experimentally, it is well known (Fri66) that in optical pumping experiments with D_2 light, there is a critical buffer-gas pressure at which no transmission monitoring signal occurs. Franz (Fra66a) has suggested that one could use these critical pressures to determine the depolarization cross section σ for excited-state orientation. Thus, if N_c is the number density which corresponds to the critical pressure, one can use Eq. (III.97) to write

$$N_c\bar{v}\sigma = 2\Gamma/3. \qquad \text{(III.98)}$$

Unfortunately, the presence of hyperfine structure complicates the interpretation of the critical pressure so that Eq. (III.98) must be considerably modified to apply to a real alkali atom with nonzero nuclear spin.

The influence of hyperfine coupling in the excited state was analyzed by Okunevich and Perel (Oku70). Further experimental studies of D_2 pumping have been reported by Zhitnikov *et al.* (Zhi70). Only in the upper hyperfine multiplet ($F=I+\frac{1}{2}$) does a change in polarization occur as a function of pressure (Fri66), (Zhi70). Furthermore, in ^{85}Rb and ^{87}Rb the critical pressure for ^{85}Rb is about 1.5 times higher than that for ^{87}Rb (Zhi70). However, the analysis of Zhitnikov *et al.* (Zhi70) can still not be considered completely satisfactory because they assumed that the ground-state relaxation was uniform. This is known to be a very poor approximation (see Sec. V).

5. *The Influence of the Excited-State Hyperfine Structure on Repopulation Pumping*

The coupling of the excited-state electronic polarization to the nuclear polarization plays an important role in repopulation pumping. A particularly detailed study of the influence of this coupling has been carried out by Lehmann (Leh67) for the Group II elements. Since the ground states of the Group II elements are diamagnetic ($^1S_0$), the ground-state polarization must be purely nuclear. Depopulation pumping can occur only for narrow-line excitation, i.e., when the different components of the hyperfine absorption lines are illuminated with different intensities [see Sec. III.A.14)]. For the singlet resonance line of cadmium ($^1S_0$–$^1P_1$), the hyperfine structure of the $^1P_1$ state is much smaller than the Doppler width of the absorption line; and, consequently, no depopulation pumping is observed. Thus, the pumping of cadmium vapor with singlet resonance radiation must result solely from repopulation pumping. From Eq. (III.83), we find that the repopulation pumping of a diamagnetic ground state is described by

$$(d^{(2)}/dt)\langle T_{LM}(II)\rangle_g = \Gamma\langle T_{LM}(II)\rangle_e. \qquad \text{(III.99)}$$

That is, the nuclear polarization of the excited state is conserved when the atom decays to the ground state. However, we recall from Eq. (III.68) that broad-line excitation from an unpolarized ground state produces no nuclear polarization in the excited state. Thus,

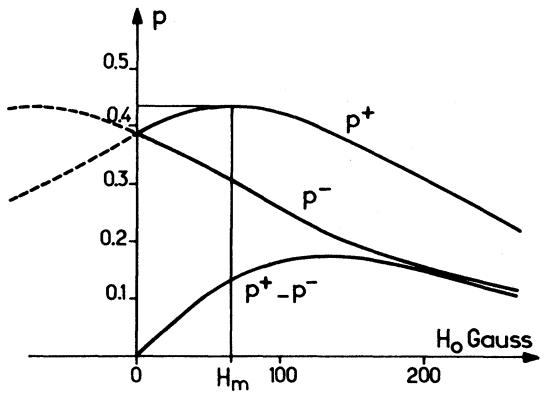

FIG. 10. Degradation of repopulation pumping due to the decoupling of I and J in a large magnetic field. Here p_+ is the probability that an atom, initially in the $-\frac{1}{2}$ ground-state sublevel, will decay spontaneously to the $+\frac{1}{2}$ ground-state sublevel after absorbing a σ_+ photon. Similarly, p_- is the probability that an atom, initially in the $+\frac{1}{2}$ ground-state sublevel, will decay to the $-\frac{1}{2}$ ground-state sublevel after absorbing a σ_- photon. Efficient repopulation pumping of diamagnetic atoms is possible only if I and J are coupled to each other in the excited state [from (Leh67)].

no repopulation pumping can occur unless the hyperfine coupling in the excited state is strong enough to transform some of the electronic polarization (which is produced by anisotropic excitation with light) into nuclear polarization before the excited state decays. This transformation can occur only if the lifetime $1/\Gamma$ of the excited state is comparable to or greater than a typical hyperfine period $1/\Delta\nu$ of the excited atom, i.e., only if

$$\Gamma \lesssim \Delta\nu. \qquad \text{(III.100)}$$

This criterion is satisfied in mercury and in cadmium, both of which have been pumped with singlet (and triplet) resonance radiation. In zinc, on the other hand, Eq. (III.100) is satisfied for the $^3P_1$ excited state but not for the $^1P_1$ excited state. As expected, attempts to pump zinc with singlet radiation have failed, but successful pumping with triplet radiation has been achieved.

6. *High Field Decoupling and Its Effect on Repopulation Pumping*

The coupling of the nuclear polarization to the electronic polarization is modified when the atom is in an external magnetic field. If the field is so large that the azimuthal quantum numbers m_I and m_J of the nucleus and of the electrons are approximately good quantum numbers, the coupling of the electronic and nuclear polarization will be negligible, and it will no longer be possible to transform appreciable amounts of electronic polarization into nuclear polarization during the excited-state lifetime. Lehman (Leh67) has shown that the repopulation pumping of cadmium with singlet resonance radiation becomes less efficient for fields above 200 G because of the decoupling of the nuclear

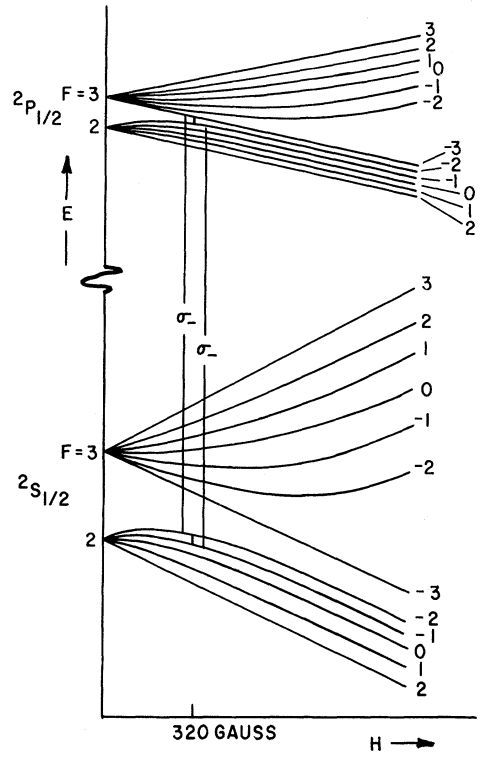

FIG. 11. Magnetic sublevels of the ^{85}Rb atom. The energy splitting between a pair of excited-state sublevels becomes equal to the energy splitting between a pair of ground-state sublevels at a magnetic field of 320 G [from (Bul71a)].

polarization from the electronic polarization (see Fig. 10). Another interesting example of the role of decoupling occurs in the pumping of alkali atoms with an unpolarized light beam. For broad-line, unpolarized excitation, there is no depopulation pumping because all components of the light-absorption operator except the equilibrium component are zero. However, the unpolarized light beam will produce an electronic alignment in the excited $^2P_{3/2}$ state. The electronic alignment of the excited state cannot be transformed into ground-state electronic alignment because the electron spin of the ground state is $\frac{1}{2}$. However, at low magnetic fields the hyperfine coupling can transform the purely electronic alignment $\rho_{20}(J_eJ_e)$ into nuclear alignment $\rho_{20}(\mathrm{II})$ and into alignment of total angular momentum $\rho_{20}(F_eF_e)$. This alignment is partially retained when the excited state decays back to the ground state. However, at high magnetic fields, the electronic polarization is decoupled from the nuclear polarization; and the excited-state electronic alignment, which is generated by unpolarized pumping light, remains purely electronic and cannot be transferred to the ground state by repopulation pumping. As expected, it is only at low magnetic fields that alkali atoms have been aligned with unpolarized or linearly polarized pumping light (Mar55).

7. *Light Shifts due to Real Transitions*

An important aspect of repopulation pumping is the phenomeenon of "light shifts due to real transitions". Barrat and Cohen-Tannoudji (Bar61d,e) pointed out that the imaginary part of the self-coupling coefficient $B(\mu\nu;\mu\nu)$ of Eq. (III.87) can be regarded as a shift $\Delta\omega_{\mu\nu}$ in the resonant frequency of the transition $\mu\rightarrow\nu$

$$\Delta\omega_{\mu\nu} = -\operatorname{Im} B(\mu\nu;\mu\nu). \qquad \text{(III.101)}$$

Equation (III.101) is valid as long as the transition frequency $\omega_{\mu\nu}$ is well resolved from other ground-state transition frequencies.

The shifts due to real transitions depend strongly on external fields because of the energy denominator of Eq. (III.91). Sizeable shifts due to real transitions can occur only if the ground-state coherence frequency $\omega_{\mu\nu}$ does not differ from the excited-state coherence frequency ω_{mn} by more than the natural width Γ of the excited state. Equation (III.79) shows this to be just the condition that large oscillating coherence be generated between the excited-state sublevels m and n.

As an example, let us consider the shift of the transition $F=2$, $m=2\rightarrow F=2$, $m=1$ in the ^{85}Rb atom. The ground-state transition frequency becomes equal to the $^2P_{1/2}$ excited-state transition frequency $F=3$, $m=-1\rightarrow F=2$, $m=-2$ at a field of 320 G (see Fig. 11). Consequently, a resonant change in the shift for σ_- pumping light occurs at 320 G (see Fig. 12). There is also a large increase in the shift at low magnetic fields, where the difference between ground-state and excited-state transition frequencies becomes less than the natural width of the excited state.

Shifts due to real transitions are always comparable to or less than the light-induced linewidth of the ground-state resonance, in contrast to shifts due to virtual transitions, which can greatly exceed the light-induced linewidth.

Shifts due to real transitions are not caused by a shift in the ground-state energy levels, although such an interpretation is quite proper for shifts due to virtual

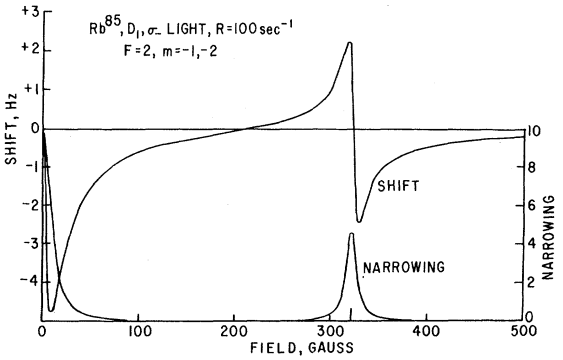

FIG. 12. Light shifts due to real transitions in ^{85}Rb. A resonant change in the shift and narrowing occurs at 320 G and at zero field (cf Fig. 11) [from (Bul71a)].

transitions. For instance, the shifts due to real transitions are not additive; i.e., if p, q, and r label three energy sublevels in descending order, the equation

$$\Delta\omega_{pq}+\Delta\omega_{qr}=\Delta\omega_{pr} \qquad \text{(III.102)}$$

is not true. However, Eq. (III.102) does hold for the shifts due to virtual transitions [see Eq. (III.61)].

Shifts due to real transitions have been studied in detail for ^{199}Hg by Cohen–Tannoudji (Coh61c,62a,b) for ^{111}Cd by Lehmann (Leh67), and for the alkali atoms by White *et al.* (Whi68), and Bulos *et al.* (Bul71a). In all of these cases, detailed studies have been restricted to single well-resolved ground-state transitions.

A theoretical analysis of shifts due to real transitions is difficult when many degenerate ground-state transitions are coupled, as in the case for the high-spin mercury and cadmium isotopes and for low-field Zeeman transitions in the alkali atoms. However, the shifts in the resonance frequencies can, in principle, be obtained by numerical solution of the Liouville equation (II.11).

8. Line Narrowing

Repopulation pumping, in addition to causing light shifts, causes a narrowing of the magnetic resonance lines of the ground state. This occurs because part of ground-state coherence survives the passage through the excited state and back to the ground state during the absorption and re-emission of a photon. Line narrowing was first predicted by Barrat and Cohen–Tannoudji (Bar61d,e), who showed that the relaxation rate γ_{mn} of the ground-state coherence between the levels μ and ν is decreased by the real part of the self-coupling coefficient of Eq. (III.87),

$$\Delta\gamma_{\mu\nu}=-\operatorname{Re}B(\mu\nu;\mu\nu). \qquad \text{(III.103)}$$

Equation (III.103) is valid only for a well-resolved ground-state resonance. For poorly resolved coupled transitions, one can solve the Liouville equation (II.11) numerically to obtain the line narrowing. The line narrowing for a typical transition is shown in Fig. 12. The narrowing is particularly pronounced at low fields and at 320 G, where efficient transfer of coherence through the excited state can occur.

Line narrowing, or more precisely, transverse ground-state relaxation rates, have been studied experimentally and theoretically by Cohen–Tannoudji (Coh61b,62a,b) for ^{199}Hg. The effects of repopulation pumping on the relaxation rates were in complete agreement with the predictions of Eq. (III.103).

IV. EVOLUTION OF THE LIGHT

In most optical pumping experiments, the behavior of the pumped atoms is determined by monitoring changes in the intensity of light that has interacted with the atoms. One can classify most detection systems as those in which the fluorescent light emitted by the atoms is observed (fluorescence monitoring) or those in which a probing, external light beam is observed after the light beam has passed through the vapor (transmission monitoring). Thus, it is natural to consider separately the forward propagation of a light beam and the production of fluorescent light. We shall see that the fluorescent light provides direct information about the polarization of the excited state, while the attenuation of a light beam provides direct information about the polarization of the ground state.

A. Forward Light Propagation

The most convenient theory to describe the forward propagation of light is the semiclassical formalism, in which the light is considered to be classical electromagnetic waves, and the atoms are considered to be quantum mechanical systems. This type of formalism has a long history and was used by Opechowski (Ope53) to describe experiments similar to modern optical pumping experiments. Recently, such theories have been worked out in detail by Corney, Kibble, and Series (Cor66), Happer and Mathur (Hap67c), Cohen–Tannoudji and Laloë (Coh67), Laloë, Leduc, and Minguzzi (Lal69a,b), and by Verchueren (Ver68).

One can think of the light beam as being composed of many monochromatic waves. The electric field of an individual wave can be written as

$$\mathbf{E}=\boldsymbol{\mathcal{E}}(\zeta t)\exp i(\mathbf{k}\cdot\mathbf{r}-\omega t)+\text{c.c.}, \qquad \text{(IV.1)}$$

where c.c. denotes the complex conjugate. The amplitude $\mathcal{E}$ will be a slowly varying function of time and distance ζ along the direction of propagation

$$\zeta=(1/k)\,\mathbf{k}\cdot\mathbf{r}. \qquad \text{(IV.2)}$$

The oscillating electric field will produce an oscillating electric dipole moment $\langle\mathbf{D}\rangle$ in each atom of the vapor:

$$\langle\mathbf{D}\rangle=\mathbf{D}\exp i(\mathbf{k}\cdot\mathbf{r}-\omega t)+\text{c.c.} \qquad \text{(IV.3)}$$

We shall only be concerned with light sources which are so weak that saturation does not occur, and the induced dipole moment is proportional to the electric field

$$\langle\mathbf{D}\rangle=\langle\boldsymbol{\alpha}\rangle\cdot\boldsymbol{\mathcal{E}}. \qquad \text{(IV.4)}$$

The constant of proportionality is the expectation value of the polarizability operator $\boldsymbol{\alpha}$, which was defined in Eq. (III.12). We can also define the dielectric susceptibility as

$$\boldsymbol{\chi}=N\boldsymbol{\alpha}, \qquad \text{(IV.5)}$$

where N is the number density of pumped atoms. We shall see that the susceptibility governs the propagation of light in much the same way that the Hamiltonian governs the time evolution of the atom (see Table I).

If oscillating ground-state coherence is present, the polarizability will also oscillate, and the induced dipole moment will oscillate not only at the driving frequency of the electric field, but at sideband frequencies that are displaced by the atomic coherence frequency from the

TABLE I. Analogous roles of the atomic wave function and the electric field of the light.

	Atom	Light
State	Ψ_g	$\mathcal{E}$
Evolution parameter	t	$\zeta=\frac{1}{2}(\xi+ct)$
Evolution equation	$i(\partial\Psi_g/\partial t)=(\mathcal{H}_0+\delta\mathcal{H})\Psi_g$	$i(\partial\mathcal{E}/\partial\xi)=(-2\pi k\chi)\mathcal{E}$
Evolution operators	$\delta\mathcal{H}=-\mathcal{E}^*\alpha\mathcal{E}$	$\chi/N=\langle\Psi_g\mid\alpha\mid\Psi_g\rangle$

driving frequency. In this way, sidebands can be generated on an initially monochromatic light wave.

Let us write the susceptibility for a light wave of frequency ω as

$$\langle\chi(\omega,\zeta,t)\rangle=\sum_{\omega'}\langle\omega'\mid\chi\mid\omega\rangle\exp i[(k'-k)\zeta-(\omega'-\omega)t]. \tag{IV.6}$$

The sum on ω' is such that all coherence frequencies of the atomic vapor are included in the set of difference frequencies $\omega-\omega'$. Equation (IV.6) represents an expansion of the susceptibility into waves that propagate along the direction of the light wave. The quantities $\langle\omega'\mid\chi\mid\omega\rangle$ are independent of time, but they may depend on position. We may think of them as matrix elements in the frequency domain, which couple a light wave of frequency ω with a wave of frequency ω'. It is convenient to introduce new independent variables

$$\xi=\tfrac{1}{2}(\zeta+ct), \tag{IV.7}$$

$$\eta=\tfrac{1}{2}(\zeta-ct). \tag{IV.8}$$

The propagation of the light wave is then determined by the infinite set of coupled equations (Hap69)

$$\partial\boldsymbol{\mathcal{E}}(\omega)/\partial\xi\,|_{\eta=\text{const}}=[\partial\boldsymbol{\mathcal{E}}(\omega)/\partial\zeta]+(1/c)[\partial\boldsymbol{\mathcal{E}}(\omega)/\partial t]$$
$$=2\pi ik\sum_{\omega'}\langle\omega\mid\chi_\perp\mid\omega'\rangle\cdot\boldsymbol{\mathcal{E}}(\omega'). \tag{IV.9}$$

Equation (IV.9) is a linearized form of the reduced Maxwell equation which occurs in the theory of nonlinear optics. It is based on the assumption that the fractional change of the field amplitudes over the distance of one wavelength or after one optical period is very small. This condition is very well satisfied in all optical pumping experiments that have been performed so far. We note that the transverse susceptibility dyadic

$$\chi_\perp=\mathfrak{T}(\hat{k})\cdot\chi\cdot\mathfrak{T}(\hat{k}) \tag{IV.10}$$

is used in Eq. (IV.9), where we have

$$\mathfrak{T}(\hat{k})=\mathbf{1}-\hat{k}\hat{k}, \tag{IV.11}$$

and $\hat{k}$ is the direction of propagation of the wave. Physically, it is clear that the longitudinal components of the susceptibility cannot affect the propagation of light to first order, since the longitudinal components of the induced polarization do not reradiate light in the direction of propagation.

There is a very close parallel between the forward propagation of the light in an optically pumped vapor and the evolution of the atoms of the vapor as a result of absorption pumping. These relationships are summarized in Table I. The state of the atoms is described by a ground-state wavefunction ψ_g, and the state of the light is represented by an electric field amplitude $\boldsymbol{\mathcal{E}}$. The ground-state wavefunction changes as time increases, and the electric field amplitude changes as the wavefront moves through the vapor, i.e., as the parameter ξ increases for a constant value of η [see Eq. (IV.9)]. The evolution of the atomic ground state is determined by a Schroedinger equation with the unperturbed Hamiltonian augmented by the effective Hamiltonian $\delta\mathcal{H}$. The evolution of the electric field is governed by the propagation equation (IV.9), which is formally analogous to the Schroedinger equation. The susceptibility plays the role of the Hamiltonian for the propagation equation. Finally, both the effective Hamiltonian and the susceptibility can be thought of as expectation values of the polarizability operator $\boldsymbol{\alpha}$. The effective Hamiltonian is the expectation value of $\boldsymbol{\alpha}$ with respect to the electric field amplitude. The susceptibility is the expectation value of $\boldsymbol{\alpha}$ with respect to the ground-state atomic wavefunction.

1. Quasistatic Susceptibilities

Let us consider a vapor in which the susceptibility is either static or very slowly varying with respect to the transit time l/c of a light wave across the length l of the vapor. Then Eq. (IV.9) reduces to

$$\partial\boldsymbol{\mathcal{E}}/\partial\zeta=2\pi ik\langle\chi_\perp\rangle\cdot\boldsymbol{\mathcal{E}}. \tag{IV.12}$$

We may seek eigensolutions to Eq. (IV.12) of the form

$$\boldsymbol{\mathcal{E}}=\hat{e}_\lambda\exp i(k_\lambda-k)\zeta, \tag{IV.13}$$

where $\hat{e}_\lambda$ is an eigenpolarization vector, and k_λ is the corresponding propagation vector. Substituting Eq. (IV.13) into Eq. (IV.12), we derive an eigenvalue equation for $\hat{e}_\lambda$

$$2\pi k\langle\chi_\perp\rangle\cdot\hat{e}_\lambda=(k_\lambda-k)\hat{e}_\lambda. \tag{IV.14}$$

For each direction of propagation, there are two solutions to Eq. (IV.14), which we may label with $\lambda=1$ and $\lambda=2$. The characteristic propagation constants k_λ are related to the phase velocities v_λ of the two eigen-

waves by

$$v_\lambda = \omega/k_\lambda. \qquad \text{(IV.15)}$$

Since the frequencies of the light used in optical pumping experiments are usually close to the atomic absorption frequencies, the vapor attenuates the light, and k_λ will usually have a small imaginary part which accounts for the attenuation. A compact way to represent the solutions to Eq. (IV.14) is to plot the real part of the phase velocity v_λ as a function of the direction of propagation. A surface is formed for each value of λ ($\lambda = 1$ or 2), and these surfaces are called normal velocity surfaces in the classical optics of crystals. A second set of two surfaces, called ray-velocity surfaces in classical optics, is defined as those wavefronts which would develop if a pulse of light were allowed to expand outward in all directions. Two different surfaces will develop in an anisotropic medium, each corresponding to a different polarization of the light wave. The ray-velocity surfaces and the normal velocity surfaces are identical to each other to first order in $\langle\chi\rangle$. Therefore, since $\langle\chi\rangle \lesssim 10^{-4}$ in most optical pumping experiments, we need not make a distinction between the ray-velocity and normal velocity surfaces, and will simply speak of the "wave surface."

As an example, consider the wave surfaces of an alkali vapor (Fig. 13). Each component of the susceptibility causes a characteristic type of wave surface. For instance, a vapor with a pure quadrupole polarization (pure alignment) will behave as a birefringent crystal; and, consequently, the quadrupole component of the susceptibility is often called the birefringent part. Similarly, a vapor with a pure dipole polarization (pure orientation) will behave as a gyrotropic optical medium birefringent. The wave surfaces are ellipsoids of revolution, and the eigenpolarizations are σ_+ and σ_- light (with respect to the direction of propagation).

When the polarization of the vapor is a combination of several multipole polarizations, the wave surfaces will be more complicated, but there will always be two eigenpolarizations for each direction of propagation.

We shall assume that the eigenpolarization vectors are linearly independent so that any initial electric field amplitude $\mathcal{E}(0)$ can be written as a linear combination of the $\hat{e}_\lambda$; i.e.,

$$\mathcal{E}(0) = a_1\hat{e}_1 + a_2\hat{e}_2. \qquad \text{(IV.16)}$$

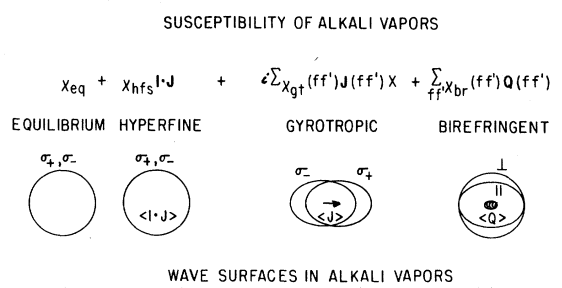

FIG. 13. Wave surfaces for light propagation in an atomic vapor. A polarized atomic vapor has optical properties similar to those of an anisotropic crystal [from (Mat70)].

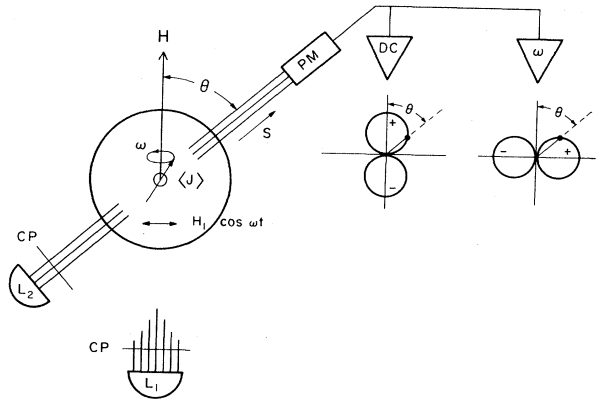

FIG. 14. Transmission monitoring of $\langle \mathbf{J} \rangle$. The precessing atomic spin $\langle \mathbf{J} \rangle$ causes a variable attenuation of the transmitted light. The angular dependences of the dc and ac components of the transmitted light are sketched.

After the wave has propagated through a length l of the vapor, the electric field amplitude will have become [see Eq. (IV.13)]

$$\mathcal{E}(l) = \sum_{\lambda=1}^{2} a_\lambda \hat{e}_\lambda \exp\left[i(k_\lambda - k)l\right]$$

$$= \exp\left[2\pi i \langle \chi_\perp \rangle kl\right] \cdot \mathcal{E}(0). \qquad \text{(IV.17)}$$

The exponential operator on the right of Eq. (IV.17) may be thought of as a power series in the dyadic $\langle \chi_\perp \rangle$.

2. *Absorption of Light by an Optically Thin Vapor*

The change in the intensity of a light wave after passage through a length l of optically pumped vapor is

$$\Delta I = (c/2\pi)\{|\,\mathcal{E}(l)|^2 - |\,\mathcal{E}(0)|^2\}. \qquad \text{(IV.18)}$$

Mathur *et al.* (Mat70) have shown that for an optically thin vapor, (i.e., to first order in $\langle \chi \rangle$), Eq. (IV.18) becomes

$$\Delta I = -\int_0^\infty d\nu \Phi(\nu) \int_0^l dz h(\nu, z, t'), \qquad \text{(IV.19)}$$

where the retarded time is

$$t' = t - (1/c)(l - z), \qquad \text{(IV.20)}$$

and the absorptivity $h(\nu, z, t)$ is

$$h = -2\pi i k N \hat{e}^* \cdot \langle \boldsymbol{\alpha}_\perp \rangle \cdot \hat{e} + \text{c.c.} \qquad \text{(IV.21)}$$

The absorptivity is the optical power absorbed by the atoms per unit volume and per unit frequency interval. From Eq. (III.11), we see that the absorptivity is related to the light-absorption operator by the equation

$$\int_0^\infty h(\nu, z, t)\, \Phi(\nu)\, d\nu = \hbar\omega N \langle \delta\Gamma(z, t) \rangle. \qquad \text{(IV.22)}$$

That is, the absorptivity is the energy per photon $\hbar\omega$ times the number of photon absorptions per second. The

intensity change for an optically thin vapor is thus

$$\Delta I(t) = -N\omega\hbar \int_0^l dz \langle \delta\Gamma(zt') \rangle. \quad \text{(IV.23)}$$

3. Transmission Monitoring

The most direct way to detect the ground-state polarization of an atomic vapor is to measure the attenuation or polarization changes of a probing light beam. Dehmelt (Deh57b), Raith (Rai61), and Bouchiat (Bou65a) have emphasized that the attenuation of a probing beam is linearly dependent on certain well-defined components of the ground-state polarization. For example, consider an optically pumped alkali vapor. If the vapor is optically thin and if its polarization is uniform along the path length l of a probing light beam, the attenuation of the beam is

$$\Delta I = lN\omega\hbar\{\delta\Gamma_{\rm eq} + \delta\Gamma_{\rm hfs}\langle \mathbf{I}\cdot\mathbf{J}\rangle + \sum_{ff'} \delta\Gamma_{gt}(ff')\langle \mathbf{J}(ff')\rangle\cdot\mathbf{s} + \sum_{ff'} \delta\Gamma_{br}(ff')\hat{e}^*\cdot\langle \mathfrak{Q}(ff')\rangle\cdot\hat{e}\}. \quad \text{(IV.24)}$$

The scalar coefficients $\delta\Gamma_i$ are convolutions of the spectral profile of the light with corresponding components $\alpha_i(\nu)$ of the polarizability operator (Mat70) of an alkali atom [cf. Eq. (III.42)]:

$$\boldsymbol{\alpha} = \alpha_{\rm eq} + \alpha_{\rm hfs}\mathbf{I}\cdot\mathbf{J} + i\sum_{ff'} \alpha_{gt}(ff')\mathbf{J}(ff')\times + \sum_{ff'} \alpha_{br}(ff')\mathfrak{Q}(ff'). \quad \text{(IV.25)}$$

For instance, in view of Eqs. (III.11) and (III.28), we have

$$\delta\Gamma_{\rm eq} = (4\pi/\hbar c)\int \Phi(\nu)\ \mathrm{Im}\ \alpha_{\rm eq}(\nu)\, d\nu. \quad \text{(IV.26)}$$

In Eq. (IV.24), the mean spin $\mathbf{s}$ of the photons is

$$\mathbf{s} = i\hat{e}\times\hat{e}^* \quad \text{(IV.27)}$$

for light of a well-defined polarization $\hat{e}$. The quadrupole operator $\mathfrak{Q}(ff')$ is defined in analogy to Eq. (III.43). The sums in Eqs. (IV.24) and (IV.25) extend over both hyperfine multiplets $f = I \pm \frac{1}{2}$ of the ground state, and $\mathbf{J}(ff')$ denotes the projection of the electronic angular momentum operator $\mathbf{J}$

$$\mathbf{J}(ff') = \sum_{\mu\nu} |f\mu\rangle\langle f\mu|\,\mathbf{J}\,|f'\nu\rangle\langle f'\nu|. \quad \text{(IV.28)}$$

Thus, the attenuation of a light beam can be used to measure the observables $\mathbf{I}\cdot\mathbf{J}$, $\mathbf{J}(ff')$, and $\mathfrak{Q}(ff')$. By a proper choice of the polarization or spectral profile of the light, the absorption signal can be made to depend on only one of these observables. For instance, for broad-line probing light, the coefficients $\delta\Gamma_{\rm hfs}$ and $\delta\Gamma_{br}(ff')$ are zero, and $\delta\Gamma_{gt}(ff')$ becomes independent of the arguments f and f'. The attentuation is then proportional to

$$\sum_{ff'} \langle \mathbf{J}(ff')\rangle\cdot\mathbf{s} = \langle \mathbf{J}\rangle\cdot\mathbf{s}. \quad \text{(IV.29)}$$

On the other hand, if the probing beam is "narrow line" but linearly polarized or unpolarized, the mean photon spin $\mathbf{s}$ will be zero, and the absorption signal will depend on $\langle \mathbf{I}\cdot\mathbf{J}\rangle$ and $\langle \mathfrak{Q}(ff')\rangle$. For the lighter alkali atoms, the coefficient $\delta\Gamma_{br}(ff')$ is negligibly small compared to $\delta\Gamma_{\rm hfs}$, so that the absorption signal is essentially a measure of $\langle \mathbf{I}\cdot\mathbf{J}\rangle$ alone.

Quite analogous considerations apply to the absorption signals of other optically pumped atoms, such as mercury and helium. In all cases, one can associate the absorption signals with certain ground-state observables, which, at low magnetic fields, include $\mathbf{J}$, $\mathfrak{Q}$, and various powers of $\mathbf{I}\cdot\mathbf{J}$.

Dehmelt (Deh57b) pointed out that the attenuation of the light beam will be time dependent if the observables of the vapor are time dependent. Thus, Bell and Bloom (Bel57), were able to use a transverse, circularly polarized beam of light to detect the rotating transverse spin of an optically pumped vapor. A typical crossed-beam experiment of the type introduced by Bell and Bloom is shown in Fig. 14. An analogous type of crossed-beam experiment, (Pan68) (Lal68a,b), (Mat70), which utilizes the birefringence of the vapor, is shown in Fig. 15.

4. Off-Resonant Light

An optically pumped vapor can be probed with either resonant or off-resonant light, since the polarization of the vapor affects both the real and imaginary parts of the index of refraction of the vapor. For instance,

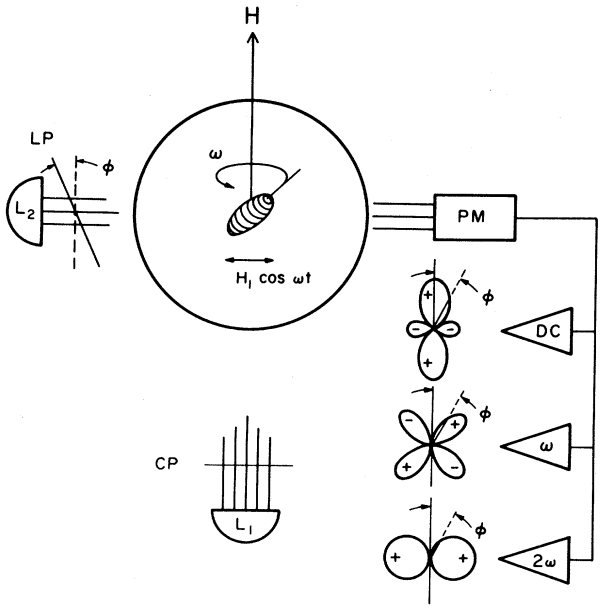

FIG. 15. Transmission monitoring of $\langle \mathfrak{Q} \rangle$. The precessing quadrupole moment (dielectric ellipsoid) of the vapor causes a variable attenuation of the linearly polarized probing beam. The dependence of the dc and ac components of the transmission monitoring signals on the angle ϕ between the polarization vector of the light and the magnetic field is sketched.

Kastler (Kas51) proposed that the parametric Faraday rotation of a polarized vapor be used to detect the degree of polarization of the vapor. Similar proposals were made by Opechowski (Ope53) and Gozzini (Goz62). Daniels and Wesemeyer (Dan58a,b) were able to use the paramagnetic rotation to detect magnetic rotation in paramagnetic salts. Early observations of the paramagnetic Faraday rotation in optically pumped atomic vapors were reported by Manuel and Cohen–Tannoudji for mercury (Man63), by Strumia for sodium (Str66), and by Mathur and Happer for rubidium (Hap67a). All paramagnetic Faraday-effect experiments are based on the fact that the gyrotropic component of the atomic polarizability causes the electric field $\mathcal{E}$ of a light wave to be rotated by an angle

$$\delta\phi = 2\pi klN\langle J_\zeta\rangle \operatorname{Re}\alpha_{0l} \qquad \text{(IV.30)}$$

after the light has passed through a length l of polarized vapor. By inserting a suitable analyzer in the path of the beam, one can detect this rotation angle even though no attenuation of the beam has occurred. A simple experimental arrangement is shown in Fig. 16.

Similar experiments can be designed to make use of the birefringence of the vapor for off-resonant light.

Off-resonant probing light has the advantage that it causes no depumping of the vapor. However, off-resonant light does cause light shifts, and the signal-to-noise ratios are not always as good as those which can be obtained with resonant light.

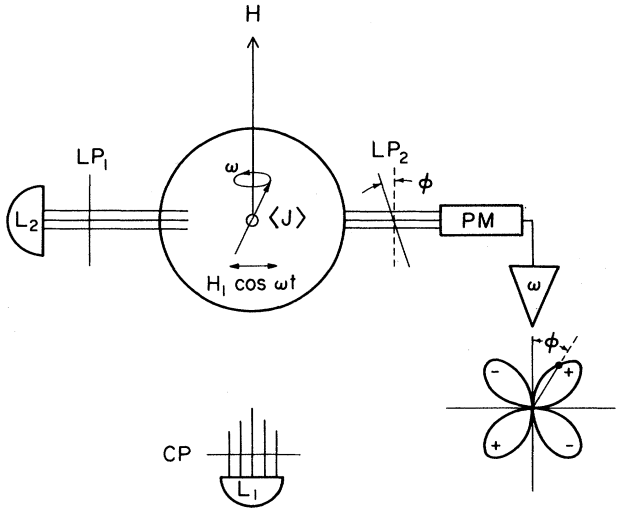

FIG. 16. Transmission monitoring of ⟨J⟩ with the parmagnetic Faraday effect. The plane of polarization of the off-resonant light is rotated about the atomic angular momentum ⟨J⟩. The dependence of the modulated signal amplitude on the angle ϕ between the linear polarizer LP_1 and the linear polarizer LP_2 is sketched.

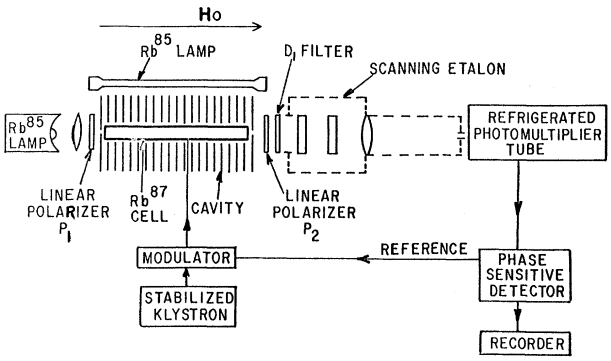

FIG. 17. Phase-matched parametric frequency conversion. Transmission monitoring techniques must be modified when the atomic coherence changes appreciably during the transit time of a probing light pulse across the vapor. The light pulse should move at the same velocity as the waves of atomic coherence. In this experiment, a dielectrically loaded cavity was used to adjust the velocity of the microwaves, which produced waves of atomic coherence. The group velocity of the light was greatly modified by the index of refraction of the vapor [from (Tan70)].

5. *Rapidly Varying Susceptibilities*

The susceptibility of the atomic vapor may vary appreciably during the time required for the light to traverse the vapor. For this to occur, the wavelength of the electromagnetic field which drives the susceptibility of the vapor must be on the order of typical cell dimensions, and the corresponding frequencies will therefore be in the microwave range. The simplest way to view the problem is to think of the vapor as a parametric medium which couples optical waves with microwaves. The quantitative details of this coupling are described by Eq. (IV.9), but several qualitative aspects can be understood without difficulty. Suppose that the susceptibility of the vapor is modulated at a frequency Ω. Then an optical carrier wave of frequency ω_0 can be coupled to upper and lower sidebands of frequencies

$$\omega_{\pm1} = \omega_0 \pm \Omega. \qquad \text{(IV.31)}$$

Suppose that the susceptibility is also spatially modulated with a propagation constant

$$K = 2\pi/\Lambda, \qquad \text{(IV.32)}$$

where Λ is the wavelength of the exciting microwave field. Then efficient conversion from carrier to sideband power can occur only if we have the condition

$$\mathbf{k}_0 n(\omega_0) \pm \mathbf{K} = \mathbf{k}_{\pm1} n(\omega_{\pm1}). \qquad \text{(IV.33)}$$

Here $\mathbf{k}_0$, $\mathbf{k}_{+1}$, and $\mathbf{k}_{-1}$ are the free-space wave vectors of the carrier and of the upper and lower sidebands, and $n(\omega)$ is the static index of refraction of the vapor at the frequency ω

$$n(\omega) = 1 + 2\pi\langle\omega \mid \chi \mid \omega\rangle. \qquad \text{(IV.34)}$$

The two conditions represented by Eqs. (IV.31) and (IV.33) are called the conditions for phase matching.

Because of the condition in Eq. (IV.33), the optimum

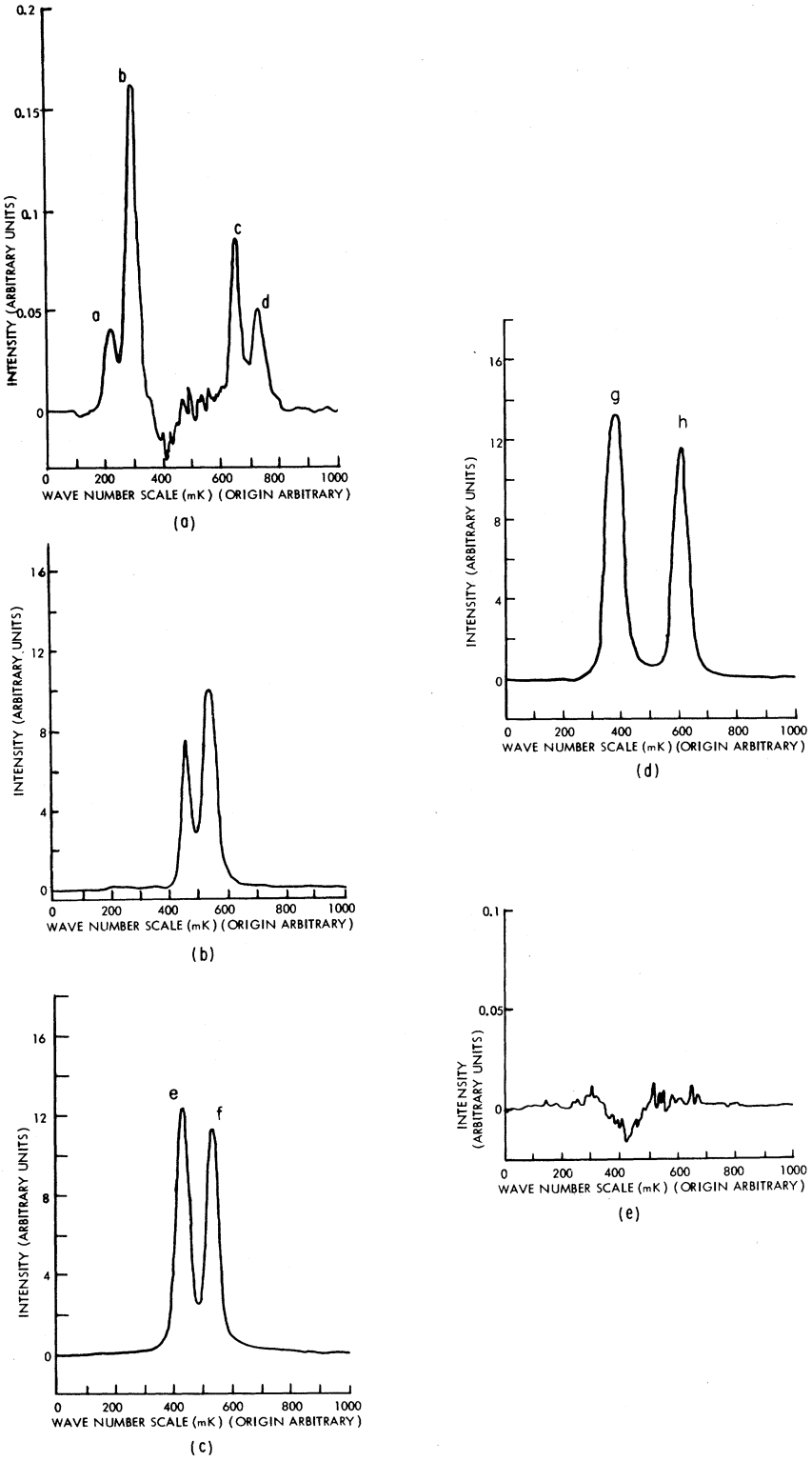

FIG. 18. Spectral line profiles observed with the apparatus of Fig. 17. (a) Sidebands; P_1 and P_2 were crossed. (b) Attenuated carrier; P_1 and P_2 were parallel; (c) Unattenuated carrier, the microwave cavity and absorption cell were removed. (d) Spectral profile of a ^{87}Rb lamp; (e) Fluorescent light; probing ^{85}Rb lamp was removed [from (Tan71)].

propagation constant for the microwaves will be shifted from the free-space value Ω/c. The shift is

$$K-\Omega/c=2\pi k[\langle\omega_1\mid\chi_\perp\mid\omega_1\rangle-\langle\omega_0\mid\chi_0\mid\omega_0\rangle] \quad \text{(IV.35)}$$

for phase matching to the sideband. The shift can be 10% or more of the free-space wavelength, since the index of refraction is very large in the neighborhood of the atomic absorption lines.

Tang and Happer (Tan70), have observed the sidebands produced by the 0–0 coherence in ^{87}Rb vapor with a Fabry–Perot interferometer. Their apparatus is shown in Fig. 17. It was necessary to pump the 45-cm rubidium cell along its entire length with an auxiliary lamp to maintain a sufficient polarization of the vapor, and a special microwave cavity was designed to allow pumping from the side. Typical sidebands are shown in Fig. 18.

Very weak sidebands are difficult to detect with a spectrometer because the intensity falls as the square of the sideband amplitude. A considerable gain in sensitivity can be obtained by beating the sideband with the carrier and looking for the difference frequency. In this heterodyne-detection scheme, the signal is linearly proportional to the sideband amplitude. The original crossed-beam light-modulation experiments of Bell and Bloom (Bel57) can be considered as a heterodyne detection of the sidebands produced by the Zeeman coherence of the vapor. Coherence between different hyperfine states was first used by Firester and Carver (Fir66,67) to produce light modulation at 458 MHz in ^{39}K. Light modulation at the 6835-MHz hyperfine frequency of ^{87}Rb was detected by Mathur *et al.* (Mat68a). In all of these experiments, one of the chief difficulties is to find a photodetector with adequate sensitivity and frequency response. At the present time, the best detector for frequencies above a few hundred MHz seems to be a crossed-field photomultiplier tube (Mat68a).

B. Fluorescent Light

Another important method of measuring the properties of an optically pumped vapor is to observe the fluorescently scattered light. Before Dehmelt's (Deh57b) suggestion of transmission monitoring, fluorescent light was always used to detect optical pumping. Fluorescence monitoring has the advantage that the large background of pumping light that accompanies the transmission-monitoring signal can be nearly eliminated, provided that instrumental scattering is kept to a minimum. However, a serious disadvantage of fluorescence monitoring is that the signal is not related as directly to the ground-state polarization as is the transmission-monitoring signal. In fact, it is the excited-state polarization that is most simply related to the fluorescent light signal.

From elementary quantum mechanics, we know that the rate of emission of light with polarization $\hat{u}$ by an atom decaying from an excited-state sublevel m to a ground-state sublevel μ is

$$I\propto|\langle m\mid\hat{u}\cdot\mathbf{p}\mid\mu\rangle|^2, \quad \text{(IV.36)}$$

where $\mathbf{p}$ is the momentum operator of the atom. Equation (IV.36) can be generalized without difficulty to include the case of excited atoms described by an arbitrary density matrix. One obtains

$$\Delta I(\hat{u})\,\Delta\Omega=\hat{u}\cdot\langle\mathfrak{R}(\hat{r})\rangle\cdot\hat{u}^*, \quad \text{(IV.37)}$$

where $\Delta I(\hat{u})/\Delta\Omega$ is the light intensity (photons per second steradian) of polarization $\hat{u}$ emitted in the direction $\hat{r}$, and the fluorescent light dyadic $\langle\mathfrak{R}(\hat{r})\rangle$ is the expectation value of the excited-state operator

$$\mathfrak{R}(\hat{r})=(1/\hbar)\,(\omega/c)^3\sum_\mu\mathfrak{T}(\hat{r})\cdot\mathbf{D}\mid\mu\rangle\langle\mu\mid\mathbf{D}\cdot\mathfrak{T}(\hat{r}). \quad \text{(IV.38)}$$

Here $\mathfrak{T}(\hat{r})$ is the transverse projection dyadic for the direction $\hat{r}$ [see Eq. (IV.11)], and the summation extends over all sublevels μ to which the atom is observed to decay. If all hyperfine components of the fluorescent light that corresponds to the transition $J_e\rightarrow J_b$ are observed, the fluorescent light dyadic is

$$\mathfrak{R}(\hat{r})=[3\Gamma(J_eJ_b)/8\pi](2J_e+1)\times\sum W(L1J_eJ_b;1J_e)\,(-1)^L\mathfrak{Q}_L(\hat{r})\cdot T_L(J_eJ_e). \quad \text{(IV.39)}$$

Here we define

$$\mathfrak{Q}_{LM}(\hat{r})=\mathfrak{T}(\hat{r})\cdot\mathfrak{Q}_{LM}\cdot\mathfrak{T}(\hat{r}), \quad \text{(IV.40)}$$

and the partial decay rate from J_e to J_b is denoted by $\Gamma(J_eJ_b)$. A completely analogous expression is obtained for $\mathfrak{R}$, when a single hyperfine transition $F_e\rightarrow F_b$ is observed. One need only replace J_e by F_e and J_b by F_b in Eq. (IV.39).

From Eq. (IV.39), we see that the fluorescent light is composed of three components, one proportional to the excited-state population ($L=0$), one proportional to the magnetic dipole moment of the excited state ($L=1$), and one proportional to the quadrupole moment of the excited state ($L=2$). By a proper choice of the polarization of the observed light, one can usually eliminate signals from either the dipole or the quadrupole polarization. For instance, the contribution from the dipole always has the form $\langle J_e\rangle\cdot\mathbf{s}$, where $\mathbf{s}=i\hat{u}\times\hat{u}^*$ is the mean spin of the observed photons. Thus, there will be no contribution from the dipole if the mean spin is zero, i.e., for linearly polarized or unpolarized light. Even if $\mathbf{s}$ is not zero, there will be no dipole signal if $\mathbf{s}$ and $\langle\mathbf{J}_e\rangle$ are orthogonal.

1. Absence of Fluorescent Signal for Broad-Band Detection

The intensity of polarized fluorescent light may be independent of the excited-state polarization if all decay branches from the excited state are observed

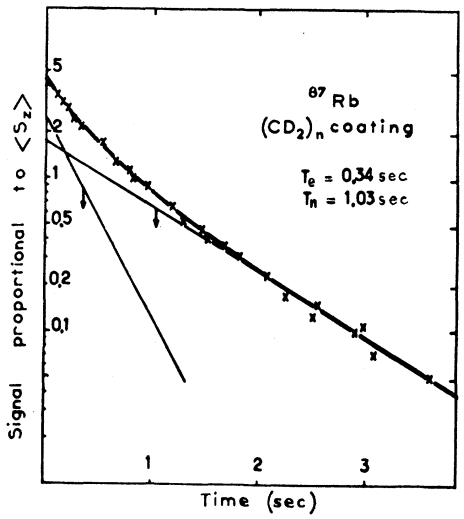

FIG. 19. Relaxation of $\langle S_z \rangle$ for ^{87}Rb atoms in a paraffin-coated cell. There are two time constants T_e and T_n [from (Bou63a, b)].

simultaneously. This is closely analogous to the absence of depopulation pumping for broad-line excitation (see Sec. III.A.14), and atomic states of the same type are involved (e.g., S states, or states with $J=0$). For example, if an excited $^2S_{1/2}$ state decays, there will normally be branches to both the $^2P_{1/2}$ and $^2P_{3/2}$ components of a fine structure doublet. The polarizations of the corresponding fluorescent intensities are very nearly equal and opposite, so that the total intensity will appear to be isotropic and unpolarized. Thus, to use fluorescence monitoring with a $^2S_{1/2}$ state, one must filter the fluorescent light in such a way that only one component of the fine structure doublet reaches the photodetector.

V. RELAXATION

Any optically pumped vapor will eventually reach a steady state if the pumping light, external fields, and other experimental parameters are maintained in a steady state. If one of the experimental parameters is changed suddenly to a new value, the atomic vapor will, after a certain time, relax to a new steady state. Relaxation can be caused by many mechanisms. Some of the most common are collisions of the polarized atoms with other atoms or molecules, collisions of the polarized atoms with the container walls, spatial diffusion of the polarized atoms from regions of high polarization to regions of lesser polarization, and trapping of resonance radiation. Indeed, optical pumping itself can be viewed as a relaxation mechanism in which an ensemble of atoms relaxes to a polarized steady state because of repeated collisions with the polarized, directional, or frequency-selected photons of the pumping light. Some of the common relaxation mechanisms that are known to play a role in optical pumping experiments are summarized in Table II.

The transient changes of atomic polarization that accompany a sudden change in external conditions are seldom characterized by a single exponential decay. For example, the decay of the longitudinal electronic spin $\langle S_z \rangle$ of ^{87}Rb atoms in a dark paraffin-coated cell is shown in Fig. 19. The decay is the sum of two exponentials with time constants T_e and T_n. Furthermore, different observables of the same atom relax in different ways. Thus, under the same conditions as those in Fig. 19, the observable $\langle \mathbf{S}\cdot\mathbf{I} \rangle$ relaxes as a single exponential and with a time constant T_H, which differs from both T_n and T_e.

A. Linear Relaxation

In a very widespread class of problems, the evolution of the density matrix in the interaction picture is governed by a set of coupled linear equations of the form

$$(d/dt)\sigma_{ij} = \sum_{rs} R_{ij;rs}\sigma_{rs} - \Gamma\sigma_{ij} + S_{ij}. \qquad \text{(V.1)}$$

Often, Eq. (V.1) is obtained by using the secular approximation (see Sec. II.E). The coupling of the various components of the density matrix is described by the constant coefficients $R_{ij;rs}$. We shall call the array of these coefficients the relaxation matrix. For instance, the rate of transfer of atoms from the sublevel j to the sublevel i is $R_{ii;jj}$. A simple example of a relaxation process is illustrated in Fig. 20, in which the $^2S_{1/2}$ ground state of an alkali atom with nuclear spin $I=\frac{3}{2}$ is sketched. We assume that the electron-spin polarization is destroyed at a rate T^{-1} but that the nuclear spin is unaffected by the collisions. We also assume that the time between collisions is much longer than the hyperfine periods of the atom. All nonzero population-transfer rates $R_{ii;jj}$ are indicated in the figure. More details about this type of relaxation by electron randomization can be found in Sec. V.C.1.

We shall assume that the process represented by the relaxation matrix neither creates nor destroys atoms. We assume that any actual destruction of atoms, which is represented by the second term on the right of Eq. (V.1), occurs at the same rate Γ from every sublevel. Such destruction might, for instance, be caused by chemical reaction with the walls, or in the case of an excited atom, by spontaneous decay. Depopulation pumping will not normally be considered a destruction

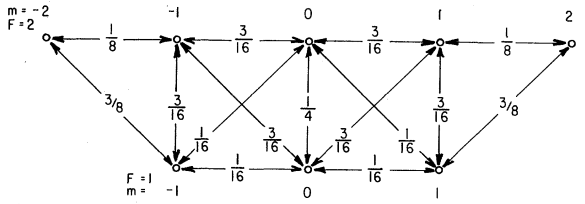

FIG. 20. The population-transfer rates between magnetic sublevels of a state with $J=\frac{1}{2}$ and $I=\frac{3}{2}$ when J is randomized but I is inert. The rates are expressed as multiples of the electron randomization rate, T^{-1}.

TABLE II. Some important relaxation mechanisms for polarized atoms.

Relaxation mechanisms	Potential	Typical relaxation phenomena	Typical σ in cm^2	References
Near field dipole–dipole	$(\mathbf{D}_A\cdot\mathbf{D}_B-3\mathbf{D}_A\cdot\hat{R}_{AB}\times\hat{R}_{AB}\cdot\mathbf{D}_B)R^{-3}$	Self-broadening of optical lines and self-depolarization of excited states; foreign gas broadening	10^{-13} (Resonant) 10^{-15} (Foreign gas)	Byr64a
Radiation-field dipole–dipole	$(\mathbf{D}_A\cdot\hat{R}_{AB}\hat{R}_{AB}\cdot\mathbf{D}_B-\mathbf{D}_A\cdot\mathbf{D}_B)k^2R^{-1}$	Radiation trapping; coherence narrowing	Relaxation times depend on container shape and can be orders-of-magnitude longer than the natural lifetime of the excited state	Bar59a, b
Spin-exchange between electrons	$V(R_{AB})\mathbf{S}_A\cdot\mathbf{S}_B$	Approach to spin temperature equilibrium. Conservation of total spin	10^{-14}	Pur56; Gro64a
Spin–orbit	$V(R)\mathbf{N}\cdot\mathbf{S}$	Disorientation of S-state atoms by wall collisions and buffer-gas collisions	10^{-19}–10^{-26}	Ber62
Spin-nuclear	$\mathbf{S}\cdot\mathfrak{T}(\mathbf{R})\cdot\mathbf{I}$	Disorientation of S-state atoms by wall collisions and buffer-gas collisions. Nuclear polarization by spin exchange with electrons	10^{-24}	Her65
Collisional modification of hfs coupling constants	$\delta A\,\mathbf{I}\cdot\mathbf{S}$	Pressure shift of hyperfine frequency	$\lvert\delta A\rvert\approx$KHz Torr^{-1}	Adr60a,b
Nuclear quadrupole	$-\frac{1}{6}\nabla\mathbf{E}:\mathfrak{Q}$	Wall relaxation of nuclear spins of diamagnetic atoms	Depends on sticking time at the wall, field gradients at wall, nuclear quadrupole moment, etc.	Coh63
Random motion in inhomogeneous magnetic field	$\dfrac{\mathbf{v}\cdot(\nabla\mathbf{H}\times\mathbf{H})\cdot\mathbf{I}}{H^2}$	Relaxation of ^{3}He ground-state atoms	Depends on field gradient and mean free path	Sch65; Gam65
Scattering of resonance light	$-(e/mc)\mathbf{p}\cdot\mathbf{A}$	Relaxation of pumped atoms to polarized equilibrium state	Typical pumping times are on the order of milliseconds or longer	Kas50
Diffusion	Diffusion rate is proportional to the kinetic mean free path and the mean velocity	Spatial motion of polarized atoms to the container walls by random walk through a buffer gas	Typical diffusion times at a few Torr pressure in a 10 cm cell are a few milliseconds	Mas67

mechanism for ground-state atoms, since the atoms return to the ground state very quickly by spontaneous decay.

We shall also assume that the process represented by the relaxation matrix does not involve the creation of atoms. We shall represent the rate of creation of polarized atoms by constant source matrix S_{ij} of Eq. (V.1). For example, the excitation rate $(d^{(2)}/dt)\rho_e$ of Eq. (III.71) can be considered to be a source matrix for the excited state.

Before obtaining the solutions to the inhomogeneous relaxation Eq. (V.1), it is convenient to discuss the solutions of the associated homogeneous equation:

$$(d/dt)\sigma_{ij}=\sum_{rs}R_{ij;rs}\sigma_{rs}. \qquad (V.2)$$

The solutions to the inhomogeneous Eq. (V.1) can be readily obtained in terms of the solutions of the homogeneous equation (V.2). In the following sections we shall discuss how a number of important properties of the solutions to Eq. (V.2) follow from physical considerations.

1. Relaxation Rates and Eigenobservables

Suppose that Eq. (V.2) has exponentially decaying solutions of the form

$$\sigma_{ij}(t)=v_{ij}\exp(-\gamma t). \tag{V.3}$$

The constant coefficients v_{ij} and the relaxation rate γ may be determined by substituting Eq. (V.3) into Eq. (V.2). In this way, one obtains the eigenvalue equations

$$\sum_{rs}[R_{ij;rs}+\delta_{ij;rs}\gamma]v_{rs}=0. \tag{V.4}$$

These equations have nontrivial solutions only when the determinant of the matrix in square brackets is zero, i.e.,

$$\det[R_{ij;rs}+\delta_{ij;rs}\gamma]=0. \tag{V.5}$$

The dimensionality of R is given by

$$N=(2I+1)^2(2J+1)^2. \tag{V.6}$$

There will be N roots,

$$\gamma=\gamma_k \qquad (k=1, 2, \cdots, N), \tag{V.7}$$

of the secular equation (V.5). Each root is a relaxation rate of the atoms, and the corresponding relaxation time is given by

$$T_k=(\gamma_k)^{-1}. \tag{V.8}$$

The relaxation rates γ_k will in general be complex; and, since the solution to Eq. (V.2) must remain finite, the real parts of the relaxation rates must be nonnegative:

$$\mathrm{Re}\gamma_k\geq 0. \tag{V.9}$$

For each relaxation rate γ_k, one can solve Eq. (V.4) for the corresponding coefficients $v_{ij;k}$. These coefficients can be used to define eigenobservables:

$$V_k=\sum_{rs}|r\rangle\langle s|\,v_{rs;k}. \tag{V.10}$$

The eigenobservables are not necessarily Hermitian, but if $V_k\neq V_k^\dagger$, then both V_k and $V_k^\dagger$ are eigenobservables, while γ_k and γ_k^* are the corresponding relaxation rates. If V_k is a relaxing eigenobservable, it is traceless (see Sec. V.A.5.a). That is

$$\mathrm{Tr}\,V_k=0, \tag{V.11}$$

if γ_k is not zero. Conversely, any eigenobservable with nonzero trace does not relax, i.e.

$$\gamma_k=0, \tag{V.12}$$

if Tr V_k is not zero.

One can assume that the V_k form a complete but not necessarily orthogonal set of operators. Although situations arise in which the V_k do not form a complete set (see Sec. V.A.3), they are quite uncommon. Thus, for any observable M, we can write

$$M=\sum_k M_k V_k \tag{V.13}$$

or

$$M_{ij}=\sum_k M_k v_{ij;k}. \tag{V.14}$$

The coefficients M_k can be determined by inverting Eq. (V.14). Then we have

$$M_k=\sum_{ij} v_{k;ij}^{-1}M_{ij}, \tag{V.15}$$

where the inverse matrix v^{-1} is defined by

$$\sum_{ij} v_{k;ij}^{-1}v_{ij;s}=\delta_{ks}. \tag{V.16}$$

The inverse matrix will exist, provided that the eigenobservables form a complete set.

The complete solution to the relaxation Eq. (V.2) is then

$$\sigma(t)=\sum_k \sigma_k(0)\,V_k\exp(-\gamma_k t), \tag{V.17}$$

and the decay of an arbitrary operator M is given by

$$\langle M\rangle=\mathrm{Tr}[\tilde{M}\sigma(t)]=\sum_k \sigma_k(0)\,\mathrm{Tr}[\tilde{M}V_k]\exp(-\gamma_k t). \tag{V.18}$$

Thus, the relaxation rate γ_k will contribute to the transient decay of $\langle M\rangle$ if the kth eigenobservable is present in the initial density matrix; i.e., if we have $\sigma_k(0)\neq 0$, and if the projection of $\tilde{M}$ on V_k is not zero; i.e., if Tr $[\tilde{M}V_k]\neq 0$.

2. The Steady-State Density Matrix

Regardless of the initial polarization of the density matrix, it will eventually relax to a unique steady state, and no further changes will occur. We can identify the steady-state density matrix with a Hermitian eigenobservable which we shall denote by V_0. The corresponding relaxation rate γ_0 is zero. Only one nonrelaxing eigenobservable can exist if the steady-state density matrix is unique.

Some simple examples will illustrate the significance of V_0. If no pumping mechanisms are present, the equilibrium density matrix is given by

$$V_0=c\exp(-H/kT), \tag{V.19}$$

where c is a constant of proportionality, H is the Hamiltonian operator of the atom, and kT is the mean thermal energy. For atomic ground states the energy splittings of the atomic sublevels are often so small compared to kT that the exponential function in Eq. (V.19) is nearly unity. Therefore, each of the G sublevels of the ground state has almost the same population, and we find

$$V_0=G^{-1}. \tag{V.20}$$

When the relaxation of the atoms is dominated by spin-exchange collisions with another polarized species, then the nonrelaxing observable will be approximately

$$V_0=N\exp(\beta F_z), \tag{V.21}$$

where F_z is the total angular momentum operator of the atom, $-\beta^{-1}$ is the spin temperature, and N is a constant of proportionality [see Sec. VI.A.3 for more details].

3. Nonexponential Decay

Although the transient decay of atomic polarization can usually be expressed as a sum of exponentials [see Eq. (V.17)], the homogeneous relaxation Eq. (V.2) can have nonexponential solutions if the decay rates γ are not all different. For instance, if two decay rates, γ_i and γ_j, are equal to each other, then in addition to the simple exponential solutions of the form $V_i \exp(-\gamma_i t)$, there may be other solutions of the form $V_i \exp(-\gamma_i t)+W_i t \exp(-\gamma_i t)$, where V_i and W_i are constant matrices. Such nonexponential transients are analogous to the response of a critically damped galvanometer, and they have been observed experimentally under special conditions by Dupont-Roc *et al.* (Dup68a) in ^{199}Hg.

Nonexponential decay does not normally occur just because several decay rates are equal. For instance, under isotropic conditions, all $(2L+1)$ components of the $(2)^L$ pole moment of an atom relax at the same rate (see Sec. V.A.5.d), but the transients still have the form of simple exponentials. Nonexponential decay occurs only if the eigenobservables V_k defined in Eq. (V.7) do not form a complete set of operators.

4. Relaxation with a Source of Polarization

The solutions to the inhomogeneous Eq. (V.1) may be obtained with the aid of the solutions to Eq. (V.2). Let us define a new relaxation matrix:

$$\bar{R}_{ij;rs}=R_{ij;rs}-\Gamma\delta_{ij;rs}. \tag{V.22}$$

Then the linear relaxation equation

$$\dot{\sigma}_{ij}=\sum_{rs} R_{ij;rs}\sigma_{rs} \tag{V.23}$$

has the same eigenobservables V_k as Eq. (V.2), but the corresponding relaxation rates differ by Γ, i.e.,

$$\bar{\gamma}_k=\gamma_k+\Gamma. \tag{V.24}$$

We note that

$$\sum_{rs} \bar{R}_{ij;rs}v_{rs;k}=-\bar{\gamma}_k v_{ij;k}. \tag{V.25}$$

Consequently, we have

$$\bar{R}_{ij;rs}=-\sum_k \bar{\gamma}_k v_{ij;k}v_{k;rs}^{-1} \tag{V.26}$$

and

$$\bar{R}_{ij;rs}^{-1}=-\sum_k \bar{\gamma}_k^{-1}v_{ij;k}v_{k;rs}^{-1}. \tag{V.27}$$

The solution to Eq. (V.1) is then

$$\sigma_{ij}(t)=\sum_k \{S_k(\bar{\gamma}_k)^{-1}[1-\exp(-\bar{\gamma}_k t))] +\sigma_k(0)\exp(-\bar{\gamma}_k t)\}v_{ij;k}. \tag{V.28}$$

The steady-state solution to Eq. (V.1) is then

$$\sigma_{ij}(\infty)=\sum_k S_k(\bar{\gamma}_k)^{-1}v_{ij;k}, \tag{V.29}$$

or, equivalently,

$$\sigma_{ij}(\infty)=\sum_{rs} R_{ij;rs}^{-1}S_{rs}. \tag{V.30}$$

5. Constraints on the Relaxation Matrix

Physical considerations place a number of important constraints on the elements of the relaxation matrix. Some of these constraints, such as those connected with the conservation of the total number of atoms or the Hermitian and positive-definite character of the density matrix, are almost always present. Other constraints, such as those connected with spherical or axial symmetry, occur in a limited but important class of problems.

a. Conservation of atoms. If the relaxation mechanism does not change the total number of atoms present in the vapor, Eq. (V.2) implies the condition

$$\sum_i R_{ii;rs}=0. \tag{V.31}$$

If we combine Eq. (V.31) with (V.4), we find

$$\gamma_k \operatorname{Tr} V_k=0. \tag{V.32}$$

Therefore, the trace of every relaxing ($\gamma_k\neq 0$) eigenobservable must be zero, and observables with nonzero trace do not relax.

b. Hermiticity of ρ. The density matrix of the system must be Hermitian at all times. Consequently, Eq. (V.2) implies

$$R_{ij;rs}^*=R_{ji;sr}. \tag{V.33}$$

An immediate consequence of Eqs. (V.33) and (V.4) is that if V_k is an eigenobservable that corresponds to the relaxation rate γ_k, then $V_k^\dagger$ is also an eigenobservable that corresponds to the relaxation rate γ_k^*. If γ_k is real, then we find $\gamma_k=\gamma_k^*$, and there are two possibilities: Either $V_k^\dagger$ and V_k are linearly independent, in which case Hermitian linear combinations can be chosen as new eigenobservables; or $V_k^\dagger$ is proportional to V_k, in which case V_k is Hermitian (or antiHermitian, so that iV_k is a Hermitian eigenobservable). In any case, real relaxation rates can be associated with Hermitian eigenobservables. If γ_k is complex, then V_k and $V_k^\dagger$ must be linearly independent, but they need not necessarily be Hermitian. Equation (V.33) also implies that population transfer rates $R_{ii;jj}$ are always real.

c. Positive definiteness of ρ. The diagonal matrix elements of ρ must be nonnegative, since they represent the probability of finding the atom in some eigenstate. Also, no diagonal matrix element of ρ can exceed unity. In order to ensure that these conditions are maintained in spite of relaxation, the following conditions must be satisfied

$$R_{ii;ii}\leq 0, \tag{V.34}$$

where $|i\rangle$ is any state of the atom. For example, suppose that $\rho_{ii}=1$ and all other components of ρ are zero. Then Eq. (V.2) implies $\dot{\rho}_{ii}=R_{ii;ii}$; and since ρ_{ii} is

already at its maximum value 1, it can only remain constant or decrease, which proves Eq. (V.34). We must also have

$$R_{jj;ii}\geq 0, \tag{V.35}$$

where $|i\rangle$ and $|j\rangle$ are any two orthogonal atomic states. If $\rho_{ii}=1$ and all other components of ρ are zero, then we have $\dot{\rho}_{jj}=R_{jj;ii}$. Therefore, since $\rho_{jj}=0$ is already at its minimum value, it can only remain constant or increase, which proves Eq. (V.35).

d. Isotropy. We now discuss a number of more specialized constraints associated with spatial rotations and reflections. The effects of these constraints on the relaxation matrix are most pronounced for an atom with a single Zeeman multiplet of spin I in the ground state, such as Hg or Cd. We shall limit our discussion to this case, although closely analogous considerations apply to atoms with hyperfine structure, e.g., the alkali atoms, in the low-field limit. It will be convenient to use the multipole representation. Then the relaxation Eq. (V.2) becomes

$$(d/dt)\sigma_{LM}=\sum_{L'M'} R_{LM;L'M'}\sigma_{L'M'}, \tag{V.36}$$

where

$$R_{LM;L'M'}=\sum_{mn}(-1)^{m-n+M-M'}C(IIL;m,M-m) \times C(IIL';n,M'-n)R_{m,m-M;n,n-M'}. \tag{V.37}$$

The coefficients $v_{LM;k}$ of the eigenobservables

$$V_k=\sum_{LM} v_{LM;k}T_{L-M}(II)(-1)^M \tag{V.38}$$

satisfy the eigenvalue equation [c.f., Eq. (V.4)]

$$\sum_{L'M'}[R_{LM;L'M'}+\gamma_k\delta_{LL'}\delta_{MM'}]v_{L'M';k}=0. \tag{V.39}$$

One can use Eq. (V.39) to show that the constraint associated with the conservation of atoms [Eq. (V.31)] becomes

$$R_{00;LM}=0, \tag{V.40}$$

and the constraint associated with Hermiticity is

$$R_{LM;L'M'}{}^*=(-1)^{M-M'}R_{L-M;L'-M'}. \tag{V.41}$$

Suppose that experimental conditions are isotropic; for instance, relaxation in the dark in the absence of any external field or other directional influences should be isotropic. Then if $\sigma(t)$ is a solution of Eq. (V.36), the density matrix

$$\sigma'(t)=\mathcal{R}\sigma(t)\mathcal{R}^{-1}, \tag{V.42}$$

which is obtained by rotating σ with any rotation operator $\mathcal{R}$, is also a solution. As a consequence, we can deduce

$$R_{LM;L'M'}=-\delta_{LL'}\delta_{MM'}\gamma_L. \tag{V.43}$$

That is, the relaxation matrix is diagonal and has only $2I+1$ different relaxation rates $\gamma_0, \gamma_1, \cdots, \gamma_{2I}$. There are $2L+1$ eigenobservables V_{LM} corresponding to the relaxation rate γ_L, and these can be chosen proportional to the spherical basis operators, i.e.,

$$V_{LM}=T_{LM}(II)\times \text{const.} \tag{V.44}$$

From Eq. (V.40) we deduce that

$$\gamma_0=0. \tag{V.45}$$

Therefore, the equilibrium density matrix is

$$V_0=T_{00}(II)(2I+1)^{-1/2}, \tag{V.46}$$

which represents a random distribution of atoms among the $2I+1$ atomic sublevels.

From Eqs. (V.41) and (V.43) we deduce that the multipole-relaxation rates are all real.

e. Axial symmetry. In many problems there is rotational symmetry about only one axis in space. For instance, the symmetry axis might be provided by the direction of an external electric or magnetic field, or, in the absence of external fields, by the propagation direction of an unpolarized or circularly polarized light beam. If $\sigma(t)$ is a solution to Eq. (V.2) then the density matrix

$$\sigma'(t)=\mathcal{R}_\phi\sigma\mathcal{R}_\phi^{-1}, \tag{V.47}$$

which is obtained by rotating σ by an angle ϕ about the symmetry axis, is also a solution of Eq. (V.2). As a consequence, the relaxation matrix obeys the constraint

$$R_{LM;L'M'}=\delta_{MM'}R_{LM;L'M}. \tag{V.48}$$

That is, when axial symmetry is present, relaxation cannot couple components of the density matrix that have different values of the axial angular momentum M. Consequently, the eigenobservables have well-defined axial angular momentum. Since the eigenobservables with nonzero M are traceless, they must all eventually relax to zero, i.e., the associated relaxation rates are nonzero. Thus, the equilibrium density matrix (the nonrelaxing eigenobservable V_0) must have no axial angular momentum.

Using Eq. (V.48) together with Eq. (V.39) one can show that if

$$V_{KM}=\sum_L v_{L-M;K}T_{LM}(-1)^M \tag{V.49}$$

is an eigenobservable with axial angular momentum M and relaxation rate γ_{LM}, then

$$V_{K-M}=(V_{KM})^\dagger(-1)^M \tag{V.50}$$

is another eigenobservable with axial angular momentum $-M$ and a relaxation rate $\gamma_{KM}{}^*$. We do not mean to imply that K is the total angular momentum of the eigenobservable. It is simply a label to distinguish different eigenobservables with the same axial angular momentum.

f. Even and odd polarizations. Let us call a multipole operator T_{LM} even if L is even, and odd if L is odd. In some axially symmetric relaxation processes, there is an additional symmetry that causes even multipoles to couple only to even multipoles and odd multipoles to

couple only to odd multipoles. We shall not discuss the underlying reasons for this even–odd symmetry, but the formal consequence is that

$$R_{LM;L'M}=0 \tag{V.51}$$

unless $(L+L')$ is even.

As a consequence of Eqs. (V.51) and (V.39), we infer that all eigenobservables will be even or odd. Since all odd eigenobservables are traceless, they must relax to zero, and the equilibrium eigenobservable is therefore even and has zero axial angular momentum $(M=0)$.

Some examples of relaxation processes where even–odd symmetry is present in addition to axial symmetry are zero-field optical pumping with unpolarized or linearly polarized light and high-field relaxation resulting from a weak, rapidly fluctuating perturbation. Some axially symmetric relaxation processes that do not have even–odd symmetry are zero-field optical pumping with circularly polarized light and relaxation by spin exchange with polarized atoms.

B. Relaxation due to a Weak Fluctuating Perturbation

In many situations, the relaxation of polarized atoms results from a very weak perturbation. For instance, a polarized mercury atom may make thousands of collisions against the walls of a quartz container before losing its polarization, and a rubidium atom can make billions of collisions against helium atoms before being depolarized. Under such conditions, one can assume that the Hamiltonian for a given atom of the vapor has the form

$$\mathcal{H}=\mathcal{H}_0+V(t). \tag{V.52}$$

The static part of the Hamiltonian, $\mathcal{H}_0$, is the same for all atoms of the vapor. A weak, fluctuating perturbation, which varies in a random manner from atom to atom, is represented by $V(t)$. In the interaction picture the perturbation is

$$\tilde{V}(t)=\exp(i\mathcal{H}_0 t)\,V\exp(-i\mathcal{H}_0 t). \tag{V.53}$$

According to the general theory of relaxation by a weak fluctuating perturbation (Abr61), the evolution of the density matrix is governed by the equation

$$\frac{d}{dt}\sigma=-\left\langle\int_0^\infty[\tilde{V}(t),[\tilde{V}(t-\tau),\sigma(t)]]d\tau\right\rangle_{\text{Av}}. \tag{V.54}$$

The symbol $\langle\ \rangle_{\text{Av}}$ denotes an ensemble average over all atoms of the vapor, and the square brackets denote commutators.

1. Relaxation on the Walls

Upon striking the wall of a container, an atom does not necessarily rebound, but may stick to the wall for a certain time. While the atom is on the wall, it may hop from site to site as a result of thermal agitation. Eventually, the atom will acquire enough thermal energy to shake loose from the wall. According to the theory of physical absorption (DeB63), the average dwell time of the atom on the wall is given by

$$\tau_s=\tau_0\exp(E_a/kT), \tag{V.55}$$

where E_a ($\sim$0.1 eV) is the binding energy of the atom to the surface, and T is the absolute temperature of the wall. The constant τ_0 ($\sim10^{-12}$ sec) is a time on the order of a vibrational period of the atom on the surface. The average dwell time of an atom at a given site on the wall is

$$\tau_s'=\tau_0'\exp(\Delta E_a/kT), \tag{V.56}$$

where ΔE_a is a measure of the difference in binding energies between different sites on the wall. During the time the atom is stuck to the walls, it will be subject to various random perturbations which will cause it to depolarize. The time dependence of the perturbation is illustrated schematically in Fig. 21.

When the atom breaks loose from the wall, it may fly undisturbed through the cell if no buffer gas is present and if the vapor pressure of the pumped atoms is low enough. Under these conditions, relaxation occurs only during those periods of time when the atom is stuck to the walls. The average time of flight from wall to wall is

$$\tau_v=l/v\sim10^{-4}\text{ sec},$$

where l is a characteristic linear dimension of the cell, and v is the mean velocity of the atom.

Equation (V.54) should therefore be modified to read

$$(d/dt)\sigma=-\tau_s/(\tau_v+\tau_s)\times\int_0^\infty\langle[\tilde{V}(t),[\tilde{V}(t-\tau),\sigma(t)]]d\tau\rangle_{\text{Av}}. \tag{V.57}$$

Here V is the interaction experienced by the atom while it is stuck to the walls.

In all experiments on wall relaxation that have been performed so far, it is found that the relaxation times are proportional to the linear dimensions of the cell. This implies that the sticking times are much shorter than the times of flight.

$$\tau_s\ll\tau_v.$$

2. The Interaction $V(t)$

In order to evaluate Eq. (V.54) or Eq. (V.57), one must have some knowledge of the perturbation V. Specifically, it is necessary to know the strength, the angular dependence, and the correlation time of V. One usually assumes that the interaction results from the coupling of some multipole moment of the atom with an external field, i.e.,

$$V(t)=\sum_m F_{lm}(t)T_{l,-m}(-1)^m. \tag{V.58}$$

Here T_{lm} is the $(2)^l$ pole moment operator of the atom. The fluctuating tensor components $F_{lm}(t)$ are further assumed to be isotropic and to have an exponential

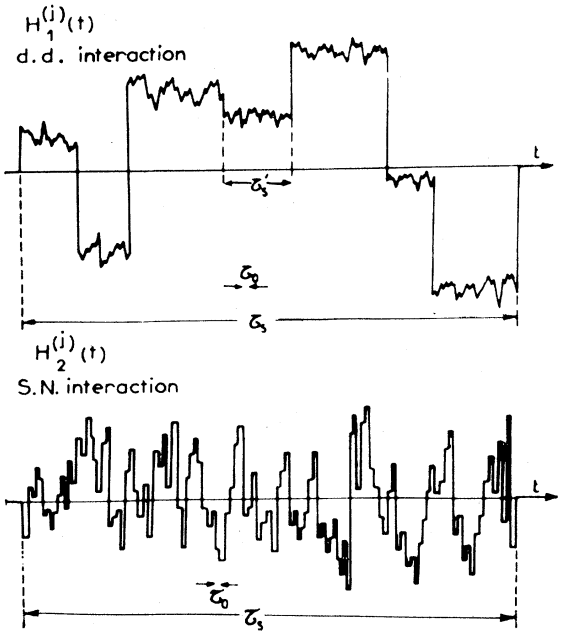

FIG. 21. Schematic time dependence of the perturbation experienced by an alkali atom on a paraffin coated wall. The nuclei of the wall material produce nearly static local fields that change abruptly as the atom hops from site to site on the wall. The vibrational motion of the atom at a given site produces a rapidly fluctuating spin-orbit interaction [from (Bou63a, b)].

autocorrelation function, i.e.,

$$\langle F_{lm}(t)F_{ln}(t-\tau)\rangle_{Av}=f^2\delta_{n,-m}(-1)^m \times \exp(-\tau/\tau_c)/(2l+1). \quad \text{(V.59)}$$

According to the Wiener–Khintchine theorem, the power spectrum $J(\omega)$ of the perturbation is proportional to the cosine Fourier transform of the autocorrelation function, so that we have

$$J(\omega)=1/[1+(\omega\tau_c)^2]. \quad \text{(V.60)}$$

Thus, the spectral width of the perturbation is on the order of $1/\tau_c$, and the perturbation will be most efficient in causing transitions between energy levels E_i and E_j such that

$$|E_i-E_j|<1/\tau_c. \quad \text{(V.61)}$$

Although the theory can be developed for more complicated autocorrelation functions, the simple exponential autocorrelation function seems adequate to describe the existing experimental data. However, it is often necessary to postulate several independent perturbations of different strength, multipolarity, and correlation time.

3. *Relaxation within a Single Zeeman Multiplet*

The relaxation caused by a weak fluctuating perturbation is particularly simple (Hap70) for an isolated Zeeman multiplet of angular momentum K, for instance, in the ground state of ^{199}Hg or ^{111}Cd. In the limit of a very small external magnetic field, the environment is essentially isotropic, and each $(2)^L$ pole relaxes independently with a relaxation rate (see Fig. 22)

$$\gamma_L(l)=2f^2\tau\{(2K+1)^{-1}-W(LKKl;KK)\}. \quad \text{(V.62)}$$

Here l is the multipolarity of the interaction, f^2 is the mean squared amplitude, and τ is the correlation time [see Eq. (V.59)]. In the special case of a fluctuating magnetic field of rms amplitude h, Eq. (V.62) reduces to

$$\gamma_L(1)=(h\gamma)^2\tau L(L+1)/3, \quad \text{(V.63)}$$

where γ is the gyromagnetic ratio of the multiplet; i.e., the Larmor frequency in radians/sec in a magnetic field H is $\omega=\gamma H$.

For nonzero magnetic fields, a simple solution of the relaxation equations can be found only for the case of a magnetic perturbation. Then, the relaxation equation becomes

$$(d/dt)\sigma_{LM}=-\gamma_{LM}\sigma_{LM}. \quad \text{(V.64)}$$

Here the relaxation rates are

$$\gamma_{LM}=\gamma_L(1)J_{LM}(\omega\tau), \quad \text{(V.65)}$$

and the function is

$$J_{LM}(x)=[1/L(L+1)] \times\{M^2+[(L^2-M^2+L)/(1+x^2)]\} -iMx[L(L+1)(1+x^2)]. \quad \text{(V.66)}$$

The imaginary parts of the relaxation rates give rise to a small frequency shift

$$\Delta\omega=(1/3)(h\gamma)^2\tau\omega\tau/[1+(\omega\tau)^2]. \quad \text{(V.67)}$$

The Zeeman splitting of the relaxation rates is illustrated in Fig. 23. High-field relaxation is rather complicated when the relaxation is caused by quadrupole or higher order interactions. Then, although M and the even–odd symmetry remain good quantum numbers, L does not. Unfortunately, there are often several independent even or odd observables of the same M, and the eigenobservables must be obtained by solving Eq. (V.39). Although the procedures are straightforward, there seems to be no simple closed-form expression for the eigenobservables and the relaxation rates.

For ^{201}Hg ($I=\frac{3}{2}$) the high-field relaxation rates that would be caused by a fluctuating electric field gradient have been calculated by Cohen–Tannoudji (Coh63). At zero magnetic field there is a curious accidental degeneracy of the dipole and octupole relaxation rates (see Fig. 22), and the quadrupole relaxation rate is twice as great as the dipole relaxation rate.

In the case of the longitudinal observables, there is in addition to the isotropic observables T_{00} only one other even observable T_{20}. Since the equilibrium polarization is a random distribution, the steady-state density matrix V_0 of Sec. V.A.2 is T_{00}. Thus, T_{20} is also an eigenobservable for arbitrary values of the external

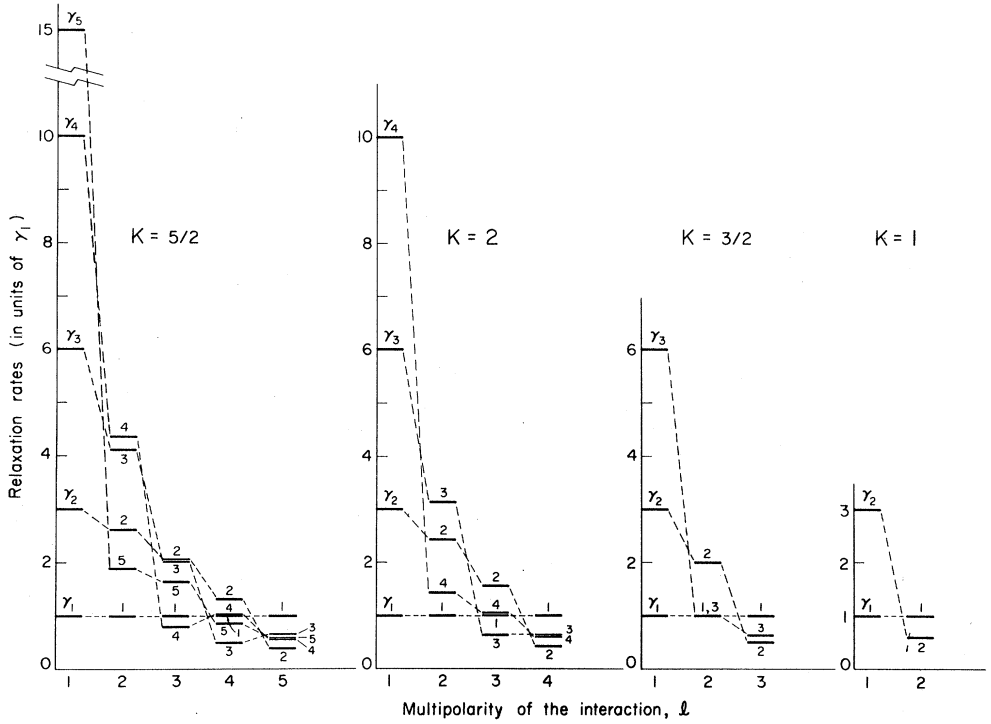

FIG. 22. Multipole-relaxation rates. For isotropic conditions the multipole polarizations of an ensemble of spin-K atoms have characteristic relaxation rates that depend on which atomic $(2)^l$ pole moment is coupled to the external perturbation [from (Hap70)].

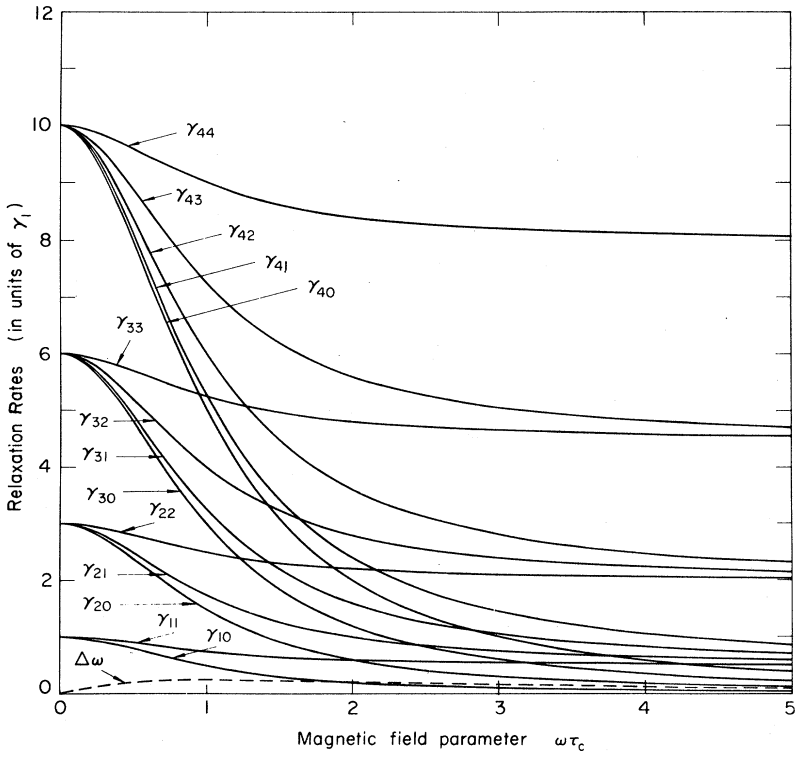

FIG. 23. Zeeman splitting of the multipole-relaxation rates. The m degeneracy of the multipole-relaxation rates is partially removed by a strong external magnetic field. [from (Hap70)].

field. The two odd eigenobservables, V_{10} and V_{30}, are linear combinations of T_{10} and T_{30}

$$V_{10}=(1/5^{1/2})(2T_{10}-T_{30}), \quad \text{(V.68)}$$

$$V_{30}=(1/5^{1/2})(T_{10}+2T_{30}). \quad \text{(V.69)}$$

The corresponding relaxation rates are

$$\gamma_{10}=\gamma_1(2)J_{10}(2\omega\tau) \quad \text{(V.70)}$$

and

$$\gamma_{30}=\gamma_1(2)J_{10}(\omega\tau), \quad \text{(V.71)}$$

where $\gamma_1(2)$ is defined by Eq. (V.62), and the function J_{10} is defined in Eq. (V.66). The relaxation rate of T_{20} is

$$\gamma_{20}=\tfrac{1}{2}\gamma_2(2)[J_{10}(\omega\tau)+J_{10}(2\omega\tau)]. \quad \text{(V.72)}$$

Analogous expressions for the transverse eigenobservables and relaxation rates have been calculated by Cohen-Tannoudji (Coh63).

4. *Relaxation of a Spin-$\frac{1}{2}$ Atom*

Consider an atom with electronic angular momentum $J=\frac{1}{2}$ and arbitrary nuclear spin I. The atom experiences a weak fluctuating magnetic field of root mean square amplitude h and correlation time τ [see Eq. (V.59)]. We assume that the interaction of the nucleus with the external field is negligibly small. In the limit of very short correlation times, this type of relaxation is completely equivalent to relaxation by electron randomization (see Sec. V.C) at a rate

$$1/T=2(h\gamma)^2\tau/3, \quad \text{(V.73)}$$

where γ is the gyromagnetic ratio of the electronic angular momentum J. For longer correlation times, the power spectrum of the perturbation is no longer constant at all the atomic transition frequencies, and the relaxation is no longer of exactly the same type as that caused by electron randomization. However, we shall still retain the time T^{-1} defined in Eq. (V.73) as a useful unit of measurement for the various relaxation rates.

We shall find it convenient to discuss the relaxation equation for several different regions of magnetic field strength.

a. Weak magnetic fields. For weak magnetic fields (we shall define "weak" more precisely later), the relaxation Eq. (V.54) reduces to

$$\begin{aligned}(d/dt)\sigma_{LM}(ff)=&-\{\Gamma(ff')/[1+(\omega_{ab}\tau)^2]\\&+L(L+1)J_{LM}(\omega_f\tau)/2T(2I+1)^2\}\sigma_{LM}(ff)\\&+\{\Gamma(f'f)/[1+(\omega_{ab}\tau)^2]\}(2f'+1)\\&\times W(1ff'L;f'f)\sigma_{LM}(f'f')\exp(2i\omega_{f'}Mt),\end{aligned} \quad \text{(V.74)}$$

where the Larmor frequency of the multiplet f is ω_f, and $f\neq f'$. The rate $\Gamma(ff')$ is

$$\Gamma(ff')=(2f'+1)/2T(2I+1). \quad \text{(V.75)}$$

The terms in Eq. (V.74) have a straightforward physical meaning. The term involving $\Gamma(ff')$ represents the transfer of atoms from the multiplet f to the multiplet f'. It is proportional to the spectral density

$$1/[1+(\omega_{ab}\tau)^2]$$

of the perturbation at the hyperfine frequency ω_{ab}. The multipole relaxation rate within a given Zeeman multiplet is given by the term proportional to $L(L+1)$ of Eq. (V.74) It is closely analogous to Eq. (V.64) for multipole relaxation of an isolated spin multiplet due to a fluctuating magnetic field. The last term of Eq. (V.74) represents the repopulation of the multiplet f due to transfer of atoms from the multipet f'. It is closely analogous to the expression of Eq. (III.83) for repopulation pumping of the ground state.

As Eq. (V.74) shows, if a $(2)^L$ pole moment exists in both Zeeman multiplets of the atomic ground state, these multipoles will be coupled to each other by the relaxation process. Let us first consider the zero-field relaxation. Equation (V.74) will in general lead to two eigenobservables for each multipolarity. We denote these eigenobservables by V_{LM}^+ and V_{LM}^-, where

$$\begin{aligned}V_{LM}^+=N(&\{[(2I+1)-L][(2I+1)+L+1]\}^{1/2}T_{LM}(aa)\\&\times\{[(2I+1)+L][(2I+1)-L-1]\}^{1/2}T_{LM}(bb)),\end{aligned} \quad \text{(V.76)}$$

and

$$\begin{aligned}V_{LM}^-=N(&\{[(2I+1)+L][(2I+1)-L-1]\}^{1/2}T_{LM}(aa)\\&-\{[(2I+1)-L][(2I+1)+L+1]\}^{1/2}T_{LM}(bb)),\end{aligned} \quad \text{(V.77)}$$

where $a=I+\frac{1}{2}$ and $b=I-\frac{1}{2}$.

The normalizing constant is

$$N=[2(2I+1)^2-2L(L+1)]^{-1/2}.$$

The corresponding relaxation rates are

$$\begin{aligned}\Gamma_{LM}^-=&J_{10}(\omega_{ab}\tau)/T+[L(L+1)/2T(2I+1)^2]\\&\times[J_{L0}(\omega_f\tau)-J_{10}(\omega_{ab}\tau)],\end{aligned} \quad \text{(V.78)}$$

$$\Gamma_{LM}^+=[L(L+1)/2T(2I+1)^2][J_{L0}(\omega_f\tau)+J_{10}(\omega_{ab}\tau)]. \quad \text{(V.79)}$$

Some of the simpler eigenobservables are

$$V_{00}^+=[2(2I+1)]^{-1/2}, \quad \text{(V.80)}$$

$$V_{00}^-=\{\sqrt{2}/[I(I+1)(2I+1)]^{1/2}\}\mathbf{I}\cdot\mathbf{S}, \quad \text{(V.81)}$$

$$V_{10}^+\propto\bar{I}_z, \quad \text{(V.82)}$$

$$V_{10}^-\propto\bar{S}_z-2\bar{I}_z/[(2I+1)^2-2]=Q_e. \quad \text{(V.83)}$$

In the last two expressions, the bar over I_z and S_z indicates that only the Zeeman components are retained. That is, for any operator M, we have

$$\bar{M}=\sum_{fmm'}|fm\rangle\langle fm|M|fm'\rangle\langle fm'|. \quad \text{(V.84)}$$

Bouchiat (Boua,b,c) designates the relaxation rates associated with I_z and Q_e, respectively, as

$$1/T_n=\Gamma_{10}^+ \quad \text{(V.85)}$$

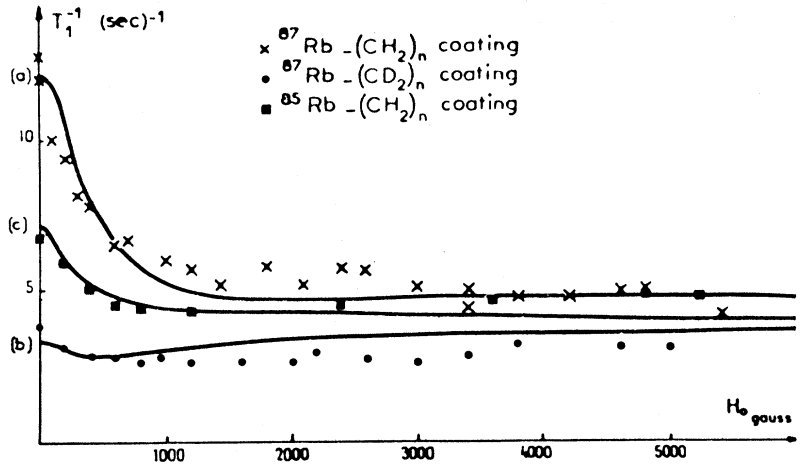

FIG. 24. Magnetic field dependence of the relaxation of $\langle S_z \rangle$. At least two different fluctuating perturbations, such as those sketched in Fig. 21, are necessary to fit these data [from (Bou63a, b)].

and

$$1/T_e = \Gamma_{10}^{-}. \tag{V.86}$$

In somewhat more generality, one can show

$$V_{LM}^{+} \propto \bar{T}_{LM}(II). \tag{V.87}$$

Since the multipolarities $L=2I$ and $L=2I+1$ can only occur in the hyperfine multiplet with $f=a=I+\frac{1}{2}$, the eigenobservables are simply

$$V_{2I,M} = T_{2I,M}(aa) \tag{V.88}$$

and

$$V_{2I+1,M} = T_{2I+1,M}(aa), \tag{V.89}$$

with relaxation rates (for $\tau \to 0$)

$$\Gamma_{2I,M} = (1/T)\,2I/(2I+1)\,;\ \Gamma_{2I+1,M} = 1/T. \tag{V.90}$$

b. Decoupling of the eigenobservables in a magnetic field. When the Larmor frequency of the atoms exceeds the characteristic relaxation rate T^{-1}, the transverse polarization components of the two hyperfine multiplets, which are coupled at zero field, become decoupled. However, in the case of the longitudinal eigenobservables, i.e., the $V_{L0}^{\pm}$ of the previous section, the magnetic field has no appreciable effect until it is so large that $\mathbf{F}=\mathbf{I}+\mathbf{J}$ ceases to be an approximately good quantum number. The eigenobservables for coherence, however, can be almost completely decoupled well before F ceases to be a fairly good quantum number.

Let us consider the transverse Zeeman coherence. Because the Larmor frequencies of the upper and lower Zeeman multiplets are approximately equal and opposite, the coupling term in Eq. (V.74) is modulated at multiples of the Larmor frequency for the transverse components. Solutions to Eq. (V.74) are readily obtained by making the substitution

$$\sigma_{LM}'(ff) = \sigma_{LM}(ff) \exp(iM\omega_f t). \tag{V.91}$$

One finds that the transverse multipole components are effectively coupled only when $\omega_f T \ll 1$. For higher fields, where $\omega_f T \lesssim 1$ but where the different ($\Delta F=0$, $\Delta m=1$) transitions are completely unresolved, the transverse multipole moments of each Zeeman multiplet relax independently at a rate

$$\gamma_{LM}(ff) = \Gamma(ff')/[1+(\omega_{ab}\tau)^2] + [L(L+1)/2I(2I+1)^2]J_{LM}(\omega_f\tau). \tag{V.92}$$

At still higher magnetic fields the different ($\Delta F=0$, $\Delta m=1$) transitions become resolved because of the repulsion of energy levels from different Zeeman multiplets. Consequently, each individual $\Delta m=1$ transition relaxes independently from all the others. A similar decoupling of individual hyperfine transitions occurs as soon as $\omega_f T \gg 1$. The secular approximation to Eq. (V.54) for a well-resolved resonance is then

$$(d/dt)\langle fm \mid \sigma \mid f'm' \rangle = -\gamma(fm; f'm')\langle fm \mid \sigma \mid f'm' \rangle. \tag{V.93}$$

The relaxation rates of Eq. (V.93) are listed in Table III. For simplicity, we have only listed values for a very short correlation time τ_c.

Relaxation rates in ^{87}Rb for arbitrary correlation times were tabulated by Bouchiat (Bou63a,b).

c. Intermediate fields. The relaxation of an alkali atom at intermediate fields, i.e., at fields where neither the quantum numbers (Fm) or $(m_I m_S)$ can be considered particularly good, is very complicated because little symmetry remains. Direct diagonalization of the relaxation matrix of Eq. (V.4) is possible with electronic computers, and this process has been used by Bouchiat (Bou63a,b) for the case of an alkali atom with nuclear spin $I=\frac{3}{2}$. In this case, there are $4I+1=7$ longitudinal relaxation rates and seven longitudinal eigenobservables, all of which contribute to the relaxation of $\langle S_z \rangle$. To extract seven relaxation rates from one somewhat noisy experimental decay curve is a hopeless task. In order to make the analysis of experimental

TABLE III. Relaxation rates $\gamma(fm; f'm)$ for well-resolved Zeeman transitions in terms of the electron randomization rate T^{-1}.

f	m	f'	m'	$T\gamma(fm; f'm')$
$I\pm\frac{1}{2}$	m	$I\pm\frac{1}{2}$	$m-1$	$\frac{3(2I+1)^2-4m(m-1)}{4(2I+1)^2}$
$I+\frac{1}{2}$	m	$I-\frac{1}{2}$	m	$\frac{3(2I+1)^2-4m^2}{4(2I+1)^2}$
$I+\frac{1}{2}$	m	$I-\frac{1}{2}$	$m\pm1$	$\frac{3(2I+1)^2+4m(m\pm1)}{4(2I+1)^2}$

data more tractable, Bouchiat (Bou63a,b) has defined a pseudorelaxation rate T_1^{-1} which describes the main features of the decay curve. The precise definition of the pseudorelaxation time and comparisons with experimental data can be found in the reference (Bou63a,b).

Studies of the magnetic field dependence (Fig. 24) of the pseudorelaxation time have contributed a great deal toward elucidating the mechanism of wall relaxation. Experiment shows (Bou63a,b) that for relaxation on paraffin walls, there seem to be at least two interactions of quite different correlation times. It is believed that a short correlation time ($\tau\simeq10^{-12}$ sec) is associated with vibrations of the alkali atom around its equilibrium position while it is stuck to a given site on the wall. A longer correlation time is believed to be associated with occasional hops from site to site on the wall. The interaction associated with the long correlation time almost certainly results from the magnetic fields produced by the nuclei of the wall, since deuterated walls cause much slower relaxation than hydrogenated walls. However, the short-correlation-time interaction is the same on both hydrogenated and deuterated walls and seems to be related to the spin–orbit interaction.

d. High fields. In the limit of extremely high magnetic fields, the nuclear spin is decoupled completely from the electronic spin and can be ignored. The relaxation then becomes very simple, and the spin-$\frac{1}{2}$ atom relaxes with a single longitudinal relaxation time (called τ_1) and a single transverse relaxation time (called τ_2). Franz (Fra71) has measured the relaxation rates of cesium at magnetic fields up to 100 kG, and finds reasonable agreement between the high-field longitudinal relaxation rate and the intrinsic spin-randomization rate deduced from low-field measurements.

5. Relaxation due to Inhomogeneous Magnetic Fields.

The relaxation of helium-3 ground-state atoms can be extremely slow because of the weak coupling of the nuclear moment to external perturbations. Relaxation times on the order of hours are not unusual. Under these conditions, relaxation is often caused largely by slight gradients in the static magnetic field through which the atoms move with thermal velocities. This type of relaxation has been investigated by Schearer and Walters (Sch65) and by Gamblin and Carver (Gam65).

If the atom moves through a magnetic field that is not constant in space, the direction of the nuclear spin will not follow the field direction adiabatically; rather, there will be slight changes in the angle between the spin and the local field direction. The rotation of the atomic spin with respect to the local field occurs as if the atom were subject to an effective field

$$\mathbf{H}_{\text{eff}}=\mathbf{v}\cdot[(\nabla\mathbf{H})\times\mathbf{H}](1/\gamma H^2), \qquad (V.94)$$

where $\mathbf{v}$ is the velocity of the atom, $\mathbf{H}$ is the local field, and γ is the gyromagnetic ratio (the Larmor frequency is $\omega=\gamma H$). The effective field is transverse to $\mathbf{H}$, and, as one can see from Eq. (V.94), it is proportional both to the velocity of the atoms and to the field gradient.

One can use Eqs. (V.94) and (V.54) to show that the longitudinal relaxation rates are

$$\gamma_{L0}=[L(L+1)\tau_c v^2(|\nabla H_x|^2 + |\nabla H_y|^2)]\{6H^2[1+(\omega\tau_c)^2]\}^{-1}. \qquad (V.95)$$

In Eq. (V.95), the correlation time τ_c is on the order of the time between velocity-changing collisions, $v=3kT/M$ is the mean square velocity, and one assumes that both the magnetic field H and the gradients are approximately constant over the volume of the container. The special case of Eq. (V.95) for $L=1$ was first derived by Schearer and Walters (Sch65) and Gamblin and Carver (Gam65). Equation (V.95) is closely related to Eq. (V.63), which describes the relaxation rates in a fluctuating magnetic field. The transverse relaxation rates are hard to define for an inhomogeneous field and will not be discussed here.

C. Relaxation due to Strong Collisions

There is another important class of relaxation phenomena, exemplified by spin-exchange relaxation, excited-state relaxation, or molecular formation, where the polarization of an atom is drastically changed by even a single collision. In the case of binary collisions, relaxation by strong collisions will be characterized by cross sections on the order of gas kinetic cross sections. The relaxation can be analyzed as follows. Suppose that the average result of a collision is to transform the initial density matrix ρ into a modified density matrix ρ^c. We denote the mean time between collisions by T. Then over any small time interval Δt, a fraction $\Delta t/T$ of atoms will have experienced collisions, and a fraction $(1-\Delta t/T)$ will not have collided. The change in the density matrix to first order in Δt is therefore

$$\Delta\rho=(1/i\hbar)[\mathcal{H},\rho]\Delta t+(\Delta t/T)(\rho^c-\rho), \qquad (V.96)$$

from whence we derive the differential equation

$$d\rho/dt=(1/i\hbar)[\mathcal{H},\rho]-(1/T)(\rho-\rho^c). \quad \text{(V.97)}$$

Equation (V.97) can be solved once ρ^c is known. In many cases ρ^c is linearly dependent on ρ, or, equivalently σ^c is linearly dependent on σ:

$$\sigma_{ij}^c=\sum_{rs} C_{ij;rs}\sigma_{rs}. \quad \text{(V.98)}$$

In this case we can immediately write the relaxation matrix

$$R_{ij;rs}=(1/T)(C_{ij;rs}-\delta_{ij;rs}). \quad \text{(V.99)}$$

The linear relationship of Eq. (V.98) does not hold for spin-exchange collisions between identical atoms. Nevertheless, the basic relaxation equation for strong collisions, Eq. (V.97), is valid whether or not a linear relationship relates ρ^c to ρ.

With the exception of "sticking" collisions, which have been discussed by Bouchiat (Bou70), strong collisions occur over a time interval on the order of 10^{-12} seconds. For such short times, the influence of external electric or magnetic fields or of hyperfine interactions on the electronic polarization is usually negligible compared to the collisional interactions. Consequently, the electronic but not the nuclear polarization is affected by the collision. However, recoupling of the electronic polarization to the nucleus or to external fields during the intervals between collisions does have an important effect on the relaxation process. Formally, the influence of the nuclear-electronic recoupling can be taken into account by proper use of the secular approximation; i.e., the rapidly oscillating parts of σ_c are simply dropped from the Liouville equation.

1. Relaxation of a Spin-$\frac{1}{2}$ Atom by Electron Randomization

As a simple example of relaxation by strong collisions, let us consider the case where the electronic spin of the atom is $J=\frac{1}{2}$, and the nuclear spin I is arbitrary. We shall suppose that every collision completely destroys the electronic polarization. The density matrix before collisions is [see Eq. (II.29)]

$$\rho=\alpha+\mathbf{A}\cdot\mathbf{J}, \quad \text{(V.100)}$$

and the density matrix after a collision is

$$\rho^c=\alpha. \quad \text{(V.101)}$$

Consequently, the evolution of the density matrix is given by [see Eq. (V.97)]

$$(d/dt)\sigma=-(1/T)\sigma+(1/T)\exp(i\mathfrak{H}t)\alpha\exp(-i\mathfrak{H}t). \quad \text{(V.102)}$$

Further reduction of Eq. (V.102) using Eq. (II.32) and the secular approximation leads to Eq. (V.74) for the limiting case $\tau_c\to 0$. That is, relaxation of an alkali-atom ground state by electron randomization is completely equivalent to relaxation by a very rapidly fluctuating magnetic field. Thus, one can use the formulas in Sec. V.B.4 to describe relaxation by electron randomization by setting $\tau_c=0$ and regarding T as the time between randomizing collisions.

2. Relaxation of Atoms with $J>\frac{1}{2}$

a. No hyperfine structure. We shall only consider the case of strong isotropic collisions. Then, according to the considerations of Sec. V.A.5.e, the relaxation of an atom without hyperfine structure is described by $(2J+1)$ relaxation rates γ_L, one for each $(2)^L$ pole moment. The relaxation equation is

$$(d/dt)\rho=-\sum\gamma_L\rho_L(JJ)\cdot T_L(JJ). \quad \text{(V.103)}$$

Unless quenching is present the atoms will not be removed from the multiplet J, and the monopole relaxation rate γ_0 will be zero. There are only a few situations in which this simple type of relaxation occurs for atoms that can be optically pumped. Such a situation can occur, for instance, in the relaxation of the $^3S_1$ state of metastable helium-4, and in the relaxation of the excited $^2P_{3/2}$ state of Sr^+.

The actual values of the multipole relaxation rates depend on the type of interaction involved during the collision. Completely depolarizing "hard" collisions relax the multipole moments at the same rate, while partially depolarizing "soft" collisions cause the different multipole moments to relax at different rates. For states with nonzero orbital angular momentum the dominant relaxation mechanism is usually the electrostatic dipole-dipole interaction

$$V=[\mathbf{D}\cdot\mathbf{P}-3(\mathbf{D}\cdot\hat{R})(\hat{R}\cdot\mathbf{P})]R^{-3} \quad \text{(V.104)}$$

between the electric dipole moment $\mathbf{D}$ of the polarized atom and the electric dipole moment $\mathbf{P}$ of the depolarizing atom. The separation between the atoms is R. Since the atomic states have well-defined parity, the odd operator (V.104) must usually be taken in second order, and rough estimates of the effective second order interaction, based on closure sum rules, are usually made. However, if the colliding atoms are identical, and one atom is in an excited state while the other is in a lower state in which the excited atom could decay by an allowed electric dipole transition, the interaction (V.104), taken in first order, leads to a resonant exchange of excitation and very large depolarization cross sections. Such resonant depolarization is almost always accompanied by strong radiation trapping. Optical pumping of the ground state is therefore quite difficult to accomplish when resonant self-depolarization of the excited state is taking place.

Some representative calculations for relative depolarization rates, resulting from the interaction (V.104), are shown in Table IV. The multipole relaxation rates seldom differ by more than 10% from each other, and it is therefore a fairly good approximation

TABLE IV. Relative multipole relaxation rates due to Van der Waals interactions between polarized atoms and inert gas atoms.

State of polarized atom	Relative relaxation rates γ_1	γ_2	γ_3	Reference
$^3P_1$	$\gtrsim 1.11$	1	···	Omo65c
	$\lesssim 1.11$			
$^2P_{3/2}$	0.92	1.11	1.01	Oku70
$^2P_{1/2}$	0	···	···	Gal67b

to assume that the collisions result in "electron randomization". The small differences in multipole relaxation rates have, however, been detected experimentally. Barrat *et al.* (Bar66) have measured the orientation ($L=1$) and alignment ($L=2$) depolarization rates for the 6^3P_1 state of mercury in various inert gases, and they have found that the orientation relaxation rates were always larger than the alignment relaxation rates by 5 to 25%. Faroux and Brossel (Far66c) have obtained similar results.

Nonresonant depolarization cross sections resulting from the interaction (V.104) are usually on the order of 10^{-15} cm^2, and are given approximately by

$$\sigma_L = K_L(eQ\alpha/\hbar v)^{2/5}, \tag{V.105}$$

where K_L is a dimensionless parameter of order unity which accounts for the slight differences between the relaxation rates of the different multipole polarizations. The other parameters are (in cgs units): e, the electron charge; Q, the static quadrupole moment of the polarized atom; α, the static polarizability of the perturbing atom; $2\pi\hbar$, Planck's constant; and v, the mean relative velocity of the colliding pair.

b. Hyperfine structure. The relaxation of atoms is greatly complicated by the presence of hyperfine structure. Although the nucleus is essentially inert during a collision and does not affect the electronic depolarization (unless the hyperfine periods are comparable to or less than the collision times), the conserved nuclear polarization regenerates electronic polarization during the time between collisions; and this tends to slow down the relaxation rates. Thus, when *hfs* is present, there remain $(2J+1)$ primary relaxation rates, one for each electronic multipole moment; but these rates must be combined with various angular factors, involving the nuclear spin I, to obtain the experimentally observed rates.

The influence of the hyperfine structure and the external magnetic fields will cause the energy eigenstates $|i\rangle$ of the atom to be complicated linear combinations of the zero-field basis states $|Fm\rangle$. In terms of the energy eigenstates, the density matrix is

$$\rho = \sum_{ij} \rho_{ij} |i\rangle\langle j| = \sum_{ij,KN,LM} T_{KN}^\dagger(II) T_{LM}^\dagger(JJ) \times \langle j | T_{KN}(II) T_{LM}(JJ) | i\rangle \rho_{ij}. \tag{V.106}$$

Because of collisional relaxation, the $(2)^L$ pole electronic component of ρ will relax at a rate γ_L, so that the relaxation of ρ is described by

$$(d/dt)\rho = -\sum_{ij,LM,KN} \gamma_L \langle j | T_{KN}(II) T_{LM}(JJ) | i\rangle \times \rho_{ij} T_{KN}^\dagger(II) T_{LM}^\dagger(JJ). \tag{V.107}$$

This can be simplified somewhat to yield

$$(d/dt)\rho_{ij} = -\sum_{L,lm,sr} \gamma_L [2L+1] W(LJJl;JJ) \times \langle r | T_{lm}^\dagger(JJ) | j\rangle\langle i | T_{lm}(JJ) | s\rangle \rho_{sr}. \tag{V.108}$$

For $J=\frac{1}{2}$, $\gamma_1 = 1/T$, and $\gamma_0 = 0$, Eq. (V.108) leads to the equations for electron randomization discussed in Sec. V.C.1. For pure electron randomization in an atom with $J>\frac{1}{2}$, i.e., when we have $\gamma_1=\gamma_2=\cdots\gamma_{2J}=\gamma$, and $\gamma_0=0$, Eq. (V.108) may be written as

$$(d/dt)\rho_{ij} = -\gamma\rho_{ij} + [\gamma(2J+1)] \times \sum_{lm,sr} \langle r | T_{lm}^\dagger(JJ) | j\rangle\langle i | T_{lm}(JJ) | s\rangle \rho_{sr}. \tag{V.109}$$

For zero-field relaxation and, in some cases, for relaxation at small magnetic fields, it is convenient to use the multipole representation. If we neglect hyperfine coherence, Eq. (V.108) becomes

$$(d/dt)\rho = -\sum_{lfF,KL} \gamma_L [2f+1][2F+1][2K+1][2L+1] \times \begin{bmatrix} I & I & K \\ J & J & L \\ f & f & l \end{bmatrix} \begin{bmatrix} I & I & K \\ J & J & L \\ F & F & l \end{bmatrix} T_l(FF) \cdot \rho_l(ff). \tag{V.110}$$

For pure electron randomization at a rate γ, Eq. (V.109) becomes

$$(d/dt)\rho = -\gamma\rho + \gamma \sum_{lfF} \{[2f+1][2F+1]/[2J+1]\} \times W(ffII;lJ) W(FFII;LJ) (-1)^{f-F} T_l(FF) \cdot \zeta_l(ff). \tag{V.111}$$

For pure electron randomization, the Zeeman projections $\bar{T}_{LM}(II)$ [see Eq. (II.35)] of the nuclear multipole moments are always eigenobservables at zero field. The corresponding relaxation rates are

$$\gamma_L = \gamma\{1 - [2J+1]^{-1} \sum_F [2F+1]^2 W^2(FFII;LJ)\}. \tag{V.112}$$

Equation (V.79) with $\tau=0$ is a special case of Eq.

(V.112). For an atom with $J=I$ we have [see Eq. (II.32)]

$$\bar{T}_{LM}(JJ)=\bar{T}_{LM}(II), \qquad \text{(V.113)}$$

so that the Zeeman components of the electronic multipole moments are also eigenobservables. This situation occurs, for instance, in the ground state of the hydrogen atom and in the $^2P_{3/2}$ states of ^{87}Rb and ^{39}K. The analysis of relaxation experiments is particularly simple in such cases, since $\bar{T}_{1M}(JJ)$ and $\bar{T}_{2M}(JJ)$ are the observables normally monitored with fluorescent light [see Sec. IV.B]

Barrat *et al.* (Bar65) have carried out detailed studies of the collisional transfer of population between the various hyperfine sublevels of the 6^3P_1 state of mercury. They found good experimental evidence that the collisions do not affect the nuclear polarization directly. Faroux and Brossel (Far65) reached similar conclusions by investigating the destruction rates for orientation and alignment in the $^3P_1$ states of ^{199}Hg and ^{202}Hg. More detailed studies by Faroux and Brossel (Far66a,b,c) support the hypothesis that nuclear polarization is not affected by a collision. Certain anomalies with helium turned out to result from impurities in the helium buffer gas (Far67a).

In summary, both theory and experiment show that the nuclear polarization is not affected by a strong collision. However, recoupling of the nuclear and electronic polarizations during the time between collisions can have a profound effect on the observed relaxation rates.

3. Radiation Trapping and Coherence Narrowing

A particularly important effect which must be considered in all optical pumping experiments is the trapping of the pumping light by multiple scattering within the vapor. Trapping occurs whenever the vapor ceases to be optically thin for some mode of fluorescent decay. Trapping strongly affects the evolution of both the ground-state and excited-state atoms. Detailed studies of the effects of trapping on the ground state have not been made, but it is well known qualitatively that trapping usually degrades the polarization produced by optical pumping. This is because the trapped light provides a weakly polarized, nearly isotropic background of resonant light that competes with the optical pumping of the primary beam and degrades the polarization of the ground state.

The trapping of resonance radiation increases the effective lifetime of excited atoms; and, hence, level-crossing or optical double-resonance signals, whose linewidths are inversely proportional to the relaxation rates of the excited-state polarization, become narrower. This effect, which was first discovered by Guichon, Blamont, and Brossel (Gui56), is called coherence narrowing. The theory of coherence narrowing was first developed by Barrat (Bar59a,b). For a single excited state with electronic angular momentum J_e and no hyperfine structure, the theory of coherence narrowing predicts that the spontaneous decay rate of the $(2)^L$ pole moment is reduced to

$$\Gamma_L=\Gamma(1-x\alpha_L), \qquad \text{(V.114)}$$

where Γ is the natural spontaneous decay rate of the state, x is the average probability that a photon will be absorbed before leaving the vapor, and α_L is a positive numerical factor which depends on the angular momenta of the atom. In some cases, the decay rate Γ_L can decrease to only 30% of the natural decay rate. However, the extent to which the dipole- and quadrupole-relaxation rates Γ_1 and Γ_2 can be reduced by trapping is limited, and the "saturation widths" $\Gamma(1-\alpha_L)$ are always greater than zero.

Coherence narrowing in the absence of spatial isotropy has been studied by Omont (Omo64) and Otten (Ott64), and coherence narrowing under the conditions that the excited state can decay to several branch states has been studied by Saloman and Happer (Sal66) and by Dumont and Decomps (Dum68), (Dec68). Meuner and Omont (Meu66b) have studied the effects of radiation trapping on the high-field level crossing of ^{201}Hg, and have also investigated the effects of ground-state polarization on the coherence narrowing. Dyakonov and Perel' (Dya65) have modified Barrat's theory to treat the velocity distribution of the atoms in a more reasonable way.

D. Diffusion to the Walls

If buffer gas is present in the cell which contains the optically pumped atoms, an atom will not be able to bounce freely from wall to wall if its mean free path λ_t in the buffer gas is comparable to or less than the dimensions of the cell. If the mean free path is much smaller than the cell dimensions, the spatial movement of the polarized atoms will be governed by the diffusion equation

$$\partial\rho/\partial t=D\nabla^2\rho, \qquad \text{(V.115)}$$

where ρ is the density matrix of the atoms and D is the diffusion constant. A comprehensive treatment of diffusion in optical pumping experiments has been published by Masnou-Seeuws and Bouchiat (Mas67).

The classical diffusion constant is related to the "transport" mean free path λ_t and the mean atomic velocity $\bar{v}$ by the equation

$$D=\lambda_t\bar{v}/3. \qquad \text{(V.116)}$$

In practice, the diffusion constants are determined experimentally, and the diffusion constant D_0 at 760 Torr of gas pressure and at 0°C is often tabulated. Representative values of D_0 are listed in Table V. Since the diffusion constant is proportional to the mean free path, it is also inversely proportional to the pressure so that the diffusion constant D at any pressure is related to D_0 by

$$D=(760\ \text{Torr}/P)D_0. \qquad \text{(V.117)}$$

TABLE V. Diffusion constants D_0 in cm^2 sec^{-1} for alkali atoms in foreign gases.

Foreign gas	Cs	Rb	Na
He	0.37 (Leg64) 0.20 (Bev71)	0.54 (Be62) 0.7 (Fra65)	0.92 (Ram64)
Ne	0.24 (Leg64) 0.40 (Fra64b) 0.15 (Bev71)	0.31 (Fra59) 0.5 (Fra65)	0.50 (Ram64)
Ar	0.19 (Leg64) 0.23 (Fra64b) 0.13 (Bev71)	0.24 (Fra59) 0.4 (Fra65)	
N_2	0.22 (Fra64b) 0.07 (Bev71)	0.33 (McN62)	0.54 (Ram64)
H_2		1.34 (McN62)	1.3 (Ram64)

The diffusion constant also depends on the gas temperature.

If we choose V to be an eigenobservable V_K for the buffer gas in question, then Eqs. (V.115) and (V.3) lead to the equation

$$\partial\langle V_K\rangle/\partial t = D\nabla^2\langle V_K\rangle - \gamma_K\langle V_K\rangle \qquad \text{(V.118)}$$

for relaxation in the dark. We may seek exponential solutions to Eq. (V.118) of the form

$$\langle V_K(\mathbf{r},t)\rangle = \sum_\nu \exp(-\Gamma_{K\nu}t) f_{K\nu}(\mathbf{r}) a_{K\nu}. \qquad \text{(V.119)}$$

Then the mode functions $f_{K\nu}(r)$ satisfy the wave equation

$$[(\Gamma_{K\nu}-\gamma_K)+D\nabla^2]f_{K\nu}=0. \qquad \text{(V.120)}$$

Because of the boundary conditions, Eq. (V.120) will have solutions only for certain discrete values of $\Gamma_{K\nu}$ which we shall label with the index ν. It is customary to define a diffusion length $\Lambda_{K\nu}$ for each decay mode

$$\Lambda_{K\nu}^2 = D(\Gamma_{K\nu}-\gamma_K)^{-1}. \qquad \text{(V.121)}$$

In terms of the diffusion length the decay rate of the νth mode is

$$\Gamma_{K\nu}=\gamma_K+D(\Lambda_{K\nu})^{-2}. \qquad \text{(V.122)}$$

The weights $a_{K\nu}$ of the various decay modes depend on the initial density matrix of the atoms, and, in practice, since the pumping cells are usually more or less uniformly illuminated, only the first few decay modes are important.

The boundary conditions for completely disorienting walls are, for all practical purposes, $f_{K\nu}=0$ at the walls (Fra59). Under such conditions the diffusion length $\Lambda_{K\nu}$ is independent of pressure. Furthermore, if the relaxation rate in the buffer gas results from binary collisions between the polarized atoms and the buffer gas molecules, then the relaxation in the buffer gas should be proportional to the buffer-gas pressure p (in Torr), and the total relaxation rate (V.122) becomes

$$\Gamma_{K\nu}=\gamma_{K0}(p/760)+D_0(\Lambda_{K\nu})^{-2}(760/p), \qquad \text{(V.123)}$$

where γ_{K0} is the relaxation rate in the buffer gas at 760 Torr of pressure. Experimental measurements of relaxation rates as a function of pressure are usually described more or less by (V.123), and by fitting experimental data to (V.123) one can determine values for γ_{K0} and D_0. Some typical experimental data is shown in Fig. 25. In analyzing experimental data, however, one must be extremely careful to account for higher-order diffusion modes (Min66b). It is frequently not clear which eigenobservable was being measured in many of the early studies of alkali spin relaxation, and some experiments probably involved three-body collisional relaxation so that Eq. (V.123) was not the correct theoretical curve to fit to the experimental data.

Cells with nondisorienting walls are of great practical importance in optical pumping experiments, and such cells must be used for studies of buffer-gas relaxation at low pressures. The atom, after diffusing to the walls and adhering to the wall for a mean time τ_s, eventually breaks loose and flies back into the vapor. During its dwell time on the wall the atom is not completely depolarized, but some relaxation may occur. For simplicity we shall assume that the eigenobservables are the same whether the atoms are on the walls or in the vapor. Let α_K be the probability that the observables $\langle V_K\rangle$ is destroyed while the atom is stuck to the walls. Then Masnou-Seeuws and Bouchiat (Mas67) have shown that the general boundary conditions for a partially disorienting wall are

$$\partial\langle V_K\rangle/\partial r = -\mu_K\langle V_K\rangle, \qquad \text{(V.124)}$$

where the parameter μ_K is

$$\mu_K = 3\alpha_K/2\lambda_t(2-\alpha_K). \qquad \text{(V.125)}$$

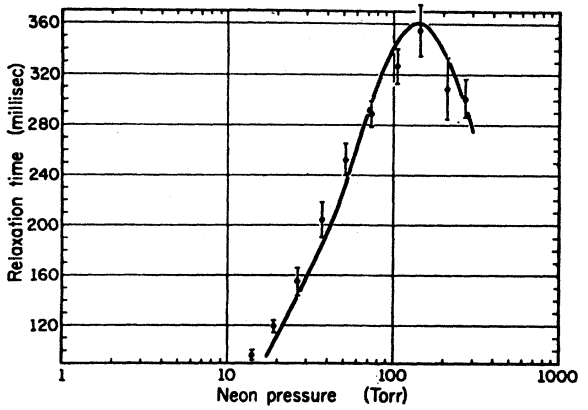

FIG. 25. Pressure dependence of the relaxation rate of polarized cesium atoms when both diffusion to the walls and collisional relaxation are present [from (Fra64b)].

Here $\partial\langle V_K\rangle/\partial r$ is the normal derivative of $\langle V_K\rangle$ at the surface of the container.

The parameter μ_K plays an important role in determining the character of the relaxation. For instance, consider a spherical cell of radius R. At sufficiently high pressures the condition

$$\mu_K R \gg 1 \qquad \text{(V.126)}$$

will be satisfied. Under such conditions the wall coating has practically no effect on the relaxation and the polarization is said to be "confined". The polarization is maximum in the region of optical pumping and falls off substantially toward the walls. A polarized atom close to the walls is much more apt to be depolarized by successive collisions with the wall than to diffuse into the center of the cell.

The opposite extreme is when

$$\mu_K R \ll 1. \qquad \text{(V.127)}$$

In this case the polarization is said to be "unconfined," and polarized atoms will tend to fill the entire container uniformly, irrespective of the spatial distribution of the pumping light. Since the diffusion equation is valid only when

$$\lambda_t \ll R, \qquad \text{(V.128)}$$

the inequalities (V.127) and (V.128) can be simultaneously satisfied only when

$$\alpha_K \ll 1, \qquad \text{(V.129)}$$

that is, only when the probability of depolarization by a wall collision is very small.

For unconfined polarized atoms one can show that the diffusion length Λ_{K0} varies inversely as the square root of the pressure. Consequently, the wall-induced relaxation rate is pressure independent for unconfined polarization. Masnou-Seeuws and Bouchiat (Mas67) have shown that the wall-induced relaxation rate is

$$D_0(\Lambda_{K0})^{-2}\left(\frac{760}{p}\right) = \frac{3\mu_K D_0}{R}\frac{760}{p} \cong \frac{3\alpha_K \bar{v}}{4R}. \qquad \text{(V.130)}$$

The rate of Eq. (V.130) turns out to be the relaxation rate for atoms in a completely evacuated cell. Equation (V.130) is of great practical significance since it shows that any pressure dependence of the relaxation rate in a good, wall-coated cell must result from changes in the intrinsic relaxation rate in the buffer gas and not from changes in the wall-induced relaxation. Unconfined, polarized rubidium vapor in paraffin-coated cells was used by Bouchiat *et al.* (Bou69) in their studies of the influence of molecular formation on the spin relaxation of rubidium atoms in krypton.

VI. SPIN EXCHANGE

Spin exchange can play a very important role in optical pumping experiments, especially in the case of alkali atoms. A simple spin-exchange collision between two $^2S_{1/2}$ atoms A and B, can be represented by the equation

$$A(\uparrow)+B(\downarrow)\rightarrow A(\downarrow)+B(\uparrow). \qquad \text{(VI.1)}$$

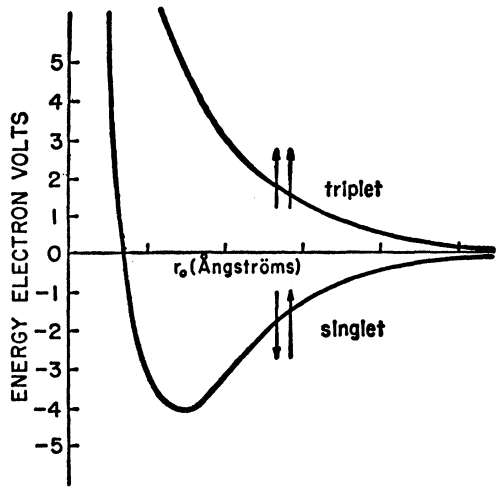

FIG. 26. Typical spin-exchange potentials [from (Car63)].

Before the collision, the spin of atom A is up, while the spin of atom B is down. After the collision the spin of atom A is down, and that of atom B is up; the spin orientations of the two atoms have been exchanged. The origin of the spin-exchange interaction is to be found in the difference between the lowest singlet and triplet potential energy curves of the molecular system AB. A typical set of potential curves is shown in Fig. 26. In this case the triplet potential is repulsive, while the singlet potential is attractive over part of its range. These potential curves can be represented by an interaction of the form

$$V(r) = V_0(r) + \mathbf{S}_A \cdot \mathbf{S}_B V_1(r), \qquad \text{(VI.2)}$$

where $\mathbf{S}_A$ and $\mathbf{S}_B$ are the spin operators of atoms A and B, respectively. The singlet and triplet interaction potentials V_s and V_t are then

$$V_s(r) = V_0(r) - \tfrac{3}{4}V_1(r) \qquad \text{(VI.3)}$$

and

$$V_t(r) = V_0(r) + \tfrac{1}{4}V_1(r). \qquad \text{(VI.4)}$$

Analogous but more complicated interaction potentials are required to describe the interaction between atoms with spins greater than $\frac{1}{2}$. Since the forces responsible for the spin-exchange interaction are of an electrostatic nature, the potentials are on the order of electron-volts, and the cross sections for spin exchange are very large ($\sigma \cong 10^{-14}$ cm^2). The most striking property of spin-exchange collisions is that even though the spin of an individual atom may flip during a collision, the total spin of a colliding pair of atoms is conserved.

The difference between the singlet and triplet potentials causes the total scattering cross section of a pair of atoms to depend strongly on their polarization. Geittner and Elbel (Gei70) reported a method for

determining the ratio of the singlet to triplet scattering cross sections of alkali atoms by observing the influence of optical pumping on the effusion rate of alkali vapors from an orifice.

A. The Mechanism of Spin Exchange

The theory of spin exchange has been developed in two alternate ways. In the original work on spin-exchange scattering by Purcell and Field (Pur56) and by Dicke and Wittke (Wit56) the colliding atoms are assumed to follow classical paths. The spins of the two atoms rotate rapidly around the resultant spin, $\mathbf{S}_A+\mathbf{S}_B$, which is conserved during the course of the collision. The total angle φ through which the spins rotate is given by the phase difference accumulated during the collision

$$\varphi=(1/\hbar)\int_{-\infty}^{\infty}(V_t-V_s)\,dt. \tag{VI.5}$$

The cross section σ for spin exchange can be obtained by averaging the exchange probability $\frac{1}{2}(1-\cos\varphi)$ over impact parameters R

$$\sigma=\pi\int_0^{\infty}(1-\cos\varphi)RdR. \tag{VI.6}$$

A partial-wave analysis of spin-exchange scattering was carried out by Dalgarno (Dal61). He determined the l-wave phase shifts $\delta_l{}^s$ and $\delta_l{}^t$ for scattering from the singlet and triplet potentials of Eqs. (VI.3) and (VI.4). The spin-exchange cross section is then

$$\sigma=\pi/k^2\sum_{l=0}^{\infty}(2l+1)\sin^2(\delta_l{}^s-\delta_l{}^t), \tag{VI.7}$$

where k is the propagation constant of the incident wave. Similar partial-wave analyses of spin-exchange scattering have been carried out by Balling and Pipkin (Bal64a) and by Glassgold (Gla63), who also studied the complications that arise when spin exchange occurs between identical atoms.

Both the classical-path theories and the partial-wave theories lead to the following fundamental equation for the evolution of the density matrix of an atomic species A which is undergoing spin exchange with atoms of a second species B

$$(d/dt)\rho_A=(1/i\hbar)[(\mathcal{H}_0-\boldsymbol{\mu}\cdot\delta\mathbf{H}),\rho_A]+(1/\tau_e)(\rho_A{}^e-\rho_A). \tag{VI.8}$$

Here

$$1/\tau_e=N_B\bar{v}\sigma \tag{VI.9}$$

is the average collision rate of an atom of species A with atoms of species B, N_B is the number density of atoms of species B, $\bar{v}$ is the mean relative velocity between an atom A and an atom B, and σ is the spin-exchange cross section defined by Eqs. (VI.6) or (VI.7). The unperturbed Hamiltonian is modified by the addition of a term $-\boldsymbol{\mu}\cdot\delta H$ which is equivalent to the interaction of the electronic-magnetic moment $\boldsymbol{\mu}$ with a small, fictitious magnetic field $\delta\mathbf{H}$ which is proportional to the mean spin $\langle\mathbf{S}\rangle$ of the ensemble. We shall discuss this term in more detail in Sec. (VI.A-6), where we shall show that it causes frequency shifts in the magnetic-resonance spectrum of the atoms.

The dominant effect of spin-exchange collisions is represented by the last term of Eq. (VI.8). The density matrix $\rho_A{}^e$ represents the atoms of species A immediately after they have undergone a spin-exchange collision with atoms of species B. We may define $\rho_A{}^e$ as

$$\rho_A{}^e=\mathrm{Tr}_B[P\rho_A\otimes\rho_BP^\dagger], \tag{VI.10}$$

where ρ_A and ρ_B are the instantaneous density matrices of species A and B, and Tr_B indicates a trace over the substates of species B. The spin-exchange operator is

$$P=\tfrac{1}{2}+2\mathbf{S}_A\cdot\mathbf{S}_B=P^\dagger=P^{-1}. \tag{VI.11}$$

It is useful to note that

$$P\mathbf{S}_AP^\dagger=\mathbf{S}_B. \tag{VI.12}$$

There are a number of ways to express $\rho_A{}^e$. If we write

$$\rho_A=\alpha+\mathbf{A}\cdot\mathbf{S}_A, \tag{VI.13}$$

where α and $\mathbf{A}$ are functions of the nuclear spin operators [see Eq. (II.29)], then Eq. (VI.10) leads to

$$\rho_A{}^e=\alpha(1+4\langle\mathbf{S}_B\rangle\cdot\mathbf{S}_A). \tag{VI.14}$$

That is, the expectation value of $\mathbf{S}_A$ immediately after a spin-exchange collision is $\langle\mathbf{S}_B\rangle$, and all correlation with the nuclear spin is lost. Grossetête (Gro64a,68) writes Eq. (VI.14) in the form

$$\rho_A{}^e=\tfrac{1}{4}\rho_A+\sum_i\mathbf{S}_A{}^i\rho_A\mathbf{S}_A{}^i-2i(\mathbf{S}_A\times\rho_A\mathbf{S}_A)\cdot\langle\mathbf{S}_B\rangle+[\mathbf{S}_A\rho_A+\rho_A\mathbf{S}_A]\cdot\langle\mathbf{S}_B\rangle, \tag{VI.15}$$

which is equivalent to Eq. (VI.14). Except in certain special cases, Eq. (VI.8) is not a linear equation, and it can be solved only with electronic computers.

It is usually assumed that in the case of identical atoms, spin-exchange collisions are adequately described by replacing $\langle\mathbf{S}_B\rangle$ and $\langle\mathbf{S}_A\rangle$ with $\langle\mathbf{S}\rangle$ in Eqs. (VI.14) and (VI.15), i.e.,

$$\rho^e=\alpha(1+4\langle\mathbf{S}\rangle\cdot\mathbf{S}). \tag{VI.16}$$

Gibbs (Gib65) has considered the approximations involved in this assumption and has concluded that, at least for the rubidium isotopes, they are well founded. Grossetête (Gro65) has also investigated the spin-exchange relaxation of identical atoms (both ^{85}Rb and ^{87}Rb) experimentally, and she has found good agreement with the predictions of Eqs. (VI.8) and (VI.16).

Contrary to some misleading suggestions in the literature, (Lam70), the nuclear spin has a profound influence on the relaxation due to spin exchange. As has been emphasized by Gibbs (Gib71a), this is because the nuclear and electron spins will re-

couple after a spin-exchange collision, since the spin-exchange rate in all experiments to date is much less than the ground-state hyperfine precession frequency.

1. *Relaxation when* $\langle \mathbf{S} \rangle = 0$

The relaxation is particularly easy to analyze if the mean spin is zero, i.e., if $\langle \mathbf{S}_A \rangle = \langle \mathbf{S}_B \rangle = 0$. Then Eq. (VI.14) or Eq. (VI.16) implies that a spin-exchange collision is equivalent to an electron-randomizing collision, and the analysis of Sec. V.C.1 applies to spin-exchange relaxation. For instance, $\langle \mathbf{S} \cdot \mathbf{I} \rangle$ relaxes with the single time constant T_e. Furthermore, if species A is very dilute compared to species B and if $\langle \mathbf{S}_B \rangle$ is zero but $\langle \mathbf{S}_A \rangle$ is not, the relaxation of $\langle \mathbf{S}_A \rangle$ will be caused mainly by spin-exchange (electron-randomizing) collisions with the unpolarized species B, and $\langle \mathbf{S}_A \rangle$ will relax with two time constants $T_e(\mathrm{AB})$ and $\frac{1}{2}(2I_A+1)^2 T_e(\mathrm{AB})$. Such a situation has been studied in detail by Grossetête (Gro64b), who pumped rubidium vapor in the presence of cesium vapor. The polarization of the cesium vapor was maintained at zero by saturating the Zeeman transitions of the cesium ground state with a resonant magnetic field. The experimental results were in good agreement with the prediction that the relaxation of the rubidium should proceed via electron randomization. Grossetête (Gro64b) has also studied the relaxation of the polarization of the $F = I + \frac{1}{2}$ hyperfine sublevel when the polarization of the $F = I - \frac{1}{2}$ sublevel is maintained at zero with a rotating rf field (the g_f values of the two hyperfine levels are approximately equal and opposite). Again, the experimental observations were in good accord with the theory of electron randomization.

Because of the relative simplicity of spin-exchange relaxation when $\langle \mathbf{S} \rangle = 0$, measurements of spin-exchange cross sections are usually made under these conditions. The most foolproof method is to measure the relaxation of $\langle \mathbf{S} \cdot \mathbf{I} \rangle$, since this gives the spin-exchange rate directly. A summary of experimental results to date is included in Table VI.

2. *Relaxation when* $\langle \mathbf{S} \rangle \neq 0$

When the average spin of the vapor is not zero, the effects of spin exchange are much more complicated, since the exchange collisions must conserve angular momentum. Let us first consider the simplest possible situation where the spin-exchange rate is much more rapid than any other relaxation rate or pumping rate of the system. Under such conditions Anderson *et al.* (And60b) have shown that the atomic polarization will be very nearly defined by a spin temperature. That is, the density matrix will be

$$\rho(\beta) = N \exp(\beta F_z), \tag{VI.17}$$

where the parameter β is called the spin–temperature parameter. One can show that the equation [see Eq. (VI.16)]

$$\rho^e(\beta) = \rho(\beta) \tag{VI.18}$$

holds, which implies that $\rho(\beta)$ is invariant to spin exchange. The equation

$$[(\mathcal{H}_0 - \boldsymbol{\mu} \cdot \delta\mathcal{H}), \rho(\beta)] = 0 \tag{VI.19}$$

is also valid; that is, $\rho(\beta)$ is invariant to the hyperfine Hamiltonian. Consequently, in view of Eqs. (VI.18) and (VI.19) one can use Eq. (VI.8) to show that

$$(d/dt)\rho(\beta) = 0; \tag{VI.20}$$

i.e., $\rho(\beta)$ is stationary with respect to internal hyperfine couplings and spin-exchange collisions.

Experimental studies by Anderson (And63) have demonstrated that under conditions easily attainable in optical pumping experiments, the polarization of the vapor is very nearly described by a spin temperature. However, one often finds that at the high temperatures where rapid spin exchange prevails, the vapor is no longer optically thin, and a precise interpretation of the experimental results is difficult to obtain.

3. *Properties of the Atomic Polarization in the Spin-Temperature Limit*

The density matrix $\rho(\beta)$ of Eq. (VI.17) can be factored into a nuclear part and an electronic part, that is

$$\rho(\beta) = N_I \exp(\beta I_z) N_S \exp(\beta S_z), \tag{VI.21}$$

where the normalizing constants are of the form

$$N_I = (\sinh \beta/2)/\sinh \beta(I+\tfrac{1}{2}). \tag{VI.22}$$

A completely analogous formula holds for N_S. One can expand the density matrix in terms of the multipole operators of the system, for instance

$$N_I \exp(\beta I_z) = \sum_L T_{L0}(II) \langle T_{L0}(II) \rangle. \tag{VI.23}$$

The expansion coefficients are

$$\langle T_{L0}(II) \rangle = (i)^L N_I (2\pi)^{1/2} f_L(I, i\beta), \tag{VI.24}$$

where the functions

$$f_L(I, x) = [i^L (2\pi)^{1/2}]^{-1} \times \sum_m \exp(-imx) C(IIL; m, -m)(-1)^{m-I} \tag{VI.25}$$

are the periodic Bessel functions defined by Happer (Hap68b). By using Eqs. (VI.23) and (VI.24), one can show that

$$\langle S_z \rangle = (1/2) \tanh \beta/2 \tag{VI.26}$$

and

$$\langle I_z \rangle = (I+1/2) \coth \beta(I+1/2) - (1/2) \coth \beta/2. \tag{VI.27}$$

In the high-temperature, low-polarization limit ($\beta \ll 1$), Eq. (VI.27) reduces to

$$\langle I_z \rangle = \beta I(I+1)/3, \tag{VI.28}$$

and Eq. (VI.26) becomes

$$\langle S_z \rangle = \beta S(S+1)/3. \tag{VI.29}$$

TABLE VI. (From Mor71) Comparison of the experimental and theoretical spin-exchange cross sections of alkali atoms (10^{-14} cm^2).

Authors and references	σ_{Na-Na}	σ_{K-K}	σ_{Rb-Rb}	σ_{Cs-Cs}	T (°K)
		Experimental values			
Jarret (Jar64)			1.85±0.23		363
Gibbs–Hull (Gib67)			1.9±0.2		351
Grossetête (Gro67c)		2.7±0.7	2.1±0.3	2.20±0.35	300 350
Ernst–Strumia (Ern68b)				2.20±0.15	300
Moretti–Strumia (Mor71)	1.109±0.005				390
Ressler–Sands–Stark (Res69)	1.03±0.21	1.45±0.21	1.9±0.2	2.06±0.2	500 700
		Theoretical values			
Smirnov–Chibisov (Smi65)	0.98	1.41	1.57	1.80	500
Dalgarno–Rudge (Dal65)	1.1	1.5	1.6	1.9	540
		1.6	1.8	2.0	300
Chang–Walker (Cha69b)	1.24	2.44	2.70	2.82	300
	1.21	2.38	2.64	2.77	405

In general, we find for $\beta \ll 1$

$$\langle T_{L0}(II)\rangle = \beta^L L![(2I+1)(2L)!]^{-1}[(2I+L+1)!]^{1/2} \times[(2L+1)(2I-L)!]^{-1/2}. \quad \text{(VI.30)}$$

An analogous formula is obtained by replacing I with S in Eq. (VI.28). Hence, for small values of β, the $(2)^L$ pole moments of the system are proportional to β^L, and the angular momenta ($L=1$) make by far the largest contribution to the polarization.

For small values of β the observable $\langle \mathbf{I}\cdot\mathbf{S}\rangle$ is

$$\langle \mathbf{I}\cdot\mathbf{S}\rangle = \langle \mathbf{I}\rangle\cdot\langle \mathbf{S}\rangle = \langle I_z\rangle\langle S_z\rangle \approx I(I+1)S(S+1)\beta^2/9. \quad \text{(VI.31)}$$

so that the hyperfine polarization $\langle \mathbf{I}\cdot\mathbf{S}\rangle$ is second order in the spin-temperature parameter β, and consequently is very small compared to the spin polarizations $\langle \mathbf{S}\rangle$ and $\langle \mathbf{I}\rangle$.

4. *Electron Randomization with Rapid Spin Exchange*

In many of the experiments on ground-state relaxation in the alkali atoms that have been reported in the literature, the experimental conditions were such that spin-exchange relaxation rates were much faster than buffer-gas relaxation rates. Anderson (And64) has pointed out that this may lead to important simplifications in the character of the relaxation. If the spin-exchange rate is very large, a spin temperature will be approximately maintained throughout the relaxation process, but the parameter β will slowly decrease because of the electron-randomizing collisions against buffer-gas molecules. One can equate the electron-randomization rate with the rate of destruction of total angular momentum, i.e.,

$$(d/dt)\langle F_z\rangle = -(1/T)\langle S_z\rangle. \quad \text{(VI.32)}$$

If the spin-temperature parameter is not too large, we may use the linear approximation for $\langle I_z\rangle$ and $\langle S_z\rangle$ [see Eqs. (VI.27) and (VI.28)] to transform Eq. (VI.31) into a relaxation equation for β:

$$d\beta/dt = -A\beta/T, \quad \text{(VI.33)}$$

where

$$A = S(S+1)/[S(S+1)+I(I+1)]. \quad \text{(VI.34)}$$

Thus, $\langle F_z\rangle$, $\langle S_z\rangle$, and $\langle I_z\rangle$ all relax at the same rate AT^{-1}, which can be considerably smaller than the electron-randomization rate because of the angular momentum stored in the nuclear polarization. Values of A are listed in Table VII.

Suppose that a mixture consists of a fraction f_1 of atoms with spin I_1, and a fraction of f_2 of atoms with

TABLE VII. The slowing-down factor for spin relaxation with rapid spin exchange.

I	$A=3/[3+4I(I+1)]$
0	1
1/2	1/2
1	3/11
3/2	1/6
2	1/9
5/2	3/38
3	1/17
7/2	1/22
4	3/83

spin I_2. Then the slowing down factor A is given by

$$A=S(S+1)/[S(S+1)+f_1I_1(I_1+1)+f_2I_2(I_2+1)]. \quad \text{(VI.35)}$$

For example, for natural mixtures of rubidium isotopes (see Table XII for f_i and I_i), the slowing down factor is $A=0.0927=(10.8)^{-1}$.

It is interesting to note that under the same conditions of rapid spin exchange, we have

$$\langle \mathbf{I}\cdot\mathbf{S}\rangle \approx I(I+1)S(S+1)\beta^2/3 \propto \exp(-2At/T), \quad \text{(VI.36)}$$

so that $\langle \mathbf{I}\cdot\mathbf{S}\rangle$ relaxes twice as fast as the angular momenta but still much more slowly than the electron-randomization rate T^{-1}, which would prevail in the absence of a spin-temperature equilibrium. Experimental studies of the relaxation of $\langle \mathbf{I}\cdot\mathbf{S}\rangle$ in the presence of spin exchange have been made by Grossetête and Bouchiat (Gro68), and they have demonstrated that spin exchange slows down the relaxation of $\langle \mathbf{S}\cdot\mathbf{I}\rangle$ when the mean spin is not zero (see Fig. 27).

5. *Spin-Exchange Relaxation of the* 0–0 *Coherence*

Spin-exchange relaxation plays an important role in the hydrogen maser, in the rubidium masers, and in various other devices which utilize the field-independent 0–0 transition ($F=a=I+\frac{1}{2}, m=0 \rightarrow F=b=I-\frac{1}{2}, m=0$). Although there is no static component of $\langle \mathbf{S}\rangle$ associated with this transition, there is an oscillating component, and the partial conservation of the oscillating component of $\langle \mathbf{S}\rangle$ after a spin-exchange collision does slow down the relaxation rate. One finds that the relaxation of the 0–0 coherence is given by (Gro68)

$$(d/dt)\rho_{a0;b0}=-[(6I+1)/(8I+4)T_e]\rho_{a0;b0}, \quad \text{(VI.37)}$$

where T_e is the time between exchange collisions, and I is the nuclear spin. The slowing down factor, $(6I+1)/(8I+4)$, is listed in Table VIII. For large values of I, the slowing down factor is nearly $\frac{3}{4}$, the value for electron randomization. We should mention that, except in the case of hydrogen where Eq. (VI.37) is exact, small nonlinear terms have been neglected. Careful experimental studies of the relaxation of the 0–0 coherence have been carried out by Vanier (Van68), who verified that the slowing down factor for the spin $\frac{3}{2}$ isotope of ^{87}Rb is $\frac{5}{8}$, as predicted by Eq. (VI.37).

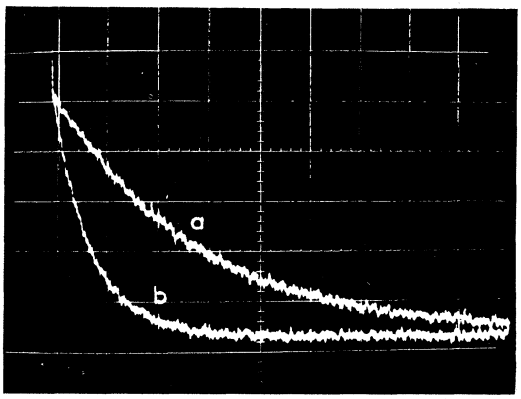

FIG. 27. The relaxation of $\langle \mathbf{S}\cdot\mathbf{I}\rangle$ due to spin exchange, buffer gas, and wall collisions. The relaxation is slower when $\langle S_z\rangle$ is nonzero (a), than when $\langle S_z\rangle$ is zero (b) [from (Gro68)].

TABLE VIII. The slowing-down factor for spin-exchange relaxation of the 0–0 coherence.

I	$(6I+1)/(8I+4)$
1/2	1/2
1	7/12
3/2	5/8
2	13/20
5/2	2/3
3	19/28
7/2	11/16
4	25/36

6. *Frequency Shifts due to Spin Exchange*

The angle of rotation φ [see Eq. (VI.5)] of the spins of a colliding atomic pair about each other is seldom exactly 180°, which would correspond to complete spin exchange. On the average, the rotation angle lies between 0° and 180° or 0° and −180°. This tendency of a spin-exchange collision to rotate the spins can be represented, as was indicated in Eq. (VI.8), by a small effective magnetic field

$$\delta\mathbf{H}=-\kappa\hbar\langle \mathbf{S}_B\rangle/\mu_0 T_e(AB), \quad \text{(VI.38)}$$

where μ_0 is the Bohr magneton, and $T_e(AB)$ is the mean exchange time for collisions between atoms of species A and B. For spin-exchange collisions between identical atoms of species A, one should replace $\langle \mathbf{S}_B\rangle$ by $\langle \mathbf{S}_A\rangle$ and $T_e(AB)$ by $T_e(AA)$ in Eq. (VI.38). The rotation parameter κ is defined as

$$\kappa=(\pi/\sigma)\int_0^\infty RdR\sin\varphi, \quad \text{(VI.39)}$$

which is seen to be the average over impact parameters of the sine of the rotation angle φ. The corresponding expression for κ in the partial-wave theory is

$$\kappa=(\pi/2k^2\sigma)\sum_{l=0}^{\infty}(2l+1)\sin 2(\delta_l{}^t-\delta_l{}^s). \quad \text{(VI.40)}$$

The static component of $\delta\mathbf{H}$ will shift the resonant frequency ω_{ij} of a field-dependent transition just as a small magnetic field would. The expression for the frequency shift is thus

$$\Delta\omega_{ij}(dc)=-(2\kappa/T_e)\langle \bar{S}_z\rangle[\langle i\,|\,S_z\,|\,i\rangle-\langle j\,|\,S_z\,|\,j\rangle], \quad \text{(VI.41)}$$

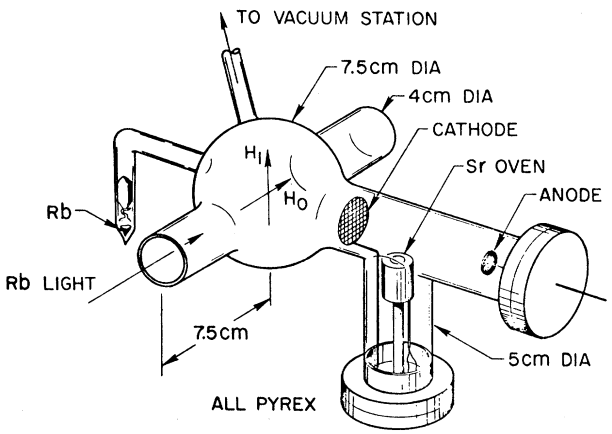

(a)

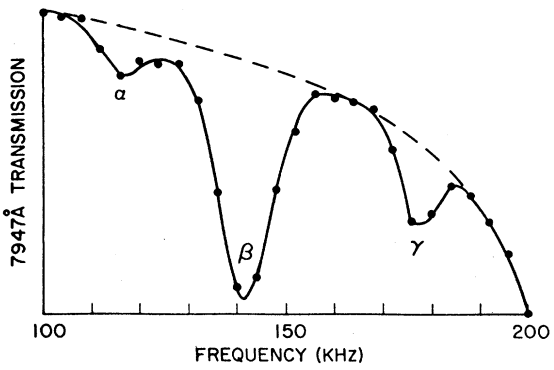

(b)

FIG. 28. A typical experiment with spin-exchange spectroscopy. Strontium ions are polarized by spin exchange with optically pumped rubidium. Changes in the Sr^+ polarization produce corresponding changes in the rubidium polarization, which is observed by transmission monitoring [from (Gib70c).]

where $\langle \bar{S}_z \rangle$ is the static component of $\langle S_z \rangle$, and T_e is the appropriate exchange time. For spin-exchange collisions between identical atoms, the oscillating parts of $\delta\mathbf{H}$ can also cause shifts of the frequency ω_{ij}, since if a population difference exists between the sublevels i and j, a resonant, oscillating field can produce additional coherence which adds to that already present. The shift due to the oscillating components of $\delta\mathfrak{K}$ is thus

$$\Delta\omega_{ij}(ac) = (2\kappa/T_e)\langle j \mid \mathbf{S} \mid i\rangle \cdot \langle i \mid \mathbf{S} \mid j\rangle \times[\langle i \mid \rho \mid i\rangle - \langle j \mid \rho \mid j\rangle], \quad \text{(VI.42)}$$

where T_e is the mean time between self-spin-exchange collisions. The total frequency shift is the sum of the terms of Eqs. (IV.41) and (VI.42).

We note in conclusion that the expected frequency shift for the 0–0 field-independent transition is given by Eq. (VI.42) and is (i is the upper state)

$$\Delta\omega = -\kappa(2T_e)^{-1}[\langle i \mid \rho \mid i\rangle - \langle j \mid \rho \mid j\rangle]. \quad \text{(VI.43)}$$

Experimental evidence on frequency shifts due to spin exchange is rather sparse so far, and for those measurements that have been made the agreement between theory and experiment is poor (Bal64a,b). The reasons for the lack of agreement are not yet clear. Bender (Ben64) has calculated explicitly the expected shifts for e–Na and e–Cs collisions and finds much larger shift-to-broadening ratios than those measured by Balling *et al.* (Bal64a) in the e–Rb system.

Balling and Pipkin (Bal64b) have suggested that spin–orbit forces must be considered together with spin exchange in electron–alkali–atom systems, and have worked out the appropriate theory. However, the role of spin–orbit interaction in frequency shifts is still inconclusive because of the paucity of experimental data.

B. Spin-Exchange Spectroscopy

Spin-exchange collisions between an optically pumped alkali vapor and a second species can be used to detect magnetic resonance in the second species. Such experiments were first suggested by Dehmelt (Deh58a). A typical experiment is shown in Fig. 28. The alkali vapor is polarized by optical pumping, and the density is high

TABLE IX. Summary of species polarized by spin exchange with optically pumped vapors.

Species polarized by spin exchange	Optically pumped species	References
e^-	Na	Deh58b
	Na	Bal66
	K	Deh58a
	Rb	Bal65
e^-	He($^3S_1$)	Sch68c
H	Na	And58
H, D, T	Rb	And60a, b
H, T	Rb	Pip62
H	Na	Ruf65
He^+	Cs	For66, Deh62a, Maj68
Rb	Na	Nov58
K	Na	Fra58a
^{21}Na	^{23}Na	Köp69
^{37}K	Rb	Bes68, Köp69
N	Rb	Hol58
N	Na	And59
N	Cs	Hol62
N	Cs	Til69a
P	Rb	Lam62
Rb^+	Rb	Mit68
Ag	Rb	Bal69
Cu	Cs	Hof69
Sr^+	Rb	Gib70b
Cd^+	Rb	Gib70b
^{3}He	Rb	Bou60, Her65
Eu	Cs	Til69b
Mn	Rb	Dav71

enough that a spin-temperature equilibrium is established between the alkali atoms and the Sr^+ ions, which are produced by a weak discharge in the sidearm. When the ion spin polarization is decreased by saturating one of the hyperfine transitions with a radio-frequency field, the rubidium spin temperature is also increased (β is decreased); this can be detected by transmission monitoring with the pumping light. Thus, spin-exchange spectroscopy allows one to carry out very precise rf spectroscopy on atoms or ions that cannot be conveniently optically pumped with their own resonance radiation.

Mitchell and Fortson (Mit68) have shown that Rb^+ ground-state ions can be polarized by charge exchange with optically pumped rubidium atoms in a helium buffer gas. This is a type of spin exchange in which one species, the Rb^+ ion, has no electronic spin but does have a nuclear spin which can be polarized. The charge exchange cross section was estimated to be about 2×10^{-14} cm^2. Hadeishi and Liu (Had66) have reported that $Xe^+(^2P_{3/2})$ ground-state atoms can be polarized by charge exchange with aligned metastable $Xe(^3P_2)$ atoms. References to most of the experiments on spin-exchange spectroscopy to date are contained in Table IX.

C. Spin Exchange Between Electron and Nucleus

A type of spin exchange can also occur between an electronically polarized atom and the nucleus of an unpolarized collision partner. For instance, Bouchiat, Carver, and Varnum (Bou60) have detected an enhancement of the nucleus polarization of a He^3 buffer gas in a cell containing optically pumped rubidium vapor. More detailed studies of He^3–Rb spin exchange have been reported by Gamblin and Carver (Gam65), who measured He^3 polarizations of 0.01%. By using aluminosilicate glass containers, which are relatively impervious to helium, Fitzsimmons *et al.* (Fit69) were able to achieve He^3 polarizations of 0.5%. The mechanism for nuclear–electronic spin exchange is almost certainly the contact interaction between the nuclear spin and the polarized electron of the optically pumped atom. Herman (Her65) and Gamblin (Gam65) have shown that this interaction is considerably enhanced by the exchange correlation between the spin of the pumped atom and the core electrons that surround the unpolarized nucleus. Herman estimates exchange cross sections on the order of 10^{-24}, 10^{-23}, and 10^{-22} cm^2 for ^{3}He, ^{21}Ne, and ^{83}Kr, respectively. Precise experimental values for the exchange cross sections are not available. Herman (Her65) has suggested that the nuclear–electronic spin-exchange collisions may be important relaxation mechanisms for polarized alkali atoms in buffer gases with nonzero nuclear spins. However, experiments by Brewer (Bre62) with H_2 and D_2, and Franz (Fra64b) with $(^{14}N)_2$ and $(^{15}N)_2$ show that for these isotope pairs, the alkali-depolarization cross sections depend very little on the nuclear spins of the buffer-gas molecules.

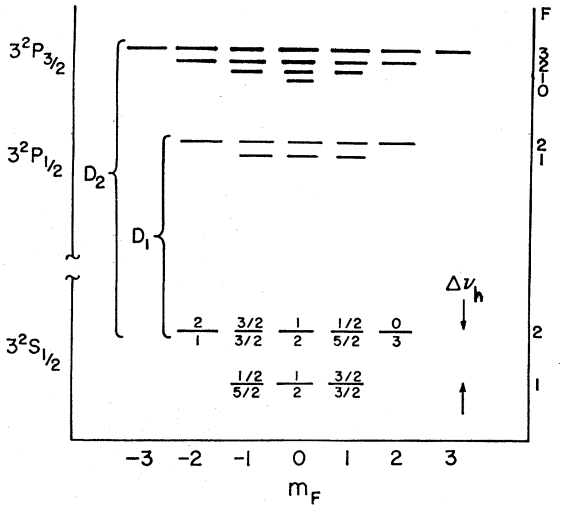

FIG. 29. The low-lying energy levels of alkali atoms. The relative absorption rates for σ_+, D_1, and D_2 light are shown above and below the respective ground-state sublevels [from (Car63)].

VII. ALKALI ATOMS AND SIMILAR ATOMS AND IONS

The alkali atoms, lithium, sodium, potassium, rubidium, and cesium, can all be optically pumped in much the same way, although there are technical problems peculiar to each species. Other atoms or ions with a $^2S_{1/2}$ ground state, such as hydrogen, or singly ionized strontium and magnesium, can also be pumped in the same manner as alkali atoms. We shall first discuss the properties that are common to all atoms and ions of this class, and we then review some of the special problems associated with each species.

A. Basic Atomic Properties

The pertinent energy levels of an alkali atom are shown in Fig. 29. The $^2S_{1/2}$ ground state is split into two hyperfine multiplets of total angular momenta $a=I+\frac{1}{2}$ and $b=I-\frac{1}{2}$, and the transition frequency between the multiplets is given by

$$\Delta\nu=(I+\tfrac{1}{2})A. \qquad \text{(VII.1)}$$

The low-field Larmor frequencies of the two multiplets are very nearly equal and opposite. The Larmor frequency of the multplet a is

$$\nu_a=[1/(2I+1)h]\{g_J\mu_0-2\mu_I\}H, \qquad \text{(VII.2)}$$

and the Larmor frequency of the multiplet b is

$$\nu_b=[-1/(2I+1)h]\{g_J\mu_0-2(I+1)\mu_I/I\}H. \qquad \text{(VII.3)}$$

The difference between the ground-state Larmor frequencies

$$|\nu_a|-|\nu_b|=-2\mu_IH/Ih \qquad \text{(VII.4)}$$

TABLE X. Basic atomic parameters of alkali atoms.

Atom	Natural abundance %	I	$\Delta\nu$ (MHz)	λ_1 (Å)	λ_2 (Å)	τ_1 (nsec)	τ_2 (nsec)	f_1	f_2	A_1 (MHz)	A_2 (MHz)	B_2 (MHz)	μ_I (Nuclear magnetons)
^{6}Li	7.5	1	228.2	6708	6708	27	27	0.25	0.50	17.5			0.8220
^{7}Li	92.5	3/2	803.5							46.2	−3.0		3.2564
^{23}Na	100	3/2	1771.6	5896	5890	16	16	0.33	0.65	94.5	18.9	2.4	2.2176
^{39}K	93.2	3/2	461.7	7699	7665	26	26	0.34	0.68	28.9	6.0	2.9	0.3914
^{41}K	6.8	3/2	254.0										0.2148
^{85}Rb	72.2	5/2	3035.7	7948	7800	28	26	0.35	0.70	121	25.0	26.0	1.3527
^{87}Rb	27.8	3/2	6834.7							409	84.9	12.6	2.7506
^{133}Cs	100	7/2	9192.6	8944	8521	34	33	0.33	0.66	280	50.9	−0.9	2.579

is proportional to the nuclear moment and can be detected experimentally in many cases (Fra66a).

For sufficiently large values of the magnetic field, the different $\Delta F=0$, $\Delta m=1$ transitions within a single Zeeman multiplet become well resolved, and an optical pumping experiment yields a magnetic resonance spectrum such as that in Fig. 30. The transition frequencies for the resolved resonances can be calculated with the Breit–Rabi formula (Köp58).

Transitions between the two hyperfine multiplets can also be observed in optical pumping experiments, and the field-independent 0–0 transition is of particular importance for frequency standards.

Optical pumping in the alkali atoms normally involves excitation of the atoms to the lowest $^2P_{1/2}$ and $^2P_{3/2}$ excited states. The $^2P_{1/2}$ state lies lower and decays with the emission of D_1 resonance light, while the $^2P_{3/2}$ state emits D_2 resonance light. The lifetimes of these two states are nearly equal.

The $^2P_{1/2}$ state is split into two hyperfine states by the magnetic dipole interaction. The splitting is much smaller than the corresponding ground-state splitting because of the absence of a large contact interaction between the nucleus and the excited valence electron.

The $^2P_{3/2}$ state can be split into as many as four different hyperfine components with total angular momenta F ranging from $|I-\frac{3}{2}|$ to $|I+\frac{3}{2}|$. The splittings in the $^2P_{3/2}$ state are somewhat smaller than those in the $^2P_{1/2}$ state, and the splittings are often noticeably affected by the nuclear quadrupole moment.

A summary of the basic atomic parameters of alkali atoms and alkalilike ions is contained in Table X.

B. Pumping

Both depopulation and repopulation pumping are effective in the alkali atoms. Theoretical calculations of pumping transients and steady-state polarizations have been carried out by Franzen and Emslie (Fra57), Hawkins (Haw61,69), and Violino (Vio66,68). Violino points out that the calculational procedure used by Hawkins is somewhat unrealistic, since Hawkins assumes that the photons are absorbed and emitted "one at a time." This procedure corresponds to rather large intervals of numerical integration of the fundamental equation of optical pumping (Vio68). In most theoretical calculations, rather unrealistic models for ground-state and excited-state relaxation are assumed.

For broad-line pumping light only gyrotropic depopulation pumping occurs. The light-absorption operators for D_1 and D_2 pumping light are, respectively,

$$\delta\Gamma_1=R_1(1-2\mathbf{J}\cdot\mathbf{s}_1) \qquad \text{(VII.5)}$$

and

$$\delta\Gamma_2=R_2(1+\mathbf{J}\cdot\mathbf{s}_2). \qquad \text{(VII.6)}$$

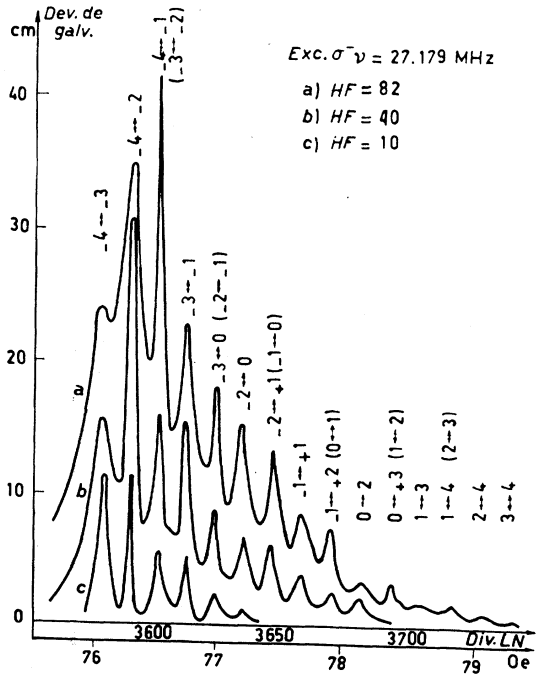

FIG. 30. Magnetic resonance spectrum of optically pumped cesium atoms. Multiple quantum transitions are seen at higher rf power [from (Ska57).]

The mean pumping rates R_1 and R_2 are related to the corresponding energy densities, u_1 and u_2, by Eq. (III.35). The mean photon spins for the D_1 and D_2 light are $\mathbf{s}_1$ and $\mathbf{s}_2$, respectively. The total light-absorption operator is therefore

$$\delta\Gamma=(R_1+R_2)-(2R_1\mathbf{s}_1-R_2\mathbf{s}_2)\cdot\mathbf{J}. \quad \text{(VII.7)}$$

Equation (VII.7) implies that if the polarizations of the D_1 and D_2 light are the same (i.e., if $\mathbf{s}_1=\mathbf{s}_2$), then no pumping will occur when $2R_1=R_2$ or when

$$u_1=(\lambda_2 f_2/\lambda_1 f_1)u_2/2. \quad \text{(VII.8)}$$

Since the ratio $(\lambda_1 f_2/\lambda_1 f_1)$ is approximately 2 for alkali atoms, efficient depopulation pumping will not occur if the intensities of the two D lines are equal. Thus, at high buffer-gas pressures, where repopulation pumping is suppressed, it is necessary to ensure that one D line is much stronger than the other if pumping is to take place. Similarly, transmission monitoring of the ground-state polarization is quite inefficient when the D-line intensities are equal, because a change in $\langle\mathbf{J}\rangle$ will increase the transparency of the vapor for one D line while decreasing it by a compensating amount for the other D line.

Good depopulation pumping can be achieved with equal intensities of the two D lines if the mean spins $\mathbf{s}_1$ and $\mathbf{s}_2$ are antiparallel. An interesting method for making $\mathbf{s}_1$ and $\mathbf{s}_2$ antiparallel for sodium light has been developed by Köpf *et al.* (Köp69). They passed sodium resonance radiation through a Lyot polarization-interference filter and replaced the exit polarizer with a $\lambda/4$ plate. Since the D_1 and D_2 components of the light were polarized at right angles to each other before entering the $\lambda/4$ plate, the D lines were circularly polarized in opposite directions after passage through the plate. Consequently, both D lines caused depopulation pumping in the same direction.

Narrow-line depopulation pumping is often used in the heavier alkali atoms to produce hyperfine population imbalances $\langle\mathbf{I}\cdot\mathbf{J}\rangle$. Methods for obtaining narrow-line pumping light in K, Rb, and Cs are discussed in Sec. VII.E.I.

Repopulation pumping is important at low buffer-gas pressures where collisional depolarization of the excited state is negligible. For circularly polarized pumping light, repopulation and depopulation pumping tend to polarize the ground-state in opposite directions. For D_2 light, repopulation and depopulation pumping can actually cancel each other at certain critical pressures of the buffer gas (see Sec. III.C.4). Because of the sensitivity of D_2 pumping to excited-state mixing, greater ground-state polarization can be obtained with circularly polarized D_1 light than with either natural or D_2 pumping light. The mechanisms of D_1 pumping have been analyzed in some detail by Franzen and Emslie (Fra57), who, with Dehmelt, first drew attention to the advantages of D_1 pumping light.

One of the most interesting aspects of repopulation pumping is that it can produce alignment of the ground state even when the light beam is unpolarized and has a broad spectral profile. This occurs only for D_2 pumping light, and Varshalovich (Var67) has suggested that hydrogen atoms in interstellar space may be aligned by the pumping action of nearby stars. The creation of alignment by unpolarized light has been observed experimentally with sodium atoms by Hawkins (Haw55) and Margerie *et al.* (Mar55). The creation of alignment by repopulation pumping becomes less and less efficient at higher magnetic fields because of the decoupling of the nuclear spin from the electronic spin in the excited $^2P_{3/2}$ state (Mar55).

Some pumping of alkali vapors seems to occur with almost any light source when optically thick samples are used. This seems to result from a self-filtering action of the pumped vapor, and an analysis of some aspects of the problem has been considered by Bloom (Blo58). The analysis of experiments in optically thick samples is difficult, however, and most quantitative work is now done with thin samples.

1. Raith's Method for Measuring Polarization

An intersting way to measure the electronic spin polarization $\langle J_z\rangle$ in absolute units has been developed by Raith (Boe61), (Rai61). For an optically thin vapor, the attenuation of a broad-line D_1 light beam, circularly polarized in the direction of propagation is

$$\Delta\Phi=lN\omega\hbar R_1(1-2\langle J_z\rangle), \quad \text{(VII.9)}$$

where l is the length of the vapor, N is the number density, and R_1 is the mean pumping rate [see Eqs. (IV.23) and (VII.5)]. The difference in attenuation between a polarized and an unpolarized atomic vapor is

$$\delta\Phi_1=2lN\omega\hbar R_1\langle J_z\rangle. \quad \text{(VII.10)}$$

One can also measure the attenuation of the unpolarized vapor at slightly different temperatures, T_1 and T_2. The difference in attenuation is then

$$\delta\Phi_2=l\omega\hbar R_1[N(T_2)-N(T_1)]. \quad \text{(VII.11)}$$

The spin polarization is therefore

$$\langle J_z\rangle=[N(T_2)-N(T_1)][2N(T_1)]^{-1}(\delta\Phi_1/\delta\Phi_2). \quad \text{(VII.12)}$$

The number densities N can be determined from tables indicating saturated vapor density versus temperature. Analogous procedures can be used with narrow-line excitation to determine the hyperfine polarization $\langle\mathbf{I}\cdot\mathbf{J}\rangle$.

Raith's method is independent of the absolute calibration of the photodetector or of the width of the probing light, provided that the profile is flat over all components of the absorption profile. It is also independent of the nuclear spin. However, it is important that the vapor density at a given temperature equal the density of a saturated vapor at the same temperature. This condition seldom holds for alkali vapors in transparent glass or quartz containers unless large amounts of clean alkali metal are present in the container.

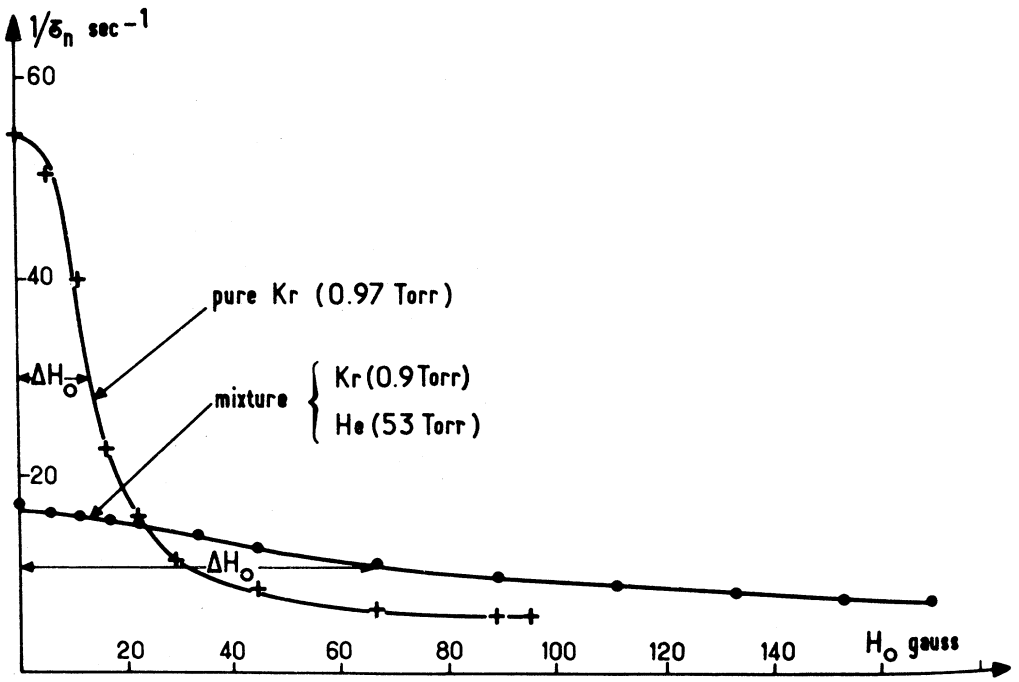

FIG. 31. Magnetic field dependence of the relaxation of polarized rubidium atoms in krypton. The rapid decrease of the relaxation rate with magnetic field indicates that the relaxation cannot be caused solely by sudden, binary collisions, which have very short correlation times. Also, the addition of helium should have almost no effect if only binary collisions were involved. The observations can be explained if it is assumed that alkali–inert-gas molecules are formed by three-body collisions and broken up by subsequent collisions [from (Aym67)].

TABLE XI. Ground-state relaxation cross sections for alkali atoms in foreign gases.[a]

Foreign gas	Cs	Rb	Na
He	2.5×10^{-24} (Leg64) 2.8×10^{-23} (Bev71)	6.2×10^{-25} (Be62) 3.3×10^{-25} (Fra65)	2.2×10^{-26} (And63)
Ne	8.4×10^{-24} (Leg64) 5.3×10^{-24} (Fra64b) 9.0×10^{-23} (Ern68a) 9.3×10^{-23} (Bev71)	5.2×10^{-23} (Fra59) 3.3×10^{-24} (Fra65)	1.8×10^{-24} (And63)
Ar	2.6×10^{-23} (Leg64) 8.0×10^{-23} (Fra64b) 1.04×10^{-21} (Bev71)	3.7×10^{-22} (Fra59) 1.1×10^{-22} (Fra65)	8.8×10^{-23} (Ram64)
Kr	2.1×10^{-21} (Fra64b)	5.9×10^{-21} (Fra59) 7.3×10^{-21} (Fra65) 2.3×10^{-20} (Bou69)	2.0×10^{-21} (Ram64)
Xe	4.6×10^{-20} (Fra64b)	1.3×10^{-20} (Fra59) 1.3×10^{-19} (Fra65)	2.5×10^{-20} (Ram64)
N_2	4.7×10^{-23} (Fra64b) 5.5×10^{-22} (Bev71)	5.7×10^{-23} (McN62)	4.1×10^{-24} (Ram64)
H_2		3×10^{-24} (McN62) 2.2×10^{-24} (Bre62a)	2.7×10^{-26} (Ram64)

[a] Most of these cross sections were deduced by observing the relaxation of $\langle S_z \rangle$. The slowing down of the relaxation rate by the nuclear spin inertia was seldom taken into account. The vapors were often optically thick, and the effects of higher diffusional modes and possible molecular formation were usually ignored. The cross sections probably differ from the true electron-randomization cross sections by as much as an order of magnitude in some cases.

C. Ground-State Relaxation of Alkali Atoms in Buffer Gas

Some of the most detailed studies of relaxation have dealt with the relaxation of polarized alkali atoms in buffer gases. The most common buffer gases are the inert gases, helium, neon, argon, krypton, and xenon; the simple diatomic gases, H_2, D_2, and N_2; and the simple organic gases, CH_4, C_2H_6, C_2H_4, cyclohexane, benzene, etc. The relaxation is now known to involve at least two different types of collision; sudden, binary collisions, which last for about 10^{-12} seconds, and sticking collisions, which lead to bound molecules. The bound molecules may have lifetimes on the order of 10^{-8} seconds at buffer-gas pressures of a few Torr.

Convincing evidence for the existence of alkali atom–inert gas molecules has been presented by Bouchiat and her co-workers (Aym67), (Bou67), who showed that the rate of relaxation of polarized rubidium atoms in krypton depended strongly on the external magnetic field for magnetic fields in the range of 0–100 G (see Fig. 31). It was also found that the relaxation rate was not proportional to buffer-gas pressure, even when the effects of diffusion were fully taken into account. Such behavior can not be explained by the mechanism of sudden binary collisions, but it is in very satisfactory accord with the behavior one would expect from molecular formation. Hartmann (Har70b) has also found evidence for Rb–Kr molecules by studying the relaxation of the 0–0 coherence of rubidium atoms in a krypton buffer gas. At the present time we do not know the extent of the phenomenon of molecular formation, but molecular formation may be important for all of the heavy noble gases, argon, krypton, and xenon. Unfortunately, at the time of the early studies of the relaxation of alkali atoms, the occurrence of molecules was not suspected, and the influence of the nuclear spin was poorly understood. Therefore, it is difficult to interpret the results of many early studies of buffer-gas relaxation.

There has been some discussion in the literature about the role of molecules with permanent electric dipole moments in alkali relaxation (McN64a,65). However, Berg (Ber65a) has pointed out that the electric dipole moment probably has no direct influence on the spin-relaxation rates of alkali atoms, since the polarizability tensor of these $S_{1/2}$ atoms is isotropic.

1. *Experimental Methods of Investigating Ground-State Relaxation*

Most experimental methods for studying the relaxation of ground-state polarization in alkali atoms are variants of the "relaxation-in-the-dark" method developed by Franzen (Fra59), (Bou66a), (Ban67). A typical experimental arrangement is shown in Fig. 32. A strong pumping beam is used to establish a large ground-state polarization in the vapor. The strong beam is suddenly removed by a shutter, and the subsequent evolution of the vapor is followed by monitoring the absorption of a very weak probing beam, which has negligible influence on the relaxation.

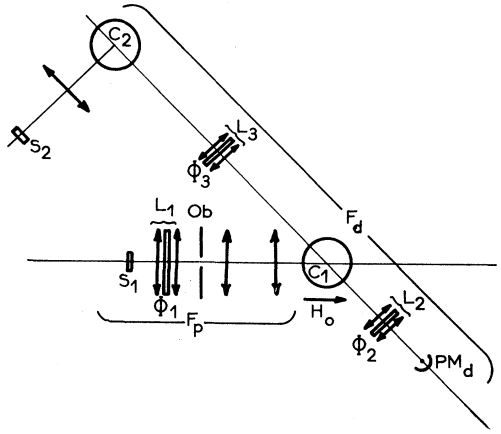

FIG. 32. A typical experimental arrangement for measuring relaxation in the dark. Atoms in the cell C_1 are polarized by a strong pumping beam F_p. A weak probing beam F_d is used to monitor the decaying polarization when the pumping beam is suddenly cut off by the shutter O_b [from (Bou66a)].

It is also possible to measure collisional relaxation rates even if the atoms do not relax in the dark, although one must usually extrapolate the results at low light intensities to distinguish the true collisional relaxation rates from the pumping rates. For instance, Dehmelt (Deh58a) has developed a simple method in which the direction of a small static field is suddenly reversed. The field reversal is fast compared to the pumping and relaxation rates but slow enough that the polarization can follow the field adiabatically. There is always a residual field of adequate magnitude to prevent non-adiabatic transitions (Deh65), although this aspect of Dehmelt's method has been misunderstood in the literature (Ale63b). The reestablishment of equilibrium polarization after the adiabatic reversal is monitored by observing the transmitted pumping light. By properly accounting for the pumping rates, collisional relaxation rates can be deduced. Bouchiat and Brossel (Bou62a) observed the polarization transients that accompany destruction of the ground-state polarization with a square-wave modulated resonant rf field. This method is similar to Dehmelt's field-reversal method, and the transients must be corrected for the pumping rates in much the same way.

Precision measurements of relaxation rates are quite difficult to make, and one should probably ignore the error estimates for most relaxation rates quoted in the literature. In a good relaxation experiment attention should be given to the following points:

(1) For gases which cause very slow relaxation, high purity samples must be used to avoid sizeable contributions to the relaxation rate from trace impurities of strongly relaxing species (Fra65).

(2) Strongly relaxing gases are sometimes diluted in

TABLE XII. Pressure shifts in Hz Torr^{-1} of the hyperfine frequency interval of alkali atoms in foreign gases.

Foreign gas	H	^{21}Na	^{39}K	^{87}Rb	^{133}Cs
He		130 (Ram65)	43 (Blo60b)	720 (Ben58)	1050 (Bea58) 1600 (Ard58a, b, c) 1200 (Ard61)
Ne		80 (Ard58a, c) 80 (Ram65)	24 (Blo60b)	392 (Ben58)	580 (Bea58) 650 (Ard58b, c)
Ar		≈0 (Ard58a, c) 5 (Ram65)	−0.4 (Blo60b)	−51 (Ben58) −52 (Ard61)	−190 (Bea58) −250 (Ard58b, c) −212 (Ard61)
Kr	−15 (Ens68)	−75 (Ram65)	−42 (Blo60b)	−580 (Ben58)	−1300 (Bea58) −1300 (Ard58b, c) −1360 (Ard61)
	−28 (Ens68)	−150 (Ram65)			−2400 (Ard58b, c) −2350 (Ard(61)
H_2		110 (Ram65)	33 (Blo60b)	660 (Ben58)	1900 (Ard58b, c)
N_2		100 (Ard58a, c) 87 (Ram65)		520 (Ben58)	890 (Bea58) 930 (Ard58b, c) 840 (Ard61)

weakly relaxing gases to yield mixtures with longer and more conveniently measured relaxation times. This can obscure the effects of molecular formation on the relaxation rates (Bou67).

(3) One should determine whether molecular formation is important by observing the pressure dependence and magnetic field dependence of the relaxation rates (Bou67).

(4) The vapor should be optically thin, so that the attentuation of the probing beam depends linearly on the atomic observables (Bou66a). The polarization and spectral profile of the probing beam should be well understood so that one can determine precisely which observable is being measured.

(5) The effects of diffusion should be eliminated if possible by the use of good wall coatings (Bou66a). It is very difficult to be sure that higher diffusion modes are not contributing to the relaxation rates, especially when the vapor is not optically thin. If the measured relaxation rates are strongly dependent on temperature, higher diffusion modes are probably present (Min66b). Both the polarization and intensity of the light may vary in a complicated way throughout the volume of the cell if the cell does not have flat windows (e.g., spherical cells). This influences the volume generation of polarized atoms and the steady state spatial dependence of the polarized atoms. The lenslike behavior and polarizing properties of curved glass surfaces should probably be avoided.

(6) Relaxation rates should be corrected for the effects of spin exchange by extrapolating the rates back to the limit of zero alkali-vapor density. However, very rapid spin-exchange rates may be useful in an optically thin sample, since under such circumstances the decay of the polarization should be very nearly single-exponential (see Sec. VI.A.4).

Experimental data on ground-state relaxation are summarized in Table XII. The cross sections are taken directly from the literature, and they may differ by several orders of magnitude from the true electron-randomization cross sections. In many of the experiments rapid spin exchange probably slowed down the measured rates appreciably (see Sec. VI.A.4) and even where spin exchange was negligible, it is seldom clear whether T_e or T_n was being measured, although it was probably T_n in most cases.

2. *Theory of Binary Collisions With Inert Gases*

The interaction of alkali atoms with inert gases has been studied in considerable detail. While it is too early to say that all aspects of alkali relaxation in inert gases are understood, it is clear that many of the observed relaxation phenomena can be interpreted by assuming that the spin-dependent interaction between an alkali atom and an inert-gas atom is given by an effective Hamiltonian

$$V=\gamma(r)\mathbf{N}\cdot\mathbf{S}+h\delta A(r)\mathbf{I}\cdot\mathbf{S}. \qquad \text{(VII.13)}$$

Here r is the interatomic separation, and $\mathbf{N}$ is the translational angular momentum of the alkali atom and the inert-gas atom around each other.

a. Change in the hyperfine coupling. The term $\delta A(r)\mathbf{I}\cdot\mathbf{S}$ represents a small change in the contact interaction between the nucleus of the alkali atom and the spin of the valence electron (Adr60a). At large

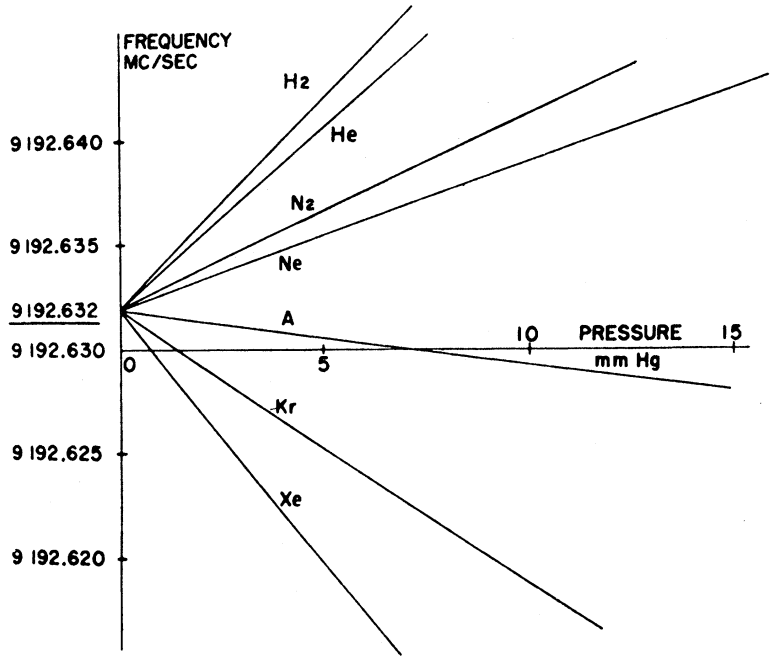

FIG. 33. Pressure shifts of the hyperfine transition frequencies of cesium atoms [from Ard61)].

interatomic separations, the term δA is caused by the electrostatic Van der Waals forces which tend to pull the electron away from the nucleus of the alkali atom and to decrease the contact interaction. Hence $\delta A(r)$ is negative at large interatomic separations. For very close interatomic separations, exchange forces between the alkali valence electron and the inert-gas electrons tend to concentrate the valence electron more strongly at the center of the atom and to increase the contact interaction. Hence, δA is positive at small distances. The term $\delta A\mathbf{I}\cdot\mathbf{S}$ is responsible for the pressure shifts observed in the hyperfine transition frequencies of alkali atoms. The observed shifts are in good qualitative agreement with the idea of a competition between exchange forces and Van der Waals forces. For heavy inert gases such as xenon or kyrpton, the pressure shifts are negative. This is reasonable since these heavy gases are highly polarizable and should have large Van der Waals interactions. For light inert gases such as helium and neon, the shifts are positive, which is not too surprising since these gases are not very polarizable and exchange forces dominate during the collisions. The pressure shifts of the hyperfine frequency of ^{133}Cs are illustrated in Fig. 33.

TABLE XIII. Depolarization cross sections in Å^2 for alkali $^2P_{3/2}$ states in inertia gases.[a]

	Na	Rb	Cs
He	50 (Elb67)	100 (Zhi70)	32 (Fri67)
Ne	48 (Elb67)	100 (Zhi70) 100 (Gal67b)	29 (Fri67)
Ar	88 (Elb67)	205 (Zhi70) 210 (Gal67b)	60 (Fri67)
Kr		290 (Zhi70)	92 (Fri67)
Xe		310 (Zhi70)	113 (Fri67)

[a] These cross sections are not always clearly defined (see text).

The pressure shift caused by binary collisions is approximately

$$\delta\nu = \langle\delta A\rangle_{Av}(I+\tfrac{1}{2})\tau_c/\tau_v, \qquad \text{(VII.14)}$$

where τ_c is the time of collision ($\simeq 10^{-12}$ sec), and τ_v is the time of flight between collisions. The mean value of δA during a collision is $\langle\delta A\rangle_{Av}$. Since τ_v is inversely proportional to the inert-gas pressure, the frequency shift due to binary collisions should be a linear function of pressure. The pressure shift also depends on temperature because the collision rate and the velocity distribution of the buffer-gas atoms change with changes in temperature.

Some representative pressure-shift measurements are included in Table XIII. Temperature dependences and pressure shifts for various mixtures can be found in the original references. Pressure shifts in organic buffer gas have been measured for ^{87}Rb by Bratty *et al.* (Bra58), and for cesium by Bernheim and Kohuth (Ber69). Although pressure shifts are found to be very nearly linear up to pressures of a few hundred Torr, Ensberg and zu Putlitz (Ens69) have observed nonlinear pressures shifts for the rubidium isotopes in argon at pressures of several atmospheres.

Theoretical estimates of pressure shifts have been made by Margenau (Mar59), Adrian (Adr60a,b),

Robinson (Rob60), Herman (Her61), Clark (Cla62), Rao (Rao69), and Ray *et al.* (Ray70). Although most of these theories are in reasonably good agreement with experimental observations, they are all based on the assumption that only binary collisions contribute to the pressure shift, whereas it may be true in some situations that molecular formation contributes a noticeable amount to the pressure shift. For instance, Brewer (Bre64) attributes an anomalously large negative pressure shift of rubidium in benzene to a molecular complex.

The interaction $\delta A\mathbf{I}\cdot\mathbf{S}$ should also contribute to the linewidth of the hyperfine transition frequencies. However, Hartmann (Har70b) has shown that for krypton the linewidth of the hyperfine transitions is probably caused mainly by the spin–orbit interaction.

b. The spin–orbit interaction. An interaction of the form $\gamma\mathbf{S}\cdot\mathbf{N}$ was first suggested by Bernheim (Ber62), who showed that two effects can lead to an effective interaction of the form $\gamma\mathbf{S}\cdot\mathbf{N}$. The first is a direct interaction between the spin of the valence electron and the electric field $\mathbf{E}$ of the inert-gas atom (the moving electron experiences an effective magnetic field of the form $(\mathbf{v}/c)\times\mathbf{E}$), while the other is a second-order interaction, involving the excitation of virtual π states of the valence electron. Herman (Her64) has shown that in most cases the second-order interaction is more important, and he has estimated spin-depolarization cross sections for various collision partners. Because of the very short duration of the binary collisions, the interaction $\gamma\mathbf{S}\cdot\mathbf{N}$ causes electron randomization with an electron-randomization cross section on the order of

$$\sigma_{\rm dis}\simeq[\gamma(b_0)I(b_0)/12\hbar^2]^2\sigma_{\rm kin}, \qquad \text{(VII.15)}$$

where b_0 is an effective distance inside which short-range interactions dominate, $I(b_0)$ is the moment of inertia of the colliding pair, and $\sigma_{\rm kin}$ is the kinetic cross section. Of course the basic electron-randomization rate gives rise to a number of different observable relaxation rates for an atom with hyperfine structure (see Sec. V.C.1).

Herman (Her68) has suggested that an interaction of the form

$$V=-[\mu_0\gamma(r)I(r)/\hbar^2][\mathbf{H}\cdot\mathbf{S}-(\mathbf{H}\cdot\mathbf{r})(\mathbf{r}\cdot\mathbf{S})/r^2] \qquad \text{(VII.16)}$$

may cause a slight shift in the effective g_J value of the atomic angular momentum. The coefficient $\gamma(r)$ is the same as the coupling constant for the spin–orbit interaction of Eq. (VII.13), and Herman has shown that the g_J shift is

$$\Delta g_J/g_J\approx-(4/3\pi)^{1/2}n(\sigma_{\rm dis})^{1/2}\sigma_{\rm kin}, \qquad \text{(VII.17)}$$

where $\sigma_{\rm kin}\approx10^{-15}$ cm^2 is the cross section for velocity-changing collisions, $\sigma_{\rm dis}$ is the cross section for electron randomization by the interaction $\gamma\mathbf{S}\cdot\mathbf{N}$ during a sudden binary collision, and n is the number density of perturbing atoms.

3. Relaxation due to Sticking Collisions

The theory of the relaxation due to sticking collisions has been developed by C. C. Bouchiat, M. A. Bouchiat, and L. C. L. Pottier (Bou69,70). An adequate description of the experimental observations can be obtained by assuming an interaction potential between the alkali atom and the inert-gas atom of the form

$$V=U(r)+h[A+\delta A(r)]\mathbf{S}\cdot\mathbf{I}+\gamma(r)\mathbf{S}\cdot\mathbf{N}. \qquad \text{(VII.18)}$$

The central potential $U(r)$ can be obtained from low-energy atom–atom scattering experiments, and the value of $U(r)$ is known for most rare-gas–alkali atom pairs. The spin-dependent terms, $\delta A(r)$ and $\gamma(r)$, play a negligible role in scattering, but they cause the polarization of the alkali vapor to relax and also cause frequency shifts in the magnetic resonance spectrum of the alkali ground state. Certain higher-order spin interactions that are allowed by symmetry are not included in Eq. (VII.18) because experimental and theoretical considerations indicate that they are negligibly small. The physical origins of the coupling constants $\delta A(r)$ and $\gamma(r)$ were discussed in the previous sections.

Because the interaction $U(r)$ is attractive at large distances, where it is determined mainly by Van der Waals forces, bound states of the alkali–inert-gas molecule can exist. The center-of-mass motion is governed by an effective potential

$$U_N(r)=U(r)+\hbar^2N(N+1)/2\mu r^2, \qquad \text{(VII.19)}$$

where N is the angular momentum of translation of the alkali atom around the inert-gas atom, and μ is the reduced mass of the system. Typical potentials $U_N(r)$ are shown in Fig. 34. Bound or quasibound states can exist for all angular momenta less than the critical value N_c. Such states can be formed by three-body collisions or by resonant two-body collisions. Bouchiat *et al.* have shown that resonant two-body collisions are not important in the regime of present day experiments, but such phenomena would be important if experiments could be performed at much lower pressures. For higher-pressure ranges, the concentration of molecules is given by the law of mass action:

$$[\text{Rb Kr}]=[\text{Rb}][\text{Kr}]K, \qquad \text{(VII.20)}$$

where K is the equilibrium constant of the reaction

$$\text{Rb}+\text{Kr}\leftrightarrow\text{Rb Kr}.$$

Bouchiat *et al.* (Bou70) have shown that an adequate description of the experimental results of spin relaxation can be obtained by a three-parameter theory. The parameters are K, the equilibrium constant of Eq. (VII.20); $\bar{\sigma}$, the mean cross section for the breakup of Rb–Kr molecules, and $\bar{\gamma}$, the mean value of the spin-rotational interaction constant in Eq. (VII.18).

For instance, for the rubidium–krypton system, Bouchiat *et al.* (Bou70) report the following values for these parameters

$$\bar{\gamma}/\hbar = 0.63 \text{ MHz}; \qquad \bar{\sigma} = 2.23\pi r_m^2;$$
$$K = 1.68\times 10^{-22} \text{ cm}^3.$$

Here $r_m = 4.53$ Å is the scale parameter of a 6–12 Lennard–Jones potential.

4. *Wall Relaxation in Alkali Atoms*

Robinson *et al.* (Rob58) discovered that alkali atoms can be pumped in evacuated cells if the glass walls of the cell are coated with weakly relaxing materials. It has been found that paraffins and certain organosilanes (Drifilm) are especially useful for pumping alkali atoms. Unfortunately, Teflon and other fluorocarbons, which work well with atomic hydrogen, are attacked by the alkali atoms. Relaxation times approaching one second can be obtained in paraffin-coated cells.

Detailed studies of the relaxation of rubidium on paraffin-coated walls have been made by Bouchiat (Bou62a,b,66a) and her associates. The relaxation rates seem to be independent of the chain length of the paraffin molecule (Bou62b). However, the relaxation rates are noticeably smaller on deuterated paraffin than on normal hydrogenated paraffin (Bou62b). This implies that the magnetic fields of the hydrogen and deuterium nuclei play a significant role in the relaxation, since the magnetic moment of deuterium is smaller than that of hydrogen by a factor of about 3. However, it is not possible to attribute all of the observed relaxation to the magnetic fields of the nuclei in the wall coating, since a number of properties of the relaxation indicate that a second (probably spin–orbit) interaction is present. For instance, Bouchiat (Bou63c) found that

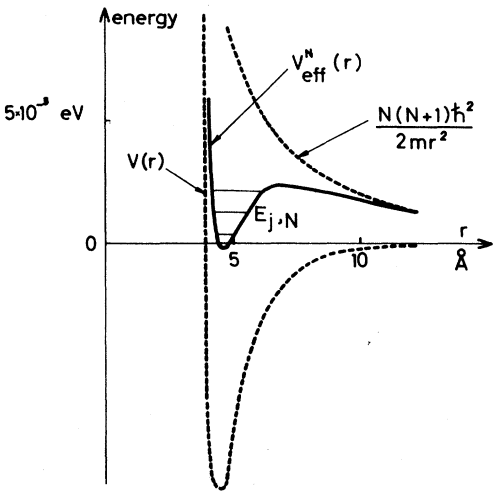

FIG. 34. Typical potentials for an alkali–inert-gas molecule. The effective potential V_{eff} is the sum of the electronic potential V and the centrifugal potential [from (Bou69)].

TABLE XIV. Depolarization cross sections in Å² for $^2P_{1/2}$ states in inert gases (ΔE is the $^2P_{1/2,\,3/2}$ fine-structure interval).[a]

Gas	Rb ($\Delta E = 238$ cm^{-1})	Cs ($\Delta E = 554$ cm^{-1})	Tl ($\Delta E = 7793$ cm^{-1})
He	9 (Gal67b)	2.1 (Gal67b)	0.0060 (Gib70a)
Ne	6 (Gal67b)	0.8 (Gal67b)	0.0014 (Gib70a)
Ar	9.7 (Gal67b)	1.7 (Gal67b)	0.0110 (Gib70a)
Kr	10.6 (Gal67b)		0.0220 (Gib70a)

[a] These cross sections are not always clearly defined (see text).

the hyperfine polarization $\langle \mathbf{S}\cdot\mathbf{I}\rangle$ relaxes at the same rate for both ^{85}Rb and ^{87}Rb on deuterated walls, but that the rates are slightly different on hydrogenated walls. On deuterated walls the interaction responsible for the relaxation of $\langle \mathbf{S}\cdot\mathbf{I}\rangle$ is believed to be mainly a spin–orbit interaction. The same spin–orbit interaction accounts for most of the relaxation of $\langle \mathbf{S}\cdot\mathbf{I}\rangle$ on hydrogenated walls, but a measurable contribution is also present from the magnetic fields of the hydrogen nuclei.

Experimental studies of the relaxation rates as a function of the external magnetic field (Vid65), (Bou66b) reveal that the interaction due to the nuclear spins has a rather long correlation time, which is probably associated with hops from site to site while the atom is bound to the wall. However, the spin–orbit interaction has a short correlation time, which is probably on the order of the vibrational period of the bound rubidium atom at a given site on the wall.

The relaxation on paraffin-coated walls is also a strong function of temperature (Bou65b). Increasing the temperature up to about 60°C lengthens the relaxation time because the rubidium atoms remain stuck to the walls for shorter periods of time. However, above 60°C the relaxation times decrease with increasing temperature, apparently because of irreversible reactions of the rubidium atoms with the paraffin or with the walls.

D. Collisional Depolarization of the Excited State

The excited $^2P_{1/2}$ and $^2P_{3/2}$ states are strongly affected by collisions with buffer-gas molecules, and the collisional depolarization cross sections are usually on the order of gas kinetic cross sections or larger. Presumably, there are three basic depolarization cross sections for the $^2P_{3/2}$ state, one for each of the electronic multipole moments of the state (see Sec. V.C.2). Although theory indicates that the basic relaxation rates are nearly the same (Oku70), no definitive experimental studies of these rates have yet been made because of the difficulty in accounting for the effects of the nuclear spin. The situation is somewhat simpler in the case of the $^2P_{1/2}$ state, where only one electronic relaxation rate exists. However, even in the $^2P_{1/2}$ state the influence of the

nuclear spin is not small, even though it is usually ignored (Bul71b).

Order-of-magnitude estimates of depolarization cross sections are listed in Tables XIII and XIV. The D_2 depolarization cross sections were estimated from critical pressure data for D_2 pumping of the ground state. The $P_{1/2}$ depolarization cross sections were obtained by Hanle-effect measurements. Neither method is very reliable because of uncertainties in the interpretation of the data. For instance, the $^2P_{1/2}$ electron-randomization cross sections should probably be about three times larger than those quoted by Gallagher (Gal67b), because of the influence of the nuclear spin on the collisional broadening of the Hanle-effect signals (Bul71b). The $^2P_{3/2}$ cross sections are probably too small for the same reason. However, to avoid confusion we have listed the cross sections as they appear in the literature.

Despite the uncertainties of these measurements, it is clear that the $^2P_{1/2}$ depolarization cross sections for rubidium and cesium are anomalously small. Experimental evidence for anomalously small collisional depolarization cross sections for the $^2P_{1/2}$ states of heavy alkali atoms was first reported by Marrus and Yellin (Mar66). Franz (Fra66b) and Gallagher (Gal67b) have pointed out that for electrostatic interactions, no collisional depolarization at all should occur in the $^2P_{1/2}$ state, provided that transitions to the $^2P_{3/2}$ state can be neglected. Such fine structure transitions would be least likely in rubidium and cesium, because their fine structure intervals are larger than the thermal energy kT. For comparison we have included in Table XIV the depolarization cross sections for the $^2P_{1/2}$ state of thallium (Gib70a). The depolarization cross sections for thallium are three or four orders of magnitude smaller than gas kinetic cross sections. Thus the smallness of the $^2P_{1/2}$ cross sections in rubidium, cesium, and thallium furnishes good evidence that the forces involved in collisional depolarization of the ^2P states are largely electrostatic in nature.

1. *Transfer between the Fine-Structure Doublets*

The transfer of population between the fine-structure doublets of the alkali atoms can be measured with some confidence, since, with proper precautions, the nuclear spin and the excited-state polarization need not complicate the experimental measurements. However, Gallagher (Gal68) has pointed out that serious errors can arise if proper account is not taken of the pressure broadening of the optical lines. Extensive studies of fine-structure transition rates have been made by Krause (Kra66b) and his co-workers. Their work showed clearly that the inert gases are very poor agents for inducing transfer between the doublets of rubidium and cesium. More detailed work by Gallagher (Gal68) has shown that the transfer cross sections are strongly velocity dependent; and, in the case of rubidium and cesium, only the very fast atoms in the high-velocity tail of the velocity distribution contribute to the transfer cross sections. Gallagher's data is reproduced in Fig. 35. Qualitatively, one can understand these results by remembering that transitions can be induced between the $^2P_{1/2}$ and $^2P_{3/2}$ states only if the

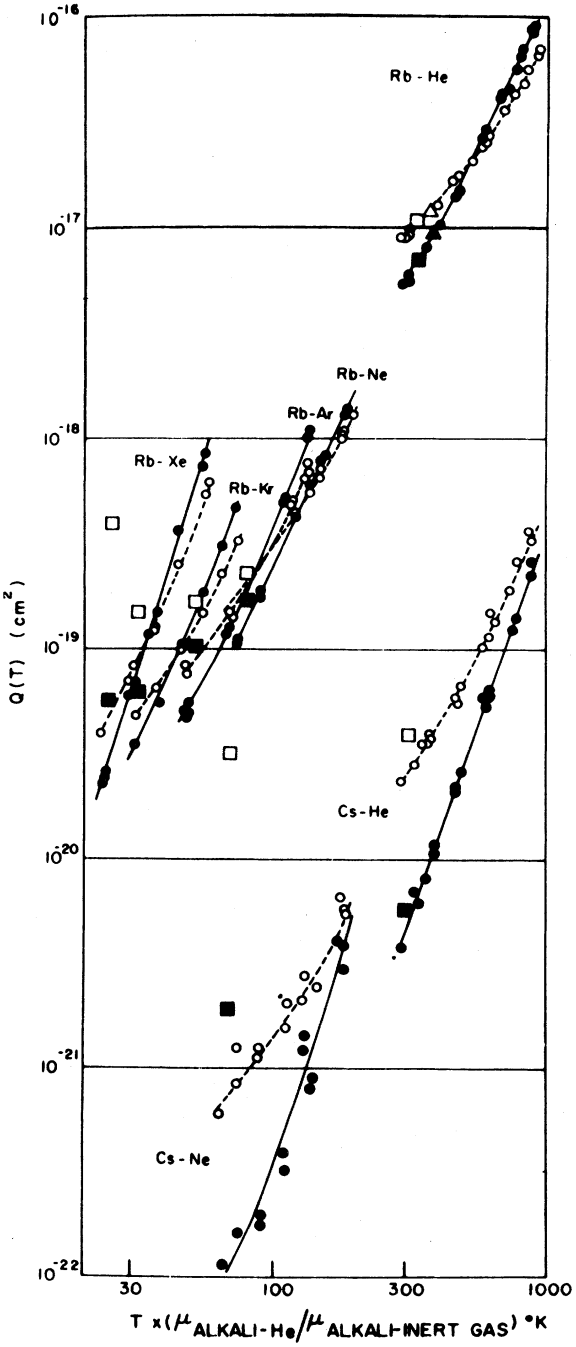

FIG. 35. Cross sections for collisional transfer between the $P_{1/2}$ and $P_{3/2}$ fine structure states of the alkali atoms. There is a pronounced temperature (velocity) dependence of the cross sections [from (Gal68)].

TABLE XV. Quenching and transfer cross sections for excited rubidium atoms in molecular buffer gases.

Gas	$\sigma(P_{1/2}\rightarrow S_{1/2})$	$\sigma(P_{3/2}\rightarrow S_{1/2})$	$\sigma(P_{1/2}\rightarrow P_{3/2})$	$\sigma(P_{3/2}\rightarrow P_{1/2})$	Reference
N_2	58	43	16	23	(Hry70)
	58	42	14	24	(Bul71c)
H_2	6	3	11	15	(Hry70)
	6	3	9	15	(Bul71c)
D_2	3	5	22	30	(Hry70)
	3	3	19	29	(Bul71c)
CH_4			30	42	(Hry70)
	0	4	32	53	(Bul71c)
C_2H_4	139	95	23	32	(Hry70)
	174	112	12	19	(Bul71c)
C_2H_6			57	77	(Hry70)
	0	5	57	86	(Bul71c)

kinetic energy of the incident atom is sufficient to supply the energy of the transition. From the viewpoint of semiclassical collision theory, it is also necessary that the Fourier components of the collisional interaction have substantial amplitude at the fine-structure frequency. Only for very fast collisions are such high-frequency Fourier components available. Thus, rubidium and cesium, with their large fine-structure intervals, are least susceptible to collisional transfer between the $^2P_{1/2}$ and $^2P_{3/2}$ states.

A completely different behavior is exhibited by molecular buffer gases. One finds that these gases induce transitions between the fine-structure doublets of all alkali atoms with about the same efficiency. Presumably, some of the internal energy of the fine-structure separation can be converted into vibrational and rotational energy of the molecules. Some typical transfer cross sections for molecular buffer gases are listed in Table XV. More details on transfer cross sections can be found in the work of Krause and his collaborators (Kra66b), (Pit66), (Mcg67), (Stu68,69), (Cop69). In these papers some of the smaller reported cross sections for transfer between the fine structure doublets may not be very reliable because of pressure broadening of the optical line.

2. *Quenching*

Buffer gases may also quench the excited atoms, i.e., the excitation energy of the atoms may be transferred to the foreign gas molecule in such a manner that no fluorescent light is observed. For all practical purposes the inert gas atoms may be regarded as nonquenching; i.e., the quenching cross sections are much less than 10^{-16} cm^2. Dodd *et al.* (Dod69) have determined experimental upper limits of about 10^{-19} cm^2 for the quenching of excited cesium atoms by helium. Molecular buffer gases, however, do quench fairly effectively, the most notable example being nitrogen, for which quenching cross sections in excess of 50 Å^2 are observed. Presumably, the rotational and vibrational degrees of freedom of a molecule are necessary to absorb the excitation energy of the atom. Direct conversion of the excitation energy into kinetic energy, which would have to occur with inert gases, is highly unlikely. Quenching cross sections for some of the common gases are included in Table XV.

Quenching is very important in optical pumping experiments, since it decreases the influence of radiation trapping. For instance, the ^{87}Rb maser has been operated successfully only with a nitrogen buffer gas (Dav66), probably because the quenching of the rubidium fluorescence by the nitrogen allows one to operate with an optically thick vapor but with little depumping resulting from fluorescent light.

E. Lithium

Lithium, which is highly corrosive, attacks quartz and glass cells in a few minutes at the high temperatures (~400°C) necessary for pumping. Sapphire and magnesium-oxide windows are more resistant to the action of lithium, and Minguzzi *et al.* (Min69) have successfully constructed a stainless steel pumping cell with sapphire windows. The cell, which could be baked at temperatures as high as 450°C, was filled with ^{7}Li and 177 Torr of helium buffer gas for operation. The D_2 line of ^{6}Li overlaps the D_1 line of ^{7}Li so that each isotope can be used in a lamp for depopulation pumping or transmission monitoring of the other isotope (Min69). The most successful lithium lamps are of the hollow cathode or flow lamp design (Bud65). Minguzzi *et al.* (Min66a) have published details of a particularly effective lithium flow lamp. The scattering of red lithium resonance radiation from pumped atoms can often be seen with the naked eye.

F. Sodium

Although sodium is much less corrosive than lithium, it still presents problems, and some care must therefore be taken in the selection of materials for cells. Most

glasses are satisfactory at low temperatures, but quartz is particularly susceptible to attack and should be avoided. Sodium-resistant glasses have been developed by several lamp manufacturers (Phillips, General Electric), and the resistance of lamps to attack can be increased by coating the glass with various glazes (Bel61).

The 6 Å separation of the yellow sodium D lines is too little to allow the use of conventional interference filters. However, very successful use has been made of Lyot polarization-interference filters to separate the D lines (Boe61), (Köp69). Carver *et al.* (Car61) have developed a magnetically scanned, sodium-vapor filter which passes 90% of the D_1 line, and only 2% of the D_2 line. The behavior of high-intensity sodium lamps in a strong magnetic field has been investigated by Ioli *et al.* (Iol70). A magnetically scanned sodium lamp has been developed by Moretti (Mor71). Such lamps are useful for hyperfine pumping and transmission monitoring of $\langle \mathbf{I} \cdot \mathbf{J} \rangle$. Electrodeless discharge lamps of the type described by Bell *et al.* (Bel61a) and by Brewer (Bre61) are adequate for Zeeman-pumping experiments. Resonance scattering of the yellow sodium D lines is often visible to the naked eye, and a change in the brightness of the vapor is readily noticed when the pumped atoms are depolarized with a resonant rf field.

Typical operating temperatures for sodium-absorption cells are 150°C. At these temperatures sodium reacts slowly with molecular buffer gases such as hydrogen and nitrogen (And64b). It also attacks many types of paraffin coatings, but Lemmerich and Raith (Lem62) have produced satisfactory polyethylene coatings. Coatings of the Drifilm type are also satisfactory (Bes67), (Köp69).

The field-independent hyperfine transitions in sodium have been studied by Arditi (Ard58a) and Bell (Bel58). Multipole quantum transitions in the ground state have been investigated by Winter (Win59). Besch *et al.* (Bes67), (Köp69) have polarized the radioactive sodium isotope ^{21}Na by spin exchange with optically pumped natural isotopes of sodium.

G. Potassium

At the typical temperatures of operation of potassium absorption cells (~100°C), the corrosive properties of potassium are similar to those for sodium but less severe. The two D lines of potassium can be separated by narrow-bandpass interference filters. The hyperfine splittings of the atomic states of ^{39}K are particularly small, so that resolution of the $\Delta m = 1$, $\Delta F = 0$ resonances of the ground state can be achieved at fields of three or four G. The $\Delta F = 1$ ground-state transitions at 458 MHz can be driven with conventional radio-frequency equipment. Electrodeless discharge lamps (Bel61) are adequate sources of pumping light.

Multiple quantum transitions and wall coatings for potassium have been studied by Kraniska-Miszczak (Kra66a). Grossetête and Brossel (Gro67a) have developed a method to measure the hyperfine polarization $\langle \mathbf{S} \cdot \mathbf{I} \rangle$ for ^{39}K by using resonantly scattered light from a ^{41}K vapor. They have also investigated the use of paraffin wall coatings for potassium-vapor cells. The potassium atoms react fairly quickly with the paraffin coatings at typical (100°C) operating temperatures.

H. Rubidium

At the low operating temperatures of rubidium absorption cells ($\leq$60°C), corrosion is seldom a problem, although rubidium atoms are known to be permanently absorbed by glass walls and to a lesser extent by paraffin-coated walls. Partial saturation of the walls with rubidium atoms seems to occur after periods of days or weeks. Similar phenomena may occur with the other alkali atoms, but only rubidium has been studied in much detail. Both Drifilm (organosilane) and paraffin wall coatings have been successfully used with rubidium (Bou66b). Rubidium pumping in wall-coated cells with buffer gas has been investigated by Kryger *et al.* (Kry64) and by Masnou-Seeuws and Bouchiat (Mas67).

There are two common isotopes of rubidium, ^{85}Rb and the weakly radioactive species ^{87}Rb. The nuclear spins and hyperfine structures of these isotopes are quite different, and they can be easily distinguished by radio-frequency spectroscopy (see Table XII). An absorption cell of one isotope can be used to filter out the low-frequency hyperfine component of light from the other isotope, and such filters have been used to prepare light for hyperfine absorption pumping in masers (Dav64). Conventional interference filters can be used to separate the D lines. A simple, effective filter that passes D_2 light but absorbs most D_1 light has been developed by Firester (Fir68) from a solution of neodymium chloride. Gibbs and Slusher (Gib70c) have used the 7944-Å line from a Hg laser to pump rubidium atoms in a magnetic field of 74.5 kG. Mathur and Happer (Hap67a) have used the 4215-Å line of a Sr^+ lamp as a probe of optically pumped rubidium vapor. Both rubidium isotopes exhibit noticeable birefringence for narrow-line probing beams. Electrodeless discharge lamps (Bel61a) are adequate sources of pumping light. However, long (40-cm) cells of rubidium vapor have been successfully pumped by long lamps with internal electrodes (Tan70).

I. Cesium

The corrosive properties of cesium are not severe and are similar to those of rubidium. There is only one stable isotope, ^{133}Cs. There is a large hyperfine splitting of all atomic states (see Table XII), which leads to a pronounced birefringence of the pumped vapor. The D lines are easily separated with interference filters. Electrodeless discharge lamps (Bel61a) are the most convenient and widely used sources of pumping light.

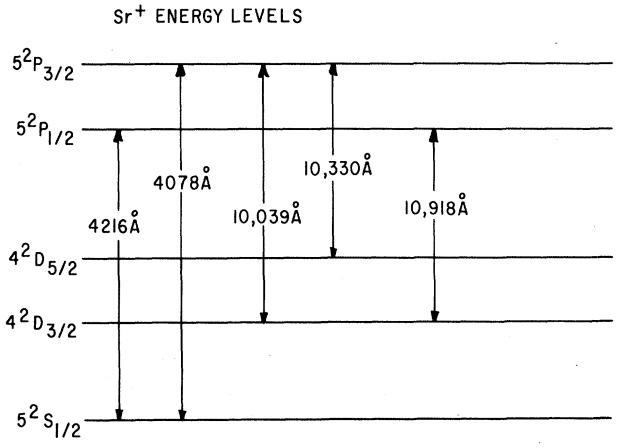

FIG. 36. Low-lying energy levels of Sr^+.

Intense pumping lamps have been described by Franz (Fra63a). Light sources for hyperfine pumping have been developed by Ernst *et al.* (Ern67,68a) and by Beverini and Strumia (Bev70). Cesium has also been probed with a gallium–arsenide laser (Sia69). The vapor can be probed with the 8521-Å line of argon (Bea58), or with the 3880-Å line of helium.

Orientation of cesium vapor was first reported by Blandin and Barrat (Bla56). Hyperfine transitions have been investigated by Beaty and Bender (Bea58), by Diamond, Legendre, and Skalinski, (Dia58), (Ska58), and by Arditi and Carver (Ard58b).

J. Singly Ionized Strontium and Barium

Optical pumping of Sr^+ ions has been reported by Ackermann *et al.* (Ack67). The energy levels involved in the optical pumping are shown in Fig. 36. The pumping mechanisms are quite similar to those in the alkali atoms, except for the presence of the low-lying metastable ^2D state to which branching occurs from the excited P states. The branching ratios to the $^2S_{1/2}$ ground state have been measured by Gallagher (Gal67a), who reports values of 15% and 13% for the $^2P_{3/2}$ and $^2P_{1/2}$ states, respectively. Ackermann *et al.* (Ack67) report ion lifetimes of several milliseconds in their experiments. In experiments with Sr^+ ions, they have also reported upper limits for ground-state depolarization cross sections of 10^{-3} Å^2 for helium, 8×10^{-3} Å^2 for Ar, and 4×10^{-2} Å^2 for Kr. Their cross sections include the effects of Sr^+–e, Sr^+–Sr, and other relaxation mechanisms, and the actual noble gas cross sections may be substantially lower.

Optical pumping of Ba^+ ions in helium buffer gas has been reported by von Sichart *et al.*, (Von70). The D_1 (4934-Å) and D_2 (4554-Å) resonance lines were generated by a high-intensity arc discharge hollow cathode lamp. Precision measurements of the ground-state hyperfine intervals for $^{135}Ba^+$ and $^{137}Ba^+$ were obtained. Ions of other Group II atoms, such as Mg^+, Ca^+, Cd^+, Hg^+, etc. can probably be pumped in the same way as Sr^+.

The oscillator strengths and branching ratios of the important optical transitions of interest in Mg^+, Ca^+, and Ba^+ have been measured by Gallagher (Gal67a) and by Smith and Gallagher (Smi66).

K. Hydrogen

Attempts to optically pump hydrogen atoms have not yet succeeded. There are severe problems with the optical components needed to handle the 1216-Å D lines, and the best material for lenses and windows, lithium fluoride, develops color centers under the influence of the pumping light. Furthermore, hydrogen atoms must be produced somehow from molecular hydrogen, and the discharges or thermal dissociators used for this purpose are an added complication in the experimental apparatus. Some of the problems associated with the optical pumping of hydrogen in the laboratory have been summarized by McIlrath (McI66). However, Varshalovich (Var70) has suggested that optical pumping of hydrogen atoms may occur in interstellar space.

VIII. ATOMS WITH $^1S_0$ GROUND STATES

Diamagnetic atoms with a $^1S_0$ ground state can be optically pumped provided that a nonzero nuclear spin is present. Perhaps the most striking feature of such atoms is their resistance to depolarization by wall collisions, and such atoms are usually pumped without buffer gas in quartz or glass containers. A typical energy-level diagram for such atoms is shown in Fig. 37. Pumping is usually done with the $^3P_1$ or $^1P_1$ excited states. Because of the breakdown of LS coupling, neither state is pure triplet or singlet; and consequently, the $^3P_1$ state can decay to the ground state by an electric-dipole transition. However, because the $^3P_1$ state has only a weak admixture of the $^1P_1$ state, the radiative lifetime of the triplet state is much longer

TABLE XVI. Basic atomic parameters of Group IIB atoms.

Atom	Triplet resonance line (Å)	Singlet resonance line (Å)	Triplet lifetime (nsec)	Singlet lifetime (nsec)
Zinc	3076	2139	20 000	1.41
Cadmium	3261	2288	2 400	1.66
Mercury	2537	1850	115	1.31

than that of the singlet state. The triplet state always lies lower in energy than the corresponding singlet state, and the triplet (intercombination) radiation therefore has a longer wavelength than the singlet radiation.

Optical pumping of the $^1S_0$ atoms can occur only if the hyperfine intervals in the excited states are larger than the natural width. Depopulation pumping can occur for narrow-line excitation but not for broad-line excitation (see Sec. III.A.14). However, efficient repopulation pumping can occur for either broad-line or narrow-line excitation provided that the hyperfine periods of the excited state are much shorter than the excited-state lifetime. A detailed study of the effects of hyperfine coupling on repopulation pumping has been made by Lehmann (Leh67), (see also Sec. VIII.B). Some of the important properties of $^1S_0$ atoms are summarized in Table XVI.

Buffer gases are seldom used in optical pumping experiments with mercury, cadmium, and zinc, since the polarized atom can make many collisions with the container walls before being depolarized. The mechanisms responsible for wall relaxation are not yet completely understood. For atoms with nuclear spins $I \geq 1$, one of the major mechanisms is known to be the interaction of the electric quadrupole moment of the nucleus with electric field gradients caused by the constituents of the wall. However, a magnetic interaction is also present, since atoms devoid of any quadrupole moment (e.g., ^{199}Hg with $I=\frac{1}{2}$) relax on the walls. The magnetic interaction probably has a number of different origins, and the strength of the interaction depends on the state of the container surface. Prolonged irradiation of quartz containers with ultraviolet light is found to increase the relaxation rate of optically pumped ^{199}Hg vapor (Coh64). Presumably, the ultraviolet light creates some sort of paramagnetic sites in the quartz surface. The relaxation rates are also strongly dependent on the wall temperature. The temperature dependence is caused at least partly by changes in the mean dwell time of an atom on the surface.

A. Mercury

Mercury has a very high vapor pressure even at room temperatures, and consequently it is a very convenient isotope to pump. The atomic density can be controlled simply by placing a drop of mercury in a long sidearm that is immersed in a cooling bath. The temperature of the cooling bath then determines the vapor pressure in the rest of the cell. Typical temperatures of operation are around 0°C for pumping with the 2537-Å intercombination line and about −43°C for pumping with the 1850-Å resonance line. Radiation trapping becomes a serious problem if these temperatures are exceeded.

Optical pumping of mercury was first reported by Cagnac, Brossel, and Kastler (Cag58a,b,d), who aligned ^{201}Hg atoms with unpolarized 2537-Å light. Optical pumping of the odd mercury isotopes is greatly facilitated by the use of lamps and absorption filters made with separated isotopes. The relative frequencies of the various isotopic components of the 2537-Å intercombination lines and the 1850-Å resonance line are shown in Fig. 38. Cagnac and Brossel (Cag59) have shown that a ^{204}Hg lamp can serve as a good narrow-line source for

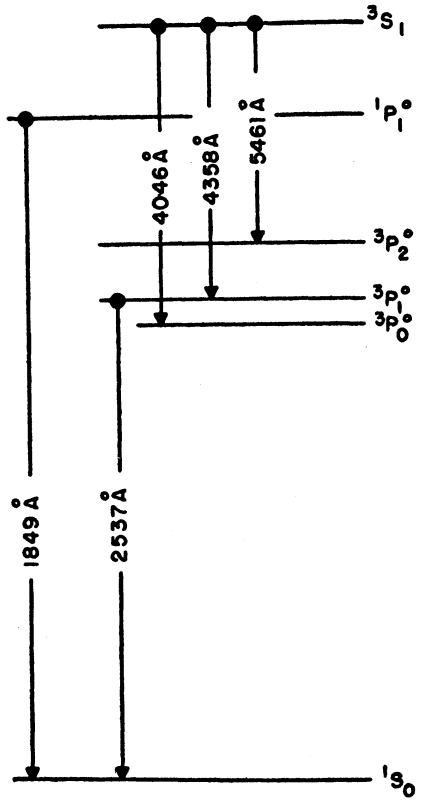

FIG. 37. Low-lying energy levels of mercury [from (Bro52)].

exciting the transition $F=\frac{1}{2}\rightarrow F=\frac{1}{2}$ in ^{199}Hg. Early work on the optical pumping of mercury is summarized in Cagnac's thesis (Cag61).

Optical pumping of ^{201}Hg with the 1850-Å resonance line from a ^{202}Hg lamp was reported by Popesku and Novikov (Pop64), (Nov65). A remarkable feature of these experiments was the appearance of a very broad magnetic resonance line, corresponding to a relaxation time of 2.2×10^{-4} sec, in addition to the expected narrow resonance line of ^{201}Hg. The broad line has not yet been positively identified, but Novikov and Popesku (Nov65) have suggested that it may be associated with the $^3P_0$ metastable state.

Mercury-199, which has only two ground-state sublevels, has served us as an important test case for the basic theory of optical pumping. Many detailed comparisons between theory and experiment for ^{199}Hg can be found in the thesis of Cohen-Tannoudji (Coh62a,b).

Optical pumping of the 6^3P_2 state of mercury has been reported by Barrat, Chéron, and Cojan (Bar64). They polarized the $^3P_2$ state both by depopulation pumping with the 5461-Å green line ($6^3P_2\rightarrow7^3S_1$) and by repopulation pumping from the 7^3S_1 level, which was populated by stepwise excitation from the $^1S_0$ ground state through the 6^3P_1 excited state with the lines at 2537 Å and 4358 Å. Up to 2% of the mercury atoms were maintained in the metastable state. Contributions to the relaxation were 18 kHz from the pumping light, 11 kHz from collisions between metastable and ground-state atoms, and 3 kHz from wall collisions. Collision-broadening cross sections for the $^3P_2$ state in various foreign gases have been measured by Tittel (Tit65).

Optical pumping of the metastable 6^3P_0 state of ^{199}Hg has been reported by Lahaye and Margerie (Lah70). Polarization was produced by repopulation pumping from the 7^3S_1 state, which is populated by excitation of 6^3P_2 metastable atoms with polarized 5461-Å light. The polarization of the 6^3P_0 state is monitored by observing the cross fluorescent 5461-Å light that is produced when the polarized 6^3P_0 states are illuminated with unpolarized 4047-Å light. A remarkable finding of these experiments was that the g_F value for the $^3P_0$ state is about 1.8 times larger than that of the ground state. This occurs because the hyperfine interaction admixes sizeable amounts of the $F=\frac{1}{2}$ component of the $^3P_1$ state to the $F=\frac{1}{2}$ component of the $^3P_0$ state. The large electronic g_J factor of the $^3P_1$ state therefore contributes to the g factor of the $^3P_0$ state.

1. *Wall Relaxation of Mercury*

Cagnac and Brossel (Cag58c,59) discovered that polarized ^{201}Hg atoms relaxed much faster than ^{199}Hg in evacuated quartz containers, and they suggested that the faster relaxation rate of ^{201}Hg was caused by the nuclear quadrupole moment of ^{201}Hg. More detailed studies by Cohen-Tannoudji (Coh63) showed that the relaxation mechanism for ^{201}Hg was indeed mainly an

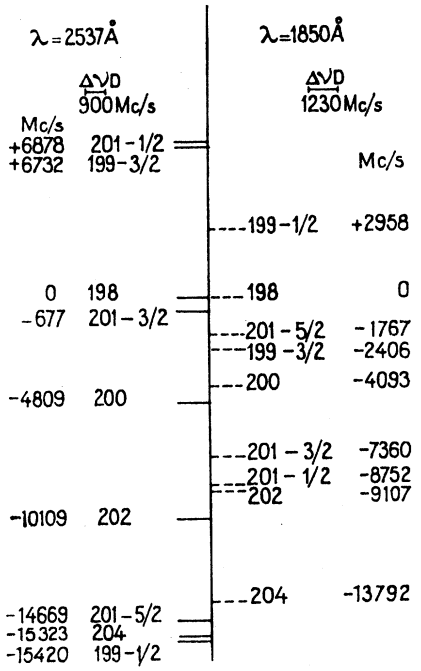

FIG. 38. Isotope shifts and hyperfine structures of the mercury isotopes [from (Pop64)].

electric quadrupole interaction. For instance, Cohen-Tannoudji found that the alignment of ^{201}Hg relaxed twice as quickly as the orientation. This is exactly what one would expect if the relaxation were caused by a weak, fluctuating electric field gradient (see Sec. V.B.3). The exact correlation time of the interaction is unknown, but it is known to be less than 10^{-7} sec (Coh63).

The relaxation of ^{199}Hg is slower than that of ^{201}Hg when the walls are at room temperature. Presumably, this results from the absence of an electric quadrupole moment in ^{199}Hg. The nature of the magnetic interactions at the walls is still unknown. Cohen-Tannoudji and Brossel (Coh64) have shown that prolonged irradiation of the cell walls with intense ultraviolet light can shorten the relaxation time of ^{199}Hg by factors of three or more. The ultraviolet light is believed to produce paramagnetic centers in the surface of the quartz cell. If the cell is removed from the ultraviolet light for several hours, the original relaxation time is re-established. Several different types of center are believed to be involved, because the recovery of the cell is characterized by several different time constants.

The relaxation times of the mercury isotopes depend strongly on the temperature of the cell walls. Initially, (see Fig. 39) there is a rapid lengthening of the relaxation time with increasing temperature in the temperature range of 20°–200°C. This decrease in the relaxation rates is believed to result mainly from a decrease in the dwell time of the atoms on the wall. Cagnac and Lemeignan (Cag67) report an anomalous increase in the

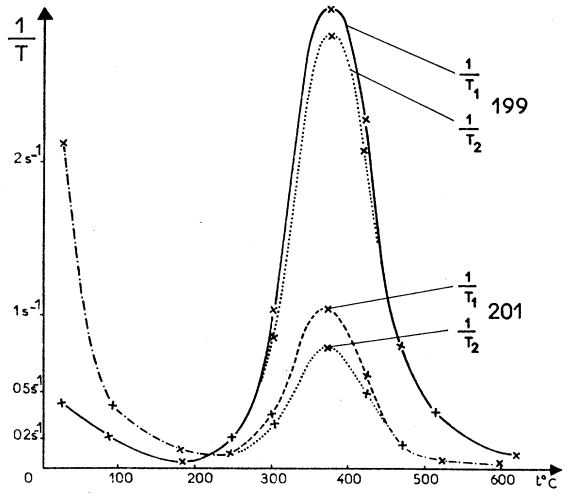

FIG. 39. Relaxation rates of polarized mercury atoms in a quartz container as a function of temperature [from (Cag67)].

relaxation rates at temperatures above 300°C. They suggest that a change in the structure of the quartz walls may occur at 300°C. Above 400°C the relaxation rates again decrease with temperature.

2. *Excited-State Relaxation of Mercury*

Buffer gases are seldom used in ground-state pumping experiments with mercury, and, consequently, excited-state depolarization cross sections are less important in practice than they are for the alkali atoms. However, excited-state relaxation has been very interesting from a more fundamental point of view, and it is in mercury that the phenomena associated with radiation trapping and the inertia of the nuclear polarization were first studied in detail.

Quenching rates and the mean depolarization cross sections for the $^3P_1$ state of mercury in various foreign gases have been measured by Cunningham and Olsen (Cun60) and by Pickely-Rives *et al.* (Pik64). Barrat *et al.* (Bar66) have made careful measurements of quenching and depolarization cross sections for orientation and alignment in the $^3P_1$ state. Very detailed studies of the relaxation of the $^3P_1$ state have been made by Faroux and Brossel in order to test the theory of relaxation in atoms with hyperfine structure (see Sec. V.C.2b and the references cited there). Resonant self-broadening of the $^3P_1$ state of mercury has been studied by Meunier, Omont, and Brossel (Meu65).

The effects of radiation trapping on excited-state relaxation have been studied by Barrat (Bar58,59a,b), and by Omont (Omo65a,c). Coherence narrowing in the $^1P_1$ state of mercury has been studied by Lecler (Lec68a,b).

B. Cadmium

Optical pumping of cadmium was first reported by Lehmann and Brossel (Leh64a,c). The isotopic structure of the 3261-Å intercombination lines is shown in Fig. 40. Both depopulation and repopulation pumping are possible with the 3261-Å intercombination line, since the $^3P_1$ excited-state hyperfine structure is well resolved optically. However, because of the small oscillator strength of the intercombination line, the pumping rates are lower than those which can be obtained with the 2288-Å resonance line. Adequate vapor pressures for pumping with the 2288-Å resonance line are obtained at 120°C, while temperatures of around 200°C are required to fully utilize the weakly absorbed 3261-Å intercombination line. Careful cell bakeout procedures are required to prevent outgassing at these high temperatures.

The 3261-Å intercombination line can be used for transmission monitoring of polarized cadmium vapor, and it is clear from Fig. 40 that several even isotopes of cadmium, among them ^{114}Cd and ^{116}Cd, can be used to probe the vapor in paramagnetic Faraday-effect experiments (Leh67).

The 2288-Å resonance line cannot be used for transmission monitoring or depopulation pumping because the $^1P_1$ excited-state hyperfine structure is small compared to the Doppler width of the absorption line. Repopulation pumping is, however, still quite effective since the hyperfine splitting of the $^1P_1$ excited state is somewhat larger than the natural width of the excited state.

Lehmann (Leh64a,67,69) has shown that the probability p_+ that the nuclear spin of a spin $\frac{1}{2}$ isotope be flipped in the excited state is at most

$$p_+ = (a/\Gamma)^2[1+2(a/\Gamma)^2]^{-1},$$

where a is the magnetic dipole-coupling constant of the excited state, and Γ^{-1} is the excited-state lifetime. The maximum flipping probability occurs at a critical magnetic field

$$H = a/2g_J\mu_0.$$

The field dependence of the flipping probabilities for Cd^{111} and Cd^{113} were shown in Fig. 10. The maximum flipping probability for various Group II isotopes is shown in Fig. 41. Note that for all the mercury isotopes, the flipping probability is close to the upper limit of 50%, while in ^{111}Cd and ^{113}Cd the flipping probability is still about 43%. However, a very small flipping probability is to be expected for ^{67}Zn, where the ratio (a/Γ) is much less than unity.

One remarkable feature of the repopulation pumping via the $^1P_1$ state is that orientation of the ground state can be achieved even with unpolarized pumping light at intermediate values of the static magnetic field (Leh67). Also, the pumping efficiency as a function of magnetic field can be used to determine the sign of "a" (Leh67). Unusual light shifts due to real transitions occur when a and Γ are approximately equal, and complete expressions for these light shifts and pumping rates have been calculated by Lehmann (Leh67,69). Most of the

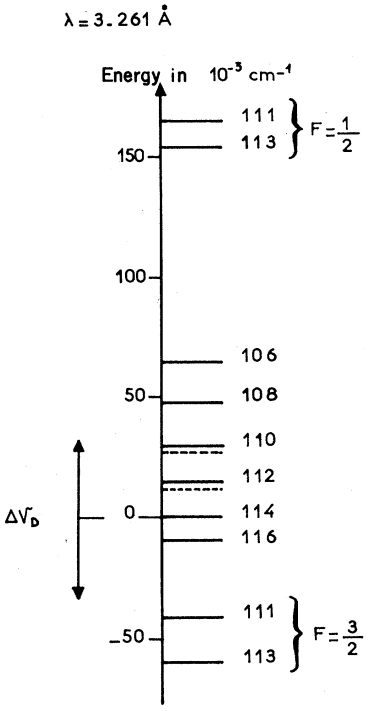

FIG. 40. Isotope shifts and hyperfine structures of the cadmium isotopes [from (Leh67)].

theoretically predicted results have been observed experimentally by Lehmann (Leh67). Since transmission monitoring is impracticable, fluorescence monitoring is used with 2288-Å resonance light.

The radioactive isotopes ^{113m}Cd, ^{115}Cd, and ^{115m}Cd have been optically pumped by Chaney and McDermott (Cha69). They used the 3261-Å intercombination line from an intense lamp, and they detected the pumping by fluorescence monitoring.

Wall relaxation of the cadmium isotopes is quite similar to that of the mercury isotopes. The spin $\frac{5}{2}$ isotope ^{109}Cd is known to relax via a quadrupolar coupling of the nucleus to the fluctuating electric field gradients, which the atom experiences while it is stuck to the walls (Led68b). The spin-$\frac{1}{2}$ isotopes ^{111}Cd and ^{113}Cd relax via some sort of magnetic interaction. A comparative study of wall relaxation in the cadmium and mercury isotopes has been reported by Lehmann and Brossel (Leh66).

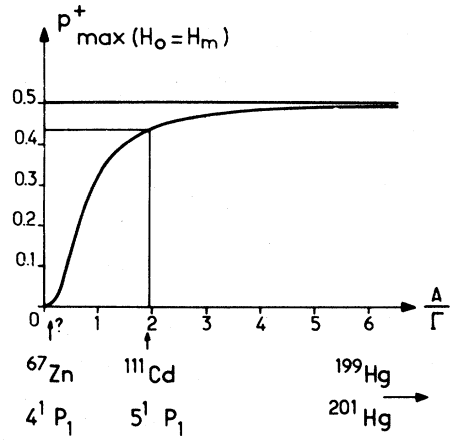

FIG. 41. Singlet pumping efficiency in Group II atoms as a function of A/Γ [from (Leh67)].

C. Zinc

Optical pumping of zinc with the 2139-Å resonance line should be quite inefficient because the hyperfine structure is small compared to the natural width of the $^1P_1$ state. No successful pumping with singlet resonance radiation has been reported. However, Spence and McDermott (Spe67) have reported optical pumping of ^{67}Zn with the 3076-Å intercombination line. Successful pumping was achieved in spite of the very small oscillator strength by using very intense lamps. Nevertheless, pumping rates probably did not exceed one hertz. Polarization was detected by fluorescence monitoring. The zinc vapor was contained in a quartz cell which was maintained at a temperature of 525°C. The transverse relaxation time was estimated to be about 60 msec, so that the zinc atoms were able to make hundreds of bounces against the cell walls without being depolarized (cell-transit times were on the order of 0.1 msec).

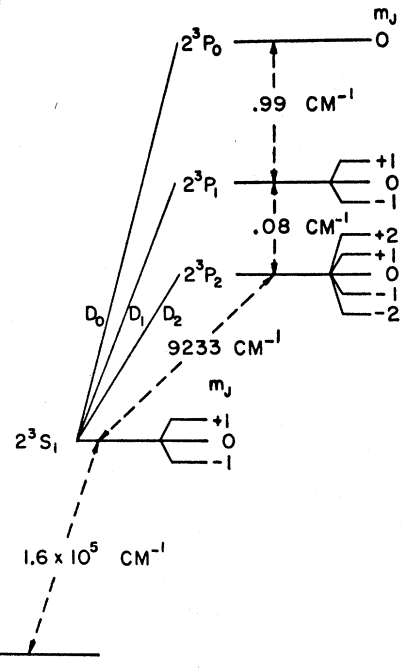

FIG. 42. The low-lying energy levels of orthohelium [from (Col60)].

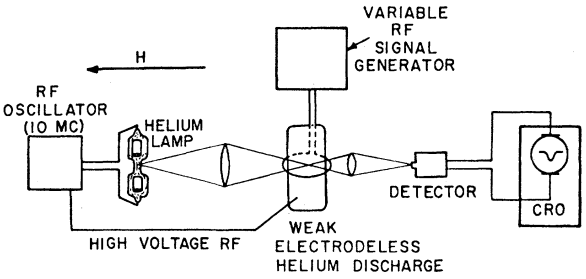

FIG. 43. A typical optical pumping experiment with metastable helium [from (Col60)].

D. Barium

Optical pumping of the barium isotopes ^{135}Ba and ^{137}Ba has been reported by Olschewski and Otten (Ols66). They used the 5535-Å resonance line ($^1S_0$–$^1P_1$), for which the pumping scheme is similar to that of the singlet pumping in mercury and cadmium. Because of the highly corrosive nature of the barium vapor, it was necessary to use a buffer gas to keep the vapor away from the glass windows.

E. Ytterbium

Optical pumping of the odd ytterbium isotopes ^{171}Yb and ^{173}Yb has been reported by Olschewski and Otten (Ols67). The pumping scheme is similar to that of mercury. Temperatures of about 350°C are required for adequate vapor pressure.

IX. HELIUM

The pumping of helium has an importance comparable to that of the alkali atoms, since optically pumped helium is used in the construction of magnetometers (Sch63b,64a), as a source of polarized electrons (McC69), to prepare polarized ^{3}He nuclei (Phi62), (Bak68), and to polarize ions via the Penning reaction with atoms and molecules (Sch69a,70a).

Franken and Colegrove (Fra58b), (Col60) have shown that the metastable $^3S_1$ state of helium can be optically pumped by the 10,830-Å resonance line of the transition 2^3S_1–2^3P_J. The pertinent energy levels are shown in Fig. 42. A simple experimental arrangement is shown in Fig. 43. Triplet metastable atoms are produced in helium gas at a few Torr pressure by a weak rf discharge. The ground-state helium atoms serve as a buffer gas for the metastable atoms, which are produced in concentrations of 10^{10}–10^{11} atoms/cm^3. Electrodeless discharge lamps or electrode-containing lamps are both used as sources of pumping light. Photomultiplier tubes suitable for use at 10 830-Å have low quantum efficiencies and high dark currents, and silicon photodetectors or lead sufide photoconductors are found to be almost as satisfactory as photomultiplier tubes.

Depopulation pumping (or transmission monitoring) is possible if the three D lines have unequal intensities, but for broad-line pumping light only repopulation pumping can occur. A typical spectral profile for the 2^3P_1–2^2S_1 line is shown in Fig. 44. The D_1 and D_2 lines overlap almost completely and are often called the D_3 line. The lifetime of the $^3P_1$ state has been measured by Landmann (Lan68) who reports a value of 99±8 nsec.

Schearer *et al.* (Sch63a) have shown that the isotope shift between the ^{3}He and ^{4}He resonance lines can be put to good use in optical pumping experiments. The D_3 line of ^{4}He overlaps the D_1 line of ^{3}He. In low-pressure experiments ($p \lesssim 0.1$ Torr) there is little depolarization of the excited state, and repopulation pumping is quite efficient. Under these conditions good pumping can be obtained by illuminating ^{4}He atoms with light from a ^{4}He lamp or by illuminating ^{3}He atoms with light from a ^{3}He lamp. However, at higher pressures, the repopulation pumping is suppressed by excited-state mixing, and narrow-line depopulation pumping is required to polarize the atoms. Under high-pressure conditions it is best to pump ^{4}He atoms with a ^{3}He lamp, or, alternatively, one should pump ^{3}He atoms with a ^{4}He lamp.

The $^3S_1$ state can be pumped with circularly polarized, linearly polarized, or unpolarized light. Schearer (Sch68b) has studied the pumping of $^3S_1$ atoms with unpolarized light in some detail.

A. Optical Pumping of He^3

Walters, Colegrove, and Schearer (Wal62), (Col63) and Greenhow (Gre63) have shown that large nuclear polarization of ^{3}He can be obtained by optically pumping the $^3S_1$ state. The nuclear polarization produced by optical pumping in the $^3S_1$ state is preserved when the excitation energy of the atom is passed on to a colliding ground-state atom. The original atom is left in the $^1S_0$ ground state with a polarized nuclear spin. Nuclear polarizations of up to 40% (Col63) have been produced in this way in gaseous ^{3}He.

Because of the nuclear spin, the ground-state ^{3}He atoms provide a large reservoir of angular momentum which takes many minutes to polarize at typical optical pumping rates. Thus, the optical pumping transients are orders of magnitude longer in ^{3}He than in any other optically pumped system. Also the polarized ^{3}He atoms are extremely resistant to depolarization by wall collisions, and relaxation times of many hours are not uncommon.

Dehmelt (Deh64) has pointed out that for optically pumped ^{3}He a small shift of the ground-state magnetic resonance frequency should occur because each ^{3}He atom spends a small fraction of time in the rapidly precessing $^3S_1$ metastable state.

More detailed studies of metastability exchange involving ^{3}He atoms have been reported by Dupont-Roc *et al.* (Dup71). They point out that the nucleus remains inert during the metastability exchange, and that this leads to a strong coupling of the ground-state nuclear polarization to the polarization of the $F=\frac{3}{2}$ and

$F=\frac{1}{2}$ components of the triplet metastable state. This coupling causes the exchange-induced linewidths of the $F=\frac{3}{2}$ and $F=\frac{1}{2}$ magnetic resonance curves to differ. Experimental confirmation of these effects was obtained by Dupont-Roc *et al.*, (Dup71).

McAdams and Walters (McA67,68) have used optical pumping of saturated ^{3}He vapor to polarize liquid ^{3}He up to 0.15%. The vapor was connected to the cold liquid by a long diffusion tube, and the ultimate degree of liquid polarization seems to be limited by the length of the diffusion tube and by the time the polarized atoms spend attached to the walls of the tube. Most angular momentum loss appears to occur on the cold parts of the tube, where the dwell time of the ^{3}He atoms on the wall is long.

B. Relaxation of Helium-3

There are at least four distinct relaxation mechanisms for optically pumped ^{3}He. The most important mechanism is the relaxation caused by the pumping light. The next most important is motion through an inhomogeneous magnetic field. The moving atom experiences a fluctuating magnetic field whose Fourier components cause transition between the magnetic sublevels (see Sec. III.B.5). Relaxation in an inhomogeneous field has been studied in detail by Gamblin and Carver (Gam65) and by Schearer and Walters (Sch65), who find good agreement between theory and experiment. The most complicated relaxation mechanism is relaxation at the walls of the container, which has been studied by Fitzsimmons, Tankersley, and Walters (Fit67). They found that their experimental results can be interpreted by assuming two different relaxation mechanisms, adsorption-controlled relaxation and permeation-controlled relaxation. At low temperatures the ^{3}He is readily adsorbed to the walls. It is believed that the ^{3}He interacts with some kind of paramagnetic centers on or near the glass surface. There does seem to be a magnetic field dependence of the relaxation rate, but so far no information about the correlation time of the perturbation has been obtained. Permeation-controlled relaxation involves the solution of the helium atoms in the material of the container walls. Since the helium dissolves more readily at higher temperatures, permeation-controlled relaxation tends to dominate at high temperatures. Support for this model comes from the fact that one can obtain much longer relaxation times with aluminosilicate glasses (Fit67), in which helium is known to dissolve poorly, than with Pyrex or quartz, in which helium dissolves more readily.

Fitzsimmons *et al.* (Fit69) have reported relaxation times as long as nine days for ^{3}He in an aluminosilicate cell at a 500-Torr pressure and at a temperature of 100°C. These relaxation times are comparable to the expected bulk relaxation due to spin–spin interactions between the helium nuclei; and ultimately, spin–spin-limited relaxation times of months to years may be attainable.

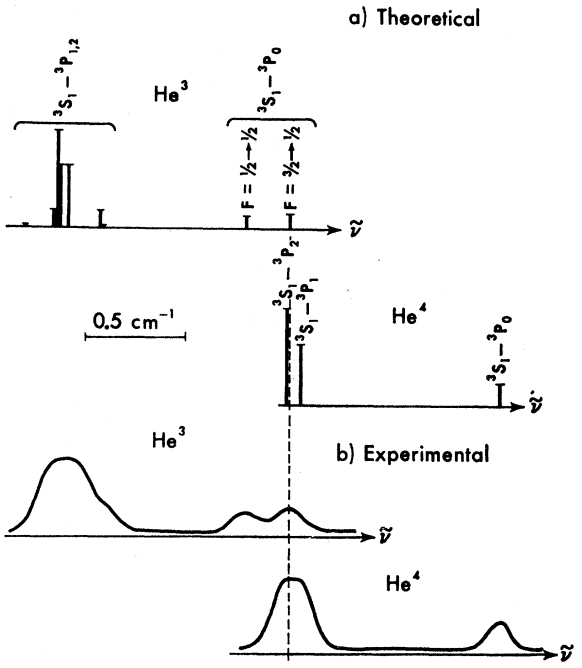

10 830 Å LINE STRUCTURE IN He^3 AND He^4

FIG. 44. Isotope shift and hyperfine structure of the helium isotopes [from (Gre64)].

C. Excitation Transfer and Diffusion of Helium Metastable Atoms

One of the most important processes in the optical pumping of ^{3}He is the exchange of excitation between polarized $^3S_1$ metastable atoms and ground-state atoms. This process has little effect on optically pumped ^{4}He, since the electronic-spin angular momentum is conserved during the process. In ^{3}He the nuclear spin is not affected during the very short excitation-transfer collision, which is completed within 10^{-12} seconds. During the intervals between collisions the nuclear and electronic spins couple together, and the whole ensemble will eventually reach a spin-temperature equilibrium. The metastability-exchange rate makes a contribution to the linewidth of the magnetic resonance transitions of the atom. Studies of the magnetic resonance linewidth by Colegrove, Schearer, and Walters (Col64) have made it possible for them to estimate the mean cross sections for metastability exchange in helium. They found (see Fig. 45) that the exchange cross section decreases rapidly with decreasing temperature. The cause of this behavior is thought to be a repulsive lip in the interaction potential between atoms in 1^1S_0 and 2^3S_1 states. The cross section measurements of Colegrove *et al.* (Col64) are consistent with those of Greenhow (Gre64), who obtained a mean metastability exchange cross section of 7×10^{-16} cm^2 at room temperature. However, as Dupont-Roc *et al.* (Dup71) have pointed

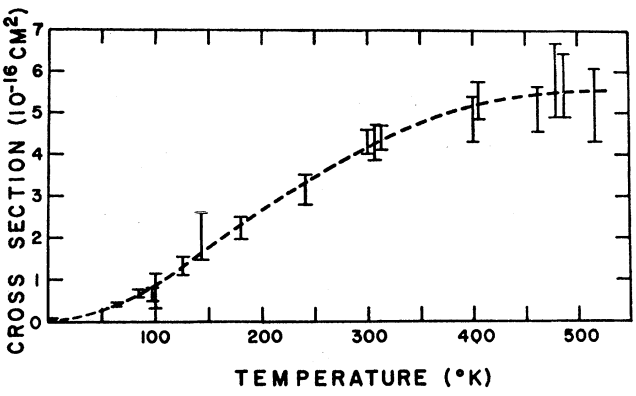

FIG. 45. Temperature dependence of the helium metastability exchange cross section [from (Fit68)].

out, it is necessary to eliminate the effects of nuclear spin to obtain true metastability exchange cross sections from data on ^{3}He.

Fitzsimmons, Lane, and Walters (Fit68) have measured the diffusion constant for metastable helium atoms in helium. The diffusion constant also drops rapidly with temperature, and it was possible to obtain empirical parameters for an adjustable potential which was consistent with the excitation-transfer rates and with the diffusion constants.

D. Depolarization of the ^3P State

The ^3P_J excited states of helium are quite sensitive to collisional depolarization, and Schearer (Sch67,68b) has measured an effective cross section for transitions out of the $^3P_0$ level of 68 Å^2, for collisions with ground-state helium atoms. Landmann (Lan68) has measured an alignment depolarization cross section of 56 Å^2 for the $^3P_1$ state.

E. Polarization by Penning Ionization

An important technique that makes use of optically pumped helium metastable atoms has been developed by Shearer (Sch69a). Metastable helium atoms are optically pumped in a flowing afterglow of a plasma (see Fig. 46). Atoms (e.g., cadmium atoms) are introduced into the afterglow from an oven. The cadmium atoms are ionized by Penning collisions with the polarized metastable helium atoms. The cadmium ions are produced in various excited states, and the ions are found to be strongly polarized because of the initial polarization of the helium metastables. The polarization of the excited ions can be easily monitored by observing the polarization of the fluorescence light that is emitted when the fluorescent ions decay. Fractional polarizations of up to 10% in the $^2D_{5/2}$ state of Cd$^+$ have been observed by Schearer (Sch67a).

Schearer and Holton (Sch70a) have reported magnetic resonance studies of some of the excited states of Cd$^+$ and Zn$^+$ which were polarized by Penning ionization with optically pumped helium metastables.

Polarization by Penning ionization is closely related to spin exchange, and is based on the fact that the electronic spin polarization of the helium metastable atom is shared by the free electron and the ion produced by the Penning reaction. The spin polarization can subsequently be transformed by the spin–orbit interaction into polarization of the orbital angular momentum of the ion. As a spectroscopic technique, polarization by Penning ionization should be at least as important as polarization by spin exchange.

F. Other Polarization Mechanisms Involving Optically Pumped Helium

Lalöe (Lal68c) has shown that the polarized nuclear spins of optically pumped ^{3}He act as flywheels for angular momentum during electron excitation. The nuclear polarization is retained in any excited state of helium produced by electron bombardment. If the coupling of the nucleus to the electrons in the excited state is strong enough, some of the nuclear polarization is converted to electronic polarization. The electronic polarization can be detected by observing the degree of polarization of the fluorescent light emitted by the excited atoms. Pavlović and Lalöe (Pav69) have measured the hyperfine structures of a number of excited states in helium by electron excitation of optically pumped ^{3}He.

Sevast'yanov and Zhitnikov (Sev69) have reported that optical pumping of the triplet metastable states of helium decreases the electron density of a weak electrical discharge in helium gas. Destruction of the polarization of the metastable state causes an increase in the

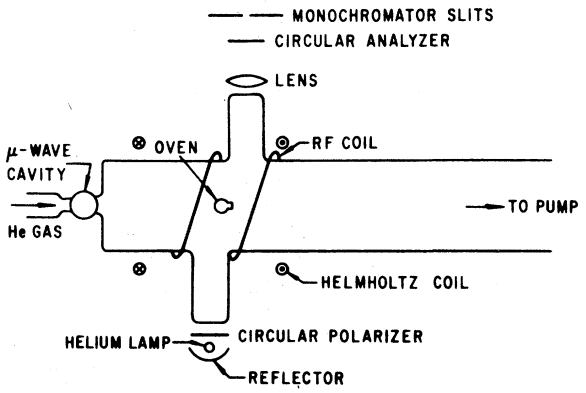

FIG. 46. Polarization by Penning ionization. Penning ionization of atoms by optically pumped helium metastable atoms produces polarized ions in the ground state and in various excited states. The polarization can be detected by observing the polarized fluorescent light emitted by the excited ions or by transmission monitoring with ionic resonance radiation [from (Sch69a)].

electron density and, for weak electrical discharges, an increase in the light emission of the plasma.

For strong electrical discharges, the increase in electron density at resonance is accompanied by a decrease in light emission. Sevest'yanov and Zhitnikov (Sev69) suggest that these effects may be associated with changes in the relative populations of the 2^3S_1 and 2^3P states at magnetic resonance.

McCusker, Hatfield, and Walters (Mc69) have shown that the rate of the reaction

$$\mathrm{He}(2^3S_1)+\mathrm{He}(2^3S_1)\rightarrow\mathrm{He}(1^1S_0)+\mathrm{He}^+ + e$$

is strongly dependent on the orientation of the metastable triplet atoms. The reaction rate almost vanishes when the metastable atoms are fully oriented since the total spin angular momentum cannot be conserved under such conditions. Shearer (Sch70b) has shown that the electron density varies by as much as 5% in an optically pumped flowing afterglow when the helium atoms are oriented.

Schearer (Sch68d) has shown that when metastable helium atoms are optically pumped in the presence of a small amount of neon, the excited neon atoms, which are produced by collisions of the second kind with helium, are polarized. Presumably, this involves the same spin-conservation rule that is responsible for polarization by spin exchange or Penning ionization.

X. OTHER OPTICALLY PUMPED ATOMS

A. Metastable States of the Heavy Noble Gases

The metastable states of neon, argon, and xenon have been optically pumped by Schearer (Sch68a,69b,c).

The metastable $^3P_2$ state has a remarkably small depolarization cross section compared to the $^3P_2$ state of an atom such as mercury. For instance, the mean depolarization cross section of the $^3P_2$ state of neon in helium is reported by Schearer (Sch68a) to be only 4.3×10^{-17} cm^2. These anomalously low depolarization cross sections are not yet completely understood, but they seem to be associated with the anomalously small tensor polarizability of the $^3P_2$ state of neon (Rob66).

Metastable $^3P_2$ atoms are produced by a weak electric discharge in an inert gas at a pressure of a Torr or less. Helium can be used as a buffer gas for the heavier inert gases (Sch69c). The states can be pumped with any one of several resonance lines, and in neon the 6402-Å line ($^3P_2\rightarrow{}^3D_3$) gives excellent pumping.

The depolarization cross sections of the $^3P_2$ metastable states in argon and xenon are larger than the corresponding depolarization cross sections for neon. Systematic studies of mean depolarization cross sections for polarized metastable states of inert gases have been made by Schearer (Sch69d). It is usually necessary to use a lighter noble gas as a buffer gas for a heavier noble gas, since excitation transfer to the buffer gas can take place otherwise, causing very rapid depolarization and de-excitation to occur.

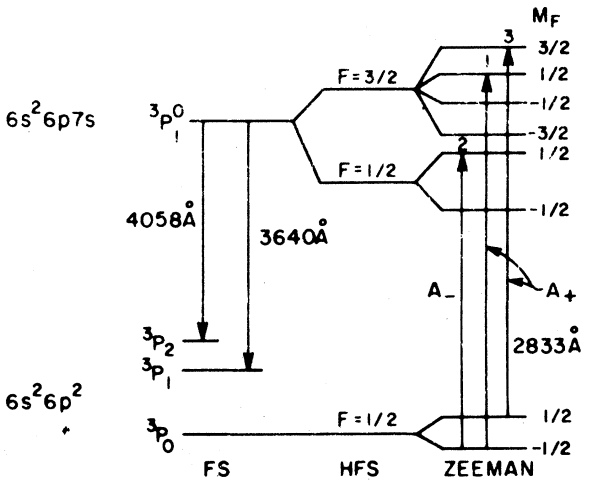

FIG. 47. The low-lying energy levels of lead [from (Gib69a)].

B. Lead

Optical pumping of lead has been reported by Gibbs, Greenhow, and Chang (Gib69a,b). The low-lying energy levels of lead are shown in Fig. 47. Temperatures of around 600°C are required to provide an adequate vapor pressure of lead atoms. The pumping mechanisms for the $^3P_0$ ground state are analogous to those of $^1S_0$ atoms, such as mercury, cadmium, and zinc. However, the repopulation pumping does not occur with maximum efficiency, because the $^3P_1^0$ excited state can decay to the $^3P_2$ and $^3P_1$ metastable states as well as to the ground state, and the branching ratio to the ground state is only about 0.27 (Sal66). Gibbs *et al.* make the reasonable assumption that the atoms which decay to the $^3P_2$ and $^3P_1$ metastable states are completely depolarized before finally reaching the $^3P_0$ ground state.

Transmission monitoring or depopulation pumping of the $^3P_0$ ground state of ^{207}Pb is possible only if the $F=\frac{1}{2}$ and $F=\frac{3}{2}$ hyperfine components ($A-$ and $A+$) of the probing light have different intensities. Gibbs ensured that the two different hyperfine components had different intensities by inserting a ^{208}Pb filter cell between the ^{207}Pb probing beam (which also served as the pumping beam) and the photo-detector. The filter cell, filled with 400 Torr of helium and operated at 550°C, removed the $A+$ component of the resonance light. A lead flow lamp, described by Churchill (Chu70), can be used to provide an intense source of resonance radiation.

Gibbs and Chang (Gib71b) have also reported pumping of the $^3P_2$ and $^3P_1$ metastable states of both ^{208}Pb and ^{207}Pb. Pure repopulation pumping from the

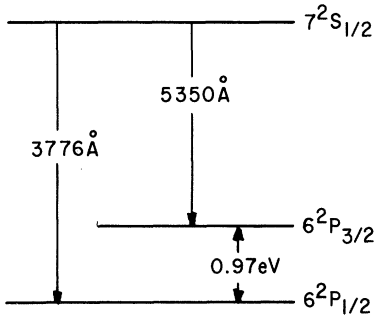

FIG. 48. The low-lying energy levels of thallium. [From (Gib70a)].

$^3P_1^0$ excited state was employed, and the degree of polarization was detected by transmission monitoring with 3639-Å and 4058-Å light.

The polarized $^3P_0$ ground-state atoms can make about 50 collisions against quartz walls before the orientation is lost (Gib69c). Buffer gases are found to have extremely small disorientation cross sections for the ground state. For ^{207}Pb, Gibbs and White (Gib69c) have shown that the cross sections do not exceed 10^{-22} cm^2 for He, Ne, Ar, Kr, Xe, H_2, and N_2. The relaxation times for an evacuated cell could be lengthened considerably by admitting several Torr of hydrogen in the cell and letting it stand for several hours. When the cell was evacuated again the relaxation times were found to increase by a factor of 2 to 3. The enhanced relaxation time persists for several hours at 625°C. The reason for this behavior is not known.

Very little information on the relaxation of the $^3P_1^0$ excited state is known. Gibbs (Gib69c) has shown that the hyperfine coupling in the excited state is so strong that at least 400 Torr of helium can be added without decoupling the electronic and nuclear spins and thereby preventing optical pumping. Saloman and Happer (Sal66) have investigated the relaxation of the $^3P_1^0$ state by coherence narrowing and resonant self-broadening. From the coherence narrowing they estimate a branching ratio to the ground state of 0.27, and the resonance self-broadening cross sections are in reasonable agreement with theoretical estimates.

Systematic studies of the depolarization and quenching cross sections of the $^3P_1$ and $^3P_2$ metastable states and of the $^3P_1^0$ excited state of lead have been reported by Gibbs (Gib71b). The disalignment cross sections ($\pm 20\%$) in Å^2 for the $^3P_1$ and $^3P_2$ states, respectively, are: He, 27, 36; Ne, 27, 35; Ar, 51, 59; Kr, 64, 76; Xe, 123, 159; H_2, 26, 39; N_2, 73, 88. The $^3P_1$ quenching cross sections were found to be less than 10^{-21} cm^2 for the rare gases, $\leq 1.3\times10^{-21}$ cm^2 for N_2, $24(5)\times10^{-20}$ cm^2 for H_2, and 0.3×10^{-20} cm^2 for D_2. Gibbs (Gib71b) also reports a radiative lifetime of 53 ± 30 msec for the $^3P_1$ metastable state.

C. Thallium

Optical pumping of thallium has been reported by Gibbs *et al.* (Gib70a). The pertinent energy levels of thallium are shown in Fig. 48. Pumping is possible because the electron randomization cross sections for the $^2P_{1/2}$ ground state are quite small, and Gibbs *et al.* (Gib70a) report the following cross sections (at 610°C, in units of 10^{-20} cm^2 with a 30% uncertainty); He, 60; Ne, 14; Ar, 110; Kr, 220; Xe, 620; H_2, 380; N_2, 920. Since the ground-state electronic spin is $\frac{1}{2}$, the nuclear spin slows down the relaxation rates in the same way as in the alkali atoms, and the eigenobservables are the same as for alkali atoms (e.g., $\mathbf{I}\cdot\mathbf{J}$, $\bar{\mathbf{I}}_z$, Q_e, etc.; see Sec. V.B.4); but since the nuclear spin is $\frac{1}{2}$ for both Tl^{203} and Tl^{205}, $\bar{I}_z$ and $\bar{S}_z$ are essentially the same eigenobservable and they relax at half the electron randomization rate. Evacuated cell-relaxation times could be lengthened by a factor of 5 by leaving H_2 gas in the cell for a few minutes before evacuation.

The small depolarization cross sections for the $^2P_{1/2}$ state of thallium in inert gases are consistent with the anomalously small depolarization cross sections for rubidium and cesium. The cross sections scale approximately as $(\Delta E)^{-2}$, where ΔE is the fine structure interval from the $^2P_{1/2}$ to the $^2P_{3/2}$ state. Earlier experiments which seemed to indicate depolarization cross sections in excess of 10^{-17} cm^2 (Fra67) have not yet been explained. Depolarization cross sections in the $^2P_{3/2}$ state are on the order of 10^4 times larger than the corresponding $^2P_{1/2}$ cross sections. Collisional transfer cross sections between the $^2P_{1/2}$ and $^2P_{3/2}$ states were too small to be measured, but Gibbs *et al.* quote an upper limit of 2×10^{-21} cm^2 for the transfer cross section in neon.

XI. REFERENCES

We have attempted to collect (and read) all papers on optical pumping of ground-state atoms and ions. We have arranged these papers by year of publication in the bibliography. For internal reference we have labeled each paper by the first three letters of the first author's name and by the last two digits of the publication year. An additional index a, b, c, etc., is added if it is necessary to distinguish between otherwise identical internal references. We have found it useful to cross reference these papers by subject matter, and we have included our Table of cross references in this section.

Pumping Theory and Basic Phenomena

Han24	Hanle Effect
Kas50	Proposal of Optical Pumping
Bro52a	Optical Double Resonance
Con53	*The Theory of Atomic Spectra*
Ope53	Paramagnetic Faraday Effect
Fra57	D_1 Pumping in Alkalis
Blo68	Self-Filtering of Pumping Light

Köp58	*Nuclear Moments*
Bar61*a*	Density Matrix in Optical Pumping
Bar61b	Density Matrix in Optical Pumping
Bar61*c*	Density Matrix in Optical Pumping
Bar61d	Density Matrix in Optical Pumping
Bar61e	Density Matrix in Optical Pumping
Bel61b	Pumping With Modulated Light
Boe61	Measurement of $\langle S_z \rangle$ in Alkalis
Coh61a	Light Shifts due to Virtual Transitions in ^{199}Hg
Coh61b	Line Narrowing Due to Real Transitions in ^{199}Hg
Coh61c	Light Shifts Due to Real Transitions in ^{199}Hg
Fra61	Level-Crossing Theory
Kas61	Excitation with Modulated Light
Rai61	Measurement of $\langle S_z \rangle$ in Alkalis
Coh62a	Density Matrix Theory of Optical Pumping, Light Shifts, Line Narrowing and Broadening.
Ale63a	Excitation with Modulated Light
Ale63b	Discussion of Field Reversal Method; see (Deh65)
Leh64a	Effect of Excited-State hfs on Pumping of $^1S_0$ Atoms
Leh64b	Ground-State Hanle Effect
Lur64	Hanle Effect
Ros64	Modulated Fluorescent Light at Ground-State Resonance
Bou65a	Proportionality and Attenuated Light to Ground-State Observables
Deh65	Clarification of Field-Reversal Method
Ros65	Modulated Fluorescent Light at Ground-State Double Quantum Resonance
Ska65	Modulated Fluorescent Light at Ground-State Double Quantum Resonance
Buc66	Detection of Optical Pumping by Atomic Beam Deflection
Car66	Monitoring Operators
Qua66	Resonant Coupling of Ground-State to Excited-State Coherence
Ros66	Resonant Coupling of Ground-State to Excited-State Coherence
Ser66	Light Modulation at Very Low Fields
Vio66	Theoretical Pumping Transients for Alkalis
Hap67c	Semiclassical Optical Pumping Theory; Multipole Representation.
Kra67	Effect of Ground-State Polarization On Level Crossings
Leh67	Pumping of $^1S_0$ Atoms with Small hfs.
Lom67	Mixing of Multipolarities by Electric Field
Nov67a	Pumping with Modulated Light
Ros67	Resonant Coupling of Ground-State to Excited-State Coherence
Bay68	Effect of Ground-State Polarization On Level Crossings
Cap68	Multipole Representation for Optical Pumping
Duc68	Polarization Transfer by Spontaneous Emission
Dup68a	Nonexponential Relaxation
Fra68	Modulated Fluorescent Light at Ground-State Double Quantum Resonances
Ham68	Comment on Semiclassical Theories
Hap68b	Partial Wave Expansion of Rotation Operator.
Pok68a	Optical Pumping Theory
Vio68	Theoretical Pumping Transients for Alkalis
Hap69	Optical Pumping Theory
Kra69	Effect of Ground-State Polarization On Level Crossing
Leh69	Pumping of $^1S_0$ Atoms with Small hfs
Van69	Optical Pumping Theory
Sch70c	Alkali Level Crossings
Var70	Polarized Atoms and Molecules in Space

Relaxation

Dic53	Collisional Narrowing of Doppler Width
Bro55b	Buffer Gas for Alkalis
Pin55	Simple Theory of Spin Relaxation
Rob58	Wall Coatings for Alkalis
Fra59	Relaxation-in-the-Dark Method
Blo60a	Alkali Relaxation
Ber62	Relaxation of Alkalis by Spin–Orbit Interaction
Bou62a	Measurement of Alkali Relaxation
Bou62b	Relaxation of Rubidium on Paraffin Walls
Bou63a	Theory of Wall Relaxation of Alkalis
Bou63b	Theory of Wall Relaxation of Alkalis
Coh63	Wall Relaxation due to Quadrupole Coupling in ^{201}Hg
Har63	Effect of UV Light on Quartz Surfaces
Byr64a	Depolarization by the Van der Waals Interaction
Her64	Relaxation of Alkalis by Spin–Orbit Interaction
McN64b	Optical Pumping and Chemical Reactions
Ber65	Absence of Electrostatic Interactions in $^2S_{1/2}$ States
Gam65	Relaxation Due to Inhomogeneous Magnetic Fields
Omo65b	Depolarization by the Van der Waals Interaction
Sch65	Relaxation Due to Inhomogeneous Magnetic Fields
Bou66a	Experimental Methods to Measure Alkali Relaxation
Erm66	Use of Polarization of Fluorescent Light to Study Relaxation
Fra66a	Effect of Excited-State Relaxation on Alkali Pumping
Fra66b	Excited-State Depolarization of Alkalis
Meu66	Comparison of Resonant Self-Broadening Theories
Min66b	Effect of Higher Diffusion Modes
Nov66	Measurement of Transverse Relaxation Time
Ruf66	Spin Echoes in Sodium
Ban67	Variant of Relaxation in the Dark
Mas67	Analysis of Diffusion with Partially Disorienting Walls
Nov67c	Spin Echoes
Elb68	Comment on Selection Rules
Bou69	Analysis of Relaxation by Molecular Formation
Elb69	Depolarization of Excited Alkali Atoms
Bou70	Analysis of Relaxation by Molecular Formation
Hap70	Multipole Relaxation Times
Oku70	Relaxation of $^2P_{3/2}$ States of Alkalis
Nov71	Spin Echoes in Cesium

Light Shifts

Ard61	Shifts of 0–0 Transition Frequency in Alkalis
Coh61a	Shift Due to Virtual Transitions in ^{199}Hg
Coh61c	Shift Due to Real Transitions in ^{199}Hg
Coh62a	Summary of Shifts in ^{199}Hg
Coh62b	Summary of Shifts in ^{199}Hg
Sch62	Light Shifts in Helium
Ale66	Shift Due to Laser
Bon66	Shift Due to Laser
Pan66	Semiclassical Theory
Dup67a	Free Precession of ^{199}Hg Around Circularly Polarized Light
Dup67b	Large Shifts in Mercury
Hap67c	Multipole Expansion of Light Shift Operator
Hap67b	Magnetic Resonance with Modulated Off-Resonance Light
Leh67	Shift Due to Real Transitions in Cadmium
Cag68	Tensor Light Shift in ^{201}Hg
Dup68b	Ground-State Level Crossings Due to Light Shifts
Dup68c	Magnetic Resonance for $\Delta m=2$ Transition with Modulated Light
Jon68	Derivation with Green's Functions
Mat68b	Shifts Due to Virtual Transitions in Alkalis
Sch68e	Shifts in Helium
Ver68	Semiclassical Theory
Coh69	Mixing of Multipoles with Tensor Light Shift
Bul71a	Shifts due to Real Transitions in Alkalis
Hap71	Light Propagation and Light Shifts

Pressure Shifts

Ard58a	Shifts of 0–0 Frequency of Sodium
Ard58b	Shifts of 0–0 Frequency of Cesium
Ard58c	Shifts of 0–0 Frequencies of Sodium and Cesium
Mar59	Theory of Shifts in Alkalis
Adr60a	Theory of Shifts for Hydrogen Atoms

Adr60b Theory of Shifts for Nitrogen Atoms
Blo60b Shifts of 0–0 Frequency of Potassium
Rob60 Theory of Shifts in Alkalis
Ard61 Shifts of 0–0 Frequency of Cesium and Rubidium
Her61 Correction to Mar59
Cla62 Shifts of 0–0 Frequency of Hydrogen in Helium
Lam63 Shifts of hfs Frequencies of Nitrogen
Bre64 Large Shift of 0–0 Frequency of Rubidium in Benzene
Ram65 Shifts of 0–0 Frequency of Sodium
Ens68 Shifts of 0–0 Frequency of Hydrogen in Krypton and Xenon
Her68 Theory of Pressure Induced g_J Shifts
Ber69 Shifts of 0–0 Frequency of Cesium in Molecular Buffer Gases
Ens69 Nonlinear Shift of Rubidium 0–0 Frequency at High Pressure
Rao69 Theory of Temperature Dependent Shifts
Ray70 Theory of Shifts for Lithium and Sodium in Helium
Wei70 Temperature Dependence of Nitrogen Pressure Shifts

Forward Light Propagation

Han33 Rapid Modulation of Diamagnetic Faraday Effect
Kas51 Paramagnetic Faraday Effect for Detection of Spin Resonance
Ope53 Paramagnetic Faraday Effect for Detection of Spin Resonance
Bel57 Modulation of Light Beam by Precessing Atoms
Deh57b Modulation of Light Beam by Precessing Atoms
Dan58a Paramagnetic Faraday Effect for Detection of Spin Resonance
Dan58b Paramagnetic Faraday Effect for Detection of Spin Resonance
Goz62 Paramagnetic Faraday Effect for Detection of Spin Resonance
Man63 Paramagnetic Faraday Effect in Mercury
Sch64b Faraday Effect in Sodium Vapor
Bou65a Proportionality of Attenuated Light to Ground-State Observables
Cor66 Effect of Excited-State Magnetic Resonance on Light Propagation
Fir66 Transmission Light Modulation at ^{39}K hfs Frequency
Par66 Transmission Light Modulation in Helium
Str66 Paramagnetic Faraday Effect in Sodium
Coh67 Theory of Light Propagation in Polarized Vapors
Fir67 Transmission Light Modulation at ^{39}K hfs Frequency
Hap67a Paramagnetic Faraday Effect and Zeeman Light Shifts
Lal68a Light Propagation in ^{201}Hg
Lal68b Light Propagation in ^{201}Hg
Mat68a Transmission Light Modulation at ^{87}Rb hfs Frequency
Nov68a Light Propagation in Cesium
Pan68 Light Propagation in Helium
Ver68 Theory of Light Propagation in Polarized Vapors
Yab68 Light Propagation in Cesium
Kor69 Light Propagation in Helium
Lal69a Relation of Light Propagation to Polarization of Vapor
Lal69b Relation of Light Propagation to Polarized Vapor
Mat70 Light Propagation in Alkali Vapors
Tan70 Parametric Frequency Conversion in ^{87}Rb Vapor
Hap71 Light Propagation and Light Shifts

Fluorescent Light

Han24 Hanle Effect
Bro52a Optical Double Resonance
Dod59 Fluorescent Light Modulation
Ale63a Excitation with Modulated Light
Kon63 Scattering of Modulated Light
Lur64 Hanle Effect
Kib65 Stepwise Excitation
Ser66 Modulated Light with Optically Pumped Ground-State
Dec68 Fluorescent Light From Laser
Dum68 Fluorescent Light From Laser
Lec68a,b Effect of Anomolous Dispersion on Hanle Effect
Pok68c Light Scattering Theory

Trapping of Resonance Radiation

Gui56 Coherence Narrowing in Mercury
Gui57 Coherence Narrowing in Mercury
Bar58 Coherence Narrowing in Mercury
Bar59a Theory of Coherence Narrowing
Bar59b Theory of Coherence Narrowing
Omo61 Coherence Narrowing in Large Magnetic Fields
Omo64 Frequency Shifts due to Trapping
Ott64 Coherence Narrowing in Large Magnetic Fields
Dya65 Multipole Relaxation with Radiation Trapping
Omo65a Multipole Relaxation with Radiation Trapping
Omo65c Frequency Shifts due to Trapping
Meu66b Effect of Ground-State Polarization on Coherence Narrowing
Dum68 Coherence Narrowing in Laser

Spin Exchange

Pur56 Spin Exchange in Hydrogen
Wit56 Spin Exchange in Hydrogen
And58 H–Na Spin Exchange
Deh58a e–Na Spin Exchange
Deh58b e–Na Spin Exchange
Fra58a K–Na Spin Exchange
Hol58 N–Rb Spin Exchange
Nov58 Rb–Na Spin Exchange
And59 N–Na Spin Exchange
And60a H, D, and T–Rb Spin Exchange
And60b H, D, and T–Rb Spin Exchange
Bou60 He^3–Rb Spin Exchange
And61 Spin Temperature in Sodium Vapor
Dal61 Partial-Wave Analysis of Spin Exchange
Deh62a He^+–Cs Spin Exchange
Hol62 N–Cs Spin Exchange
Lam62 P–Rb Spin Exchange
Pip62 H and T–Rb Spin Exchange
And63 Spin Temperature in Sodium Vapor
Ben63 Theory of Frequency Shift and Linewidth for H–H Exchange
Gla63 Spin–Exchange Theory
And64 Spin Temperature in Alkali Vapors
Bal64a Frequency Shifts for Rb–e Exchange
Bal64b Frequency Shifts for Cs–e Exchange
Ben64 Frequency Shifts due to Electron Exchange
Gro64a Theory of Spin Exchange in Alkali Vapors
Gro64b Rb–Cs Spin Exchange; No Cs Polarization.
Gro64c Rb–Cs Spin Exchange; Relaxation of $\langle \mathbf{I}\cdot\mathbf{S} \rangle$.
Jar64 ^{85}Rb–^{87}Rb Spin–Exchange Cross Section
Bal65 H, T, e^-, g Values by Spin Exchange with Rubidium
Dal65 Calculated Spin-Exchange Cross Sections For Alkalis
Gib65 Effect of Nucleus in Spin Exchange
Gro65 Relaxation of Polarization in $F=I+\frac{1}{2}$ Level of Alkalis
Her65 Theory of Electron-Nuclear Spin Exchange
Ruf65 Na–H Coherence Transfer by Spin Exchange
Smi65 Calculated Spin–Exchange Cross Sections for Alkalis
Bal66 Na–e Spin Exchange; Frequency Shifts
For66 He^+–Cs Spin Exchange
Gib67 Rb^{87}–Rb^{87} and Rb^{87}–Cs^{133} Spin–Exchange Cross Sections
Gro67a K–K Spin-Exchange Cross Section
Gro67c Spin-Exchange Theory and Experiments
Bes68 K^{87}–Rb Spin Exchange
Gro68 Spin–Exchange Theory
Maj68 He^+–Cs Spin-Exchange

Mit68	Rb^+–Rb Spin (Charge) Exchange
Bal69	Rb–Ag Spin-Exchange
Cha69b	Calculated Spin-Exchange Cross Sections for Alkali Atoms
Hof69	Cs–Cu Spin-Exchange
Köp69	K^{37}–Rb^{87} and Na^{21}–Na^{23} Spin–Exchange
Res69	Cs^{133}, Rb^{87}, Rb^{85}, and K^{39} Self-Spin-Exchange Cross Sections
Til69a	N–Cs Spin-Exchange
Til69b	Eu–Cs Spin-Exchange
Gei70	Influence of Spin Polarization on Effusion of Alkali Atoms from an Orifice.
Gib70b	Sr^+–Rb and Cd^+–Rb Spin Exchange
Lam70	Discussion of Nuclear Effects in Spin Exchange
Cra71	Clarification of Lam70
Dav71	Mn–Rb Spin Exchange
Ens71	Effects of Rapid Spin Exchange
Gib71a	Clarification of Lam70
Val71a	Rb^{87}–H Spin Exchange
Val71b	Discussion of Spin Exchange

Interaction With Radio-Frequency Fields

Bro53	Multiple Quantum Transitions in Sodium
Rab54	Analysis of Magnetic Resonance in Rotating Coordinates
Bro55a	Bloch–Siegert Shifts
Red55	Magnetic Resonance in Rotating Coordinate System
Win59	Multiple Quantum Transitions
Ale64	Parametric Resonance
Fav64	Parametric Resonance
Fra64c	Multiple Quantum Transitions
Ale65	Parametric Resonance
Coh65	Parametric Resonance
Pol65a	Parametric Resonance
Pol65b	Parametric Resonance
Pol65c	Interpretation of Parametric Resonance with Quantized Fields
Coh66a	Interpretation of Parametric Resonance with Quantized Fields
Coh66b	g-Factor Shifts
Dön67b	Parametric Resonance
Nov68b	Parametric Resonance in Rotating Coordinate System
Pok68b	Parametric Resonance in Rotating Coordinate System

Precision Measurements

Ben62	Rb^{87}–H Zeeman Frequency Ratio
Led66a	Hg^{199}–Cd^{111} Zeeman Frequency Ratio
Led66b	Cd^{111}–Cd^{113} Zeeman Frequency Ratio
Ens67a	Upper Limit on Electric Dipole Moment of Rb^{85}
Ens67b	Upper Limit on Electric Dipole Moment of Rb^{85}
Hay68	g_J Ratios for H, D, Rb^{85}, and Rb^{87}
Lad68a	Cd^{111}–Cd^{109} Zeeman Frequency Ratio
Whi68	g Factor Ratios for Rubidium Isotopes

Lithium

Min69	Lithium Pumping; Special Container

Sodium

Bro52b	Optical Pumping of Sodium Beam
Bro53	Multiple Quantum Transitions in Sodium
Haw53	Optical Pumping of Sodium Beam
Bar54	Optical Pumping of Sodium Cell
Bro55b	H_2 Buffer Gas for Sodium
Haw55	Optical Pumping of Sodium Beam
Mar55	Alignment of Sodium Vapor
Coh57	He Buffer Gas for Sodium
Deh57a	Ar Buffer Gas for Sodium
Ard58a	Hyperfine Pumping of Sodium
Bel58	Hyperfine Pumping of Sodium
Har58	Buffer Gases for Sodium
Boe61	Measurement of $\langle S_z \rangle$ in Polarized Sodium Vapor
Lem62	Wall Coatings for Sodium
Ram64	Ground-State Relaxation of Sodium in Buffer Gases
Ros65	Modulated Fluorescent Light at Ground-state Double Quantum Resonance
Jor66	Excited-State Relaxation of Sodium in Buffer Gases
Bes67	Optical Pumping of Radioactive Na^{21}
Elb67	Excited-State Relaxation of Sodium in Buffer Gases
Luk68	Excited-State Relaxation of Sodium in Buffer Gases
Stu68	Excited-State Relaxation of Sodium in Buffer Gases
Stu69	Excited-State Relaxation of Sodium in Buffer Gases
Tol70	High-Intensity Sodium Lamp in Magnetic Field
Mor71	Hyperfine Pumping of Sodium

Potassium

Buc56	Optical Pumping of Potassium Beam
Cha65	Excited-State Relaxation of Potassium in Buffer Gases
Jor66	Excited-State Relaxation of Potassium in Buffer Gases
Kra66a	Optical Pumping of Potassium Cell
Cop69	Excited-State Relaxation of Potassium in Buffer Gas
Kra69	Effect of Ground-State Polarization on Level Crossings

Rubidium

Ben58	Hyperfine Pumping of Rudidium
Fra59	Ground-State Relaxation of Rudibium in Buffer Gases
Bou62b	Wall Relaxation of Rubidium on Paraffin
Bre62a	Ground-State Relaxation of Rubidium in Buffer Gases
McN62	Ground-State Relaxation of Rubidium in Buffer Gases
Bou63a	Wall Relaxation of Rubidium on Paraffin
Bou63b	Wall Relaxation of Rubidium on Paraffin
Bou63c	Wall Relaxation of Rubidium on Paraffin
Ard64	Ground-State Relaxation of Rubidium in Buffer Gases
Bre64	Evidence for Rb–Benzene complex
Dav64	Rb^{85} Filter Cell For Hyperfine Pumping of Rb^{87}
Fra64a	Ground-State Relaxation of Rubidium in Buffer Gases
Her64	Theory of Ground-State Relaxation in Buffer Gas
Kry64	Optical Pumping With Wall Coating and Buffer Gases
McN64a	Ground-State Relaxation of Rubidium in Buffer Gases
Bou65b	Wall Relaxation of Rubidium on Paraffin
Fra65	Ground-State Relaxation of Rubidium in Buffer Gases
McN65	Comment on McN64a
Roz65	Vapor Pressure of Cs–Rb Mixtures
Vid65	Wall Relaxation of Rubidium on Paraffin
Win65	Sr^+ Probing Light For Rubidium
Bou66b	Wall Relaxation of Rubidium on Paraffin
Mar66	Excited-State Relaxation of Rubidium in Buffer Gases
Pit66	Excited-State Relaxation of Rubidium in Buffer Gases
Aym67	Evidence for Rb–Kr Molecular Formation
Bou67	Evidence for Rb–Kr Molecular Formation
Gal67b, c	Excited-State Relaxation of Rubidium in Buffer Gases
Fir68	Neodymium-Solution Filter for Rubidium Pumping
Gal68	Excited-State Relaxation of Rubidium in Buffer Gases
Rou69	Rb–Kr Molecular Formation Theory
Haw69	Theory of Rubidium Pumping

Bou70 Analysis of Relaxation by Molecular Formation
Gib70c Hg^{202} Laser for Pumping Rubidium
Har70 Effect of Molecular Formation on 0–0 Coherence
Hry70 Excited-State Relaxation of Rubidium in Buffer Gases
Zhi70 Ground-State Relaxation of Rubidium in Buffer Gases
Bul71b Nuclear Spin Inertia in $^2P_{1/2}$ State

Cesium

Bla56 Optical Pumping of Cesium Vapor
Ska57 Buffer Gas (H_2 and Xe) for Cesium 0–0 Transition
Bea58 Pressure Shifts in Cesium
Dia58 $\Delta F=1$ Transitions in Cesium
Ska58 Optical Pumping of Cesium Vapor
Haw61 Theory of Cesium Pumping
Fra63b Ground-State Relaxation of Cesium in N_2
Fra64b Ground-State Relaxation of Cesium in Buffer Gases
Leg64 Ground-State Relaxation of Cesium in Buffer Gases
Cza65 Excited-State Relaxation of Cesium
Kan65 Ground-State Relaxation of Cesium in Benzene
Roz65 Vapor Pressure of Cesium–Rubidium Mixtures
Cza66 Excited-State Relaxation of Cesium
Fri66 D_2 Pumping of Cesium in Buffer Gas
Che67 Pressure Broadening of Optical Absorption Lines
Fri67 Excited-State Relaxation Studied with D_2 Pumping
Gal67b, c $^1P_{1/2}$ Depolarization in Buffer Gas
Mcg67 Excited-State Relaxation in Buffer Gases
Ern68a Relaxation of $\langle \mathbf{S}\cdot\mathbf{I} \rangle$ With Neon Buffer Gas
Ern68b Hyperfine Pumping of Cesium
Gal68 Excited-State Relaxation of Cesium in Buffer Gases
Dod69 Quenching by Helium
Sia69 Gallium–Arsenide Laser for Probing Cesium Vapor
Bev70 Hyperfine Pumping of Cesium
Bev71 Relaxation of $\langle \mathbf{S}\cdot\mathbf{I} \rangle$ in He, Ne, Ar, N_2
Fra71 Optical Pumping at 10^5 Gauss
Nov71 Spin Echoes in Cesium

Hydrogen

McI66 Attempts to Optically Pump Hydrogen
Var67 Theory of Pumping with an Unpolarized Light Beam

$^2S_{1/2}$ Ions

Smi66 Radiative Lifetimes of Ca^+ and Mg^+ P States
Ack67 Optical Pumping of Sr^+
Gal67a Radiative Lifetimes of Excited States of Ca^+, Sr^+, and Ba^+
Ack68 Ground-State Relaxation of Sr^+
Von70 Optical Pumping of Ba^+

Mercury

Mro32 Excited-State Relaxation of Mercury
Han33 Diamagnetic Faraday Rotation at High Frequencies
Cag58a Optical Pumping of Hg^{201}
Cag58b Optical Pumping of Hg^{201}
Cag58c Optical Pumping of Hg^{199} and Hg^{201}
Cag58d Ground-State Relaxation of Hg^{199}
Cag59 Wall Relaxation of Hg^{201} and Hg^{199}; Quadrupole Interaction
Cun60 Excited-State Relaxation in Buffer Gases
Cag61 Optical Pumping of Mercury Isotopes
Bau63 Relaxation of $^3P_2$ State
Coh63 Wall Relaxation due to Quadrupole Coupling in Hg^{201}
Leh63 Hg^{199}–Hg^{201} Zeeman Frequency Ratio
Bar64 Optical Pumping of $^3P_2$ State
Coh64 Effect of uv Light On Wall Relaxation
Pik64 Excited-State Relaxation in Buffer Gases
Pop64 Optical Pumping with 1850-Å Line
Bar65 Excited-State Relaxation in Rare Gases
Far65 Excited-State Relaxation in Rare Gases
Meu65 Self-Depolarization of Excited State
Nov65 Optical Pumping With 1850-Å Line
Tit65 Relaxation of $^3P_2$ State in Noble Gases
Bar66 Excited-State Relaxation in Buffer Gases
Far66a Excited-State Relaxation in Helium
Far66b Excited-State Relaxation in Helium
Far66c Excited-State Relaxation in Rare Gases
Big67 $6^1S_0 \rightarrow 6^3P_0$ Transition Rates for Odd Isotopes
Cag67 Temperature Dependence of Wall Relaxation
Far67a Excited-State Relaxation in Helium
Far67b Excited-State Relaxation in Rare Gases
Far67c Excited-State Relaxation in Rare Gases
Far67d Temperature Dependence of Excited-State Relaxation
Omo67 Self-Depolarization of Excited State
Lec68a,b Effect of Anomolous Dispersion on Hanle Effect
Lah70 Optical Pumping of the $^3P_0$ State of Odd Isotopes
Mor70 Magnetic Scanning for Optical Pumping with UV Light

Cadmium

Byr64b Self-Depolarization of Excited State
Leh64c Optical Pumping of Cadium
Leh66 Wall Relaxation of Cadium
Led68b Wall Relaxation of Cd^{109}
Cha69a Optical Pumping of Cd^{113m}, Cd^{115}, Cd^{115m}
Leh69 Optical Pumping of Cadmium

Other $^1S_0$ Atoms

Ols66 Optical Pumping of Ba^{135} and Ba^{137}
Osl67 Optical Pumping of Yb^{171} and Yb^{173}
Spe67 Optical Pumping of Zn^{67}

Helium

Fra58b Optical Pumping of $^3S_1$ State of He^4
Col60 Optical Pumping of $^3S_1$ State of He^4
Sch61a Optical Pumping of $^3S_1$ State of He^4
Sch61b Magnetic Field Stabilization
Phi62 Polarized He^3 Target for Nuclear Reactions
Sch62 Light Shifts in Helium
Wal62 Optical Pumping of He^3
Col63 Optical Pumping of He^3
Sch63a Optical Pumping of He^3
Col64 Temperature Dependence of Metastability Exchange Rate
Deh64 Frequency Shifts in He^3 Metastability Exchange
Gre64 Optical Pumping of He^3
Gam65 Relaxation of He^3
Fit67 Temperature Dependence of Wall Relaxation of He^3
Gro67b Electron Excitation of Polarized He^3
McA67 Polarization of Liquid He^3 By Optical Pumping
Sch67 Excited-State (^3P_J) Relaxation of Helium
Skr67 Optical Pumping of Helium
Bak68 Polarized He^3–Ion Beam
Fit68 Diffusion of $^3S_1$ Atoms in Helium
Lal68c Electron Excitation of Polarized He^3
Lan68 Excited-State ($^3P_1$) Relaxation of Helium
McA68 Polarization of Liquid He^3 By Optical Pumping
Sch68b Excited-State (^3P_J) Relaxation of Helium
Sch68c Spin Exchange between He ($^3S_1$) and Electrons
Sch68d Polarization Transfer between He ($^3S_1$) and Neon
Sch68e g-Value of He ($^3S_1$)
Fit69 Wall Relaxation of He^3
McC69 Polarized Electron Beams from He ($^3S_1$)
Pav69 Electron Excitation of Polarized He^3
Sch69a Polarization by Penning Ionization
Sev69 Effect of He ($^3S_1$) Polarization on a Plasma
Sch70a Polarization by Penning Ionization
Sch70b Effect of He ($^3S_1$) Orientation on a Plasma

Dup71	Metastability Exchange Rate
Led71	He^{3+} Polarization

Neon, Argon, Krypton, and Xenon

Rob66	Metastable $^3P_2$ Rare Gas Polarizabilities
Hän68	Excited-State Relaxation in Neon
Lan68	Excited-State Relaxation in Argon
Sch68a	Optical Pumping on Neon $^3P_2$ Atoms
Sch69b	Optical Pumping of Argon and Xenon $^3P_2$ Atoms
Sch69c	Optical Pumping of Neon $^3P_2$ Atoms
Sch69d	Relaxation of Polarized $^3P_2$ Atoms

Lead

Sal66	Lifetime and Branching Ratios of $^3P_1{}^0$ State
Gib69a	Optical Pumping of the $^3P_0$ Ground State
Gib69b	Optical Pumping of the $^3P_0$ Ground States
Gib69c	Ground-State Relaxation
Chu70	Flow Lamp For Optical Pumping
Gib71b	Relaxation of the $^3P_1$, $^3P_2$, and $^3P_1{}^0$ States

Thallium

Fra67	Relaxation of $^2P_{1/2}$ State
Bel70	Relaxation of $^2P_{3/2}$ State
Gib70a	Optical Pumping of Thallium $^2P_{1/2}$ State
Rit70	Relaxation of the $6^2D_{3/2}$ State

Miscellaneous Polarization Techniques

Deh62b	Photodissociation of Molecules
Had66	Resonant Charge Exchange Xe–Xe^+
Had67	Metastability Exchange and Electron Pumping
Lal68c	Electron Excitation of Polarized He^3
Mit68	Resonant Charge Exchange Rb–Rb^+
Ric68	Photodissociation of Molecules
Sch68d	Metastability Exchange; He^m–Ne
Fan69	Photoionization of Atoms
Liu69	Ionization by Electron Beam
Lub69	Photoionization of Atoms
Pav69	Electron Excitation of Polarized He^3

Devices and Experimental Technique

Bel61a	Electrodeless Lamps for Alkalis
Bre61	Electrodeless Lamps for Alkalis
Car61	Na–Vapor Filter for D_1 Pumping
Sch61b	Magnetic Field Stabilization
Blo62	Rb–Vapor Magnetometer
Bre62b	Slow Transient Response of Infrared Phototubes
Ard63	Alkali–Vapor Frequency Standards
Fra63a	Electrodeless Discharge Lamp for Cesium
Sch63b	He^3 Magnetometer
Dav64	Rb^{85} Filter Cell for *hfs* Pumping or Rb^{87}
Deh64	He^3 Magnetometer
McN64b	Optical Pumping and Chemical Reactions
Sch64a	He^3 Magnetometer
Ard65	Rb^{87} Regenerative Maser Oscillator
Bud65	Lamps for Optical Pumping
Dav65	Field-Independent Rb^{87} Maser
Dav66	Field-Independent Rb^{87} Maser
Min66a	Lithium Lamp
Dön67a	Rb Magnetometer
Ern67	Magnetically Scanned *Cs* Vapor Filter
Har67a	Rb^{85} Maser Oscillator with External Gain
Har67b	Rb^{85} Maser
Har67c	Rb^{85} Maser
Cer68	Rb^{87} Atomic-Beam Frequency Standard
Har68	Rb^{85} Maser
Van68	Relaxation in the Rb^{87} Maser
Har69	Lineshape and Filling Factor for Alkali-Vapor Maser
Bev70	Magnetically Scanned Cs Vapor Filter
Chu70	Lead Flow Lamp
Iol70	Operation of Lamps in Strong Magnetic Fields
Mor70	Optical Pumping in Vacuum Ultraviolet
Van70	Rb^{85} Maser
Slo71	Self-Oscillating He^4 Magnetometer

Review Articles and Books

Con53	*The Theory of Atomic Spectra*
Che57	Pressure Broadening and Shifts of Spectral Lines
Fan57	Irreducible Tensors and Density Matrix
Kas57	Optical Pumping
Köp58	*Nuclear Moments*
Ser59	Radio-Frequency Spectroscopy of Excited Atoms
Ska60	Optical Pumping
deZ60	Optical Pumping
Abr61	*The Principles of Nuclear Magnetism*
Fri61	*The Plasma Dispersion Function*
Skr61	Optical Pumping
Cor62	*Experimental Transition Probabilities for Spectral Lines of Seventy Elements*
Car63	Optical Pumping
DeB63	*The Dynamical Character of Adsorption*
Kas63	Light Shifts
Fos64	Oscillator Strengths
Ber65b	Reprint Collection on Optical Pumping
ZuP65	Radio-Frequency Spectroscopy of Excited Atoms
Coh66c	Optical Pumping
Kra66b	Collisional Transfer Between $^2P_{1/2}$ and $^2P_{3/2}$ Levels of Alkalis
Wie66	Tables of Oscillator Strengths
Bud67	Level-Crossing and Optical Double-Resonance Spectroscopy
Kas67	Optical Pumping
Hap68	The Hanle Effect
Maj68b	Optical Pumping
Hap70b	Light Shifts and Light Propagation
Nov70	Coherence Effects

References

Pre 1955

Han24	W. Hanle, Z. Physik **30,** 93 (1924).
Mro32	S. Mrozowski, Z. Physik **78,** 826 (1932).
Han33	W. Hanle, Z. Physik **85,** 304 (1933).
Kas50	A. Kastler, J. Phys. Radium **11,** 225 (1950).
Kas51	A. Kastler, Compt. Rend. **232,** 953 (1951).
Bro52a	J. Brossel and F. Bitter, Phys. Rev. **86,** 308 (1952).
Bro52b	J. Brossel, A. Kastler, and J. Winter, J. Phys. Radium **13,** 668 (1952).
Bro53	J. Brossel, B. Cagnac, and A. Kastler, Compt. Rend. **237,** 984 (1953).
Con53	E. U. Condon and G. H. Shortley, *The Theory of Atomic Spectra* (Cambridge U. P., New York, 1953).
Dic53	R. H. Dicke, Phys. Rev. **89,** 472 (1953).
Haw53	W. B. Hawkins and R. H. Dicke, Phys. Rev. **91,** 1008 (1953).
Ope53	W. Opechowski, Rev. Mod. Phys. **25,** 264 (1953).
Bar54	J. P. Barrat, J. Brossel, and A. Kastler, Compt. Rend. **239,** 1196 (1954).
Rab54	I. I. Rabi, N. F. Ramsey, and J. Schwinger, Rev. Mod. Phys. **26,** 167 (1954).

1955

Bro55a	J. Brossel, J. Margerie, and J. M. Winter, Compt. Rend. **241,** 556 (1955).
Bro55b	J. Brossel, J. Margerie, and A. Kastler, Compt. Rend. **241,** 865 (1955).
Haw55	W. B. Hawkins, Phys. Rev. **98,** 478 (1955).
Mar55	J. Margerie, J. Brossel, and A. Kastler Compt. Rend. **241,** 474 (1955).

Pin55 D. Pines and C. P. Slichter, Phys. Rev. **100,** 1014 (1955).

Red55 A. G. Redfield, Phys. Rev. **98,** 1787 (1955).

1956

Bla56 A. Blandin and J. P. Barrat, Compt. Rend. **243,** 2041 (1956).

Buc56 P. Buck, I. I. Rabi, and B. Senitzky, Phys. Rev. **104,** 553 (1956).

Gui56 M. A. Guichon, J. E. Blamont, and J. Brossel, Compt. Rend **243,** 1859 (1956).

Pur56 E. M. Purcell and G. B. Field, Astrophys. J. **124,** 542 (1956).

Wit56 J. P. Wittke and R. H. Dicke, Phys. Rev. **103,** 620 (1956).

1957

Bel57 W. E. Bell and A. L. Bloom, Phys. Rev. **107,** 1559 (1957).

Che57 S. Y. Chen and M. Takeo, Rev. Mod. Phys. **29,** 20 (1957).

Coh57 C. Cohen-Tannoudji, J. Brossel, and A. Kastler, Compt. Rend. **244,** 1027 (1957).

Deh57a H. G. Dehmelt, Phys. Rev. **105,** 1487 (1957).

Deh57b H. G. Dehmelt, Phys. Rev. **105,** 1924 (1957).

Fan57 U. Fano, Rev. Mod. Phys. **29,** 74 (1957).

Fra57 W. Franzen and A. G. Emslie, Phys. Rev. **108,** 1453 (1957).

Gui57 M. A. Guichon, J. E. Blamont, and J. Brossel, J. Phys. Radium **18,** 99 (1957).

Kas57 A. Kastler, J. Opt. Soc. **47,** 460 (1957).

Ska57 T. Skalinsky, Compt. Rend. **245,** 1908 (1957).

1958

And58 L. W. Anderson, F. M. Pipkin, and J. C. Baird, Phys. Rev. Letters **1,** 229 (1958).

Ard58a M. Arditi and T. R. Carver, Phys. Rev. **109,** 1012 (1958).

Ard58b M. Arditi and T. R. Carver, Phys. Rev. **112,** 449 (1958).

Ard58c M. Arditi, J. Phys. Radium **19,** 873 (1958).

Bar58 J. P. Barrat and J. Brossel, Compt. Rend **246,** 2744 (1958).

Bea58 E. C. Beatty, P. L. Bender, and A. R. Chi, Phys. Rev. **112,** 450 (1958).

Bel58 W. E. Bell and A. L. Bloom, Phys. Rev. **109,** 219 (1958).

Ben58 P. L. Bender, E. C. Beatty, and A. R. Chi, Phys. Rev. Letters **1,** 311 (1958).

Blo58 A. Bloom, J. Phys. Radium **19,** 881 (1958).

Cag58a B. Cagnac, J. Phys. Radium **19,** 863 (1958).

Cag58b B. Cagnac, J. Brossel, and A. Kastler, Compt. Rend. **246,** 1827 (1958).

Cag58c B. Cagnac and J. Brossel, Compt. Rend. **249,** 77 (1958).

Cag58d B. Cagnac and J. Brossel, Compt. Rend. **249,** 253 (1958).

Can58a J. M. Daniels and H. Wesemeyer, Can. J. Phys. **36,** 405 (1958).

Dan58b J. M. Daniels and H. Wesemeyer, Z. Physik **152,** 591 (1958).

Deh58a H. G. Dehmelt, Phys. Rev. **109,** 381 (1958).

Deh58b H. G. Dehmelt, J. Phys. Radium **19,** 866 (1958).

Dia58 F. Diamond, J. M. Legendre, and T. Skalinski, Compt. Rend. **246,** 90 (1958).

Fra58a P. Franken, R. Sands, and J. Hobart, Phys. Rev. Letters **1,** 52 (1958).

Fra58b P. A. Franken and F. D. Colegrove, Phys. Rev. Letters **1,** 316 (1958).

Har58 F. Hartmann, M. Rambosson, J. Brossel, and A. Kastler, Compt. Rend. **246,** 1522 (1958).

Hol58 W. W. Holloway, Jr. and R. Novick, Phys. Rev. Letters **1,** 367 (1958).

Köp58 H. Köpfermann, *Nuclear Moments* (Academic, New York, 1958).

Nov58 R. Novick and H. E. Peters, Phys. Rev. **1,** 54 (1958).

Rob58 H. G. Robinson, E. S. Ensberg, and H. G. Dehment, Bull. Am. Phys. Soc. **3,** 9 (1958).

Ska58 T. Skalinski, J. Phys. Radium **19,** 890 (1958).

1959

And59 L. W. Anderson, F. M. Pipkin, and J. C. Baird, Phys. Rev. **116,** 87 (1958).

Bar59a, b, c J. P. Barrat, J. Phys. Radium **20,** 541, 633, 657 (1959).

Cag59 B. Cagnac and J. Brossel, Compt. Rend. **249,** 77 (1959).

Dod59 J. M. Dodd, W. N. Fox, G. W. Series, and M. J. Taylor, Proc. Phys. Soc. (London) **74,** 789 (1959).

Fra59 W. Franzen, Phys. Rev. **115,** 850 (1959).

Mar59 H. Margenau, P. Fontana, and L. Klein, Phys. Rev. **115,** 87 (1959).

Ser59 G. W. Series, Rept. Progr. Phys. **22,** 280 (1959).

Win59 J. M. Winter, Ann. Phys. (Paris) **4,** 745 (1959).

1960

Adr60a F. J. Adrian, J. Chem. Phys. **32,** 972 (1960).

Adr60b F. J. Adrian, Phys. Rev. **127,** 837 (1960).

And60a L. W. Anderson, F. M. Pipkin, and J. C. Baird, Phys. Rev. Letters **4,** 69 (1960).

And60b L. W. Anderson, F. M. Pipkin, and J. C. Baird, Phys. Rev. **120,** 1279 (1960).

Blo60a A. L. Bloom, Phys. Rev. **118,** 664 (1960).

Blo60b A. L. Bloom and J. B. Carr, Phys. Rev. **119,** 1946 (1960).

Bou60 M. A. Bouchiat, T. R. Carver, and C. M. Varnum, Phys. Rev. Letters **5,** 373 (1960).

Col60 F. D. Colegrove and P. A. Franken, Phys. Rev. **119,** 680 (1960).

Cun60 D. E. Cunningham and L. O. Olsen, Phys. Rev. **119,** 691 (1960).

DeZ60 R. L. de Zafra, Am. J. Phys. **28,** 646 (1960).

Rob60 L. B. Robinson, Phys. Rev. **117,** 1275 (1960).

Ska60 T. Skalinski, Rendiconti S. I. F. XVII Corso 212–239 (1960).

1961

Abr61 A. Abragam, *The Principles of Nuclear Magnetism* (Clarendon Press, Oxford, 1961).

And61 L. W. Anderson and A. T. Ramsey, Phys. Rev. **124,** 1862 (1961).

Ard61 M. Arditi and T. R. Carver, Phys. Rev. **124,** 800 (1961).

Bar61a J. P. Barrat, Proc. Roy. Soc. (London) **A263,** 371 (1961).

Bar61b J. P. Barrat and C. Cohen-Tannoudji, Compt. Rend. **252,** 93 (1961).

Bar61c J. P. Barrat and C. Cohen-Tannoudji, Compt. Rend. **252,** 255 (1961).

Bar61d J. P. Barrat and C. Cohen-Tannoudji, J. Phys. Radium **22,** 329 (1961).

Bar61e J. P. Barrat and C. Cohen-Tannoudji, J. Phys. Radium **22,** 443 (1961).

Bel61a W. E. Bell, A. L. Bloom, and J. Lynch, Rev. Sci. Instr. **32,** 688 (1961).

Bel61b W. E. Bell and A. L. Bloom, Phys. Rev. Letters **6,** 280 (1961).

Boe61 H. Boersch, W. Raith, and M. Rehmet, Z. Physik **163,** 197 (1961).

Bre61 R. G. Brewer, Rev. Sci. Instr. **32,** 1356 (1961).

Cag61 B. Cagnac, Ann. Phys. (Paris) **6,** 467 (1961).

Car61 T. R. Carver, F. R. Lewis, Jr., R. E. Pollock, and G. E. Schrank, Rev. Sci. Instr. **32,** 861 (1961).
Coh61a C. Cohen-Tannoudji, Compt. Rend. **252,** 394 (1961).
Coh61b C. Cohen-Tannoudji, Compt. Rend. **253,** 2662 (1961).
Coh61c C. Cohen-Tannoudji, Compt. Rend. **253,** 2899 (1961).
Dal61 A. Dalgarno, Proc. Roy. Soc. (London) **A262,** 132 (1961).
Fra61 P. A. Franken, Phys. Rev. **121,** 508 (1961).
Fri61 B. D. Fried and S. D. Conte, *The Plasma Dispersion Function* (Academic Press, New York, 1961).
Haw61 W. B. Hawkins, Phys. Rev. **123,** 544 (1961).
Her61 R. Herman and H. Margenau, Phys. Rev. **122,** 1204 (1961).
Kas61 A. Kastler, Compt. Rend. **252,** 2396 (1961).
Omo61 A. Omont, Compt. Rend. **252,** 861 (1961).
Rai61 W. Raith, Z. Physik **163,** 467 (1961).
Sch61a L. D. Schearer, *Advances in Quantum Electronics*, (Columbia U. P., New York, 1961), p. 239.
Sch61b L. D. Schearer, Rev. Sci. Instr. **32,** 1190 (1961).
Skr61 G. V. Skrotskii and T. G. Izyumova, Soviet Phys. Usp. **4,** 177 (1971).

1962

Ben62 P. L. Bender, Phys. Rev. **128,** 2218 (1962).
Ber62 R. A. Bernheim, J. Chem. Phys. **36,** 135 (1962).
Blo62 A. L. Bloom, Appl. Opt. **1,** 61 (1962).
Bou62a M. Bouchiat and J. Brossel, Compt. Rend. **254,** 3650 (1962).
Bou52b M. A. Bouchiat and J. Brossel, Compt. Rend. **254,** 3828 (1962).
Bre62a R. G. Brewer, J. Chem. Phys. **37,** 2504 (1962).
Bre62b R. G. Brewer, J. Opt. Soc. Am. **52,** 832 (1962).
Cla62 G. A. Clarke, J. Chem. Phys. **36,** 2211 (1962).
Coh62a, b C. Cohen-Tannoudji, Ann. Phys. (Paris) **7,** 423, 469 (1962);
Cor62 C. R. Corliss and W. R. Bozmann, Nat. Bur. Stand. Monograph No. 53 (1962).
Deh62a H. G. Dehmelt and F. G. Major, Phys. Rev. Letters **8,** 213 (1962).
Deh62b H. G. Dehmelt and K. B. Jafferts, Phys. Rev. **125,** 1318 (1962).
Goz62 A. Gozzini, Compt. Rend. **255,** 1905 (1962).
Hol62 W. W. Holloway, E. Lüscher, and R. Novick, Phys. Rev. **126,** 2109 (1962).
Lam62 R. H. Lambert and F. M. Pipkin, Phys. Rev. **128,** 198 (1962).
Lem62 J. Lemmerich and W. Raith, Naturwiss. **49,** 127 (1962).
McN62 R. J. McNeal, J. Chem. Phys. **37,** 2726 (1962).
Phi62 G. C. Phillips, R. R. Perry, P. M. Windham, G. K. Walters, L. D. Schearer, and F. D. Colegrove, Phys. Rev. Letters **9,** 502 (1962).
Pip62 F. M. Pipkin and R. H. Lambert, Phys. Rev. **127,** 787 (1962).
Sch62 L. D. Schaerer, Phys. Rev. **127,** 512 (1962).
Wal62 G. K. Walters, F. D. Colegrove, and L. D. Schearer, Phys. Rev. Letters **8,** 439 (1962).

1963

Ale63a E. B. Aleksandrov, Opt. Spectry. (USSR) **14,** 233 (1963).
Ale63b E. B. Aleksandrov and V. A. Khodovvi, Opt. Spectry. (USSR) **14,** 436 (1963).
And63 L. W. Anderson and A. T. Ramsey, Phys. Rev. **132,** 712 (1963).
Ard63 M. Arditi and T. R. Carver, Proc. IEEE **51,** 190 (1963).
Bau63 M. Baumann, Z. Physik **173,** 519 (1963).
Ben63 P. L. Bender, Phys. Rev. **132,** 2154 (1963).
Bou63a M. A. Bouchiat, J. Physique **24,** 379 (1963).
Bou63b M. A. Bouchiat, J. Physique **24,** 611 (1963).
Bou63c M. Bouchiat and J. Brossel, Compt. Rend. **257,** 2825 (1963).
Car63 T. R. Carver, Science **141,** 599 (1963).
Coh63 C. Cohen-Tannoudji, J. Physique **24,** 653 (1963).
Col63 F. D. Colegrove, L. D. Schearer, and G. K. Walters, Phys. Rev. **132,** 2561 (1963).
DeB63 J. H. DeBoer, *The Dynamical Character of Adsorption* (Oxford U. P., New York, 1963).
Fra63a F. A. Franz, Rev. Sci. Instr. **34,** 589 (1963).
Fra63b F. A. Franz and E. Lüscher, Physics Letters **7,** 277 (1963).
Gla63 A. E. Glassgold, Phys. Rev. **132,** 2144 (1963).
Har63 P. Hartmann, Compt. Rend. **257,** 2447 (1963).
Kas63 A. Kastler, J. Opt. Soc. Am. **53,** 902 (1963).
Kon64 O. V. Konstantinov and V. I. Perel', Soviet Phys.—JETP **18,** 195 (1964).
Lam63 R. H. Lambert and F. M. Pipkin, Phys. Rev. **129,** 1233 (1963).
Leh63 J. C. Lehmann and R. Barbé Compt. Rend. **257,** 3152 (1963).
Man63 J. Manuel and C. Cohen-Tannoudji, Compt. Rend. **257,** 413 (1963).
Sch63a L. D. Schearer, F. D. Colegrove, and G. K. Walters, Phys. Rev. Letters **10,** 108 (1963).
Sch63b L. D. Schearer, F. D. Colegrove, and G. K. Walters, Rev. Sci. Instr. **34,** 1363 (1963).

1964

Ale64 E. B. Aleksandrov, O. V. Konstantinov, V. I. Perel', and V. A. Khodovoi, Soviet Phys.—JETP **18,** 346 (1964).
And64 L. W. Anderson, Nuovo Cimento **31,** 986 (1964).
Ard64 M. Arditi and T. R. Carver, Phys. Rev. **136,** A643 (1964).
Bal64a L. C. Balling, R. J. Hanson, and F. M. Pipkin, Phys. Rev. **133,** A607 (1964).
Bal64b L. C. Balling and F. M. Pipkin, Phys. Rev. **136,** A461 (1964).
Bar64 J. P. Barrat, B. Chéron, and J. L. Cojan, Compt. Rend. **259,** 3475 (1964).
Ben64 P. L. Bender, Phys. Rev. **134,** A1174 (1964).
Bre64 R. G. Brewer, J. Chem. Phys. **40,** 1077 (1964).
Byr64a F. W. Byron and H. M. Foley, Phys. Rev. **134A,** 625 (1964).
Byr64b F. W. Byron, M. N. McDermott, and R. Novick, Phys. Rev. **134,** A615 (1964).
Coh64 C. Cohen-Tannoudji and J. Brossel, Compt. Rend. **258,** 6119 (1964).
Col64 F. D. Colegrove, L. D. Schearer, and G. K. Walters, Phys. Rev. **135A,** 355 (1964).
Dav64a P. Davidovits and N. Knable, Rev. Sci. Instr. **35,** 857 (1964).
Deh64 H. G. Dehmelt, Rev. Sci. Instr. **35,** 768 (1964).
Fav64 C. J. Favre and E. Geneux, Physics Letters **8,** 190 (1964).
Fos64 E. W. Foster, Rept. Progr. Phys. **27,** 469 (1964).
Fra64a F. A. Franz, Physics Letters **13,** 123 (1964).
Fra64b F. Franz and E. Lüscher, Phys. Rev. **135,** A582 (1964).
Fra64 W. Franzen and M. Alam, Phys. Rev. **133,** A460 (1964).
Gre64 R. C. Greenhow, Phys. Rev. **136,** A660 (1964).
Gro64a F. Grossetête, J. Physique **25,** 383 (1964).
Gro64b F. Grossetête, Compt. Rend. **258,** 3668 (1964).
Gro64c F. Grossetête, Compt. Rend. **259,** 3211 (1964).
Her64 R. H. Herman, Phys. Rev. **136,** A1576 (1964).
Jar64 S. M. Jarrett, Phys. Rev. **133,** A111 (1964).
Kry64 E. Kryger, B. Mioduszewsku, and K. Rosinski, Bull. Acad. Polonaise Sci. **12,** 503 (1964).
Leg64 S. Legowski, J. Chem. Phys. **41,** 1313 (1964).
Leh64a J. C. Lehmann, J. Phys. Radium **25,** 809 (1964).
Leh64b J. C. Lehmann and C. Cohen-Tannoudji, Compt. Rend. **258,** 4463 (1964).
Leh64c J. C. Lehmann and J. Brossel, Compt. Rend. **258,** 869 (1964).
Lur64 A. Lurio, R. L. DeZafra, and R. Goshen, Phys. Rev. **134,** 1198 (1964).

McN64a R. J. McNeal, J. Chem. Phys. **40,** 1089 (1964).
McN64b R. J. McNeal, R. A. Bernheim, R. Bersohn, and M. Dorfman, J. Chem. Phys. **40,** 1678 (1964).
Omo64 A. Omont, Compt. Rend. **258,** 1193 (1964).
Ott64 E. Otten, Naturwiss. **7,** 157 (1964).
Pik64 C. A. Piketty-Rives, F. Grossetête, and J. Brossel, Compt. Rend. **258,** 1189 (1964).
Pop64 I. M. Popescu and L. N. Novikov, Compt. Rend. **259,** 1321 (1964).
Ram64 A. T. Ramsey and L. W. Anderson, Nuovo Cimento **32,** 1151 (1964).
Ros64 K. Rosinski, Bull. Acad. Polonaise Sci. **12,** 497 (1964).
Sch64 L. D. Schearer, F. D. Colegrove, and G. K. Walters, Rev. Sci. Instr. **35,** 767 (1964).
Sch64 B. M. Schmidt, J. M. Williams, and D. Williams, J. Opt. Soc. Am. **54,** 454 (1964).

1965

Ale65 E. B. Aleksandrov, O. V. Konstantinov, and V. I. Perel', Soviet Phys.—JETP **22,** 70 (1966).
Ard65 M. Arditi and T. R. Carver, J. Appl. Phys. **36,** 443 (1965).
Bal65 L. C. Balling and F. M. Pipkin, Phys. Rev. **139,** A19 (1965).
Bar65 J. P. Barrat, J. L. Cojan, and F. Lacroix-Desmazes, Compt. Rend. **261,** 1627 (1965).
Ber65a H. C. Berg, J. Chem. Phys. **43,** 1851 (1965).
Ber65b R. A. Bernheim, *Optical Pumping* (Benjamin, New York, 1965).
Bou65a M. A. Bouchiat, J. Physique **26,** 415 (1965).
Bou65b M. A. Bouchiat and J. Brossel, Compt. Rend **260,** 6823 (1965).
Bud65 B. Budick, R. Novick, and A. Lurio, Appl. Optics **4,** 229 (1965).
Cha65 G. D. Chapman and L. Krause, Can. J. Phys. **44,** 753 (1965).
Coh65 C. Cohen-Tannoudji and Serge Haroche, Compt. Rend. Acad. Sci. Paris **261,** 5400 (1965).
Cza65 M. Czajkowski and L. Krause, Can. J. Phys. **43,** 1259 (1965).
Dal65 A. Dalgarno and H. R. Rudge, Proc. Roy. Soc. (London) **A286,** 519 (1965).
Dav65 P. Davidovits and W. A. Stern, Applied Physics Letters **6,** 20 (1965).
Deh65 H. G. Dehmelt, J. Opt. Soc. Am. **55,** 335 (1965).
Dya65 M. J. Dyakonov and V. I. Perel', Soviet Phys.—JETP **20,** 997 (1965).
Far65 J. P. Faroux and J. Brossel, Compt. Rend. **261,** 3092 (1965).
Fra65 F. A. Franz, Phys. Rev. **139,** A603 (1965).
Gam65 R. L. Gamblin and T. R. Carver, Phys. Rev. **138,** A946 (1965).
Gib65 H. Gibbs, Phys. Rev. **139,** A1374 (1965).
Gro65 F. Grossetête, Compt. Rend. **260,** 3327 (1965).
Her65 R. M. Herman, Phys. Rev. **137,** A1062 (1965).
Kan65 T. Kandu and T. Minemoto, J. Phys. Soc. Japan **20,** 1532 (1965).
Kib65 B. P. Kibble and S. Pancharatnam, Proc. Phys. Soc. London **86,** 1351 (1965).
Meu65 J. Meunier, A. Omont, and J. Brossel, Compt. Rend. **261,** 5033 (1965).
McN65 R. J. McNeal, J. Chem. Phys. **43,** 1851 (1965).
Nov65 L. N. Novikov and I. M. Popesku, Opt. Spectry. (USSR) **19,** 375 (1965).
Omo65a A. Omont, Compt. Rend. **260,** 3331 (1965).
Omo65b A. Omont, J. Physique **26,** 26 (1965).
Omo65c A. Omont, J. Physique **26,** 576 (1965).
Pol65a N. Polonsky and C. Cohen-Tannoudji, Compt. Rend. **260,** 5231 (1965).
Pol65b N. Polonsky and C. Cohen-Tannoudji, Compt. Rend. **261,** 369 (1965).
Pol65c N. Polonsky and C. Cohen-Tannoudji, J. Physique **26,** 409 (1965).
Ram65 A. T. Ramsey and L. W. Anderson, J. Chem. Phys. **43,** 191 (1965).
Ros65 K. Rosinski, Bull. Acad. Polonaise Sci. **23,** 847 (1965).
Roz65 M. Rozwadowski and E. Lipworth, J. Chem. Phys. **43,** 2347 (1965).
Ruf65 G. A. Ruff and T. R. Carver, Phys. Rev. Letters **7,** 282 (1965).
Sch65 L. D. Schearer and G. K. Walters, Phys. Rev. **139,** A1398 (1965).
Ska65 T. Skalinski and K. Rosinski, Journal of Applied Mathematics and Physics **16,** 15 (1965).
Smi65 B. Smirnov and M. Chibisov, Soviet Phys.—JETP **21,** 624 (1965).
Tit65 K. Tittel, Z. Physik **187,** 421 (1965).
Vid65 J. Vidal-Couret, M. A. Bouchiat, J. Nasser, and J. Brossel, Compt. Rend. **260,** 1904 (1965).
Win65 J. Winocur and R. V. Pyle, J. Appl. Phys. **36,** 2740 (1965).
zuP65 G. zuPutlitz, Ergeb. Exakt. Naturwiss. **37,** 105 (1965).

1966

Ale66 E. B. Aleksandrov, A. M. Bonch-Bruevich, N. N. Kostin, and V. A. Khodovoi, Soviet Phys. Letters—JETP **3,** 85 (1966).
Bal66 L. C. Balling, Phys. Rev. **151,** 1 (1966).
Bar66 J. P. Barrat, D. Casalta, J. L. Cojan, and J. Hamel, J. Physique **27,** 608 (1966).
Bon66 A. M. Bonch-Bruevich, N. N. Kostin, and V. A. Khodovoi, Soviet Phys.—JETP **3,** 425 (1966).
Bou66a M. Bouchiat and F. Grossetête, J. Physique **27,** 353 (1966).
Bou66b M. A. Bouchiat and J. Brossel, Phys. Rev. **147,** 41 (1966).
Buc66 H. Bucka, Z. Physik **191,** 199 (1966).
Car66 T. R. Carver and R. B. Partridge, Am. J. Phys. **34,** 339 (1966).
Coh66a C. Cohen-Tannoudji and S. Haroche, Compt. Rend. **262,** 37 (1966).
Coh66b C. Cohen-Tannoudji and S. Haroche, Compt. Rend. **262,** 268 (1966).
Coh66c C. Cohen-Tannoudji and A. Kastler Progress in Optics **5,** 3 (1966).
Cor66 A. Corney, B. P. Kibble, and G. W. Series, Proc. Roy. Soc. (London) **A293,** 70 (1966).
Cza66 M. Czajkowski, D. McGillis, and L. Krause, Can. J. Phys. **44,** 91 (1966).
Dav66 P. Davidovits and R. Novick, Proc. IEEE **54,** 155 (1966).
Erm66 W. Ermisch, Ann. Physik **18,** 271 (1966).
Far66a J. P. Faroux and J. Brossel, Compt. Rend. **262,** 41 (1966).
Far66b J. P. Faroux, Compt. Rend. **262,** 1385 (1966).
Far66c J. P. Faroux and J. Brossel, Compt. Rend. **263,** 612 (1966).
Fir66 A. H. Firester and T. R. Carver, Phys. Rev. Letters **17,** 947 (1966).
For66 E. N. Fortson, F. G. Major, and H. G. Dehmelt, Phys. Rev. Letters **16,** 221 (1966).
Fra66a F. A. Franz, Phys. Rev. **141,** 105 (1966).
Fra66b F. A. Franz and J. R. Franz, Phys. Rev. **148,** 82 (1966).
Fri66 J. Fricke and J. Haas, Z. Naturforsch. **21a,** 1319 (1966).
Had66 T. Hadeishi and C. H. Liu, Phys. Rev. Letters **17,** 513 (1966).
Jor66 J. A. Jordan and P. A. Franken, Phys. Rev. **142,** 20 (1966).
Kra66a M. Krainska-Miszczak, Bull. Acad. Polonaise Sci. **14,** 223 (1966).
Kra66b L. Krause, Appl. Optics **5,** 1375 (1966).
Led66a M.Leduc, J. Brossel, and J. C. Lehmann, Compt. Rend. B 263, 740 (1966).
Led66b M. Leduc and J. C. Lehmann, Compt. Rend. **262,** 736 (1966).
Leh66 J. C. Lehmann, and J. Brossel, Compt. Rend. **262B,** 624 (1966).

Mar66 R. Marrus and J. Yellin, Phys. Rev. **141,** 130 (1966).
McI66 T. McIlrath, Thesis, Princeton, 1966 (unpublished).
Meu66a J. Meunier and A. Omont, Compt. Rend. **262,** 190 (1966).
Meu66b J. Meunier and A. Omont, Compt. Rend. **262,** 260 (1966).
Min66a P. Minguzzi, F. Strumia, and P. Violino, J. Opt. Soc. Am. **56,** 707 (1966).
Min66b P. Minguzzi, F. Strumia, and P. Violino, Nuovo Cimento **46B,** 145 (1966).
Nov66 L. N. Novikov, Pribory i Tex. Exper. **4,** 121 (1966).
Ols66 L. Olschewski and E. W. Otten, Z. Physik **196,** 77 (1966).
Pan66 S. Pancharatnam, J. Opt. Soc. Am. **56,** 1636 (1966).
Par66 R. B. Partridge and G. W. Series, Proc. Phys. Soc. (London) **88,** 983 (1966).
Pit66 B. Pitre, A. G. A. Rae, and L. Krause, Can. J. Phys. **44,** 731 (1966).
Qua66 F. Quarré and A. Omont, Compt. Rend. **263B,** 41 (1966).
Rob66 E. J. Robinson, J. Levine, and B. Bederson, Phys. Rev. **146,** 95 (1966).
Ros66 K. Rosinski, Bull. Acad. Polonaise Sci. **24,** 239 (1966).
Ruf66 G. A. Ruff, Phys. Rev. Letters **16,** 976 (1966).
Sal66 E. B. Saloman and W. Happer, Phys. Rev. **144,** 7 (1966).
Ser66 G. W. Series, Proc. Phys. Soc. (London) **88,** 957 (1966).
Smi66 W. W. Smith and A. Gallagher, Phys. Rev. **145,** 26 (1966).
Str66 F. Strumia, Nuovo Cimento **44B,** 387 (1966).
Vio66 P. Violino, Nuovo Cimento **45B,** 166 (1966).
Wie66 W. L. Wiese, M. W. Smith, and B. M. Glennon, *Atomic Transition Probabilities* (National Standard Reference Data Series, National Bureau of Standards **4,** 1966).

1967

Ack67 H. Ackermann, G. zuPutlitz, and E. W. Weber, Physics Letters **24A,** 567 (1967).
Aym67 M. Aymar, M. A. Bouchiat, and J. Brossel, Physics Letters **24A,** 753 (1967).
Ban67 I. Bany and B. Mioduszewska-Grochowska, Bull. Acad. Polonaise Sci. **25,** 369 (1967).
Bes67 H. J. Besch, U. Köpf, and E. W. Otten, Physics Letters **25B,** 120 (1967).
Big67 M. C. Bigeon, J. Physique **28,** 51 (1967).
Bou67 M. A. Bouchiat, J. Brossel, and L. Pottier, Phys. Rev. Letters **19,** 817 (1967).
Bud67 B. Budick, *Advances in Atomic and Molecular Physics,* **3,** (1967).
Cag67 B. Cagnac and G. Lemeignan, Compt. Rend. **264,** 1850 (1967).
Che67 S. Y. Ch'en, R. O. Garrett, and E. C. Looi, Phys. Rev. **156,** 48 (1967).
Coh67 C. Cohen-Tannoudji and F. Laloë, J. Physique **28,** 505, 722 (1967).
Dön67a A. Dönzelmann, A. P. M. Baede, E. J. M. Overboom, and J. M. Rozing, Appl. Sci. Res. **18,** 61 (1967).
Dön67b A. Dönzelmann, C. J. Van der Berg, and P. Voetalink, Physics Letters **26A,** 83 (1967).
Dup67a J. Dupont-Roc, N. Polonsky, C. Cohen-Tannoudji, and A. Kastler, Physics Letters **25A,** 87 (1967).
Dup67b J. Dupont-Roc, N. Polonsky, C. Cohen-Tannoudji, and A. Kastler, Compt. Rend. **264,** 1811 (1967).
Elb67 M. Elbel and F. Naumann, Z. Physik **204,** 501 (1967).
Ens67a,b E. S. Ensberg, Phys. Rev. **153,** 36 (1967); Phys. Rev. **164,** 270 (1967).
Ern67 K. Ernst, P. Minguzzi, and F. Strumia, Nuovo Cimento **51B,** 202 (1967).
Far67a J. P. Faroux and J. Brossel, Compt. Rend. **264,** 1452 (1967).
Far67b J. P. Faroux, Compt. Rend. **264,** 1573 (1967).
Far67c J. P. Faroux, Compt. Rend. **265,** 393 (1967).
Far67d J. P. Faroux and J. Brossel, Compt. Rend. **265,** 1412 (1967).
Fir67 A. H. Firester and T. R. Carver, Phys. Rev. **164,** 76 (1967).
Fit67 W. A. Fitzsimmons and G. K. Walter, Phys. Rev. Letters **19,** 943 (1967).
Fra67 F. A. Franz, G. Leutert, and R. T. Shuey Helv. Phys. Acta **40,** 778 (1967).
Fri67 J. Fricke, J. Haas, E. Lüscher, and F. A. Franz, Phys. Rev. **163,** 45 (1967).
Gal67a A. Gallagher, Phys. Rev. **157,** 24 (1967).
Gal67b A. Gallagher, Phys. Rev. **157,** 68 (1967); **163,** 206 (1967).
Gib67 H. M. Gibbs and R. J. Hull, Phys. Rev. **153,** 132 (1967).
Gro67a F. Grossetête and J. Brossel, Compt. Rend. **264,** 381 (1967).
Gro67b F. Grossetête, F. Laloë, C. Cohen-Tannoudji, and J. Brossel, Compt. Rend. **265,** 1247 (1967).
Gro67c F. Grossetête, D. Sci. Dissertation University of Paris, 1967, (unpublished).
Had67 T. Hadeishi and C. H. Liu, Phys. Rev. **19,** 211 (1967).
Hap67a W. Happer and B. S. Mathur, Phys. Rev. Letters **18,** 577 (1967).
Hap67b W. Happer and B. S. Mathur, Phys. Rev. Letters **18,** 727 (1967).
Hap67c W. Happer and B. S. Mathur, Phys. Rev. **163,** 12 (1967).
Har67a F. Hartmann, Physics Letters **24A,** 767 (1967).
Har67b F. Hartmann, Ann. Phys. (Paris) **2,** 329 (1967).
Har67c F. Hartmann, J. Physique **28,** 288 (1967).
Kas67 A. Kastler, Science **158,** 214 (1967).
Kra67 M. Krainska-Miszczak, Bull. Acad. Polonaise Sci. **15,** 595 (1967).
Leh67 J. C. Lehmann, Ann. Phys. (Paris) **2,** 345 (1967).
Lom67 H. Lombardi, Compt. Rend. **265B,** 191 (1967).
Mas67 F. Masnou-Seeuws and M. A. Bouchiat, J. Physique **28,** 406 (1967).
McA67 H. McAdams and G. K. Walters, Phys. Rev. Letters **18,** 436 (1967).
McG67 D. A. McGillis and L. Krause, Phys. Rev. **153,** 44 (1967).
Nov67a L. N. Novikov and V. G. Polazan'ev, Soviet Phys.—JETP **53,** 699 (1967).
Nov67b L. N. Novikov, V. G. Polazan'ev, and L. T. Yakub, Soviet Phys.—JETP **26,** 752 (1968).
Nov67c L. N. Novikov, Opt. i Spektroskopiya **23,** 677 (1967).
Nov67d L. N. Novikov, Pribory i Tekhnika Experimenta **4,** 136 (1967).
Ols67 L. Olschiwski and E. W. Otten, Z. Physik **200,** 224 (1967).
Omo67 A. Omont, Compt. Rend. **265,** 31 (1967).
Ros67 K. Rosinski, Acta Phys. Polon. **31,** 173 (1967).
Sch67 L. D. Schearer, Phys. Rev. **160,** 76 (1967).
Skr67 G. V. Skrotzky, V. G. Pokazan'ev, and L. T. Yakub, Nuovo Cimento **52B,** 469 (1967).
Spe67 P. W. Spence and M. N. McDermott, Physics Letters **24A,** 430 (1967).
Var67 D. A. Varshalovich, Soviet Phys.—JETP **25,** 157 (1967).

1968

Ack68 H. Ackermann, E. W. Weber, and G. zuPutlitz, Abstracts of the International Conference on Atomic Physics, New York, 1968.
Bak68 S. D. Baker, E. B. Carter, D. D. Findley, L. L. Hatfield, G. C. Phillips, N. D. Stockwell, and G. K. Walters, Phys. Rev. Letters **20,** 738 (1968).
Bay68 W. E. Baylis, Physics Letters **26A,** 414 (1968).
Bes68 H. J. Besch, U. Köpf, E. W. Otten, and Ch. Von Platten, Physics Letters **26B,** 721 (1968).
Cag68 B. Cagnac, A. Izraël, and M. Nogaret, Compt. Rend. **267,** 274 (1968).

Cap68 U. Cappeller and L. Dellit, Physics Letters **26A,** 535 (1968).

Cer68 P. Cerez, M. Arditi, and A. Kastler, Compt. Rend. **267,** 282 (1968).

Dec68 B. Decomps and M. Dumont, J. Physique **29,** 443 (1968).

Duc68 M. Duclay and M. Dumont, Compt. Rend. **266,** 340 (1968).

Dum68 M. Dumont and B. Decomps, J. Physique **29,** 181 (1968).

Dup68a J. Dupont-Roc, N. Polonsky, and C. Cohen-Tannoudji, Compt. Rend. **266,** 613 (1968).

Dup68b J. Dupount-Roc and C. Cohen-Tannoudji, Compt. Rend. **267,** 1211 (1968).

Dup 68c J. Dupont-Roc and C. Cohen-Tannoudji, Compt. Rend. **267,** 1275 (1968).

Elb68 M. Elbel, Physics Letters, **28A,** 4 (1968).

Ens68 E. S. Ensberg and C. R. Morgan, Physics Letters **28A,** 106 (1968).

Ern68a K. Ernst, P. Minguzzi, and F. Strumia, Physics Letters **27A,** 418 (1968).

Ern68b K. Ernst and F. Strumia, Phys. Rev. **170,** 48 (1968).

Fir68 A. H. Firester, Am. J. Phys. **36,** 366 (1968).

Fit68 W. A. Fitzsimmons, N. F. Lane, and G. K. Walters, Phys. Rev. **174,** 193 (1968).

Fra68 W. Franzen, P. B. Newell, and D. S. Edmonds, Jr., Phys. Rev. **170,** 17 (1968).

Gal68 A. Gallagher, Phys. Rev. **173,** 88 (1968).

Gro68 F. Grossetête, J. Physique **29,** 456 (1968).

Ham68 Peter Hammerling, Acta. Phys. Austracia **28,** 299 (1968).

Hän68 T. Hänsch, R. Odenwald, and P. Toschek, Z. Physik **209,** 478 (1968).

Hap68a W. Happer, *Beam Foil Spectroscopy*, edited by S. Bashkin (Gordon & Breach, 1968, New York), p. 305.

Hap68b W. Happer, Ann. Phys. (N.Y.) **48,** 579 (1968).

Har68 F. Hartmann, Physics Letters **28A,** 193 (1968).

Hay68 G. S. Hayne, E. S. Ensberg, and H. G. Robinson, Phys. Rev. **171,** 20 (1968).

Her68 R. M. Herman, Phys. Rev. **175,** 10 (1968).

Jon68 B. L. Jones and M. Verschueren, Phys. Rev. **176,** 42 (1968).

Lal68a F. Lalöe, M. Leduc, and P. Minguzzi, Compt. Rend. **266,** 1517 (1968).

Lal68b F. Lalöe, M. Leduc, and P. Minguzzi, Compt. Rend. **267,** 328 (1968).

Lal68c F. Lalöe, Compt. Rend. **267,** 208 (1968).

Lan68 D. A. Landmann, Phys. Rev. **173,** 33 (1968).

Lec68a D. Lecler, J. Physique **29,** 611 (1968).

Lec68b D. Lecler, J. Physique **29,** 739 (1968).

Led68a M. Leduc and J. Brossel, Compt. Rend. **266,** 12 (1968).

Led68b M. Leduc and J. Brossel, Compt. Rend. **266,** 287 (1968).

Luk68 M. Lukaszewski and K. Rosinski, Bull. Acad. Polonaise Sci. **16,** 359 (1968).

Maj68a F. G. Major and H. G. Dehmelt, Phys. Rev. **170,** 91 (1968).

Maj68b F. G. Major, *Methods of Experimental Physics* (Academic, New York, 1968), Vol. 7, Part B.

Mat68a B. S. Mathur, H. Tang, R. Bulos, and W. Happer, Phys. Rev. Letters **21,** 1035 (1968).

Mat68b B. S. Mathur, H. Tang, and W. Happer, Phys. Rev. **171,** 11 (1968).

McA68 H. H. McAdams, Phys. Rev. **170,** 276 (1968).

Mit68 J. K. Mitchell and E. N. Fortion, Phys. Rev. Letters **21,** 1621 (1968).

Nov68a L. N. Novikov, Opt. i Spektroscopiya **24,** 866 (1968).

Nov68b L. N. Novikov, V. L. Pokazan'ev, and L. I. Yakub, Izvestia Vyshikx, Uchebnikh Zavedenii **11,** 714 (1968).

Pan68 S. Pancharatnam, J. Phys. B (Proc. Phys. Soc. London) **1,** 250 (1968).

Pok68a V. G. Pokazanev, Opt. i Spektroskopiya (USSR) **24,** 348 (1968).

Pok68b V. G. Pokazan'ev and L. N. Novikov, Soviet Phys.—JETP **54,** 1297 (1968).

Pok68c V. Pokazan'ev, Opt. i Spektroskopiya **24,** 174 (1968).

Ric68 C. B. Richardson, K. B. Jefferts, and H. G. Dehmelt, Phys. Rev. **165,** 80 (1968).

Sch68a L. D. Schearer, Phys. Rev. Letters **21,** 660 (1968).

Sch68b L. D. Schearer, Phys. Rev. **166,** 30 (1968).

Sch68c L. D. Schearer, Phys. Rev. **171,** 81 (1968).

Sch68d L. D. Schearer, Phys. Letters **27A,** 544 (1968).

Sch68e L. D. Schearer and F. D. Sinclair, Phys. Rev. **175,** 36 (1968).

Sta68 M. Stapavsky and L. Krause, Can. J. Phys. **46,** 2127 (1968).

Van68 J. Vanier, Phys. Rev. **168,** 129 (1968).

Ver68 M. Verschueren, Can. J. Phys. **46,** 1753 (1968).

Vio68 P. Violino, Nuovo Cimento **54,** 61 (1968).

Whi68 C. W. White, W. M. Hughes, G. S. Hayne, and H. G. Robinson, Phys. Rev. **174,** 23 (1968).

Yab68 T. Yabuzaki and T. Ogawa, J. Opt. Soc. Am. **58,** 587 (1968).

1969

Bal69 L. C. Balling, R. H. Lambert, J. J. Wright, and R. E. Weiss, Phys. Rev. Letters **22,** 61 (1969).

Ber69 R. A. Bernheim and L. M. Kohuth, J. Chem. Phys. **50,** 899 (1969).

Bou69 C. C. Bouchiat, M. A. Bouchiat, and L. C. L. Pottier, Phys. Rev. **181,** 144 (1969).

Cha69 R. L. Chaney and M. N. McDermott, Physics Letters **29A,** 103 (1969).

Cha69b C. K. Chang and R. H. Walker, Phys. Rev. **178,** 198 (1969).

Coh69 C. Cohen-Tannoudji and J. Dupont-Roc, Optics Communications **1,** 184 (1969).

Cop69 G. Copley and L. Krause, Can. J. Phys. **47,** 533 (1969).

Dod69 J. N. Dodd, E. Enemark, and Alan Gallagher, J. Chem. Phys. **50,** 4838 (1969).

Elb69 M. Elbel, Ann. Physik **22,** 289 (1969).

Ens69 E. S. Ensberg and G. zuPutlitz, Phys. Rev. Letters **22,** 1349 (1969).

Fan69 U. Fano, Phys. Rev. **178,** 131 (1969).

Fit69 W. A. Fitzsimmons, L. L. Tankersley, and G. K. Walters, Phys. Rev. **179,** 156 (1969).

Gib69a H. M. Gibbs, B. Chang, and R. S. Greenhow, Phys. Rev. Letters **22,** 270 (1969).

Gib69b H. M. Gibbs, B. Chang, and R. C. Greenhow, Phys. Rev. **188,** 172 (1969).

Gib69c H. M. Gibbs and C. W. White, Phys. Rev. **188,** 180 (1969).

Hap69 W. Happer, *Optical Pumping Theory*, (Gordon and Breach, New York, 1969), Vol. XIc.

Har69 F. Hartmann, IEEE J. Quantum Electron **QE5,** 595 (1969).

Haw69 W. Bruce Hawkins, Phys. Rev. **182,** 39 (1969).

Hof69 H. Hofmann-Reinecke, J. Haas, and J. Fricke, Z. Naturforsch. **24a,** 182 (1969).

Köp69 U. Köpf, H. J. Besch, E. W. Otten, and Ch. von Platten, Z. Physik **226,** 297 (1969).

Kor69 V. S. Korol' and A. N. Kozlev, Soviet Phys.—JETP **56,** 1100 (1969).

Kra69 M. Krainska-Miszczak, Acta Phys. Polon. **35,** 745 (1969).

Lal69a F. Laloë, M. Leduc, and P. Minguzzi, J. Physique **30,** 277 (1969).

Lal69b F. Lalöe, M. Leduc, and P. Minguzzi, J. Physique **30,** 341 (1969).

Leh69 J. C. Lehmann, Phys. Rev. **178,** 153 (1969).

Liu69 C. H. Liu, R. L. King, and H. H. Stroke, Phys. Rev. Letters **23,** 209 (1969).

Lub69 M. S. Lubell and W. Raith, Phys. Rev. Letters **23,** 211 (1969).

McC69 M. V. McCusker, L. L. Hatfield, and G. K. Walters, Phys. Rev. Letters **22,** 817 (1969).

Min69 P. Minguzzi, F. Strumia, and P. Violino, Optics Communications **1,** 1 (1969).

Pav69 M. Pavlovič and F. Laloë, J. Physique **31,** 173 (1969).
Rao69 B. K. Rao and T. P. Das, Phys. Rev. **185,** 95 (1969).
Res69 N. W. Ressler, R. H. Lands, and T. E. Stark, Phys. Rev. **184,** 109 (1969).
Sch69a L. D. Schearer, Phys. Rev. Letters, **22,** 629 (1969).
Sch69b L. D. Schearer, Physics Letters **28A,** 660 (1969).
Sch69c L. D. Schearer, Phys. Rev. **180,** 83 (1969).
Sch69d L. D. Schearer, Phys. Rev. **188,** 505 (1969).
Lev69 B. N. Sevastiyanov and R. A. Zhitnikov, Soviet Phys.—JETP **56,** 1508 (1969).
Sia69 S. Siahatgar and U. E. Hochuli, IEEE J. Quantum Electron **QE-5,** 295 (1969).
Stu69 M. Stupavsky and L. Krause, Can. J. Phys. **47,** 1249 (1969).
Til69a R. Tilgner, J. Fricke, and J. Haas, Z. Naturforsch. **24A,** 337 (1969).
Til69b R. Tilgner, J. Fricke, and J. Haas, Helv. Phys. Acta **42,** 740 (1969).
Van69 J. Vanier, Can. J. Phys. **47,** 1461 (1969).

1970

Bel70 J. A. Bellisio and P. Davidovits, J. Chem. Phys. **53,** 3474 (1970).
Bev70 N. Beverini and F. Strumia, Optics Communications **2,** 189 (1970).
Bou70 C. C. Bouchiat and M. A. Bouchiat, Phys. Rev. **2A,** 1274 (1970).
Chu70 G. G. Churchill, Rev. Sci. Instr. **41,** 891 (1970).
Gei70 P. Geittner and M. Elbel, Z. Physik **243,** 319 (1970).
Gib70a H. M. Gibbs, G. C. Churchill, T. R. Marshall, J. F. Papp, and F. A. Franz, Phys. Rev. Letters **25,** 263 (1970).
Gib70b H. M. Gibbs and G. G. Churchill, Phys. Rev. **3,** 1617 (1971).
Gib70c H. N. Gibbs and R. E. Slusher, Phys. Rev. Letters **24,** 638 (1970).
Hap70a W. Happer, Phys. Rev. B **1,** 2203 (1970).
Har70 Francis Hartmann and Francoise Hartmann-Bourton, Phys. Rev. A **2,** 1885 (1970).
Hry70 E. S. Hrycyshyn, and L. Krause, Can. J. Phys. **48,** 2761 (1970).
Iol70 N. Ioli, P. Minguzzi, and F. Strumia, J. Opt. Soc. Am. **60,** 1192 (1970).
Lah70 B. Lahaye and J. Margerie, Optics Communications **1,** 259 (1970).
Lam70 R. H. Lambert, Phys. Rev. A **1,** 1841 (1970).
Mat70 B. S. Mathur, H. Y. Tang, and W. Happer, Phys. Rev. **2,** 648 (1970).
Mor70 G. Moruzzi and F. Strumia, Optics Communications **2,** 279 (1970).
Nov70 L. N. Novikov, V. G. Pokazan'ev, and G. V. Skrotskii, Soviet Phys.—Usp. **101,** 273 (1970).
Oku70 A. T. Okunevich and V. I. Perel', Soviet Phys.—JETP **31,** 356 (1970).
Ray70 S. Ray, G. Das, P. Maldonado, and Arnold C. Wahl, Phys. Rev. **2,** 2196 (1970).
Rit70 E. Rityn, M. Chaika, and V. Cherenkovskii, Opt. Spectry. (USSR) **28,** 344 (1970).
Sch70a L. D. Schearer and W. C. Holton, Phys. Rev. **24,** 1214 (1970).
Sch70b L. D. Schearer and L. A. Riseberg, Physics Letters **33A,** 325 (1970).
Sch70c R. W. Schmieder, A. Lurio, W. Happer, and A. Khadjavi, Phys. Rev. A **2,** 1216 (1970).
Tan70 H. Tang and W. Happer, Phys. Rev. Letters **24,** 551 (1970).
Van70 J. Vanier, R. Vaillancourt, G. Missout, and M. Têtu, J. Appl. Phys. **41,** 3188 (1970).
Var70 D. A. Varshalovich, Uspekhi Fiz. Nauk **101,** 369 (1970).
Von70 F. von Sichart, H. T. Stöckmann, H. Ackermann, and G. zuPutlitz, Z. Physik **236,** 97 (1970).
Wei70 R. E. Weiss, R. H. Lambert, and L. C. Balling, Phys. Rev. **2,** 1745 (1970).
Zhi70 R. A. Zhitnikov, P. P. Kuleshov, A. T. Okunevich, and B. N. Sevastanov, Soviet Phys.—JETP **31,** 445 (1970).

1971

Bev71 N. Bevirini, P. Minguzzi, and F. Strumia, Phys. Rev. A **4,** 550 (1971).
Bul71a B. R. Bulos, A. Marshall, and W. Happer, Phys. Rev. **4,** 51 (1971).
Bul71b R. B. Bulos and W. Happer, Phys. Rev. **A4,** 849 (1971).
Bul71c B. R. Bulos, Thesis, Columbia University, 1971 (unpublished).
Cra71 S. B. Crampton, Phys. Rev. A **3,** 515 (1971).
Dav71 S. J. Davis, J. J. Wright, and L. C. Balling, Phys. Rev. A **3,** 1220 (1971).
Dup71 J. Dupont-Roc, M. Léduc, and F. Laloë, Phys. Rev. Letters **27,** 467 (1971).
Ens71 E. S. Ensberg and C. L. Morgan, Phys. Rev. **3,** 2143 (1971).
Fra71 F. A. Franz, T. R. Marshall, and J. A. Munarin, Physics Letters **36A,** 31 (1971).
Gib71a Hyatt M. Gibbs, Phys. Rev. **3A,** 500 (1971).
Gib71b H. M. Gibbs, Phys. Rev. (to be published).
Hap71 W. Happer, Progress in Quantum Electronics (Pergamon Press, Oxford, 1971), Vol. 1, p. 51.
Led71 M. Leduc and F. Laloe, Optics Communications **3,** 56 (1971).
Mor71 A. Moretti and F. Strumia, Phys. Rev. **3,** 349 (1971).
Nov71 L. N. Novikov, Opt. i Spektroskopiya **18,** 740 (1971).
Slo71 R. E. Slocum, P. C. Caniness, and L. L. Blevins, Rev. Sci. Instr. **42,** 763 (1971).
Ste71 W. A. Stern, Thesis, Columbia University, 1971 (unpublished).
Tan71 H. Y. Tang, Thesis, Columbia University (unpublished).
Val71a P. A. Valberg and N. F. Ramsey, Phys. Rev. **3A,** 554 (1971).
Val71b P. A. Valberg, Phys. Rev. **3A,** 505 (1971).

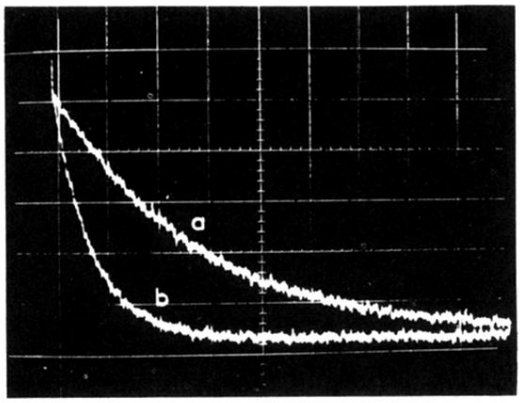

FIG. 27. The relaxation of $\langle \mathbf{S} \cdot \mathbf{I} \rangle$ due to spin exchange, buffer gas, and wall collisions. The relaxation is slower when $\langle S_z \rangle$ is nonzero (a), than when $\langle S_z \rangle$ is zero (b) [from (Gro68)].